COMPETITIVE PHOTOCATALYTIC REMOVAL OF AQUEOUS PHASE SELENOCYANATE ($SECN^-$) IN THE PRESENCE OF SOME CRITICAL CO-POLLUTANTS: ADSORPTION MODELLING, PROCESS KINETICS, AND REACTION MECHANISMS

BY

BASHIR ALHAJI LABARAN

A Dissertation Presented to the

DEANSHIP OF GRADUATE STUDIES

KING FAHD UNIVERSITY OF PETROLEUM & MINERALS

DHAHRAN, SAUDI ARABIA

In Partial Fulfillment of the
Requirements for the Degree of

DOCTOR OF PHILOSOPHY

In

CIVIL ENGINEERING

May 2017

KING FAHD UNIVERSITY OF PETROLEUM & MINERALS

DHAHRAN- 31261, SAUDI ARABIA

DEANSHIP OF GRADUATE STUDIES

This thesis, written by **Bashir Alhaji Labaran** under the direction of his thesis advisor and approved by his thesis committee, has been presented and accepted by the Dean of Graduate Studies, in partial fulfillment of the requirements for the degree of **DOCTOR OF PHILOSOPHY IN CIVIL ENGINEERING.**

Dr. Muhammad S. Vohra
(Advisor)

Dr. Mohammad S. Al-Suwaiyan
(Co-Advisor)

Dr. Salah U. Al-Dulaijan
Department Chairman

Dr. Muhammad H. Al-Malack
(Member)

Dr. Salam A. Zummo
Dean of Graduate Studies

28/5/17
Date

Dr. Alaadin A. Bukhari
(Member)

Shaikh Abdur Razzak

Dr. Shaikh Abdur Razzak
(Member)

Dedicated to My Parents, Family, and Siblings

ACKNOWLEDGMENTS

All thanks and praise is due to Allah (SWA) the most exalted, most high, for all his blessings and for taken me through this academic journey successfully. May the peace and blessings of Allah be upon the last and seal of the prophets (PBUH). I would like to express my special thanks to King Fahd University of Petroleum and Minerals for providing scholarship, Civil and Environmental Engineering Department for their support, Deanship of Scientific Research for financing part of this research through research grant SB141004. I would like to express my deepest gratitude to Dr. Salah U. Al-Dulaijan, Chairman, Civil and Environmental Engineering Department for his academic and moral support throughout my graduate study. My greatest and warmest gratitude and appreciation goes to my advisor, Dr. M. S. Vohra for his omnipresence in providing help, support, inspiration, encouragement, guidance and never being tired of reading my work. I am particularly grateful to him for been kind and considerate when advising either academically or morally. I am also grateful to my co-advisor, Dr. M. S. Al-Suwaiyan, and my committee members, Dr. M. H. Malack, Dr. Alaadin Bukhari and Dr. Shaikh Abdur Razzak for their help, guidance, valuable advice, and patience in reading my work despite their tight schedules. Special thanks go to Dr. M. H. Essa, Engineer Sameh AbdulFattah Araby and the staffs of Environmental Engineering lab for their assistance. This acknowledgement cannot be complete without the mention of my friend, Engineer Sagir Adamu, who helped in teaching, correcting, and assessing my Mathematica models.

Most importantly, I am thankful to my parents for their guidance, encouragement, prayers, and moral/financial support throughout my life and for laying a good foundation at my tender age that makes me what I am today. I am also grateful to all my brothers, sisters, friends, and other relatives, for their moral and emotional support. Last but not the least, the continued support, patience, prayer, love and care from my wife and children are sincerely and gratefully appreciated.

TABLE OF CONTENTS

LIST OF TABLES

LIST OF FIGURES

LIST OF ABBREVIATIONS

PCD:	Photocatalytic Degradation
SPCD:	Solar Photocatalytic Degradation
DLM:	Diffused Layer Model
TLM:	Triple Layer Model
CD MUSIC:	Charge Distribution Multi-Site Complexation
CSTR:	Continuous Stirred Tank Reactors
UV:	Ultraviolet
CCD:	Central Composite Design
FCC:	Face-Centred Central Composite Design
DOE:	Design of Experiment
CB:	Conduction Band
VB:	Valence Band

ABSTRACT

Full Name : Bashir Alhaji Labaran

Thesis Title :Competitive photocatalytic removal of aqueous phase selenocyanate ($SeCN^-$) in the presence of some critical co-pollutants: adsorption modelling, process kinetics, and reaction mechanisms

Major Field : Civil Engineering

Date of Degree : May 2017

Present study investigated removal of selenocyanate species from aqueous phase using TiO_2 based adsorption and photocatalysis. Initially, competitive adsorption of selenite, selenate and selenocyanate onto TiO_2 was studied under varying mixed scenarios that was followed by a detailed investigation on the efficiency of TiO_2 based photocatalytic degradation (PCD) process for the competitive destruction of selenocyanate complex along with simultaneous removal of co-pollutants ammonia, cyanide, thiocyanate, and phenol from simulated mixed wastewater streams. For mixed selenite & selenate binary systems we noted high selenite adsorption with no noticeable selenate effect onto selenite adsorption even up to 10 ppm selenate. However, selenate adsorption was markedly affected by the selenite species. Nevertheless, results from the binary selenite & selenocyanate mixed systems indicated no such competitive adsorption trend and similar was also noted for the binary selenate & selenocyanate mixed adsorption studies. Findings from the tertiary mixed selenite, selenate, and selenocyanate studies showed similar adsorption trends. In general, the adsorption results above pH 4 showed selenite > selenocyanate > selenate. For adsorption modelling an inner sphere type complex i.e., **Ti**-SeO_3^- reasonably predicted selenite adsorption whereas selenate & selenocyanate adsorptions were well predicted considering outer sphere complexes, i.e., **Ti**-H_2O-SeO_4^- and **Ti**-H_2O-SeCN respectively. The adsorption results from the present work indicate that selenite, selenate, and selenocyanate species can be effectively removed from respective aqueous streams under varying mixed competitive conditions using the TiO_2 based adsorption process with a careful control of process parameters. The present study also investigated the efficiency of both UV and solar light assisted photocatalysis for the removal of selenocyanate from aqueous phase under a varying set of mixed conditions. Higher solar photocatalytic removal of selenium species transpired at pH 4 and it increased with an increase in both initial selenium and initial EDTA concentrations. The mechanism for selenocyanate removal is via SeCN complex destruction followed by stepwise oxidation to selenite and then to selenate, which in turn are reduced to elemental

selenium using hole scavenger EDA. Solar photocatalysis in the presence of co-pollutants follows the following order: SeO_3^{2-} > SCN^- > CN^- > $CN^-/SCN^-/NH_4^+$. It is worth noting that while selenium and thiocyanate species were converted to elemental selenium and sulfate respectively, no significant removal of ammonia and cyanide was noted for other experimental conditions. The mechanism of phenol removal in the presence of selenocyanate involves the formation of benzeneseleninic acid, hydroquinone, resorcinol, and pyrocatechol as primary intermediates. Secondary intermediates include maleic acid, formic acid and fumaric acid among others.

Linear and two factor interaction mathematical models were developed for photocatalytic removal of selenocyanate and phenol under competitive environment using face-centered central composite design. Higher R^2, adjusted R^2, predicted R^2 were obtained from regression analysis establishing the prediction ability of the models. Natural log transformation was applied to selenocyanate model as suggested by Box-Cox plot while perturbation plot was utilized for identifying relative significance of the factors. After successful model diagnosis and validation using various statistical approaches, the models were also validated experimentally. Optimal process conditions for photocatalytic removal of selenocyanate and phenol form aqueous phase were pH 4, 10 ppm selenocyanate, 5 ppm phenol and 450 ppm EDTA concentrations. RSM modelling prove to be an economical way for the removal of selenocyanate and phenol from aqueous phase using the optimization techniques.

Lastly, kinetic models for photocatalytic removal of selenocyanate and phenol under varying experimental conditions were developed by considering degradation of reactants and the formation and disappearance of reaction intermediates. Considering steady state assumption, ordinary differential equations representing the rate of change of each reactant were setup and solved using Mathematica to obtain reaction rate constants. *ParametricNDSolve* and *NonlinearModelfit* command were utilized for solving the differential equation and fitting the experimental data to the model respectively. Excellent to very good model fits were achieved as suggested by adjusted R^2 values as high as 0.999. Modeling results suggest selenocyanate removal via oxidation to selenite and then selenate and reaction of selenocyanate and phenol to form benzeneseleninic acid especially at low pH values. Formation of benzenediols and benzeneseleninic acid were the dominant mechanisms for phenol removal at high and low pH values respectively.

ملخص الرسالة

الاسم الكامل: بشير الحاجي لاباران

عنوان الرسالة: إزالة سيلينوسيانات من المرحلة المائية بالتحفيز الضوئي في وجود بعض الملوثات الحرجة: النمذجة الامتزازية، العملية الحركية، وآليات التفاعل

التخصص: الهندسة المدنية

تاريخ الدرجة العلمي: مايو 2017 م

إن هذ الدراسة تهدف الي معالجه ميا ة الصرف من مركبات $SeCN^-$ باستخدام كلا من طريقة Adsorption و Photocatalysis. بداية, تم اختبار معالجة مياه الصرف الملوثه بمركب -SeCN في وجود بعض مصادر السيلينيوم الاخري مثل SeO_3^{2-} و SeO_4^{2-} عن طريق امتزازها علي سطح TiO_2 متبوعة بكسر الرابطة في مركب $SeCN^-$ باستخدام طريقة Photocatalysis معتمدة علي TiO_2 في وجود بعض الملوثات الاخري مثلammonia, cyanide, thiocyanate, and phenol. لوحظ انه في حالة معالجة نظام مكون من SeO_3^{2-} و SeO_4^{2-}, ازالة مكون SeO_3^{2-} لا تتاثر بوجود مركب SeO_4^{2-} في حالة استخدام عملية Adsorption والعكس بالعكس. ايضا, تم نمذجة عملية Adsorption للثلاث مركبات مجتمعة ($SeCN^-$, SeO_3^{2-}, SeO_4^{2-}) عبارة عن حبيبات كروية من TiO^2 متصلة من الخارج في حالة $SeCN^-$ و SeO_4^{2-} او الداخل في حالة SeO_3^{2-}. لذا فإنه يمكننا القول ان عملية Adsorption للمركبات الثلاث تكون فعالة جدا في معالجة مياة الصرف تحت ظروف معينة. ان هذا البحث تطرق الي امكانية استخدام الاشعة الفوق بنسفجية (UV-light) من مصادر مختلفة مثل ضوء الشمس (Solar Photocatalysis) او من مصدر اصطناعي (UV-lamp) لمعالجة مياة الصرف الملوثة بمركبا السلينيوم ($SeCN^-$). اولا بالنسبة الي استخدام solar photocatalysis, فانه تم ملاحظة اكبر نسبة معالجة عند الاوساط الحامضية وتزداد بزيادة تركيز مركبات السيلينوم الابتدائية وكذلك تركيز EDTA. ايضا في وجود بعض المركبات الاخري السابق ذكرها, فانه استخدام طريقة solar photocatalysis تعالج مياة الصرف من مركبات SeO_3^{2-} بصوره اكبر من مركب -SeCN والتي بدورها اكبر من معالجة مركبات SeO_4^{2-}. ايضا شهدت عملية المعالجة عدم

ازالة مركب ammonia ولكن في حالة مركب phenol فانه يتحول الي مركب النزين وبعض المركبات الاخري. ايضا تم استخدم النمذجة الرياضية (RSM) لتوقع نسبة معالجة مياة الصرف من مركبات $SeCN^-$ في وجود مركبات phenol باستخدام طريقة Photocatalysis. استخدام هذه الطريقة ف النمذجة اثبتت انها اقتصاديه وسريعة بشكل كافي حيث كانت اوضحت ان انسب الظروف لازالة مركب $SeCN^-$ و phenol هي عند درجة حامضية 4 و 10 وتركيز 450 مجم/لتر من EDTA.

INTRODUCTION

Though selenium is an essential micronutrient, however intake of elevated selenium amounts could result in to serious human health concerns and diseases [1-9]. Considering the respective health issues, several countries have imposed very low selenium regulatory limits both for water and wastewater treatment, for example the U.S. EPA has set 50 ppb selenium limit for drinking water whereas the WHO has set 10 ppm as selenium limit. Though typically selenite (SeO_3^{2-}) and selenate (SeO_4^{2-}) account for most Se-species in selenium contaminated water bodies however selenocyanate ($SeCN^-$) is another dominant Se-species in specific industrial effluents including those from petroleum refineries, mining, and power plants using fossil fuels [10-15]. This becomes more of a concern as selenocyanate species is not only toxic but also poses a removal challenge. Furthermore co-pollutants ammonia, thiocyanate, and cyanide [5, 12, 16, 17] which are also noted in respective streams are also of environmental concern. Likewise, phenol which co-exists with selenium species especially in petroleum refinery wastewater [18-22] is also toxic and thus of great environmental concern. Furthermore, these co-pollutants will render selenocyanate treatment even more challenging because of synergistic effects. Traditional technologies such as using ferric chloride based coagulation is not feasible because of reasons including low attachment of selenocyanate on to formed iron hydroxide precipitate whereas traditional biological wastewater treatment oxidizes selenocyanate to

oxyanions selenite and selenate with no further removal. Considering this, several studies have investigated and reported the removal of selenocyanate species from the aqueous phase using specific technologies. For example, a patented technology mentions selenocyanate complex destruction using a proprietary chemical oxidant along with co-precipitation of oxidized selenium species employing ferric coagulant [23]. Two employed two continuous stirred tank reactors (CSTR) in series were employed for the removal of aqueous phase selenium species. In the first CSTR, ferric salt was added to the waste stream with formation of ferric hydroxide and ferric oxyhydroxide precipitates. In the second CSTR, permanganate salt was added to facilitate the oxidation of selenium species in the effluent of the first CSTR to selenite which is later adsorbed by the respective metal precipitates and removed from aqueous phase. Furthermore selenocyanate removal via direct reaction with zero valent iron (ZVI) or copper based salts has also been reported [5, 16]. These processes though reported to be successful have concerns such as significant sludge production or high co-precipitant requirement. Furthermore, as mentioned above that selenocyanate often noted with the other toxic co-pollutants and hence synergistic effect may render the selenocyanate removal more challenging. For example, the presence of co-pollutants thiocyanate, ammonia, cyanide, and phenol with selenocyanate has been reported for specific fossil fuel based industries [5, 12, 16, 17] which will render selenocyanate removal even more challenging from respective mixed streams. These concerns therefore require either development of new technologies or a careful study of existing technologies for the removal of selenocyanate under a competitive environment. The titanium dioxide (TiO_2) mediated photocatalytic

degradation (PCD) process which is an advanced oxidation/reduction treatment process for contaminated streams has been reported to successfully remove several aqueous phase pollutants [24-27]. A few TiO_2 based studies (both adsorption and photocatalysis), do report removal of selenite and selenate from the aqueous phase under a varying set of conditions [1, 28-35]. In this regard role of several h^+/hole scavengers including formic acid has also been explored to expedite the reduction of selenite species to elemental selenium and latter's enhanced removal from the respective wastewater streams [1, 28, 31, 36]. Adsorption of selenium species is reported to be a prerequisite for such photocatalytic applications [28, 32, 37]. Furthermore, successful destruction of selenocyanate complex and removal of resulting selenite and selenate species from synthetic wastewater using the TiO_2 assisted photocatalysis has also been reported [37]. Nevertheless, no study so far has explored the effect of co-pollutants selenite, selenate, thiocyanate, cyanide, ammonia, and phenol on to competitive destruction of selenocyanate along with simultaneous removal of respective co-pollutants using the TiO_2 photocatalysis. Additionally, the use of adsorption process has also been widely reported for the removal of various aqueous phase pollutants [38-42], and various studies have also explored the adsorption of selenium species onto different materials including iron oxides [43], montmorillonites [44], chitosan–clay composites and iron oxides [2], aluminum oxide [45], etc. However, investigations on selenium species adsorption onto TiO_2 are limited [1, 29-34, 46-49], with only few detailed selenium adsorption work onto TiO_2 [30]. Furthermore, there is no work on competitive adsorption of selenite, selenate and selenocyanate species onto TiO_2 surface. However, understanding such an adsorption

behaviour is important not only to realize the application of TiO_2 based adsorption for selenium species removal but also understand its role in photocatalysis [50-53] as synergistic effects might also affect the adsorption of selenite, selenate and selenocyanate onto TiO_2 in mixed binary or tertiary competitive adsorption systems. For example, adsorption of selenium species onto TiO_2 is noted to be affected by the presence of other anionic species such as phosphate [54, 55], sulphate [54], chromate [56], molybdate [56], silicate [57], fluoride [57], citrate, oxalate, and carbonate/bicarbonate [58] due to competition for the limited TiO_2 surface sites [48]. As TiO2 based adsorption is also a reliable treatment technology, studying the competitive adsorption behaviour of respective selenium species i.e., selenite, selenate and selenocyanate is important to better understand the respective adsorption trends under mixed conditions. Hence the present study's main objective is to investigate the efficiency of TiO_2 based adsorption and photocatalytic degradation processes for the removal of selenocyanate complex along with simultaneous removal of selenite and selenate species. Furthermore, the effect of co-pollutants cyanide, thiocyanate, ammonia, and phenol as mentioned earlier, onto selenocyanate removal from simulated mixed wastewater streams will also be investigated. We intend to determine the efficiency of PCD process for the treatment of said streams under a varying set of conditions and extend fundamental knowledge on subject for possible practical applications. Furthermore, use of hole scavenger EDTA during the PCD process for enhanced *reduction* initiated removal of selenite and selenate species (that will result from selenocyanate oxidation) will also be probed. Selective solar photocatalysis experiments will also be completed to assess the efficiency of solar

photocatalytic degradation (SPCD) process for the said application. The present work will use the diffuse layer model to model the adsorption of selenite, selenate, and selenocyanate onto TiO_2 under a varying set of pH and process conditions. Furthermore, the Response Surface Methodology (RSM) and kinetic modelling will also be completed for selective PCD experiments. The findings from the present study will be of use to better treat respective wastewater streams under the optimum operational conditions. To the best of our knowledge, no once has reported the abovementioned areas and considering the Se-based pollution and toxicity concerns, these topics should be studied. Further details are reported in the subsequent chapters.

LITERATURE REVIEW

The present work proposes to investigate the competitive adsorption of Se-species selenite, selenate, and selenocyanate onto TiO_2 surface along with adsorption modelling and respective findings will help to explain the TiO_2 surface based phenomena that may take part in the removal of respective Se-species. In addition, the proposed work will also investigate use of TiO_2 mediated photocatalysis or photocatalytic degradation (PCD) process for the competitive removal of selenocyanate species along with simultaneous removal of co-pollutants thiocyanate, ammonia, cyanide and phenol from simulated industrial wastewaters under a varying set of conditions. As a first step, a brief overview of the PCD and adsorption processes and review of specific selenium removal processes is given below.

2.1 Photocatalytic Degradation Process

The photocatalytic degradation (PCD) process has been widely studied to remove a variety of pollutants from the aqueous phase [24, 59, 60]. The process employs TiO_2 as a photocatalyst and UV light as an energy source to remove the concerned pollutants [61-67]. Also studies completed in the absence of TiO_2 or UV light show no or negligible removal of the target pollutants [62, 68, 69]. Some background information related to the TiO_2 catalyst and PCD process is given below for a better process understanding.

2.1.1 Catalyst TiO_2 Surface Characteristics

TiO_2 is an amphoteric compound and hence its surface (**Ti**-) in contact with water is highly hydroxylated [70, 71]. Reactions 2.1 and 2.2 are typically used to represent the naked-TiO_2 surface in contact with the water molecules:

$$\underline{Ti}\text{-}OH_2^+ \leftrightarrow \underline{Ti}\text{-}OH + H^+ \qquad 2.1$$

$$\underline{Ti}\text{-}OH \leftrightarrow \underline{Ti}\text{-}O^- + H^+ \qquad 2.2$$

For Degussa P25 TiO_2, pK_1 and pK_2 values of 3.9 and 8.7 have been reported for reactions 2.1 and 2.2, respectively [72]. Also, Turchi and Ollis (1990) report the OH^- concentration on the TiO_2 surface between 5-15/nm^2 [26]. The pH_{zpc} and other surface characteristics of TiO_2 are summarized later in Table 4.1.

2.1.2 $OH^\cdot$ Radicals: Formation and Related Reactions

The $OH^\cdot$ radicals are the dominant oxidizing species in the PCD processes and there is a considerable amount of experimental evidence to support this claim, e.g., the electron spinning resonance results as mentioned by [26]. Maruyama and Nishimoto (1991) have also reported a change in photoactivity of TiO_2 particles (H_2 production) due to a change in the surface density of OH^- ions [73]. The generation mechanism of $OH^\cdot$ radicals, is briefly explained here.

TiO_2 possesses a wide energy gap between its valence band (VB) and conduction band (CB) also known as band gap (BG). The BG extends from the top of the electron-filled VB to the bottom of the vacant CB. Upon exposure to a UV light source with energy h_v equivalent to or higher than the bandgap energy (BGE) the VB electron (e^-) is transferred to the CB. This creates a positive vacancy or hole (h^+) in the VB as shown in Scheme 2.1. Navio and Marchena (1991) have

reported BGE of 3.0 eV for TiO_2 [74]. When a TiO_2 particle is exposed to a UV radiation source (near 352 nm) it absorbs the light energy and produces an e^-/h^+ pair (Equation 2.3):

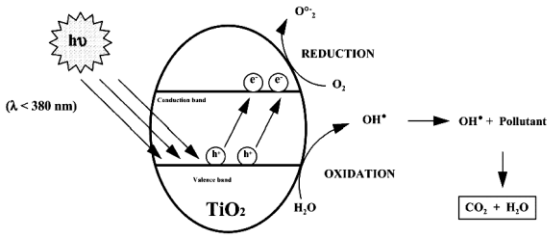

Figure 2.1 Electron excitation and related redox reactions.

$$TiO_2 + h\upsilon \rightarrow e^- + h^+ \qquad 2.3$$

The h^+ species that is electron deficient reacts with an adsorbed hydroxyl molecule OH^- on the TiO_2 surface and produces an $OH^\cdot$ radical:

$$\underline{Ti}\text{-}OH^- + h^+ \rightarrow \underline{Ti}\text{-}OH^\cdot \qquad 2.4$$

The $OH^\cdot$ radicals produced in equation 2.4 are dominant oxidizing species in the PCD process [25, 26]. These $OH^\cdot$ radicals are very powerful and non-selective oxidants. For example, they typically mineralize the organic pollutants to end products such as CO_2 and H_2O:

$$\text{Organic Pollutant} + OH^\cdot \rightarrow CO_2 + H_2O \qquad 2.5$$

It should be noted that direct oxidation of organics by holes (equation 2.6) has also been reported [61, 75, 76]. In addition to organic pollutants, inorganic pollutants such as ammonia can also be removed using the PCD technique [77].

$$\text{Organic Pollutant} + h^+ \rightarrow CO_2 + H_2O \qquad 2.6$$

The excited e^- species from equation 2.3 can be donated to an acceptor such as O_2 forming the superoxide radicals, $O_2^{\cdot}$ and hydrogen peroxide:

$$e^- + O_2 \rightarrow O_2^{\cdot} \qquad 2.7$$

$$2e^- + 2H^+ + O_2 \rightarrow H_2O_2 \qquad 2.8$$

The excited state CB electrons and VB holes can also recombine, producing heat:

$$e^- + h^+ \rightarrow \text{heat} \qquad 2.9$$

However, an increased e^-/h^+ recombination would decrease the efficiency of PCD process by reducing the e^-/h^+ pairs available for the redox reactions. Thus, the presence of a suitable electron acceptor such as O_2 which reduces the pair's recombination typically results in increased PCD efficiency. Similarly, an organic hole scavenger such as EDTA, would leave more e^- for the reduction based removal of pollutants such as heavy metals, etc, The e^- transfer process is more efficient if the receiving species is adsorbed on the surface. The respective position of photocatalyst's VB/CB w.r.t. to the adsorbed target pollutant's redox potential also determines

the e^-/h^+ transfer efficiency. The redox potential of the electron acceptor should be more positive (i.e., below) than the photocatalyst's CB redox potential. On the other hand, the redox potential of the species donating electron to the VB hole should be more negative (i.e., above) than the photocatalyst's VB redox potential.

2.1.3 Optimum TiO_2 Amount

Most PCD studies report optimum TiO_2 amounts between 0.5 and 2 g/l [78-88]. An initial increase in the TiO_2 amount added result in increased photocatalysis efficiency because of higher availability of e^-/h^+ pairs for reaction 2.1 to 2.5. However, decreased penetration of UV light into the TiO_2 suspension at higher catalyst amounts and in turn reduced excitation of TiO_2 particle is the main reason behind this maximum limiting value.

2.1.4 pH Effect

pH and its role in the PCD process is multi-dimensional. Compounds with pH dependent speciation such as phenols, organic acids and amines, show a degradation trend that significantly varies with the aqueous pH. This is mostly related to the varying adsorption of target pollutants on to the catalyst surface with pH, which in turn is related to the pH dependent speciation of target pollutant and also the surface speciation of catalyst TiO_2 (equations 2.1 & 2.2). $OH^{\cdot}$ radicals are considered to be dominant at neutral and high pH values [69, 89]. Decreased TiO_2 surface area because of particles agglomeration at acidic pH values would also cause reduced pollutant removal. Furthermore, the CB edge also show a negative shift of 59 mV/pH unit with an increase in pH.

2.1.5 Light Intensity Effect

Wei and Wan (1991) studied the PCD of phenol at several light intensities, between low-to-2.3 x 10^{-4} Einstein/s values and noticed an increase in phenol removal with light intensity [69]. Peterson et al. (1991) report both a linear and square-root type relationships between the light intensity and the PCD rate; e.g., at higher light intensities the PCD rate was noted to be directly proportional to the $I_o^{1/2}$ (I_o is the light intensity) [90]. Generally linear and then square root type relationship between an increasing-light-intensity and PCD rate are noted; this is followed by PCD rate independent of light intensity at even more high light intensities. (It would be useful to mention that the efficiency of the photocatalytic processes is often defined in terms of quantum yield, i.e., the number of specific conversions per photon absorbed.)

2.2 Adsorption

Adsorption is widely applied for the removal of various aqueous phase pollutants [39-41, 91]. Though activated carbon is the most widely applied adsorbent [38], studying the adsorption of pollutants onto TiO_2 surface is significant since their effective photocatalytic removal from aqueous phase is highly dependent on their adsorption on to the TiO_2 surface [50-53]. Various parameters can affect the adsorption of pollutants onto adsorbents. For example, temperature can influence adsorption by leading to creation of active sites [92], increasing the penetration of solutes into the adsorbent, or by affecting the solubility of the solutes. pH on the other hand can affect the surface chemistry of both the adsorbent and adsorbate and thus can greatly influence adsorption processes [93]. This is due to electrostatic interactions between the adsorbate and the adsorbent. In addition to the above-

mentioned parameters, concentrations of adsorbent and the adsorbate also play significant role on the efficiency of adsorption process [94].

Surface complexation models are widely used for modelling adsorption data [95, 96]. These models are capable of simulating the adsorption of aqueous solution species as a function of pH, solute concentration, and ionic strength [97]. Unlike isotherm models, surface complexation models account for the effect of surface charge on the adsorption of solutes [98]. Therefore, surface complexation models utilize an equilibrium approach to describe adsorption phenomena on surfaces [99]. Unlike, isotherm models, SCMs define surface species, chemical reactions on the surface, equilibrium constants, surface activity coefficients, mass balance, and charge balance. Some widely used surface complexation models are diffuse-layer model (DLM), constant capacitance model (CCM), and the triple layer model (TLM). The difference in these models is highlighted by their structural representation of electrical interfacial layer. Application of these models is simplified by the present of computer based programs like Visual MINTEQ that has several versions of adsorption and surface complexation models [100]. For example, Shi et al. (2009) applied constant capacitance model for modelling the adsorption of selenite on TiO_2 (anatase) [30]. They were able to fit the experimental data to the above model under different pH and concentrations.

As outlined earlier, surface complexation models differ in their structural representation of electric interfacial layer. The surface configuration of the adsorbed ions is what distinguishes the models. To describe a model, several surface planes are assumed. Figure

2.2 below shows a schematic representation of electrostatic potential for diffuse layer model. The 0-plane is where surface charges are located, while d-plane characterizes the position of centres of associated counterions and marks the onset of the diffuse layer. Counter ions are attracted to the charged mineral surface in the diffuse layer, but remain in the bulk fluid phase. There is also slipping plane otherwise known as the s-plane with electrokinetic zeta potential (ζ-potential). The uncharged region between the surface and the locus of hydrated counterions is called the stern layer whereas the charged layer beyond is called the diffuse layer [101, 102]. Though in diffuse-layer model, all surface complexes are inner-sphere and located in a single surface plane, adsorption of some ions have been successfully represented by an outer-sphere complex in DLM [103-105]. Diffuse layer model, like other surface complexation models account for the effect of electrostatic forces in describing surface reactions. This is for obtaining mass law constants that does not vary with surface charge. This is achieved by separating chemical and electrical contributions to the total free energy change as shown in equation 2.10.

$$\Delta G_{total} = \Delta G_{intrinsic} + \Delta G_{couloumbic} \qquad 2.10$$

where ΔG_{total} is the total free energy of adsorption, $\Delta G_{\text{intrinsic}}$ is the chemical contribution (or intrinsic part), whereas the $\Delta G_{\text{coulombic}}$ is the electrostatic contribution. Intrinsic equilibrium constants that do not depend on surface potential are obtained by multiplying apparent equilibrium constants with coulombic correction factor as in equation 2.11

$$K^{int} = K^{app} e^{\frac{\Delta ZF\psi}{RT}} \qquad 2.11$$

Where K^{int} = intrinsic rate constant

K^{app} = apparent rate constant

ΔZ = change of equivalent charge taking place in the reaction

F = Faraday's constant = 96485.33289 C mol^{-1}

ψ = Surface potential (V)

R = molar gas constant = 8.3144598 J mol^{-1} K^{-1}

T = absolute temperature (K)

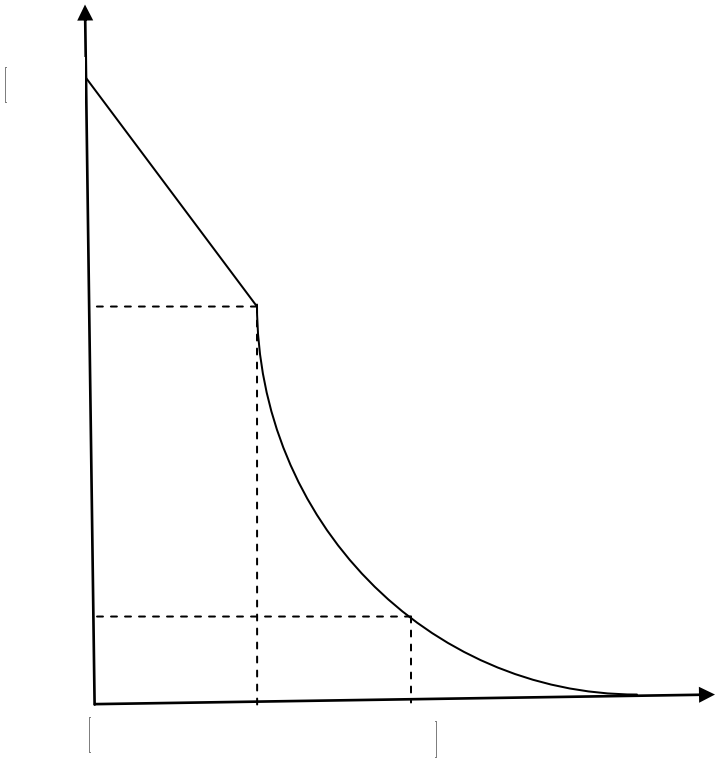

Figure 2.2: Schematic representation of electrostatic potential for diffuse layer model (Ψ_0 is the surface potential, Ψ_d is the diffuse layer potential, ζ is the zeta potential).

2.3 Previous Studies

2.3.1 Selenium Species Removal

A brief literature review on the removal of aqueous phase selenium is provided here. Aman et al. (2011) report on simultaneous photo-reductive removal of copper (II) and selenium (IV) using Ti, Ti-Zr, and Ti-Si binary oxide photocatalysts and visible light under a varying set of conditions including single and mixed copper and selenium systems [1]. The prepared catalysts had high specific surface area and were mesoporous. TiZr-10 was noted to be thse best photocatalyst. Also pH 3 was noted to be the optimum and yielded highest photocatalytic selenite reduction in a mixed solution. Out of many hole scavengers tested, formic acid and ethylenediaminetetraacetic acid (EDTA) were best for the reduction of selenium oxyanions. The h^+ species produced in Equation 2.3 are consumed by the h^+ scavengers (equation 2.6), resulting in reduced e^-/h^+ recombination (Equation 2.9) and thus leaving more e^- species for reduction of selenite (analogous to Equation 2.7 and 2.8). Furthermore, for single pollutant system, formic acid yielded better results for Se(IV) reduction whereas EDTA was noted to be better for Cu(II) reduction. However for mixed systems, both formic acid and EDTA showed better metal reduction results and the copper selenide was noted to be deposited at the catalyst surface. Nguyen et al. (2005) noted that in the presence of formic acid as a hole scavenger both selenite and selenate were photo-reduced to Se(0) in illuminated TiO_2 suspensions [29]. Findings from the UV-Vis reflectance indicated that compared to pure TiO_2 the Se/TiO_2 sample had a red-shift; an additional absorbance peak at approx. 680 nm was assigned to Se(0) and the elemental selenium species was noted to accumulate on

the TiO_2 particles either in a particulate or film form. It was proposed that the formation of Se(0) particles was due to a chemical reaction between Se(IV) and Se^{2-} whereas a direct reduction of Se(IV) by the conduction band electrons (TiO_2) resulted in the formation of a Se(0) film. The Se^{2-} species was suggested to result either from photoreduction of Se(0) or because of reduction of Se(IV). Labaran and Vohra (2014) also recently reported on the removal of selenite and selenate species from synthetic wastewater using the TiO_2 assisted photocatalytic degradation (PCD) process in presence of EDTA as a hole scavenger [28]. Authors noted better selenite and selenate removal via reduction route at acidic pH values. Shi et al. (2009) who investigated selenite sorption on TiO_2 indicated that selenite sorption is a function of pH and its kinetics can be given as a pseudo-second-order model [30]. The authors also employed the constant capacitance model to predict selenite sorption on to TiO_2. Tan et al. (2003a) also investigated the reduction of selenium oxyanions (selenite and selenate) to elemental selenium using TiO_2 assisted photocatalysis [31]. The authors employed several hole scavenging agents including acetic acid, methanol, ethanol, salicylic acid, formic acid, and sucrose. Significant reduction of selenium oxyanions was possible using ethanol, formic acid, and methanol, with following order: formic acid > methanol > ethanol. This high capability of formic acid to reduce selenium oxyanions was explained based on its effective mineralization, formation reducing radicals, and adsorption of both the selenium species and formic acid onto TiO_2. Insignificant adsorption of ethanol and methanol was explained based on competitive selenium species adsorption on to TiO_2 surface, resulting in reduced role of hole scavenger ethanol and methanol resulting in their reduced

efficiency. For the formic acid case the optimum pH for selenium oxyanions photoreduction was 3.5-4. For methanol and ethanol the optimum pH value was 2.2. Tan et al. (2003b) investigated the PCD initiated reduction of selenate using TiO_2 and Ag-loaded TiO_2 and formic acid; selenate was successfully reduced to elemental selenium species employing the said photocatalysts and hole scavenger [34]. The formation of Se^{2-} followed by H_2Se formation was noted using pure TiO_2 whereas using Ag-loaded TiO_2 photocatalyst H_2Se and selenate reduction were noted to occur in parallel. Also pH 3.5 was noted to be optimum for reduction of selenate using 0.5 % Ag loading. This high efficiency was explained based on electronic changes from TiO_2-Ag-Se interaction and decreased e^-/h^+ recombination. In another study, Tan et al. (2003c) report that the adsorption of formate and selenate onto TiO_2 surface is prerequisite for selenate reduction to elemental selenium which could further be reduced to H_2Se (after selenate reduction to elemental form) [32]. The authors also report for optimum selenate reduction, a 3:1 formate:selenate ratio (on to TiO_2 surface). This ratio could be maintained by controlling factors such as concentration of respective species and the aqueous phase pH. Also the noted 3:1 of formate:selenate ratio (on to TiO_2 surface) strongly co-related with the stoichiometric ratio of 3 moles of formic acid to 1 mole of selenate for effective reduction. Tan et al. (2003d) described selenate reduction rates in presence of formic acid employing Langmuir-Hinshelwood competitive adsorption models for selenate and formate ions onto TiO_2 surface [33]. The respective models allowed for the modelling of formic acid and selenate adsorption on to TiO_2. Furthermore a 3:1 formate:selenate ratio (on to TiO_2 surface) was also obtained using the kinetic modelling exercise. Zhang et al.

(2009) also investigated sorption of selenium species on to TiO_2 [35]. The maximum sorption was noted at pH 2-6. Also the sorption reached equilibrium within 5 min. The authors suggest that the adsorption could be described both by boundary layer diffusion and intra-particle diffusion. Furthermore the adsorption kinetics results showed a second order kinetic model and the Langmuir adsorption isotherm was useful in modelling the respective findings. De Souza et al. (2002) investigated phytoremediation technique using muskgrass and Indian mustard to remove selenocyanate from the aqueous phase. [11] The authors report that Indian mustard can successfully remove and phyto-extract selenocyanate from respective aqueous and soil phases. The Indian mustard removed approx. 30% w/v of initial selenium treated whereas selenium accumulated (µg/g-dry-weight) values were 554 and 86 for roots and shoots, respectively. Furthermore Indian mustard exposed to selenate and selenite, showed a greater tolerance level for selenate species. However no overall and specific judgment was reported regarding differences in selenium tolerance (for the three respective selenium species, i.e., selenite, selenate, and selenocyanate) of Indian mustard. On the other hand, using muskgrass approx. 9% (w/v) of the initial selenium was removed whereas approx. 27 % w/w selenium transferred to muskgrass. Nevertheless both plant types (i.e., Indian mustard and muskgrass) destroyed the selenocyanate species given that this form of selenium was not noted in the respective system-samples. Furthermore muskgrass had selenium mostly in organic and inorganic (selenite form), whereas Indian mustard had selenium in the organic (volatile) dimethylselenide form. The authors report a rate limiting step of dimethylselenide formation from organic selenium and thus an insignificant loss of 0.7% w/v

(selenocyanate) was noted from dimethylselenide species. Lim and Joo (2007) who studied organic selenocyanate species conversion on to Au nano particles report its break down to cyanide and selenium species [106]. These species were reported to be bound to the Au surface. Manceau and Gallup (1997) report treatment of selenocyanate containing wastewaters using copper (II) salts and via precipitation [5]. The authors also investigated the form in which selenocyanate based selenium was eventually removed. It was noted that the selenium is bound with copper thiocyanate whereas native selenium species was disregarded as per both XANES (X-ray absorption near-edge structure) and EXAFS (extended X-ray absorption fine structure) spectroscopy findings. Selenium was shown by EXAFS to be present '*as selenide and surrounded by one nearest C atom and three next-nearest Cu atoms*'. The respective findings from the treatment of selenocyanate containing wastewater streams indicate that the Cu(II) species are reduced by sulfites and thiosulfate and produces cuprous-thiocyanate/selenocyanate type species. Ye et al. (2003) investigated use of constructed wetlands for the treatment of a coal gasification plant wastewater containing boron, arsenic, and selenocyanate species [107]. The authors report that treatment of respective effluent streams caused a greater reduction in toxicity (as per standard toxicity tests) as compared to effluents that were not treated. Also the reported reductions for selenium, arsenic, boron, and cyanide were 64, 47, 31, and 30%, respectively. The local sediment within the constructed wetland contributed significantly towards the respective objective. However removal because of assimilation of said pollutants within plant tissues and also because of volatilization was noted to be minimal. The authors investigated use of fourteen plant types out of which rabbit foot, cattail, and

Thalia, showed no negative impact on to their growth and thus were of high tolerance while removing the said pollutants. The findings from the respective work indicate that constructed wetland along with the plant type rabbitfoot, cattail, and Thalia can be successfully employed to treat wastewater containing cyanide, boron, arsenic, and selenocyanate species. Meng et al. (2002) studied reduction of aqueous phase selenocyanate using effluents from an oil refinery and also synthetic wastewater, employing Fe(0) elemental iron [16]. The oil refinery wastewater analysis indicated to have 5 ppm selenium-total (98% selenocyanate soluble), 40 mg/L sulfate, 10 mg/L thiocyanate, and 20 mg/L thiosulfate. The authors report successful removal of selenocyanate species from respective streams at an optimum pH value of 6. The reduction of selenocyanate was attributed to formation of elemental selenium and ferrous selenide, as determined using XPS (X-ray photoelectron spectroscopy) technique. The authors suggest a stepwise degradation of selenocyanate species via breakdown of selenium and its reduction to elemental selenium form followed by formation of selenide species. Furthermore, a recent study by Vohra (2015) has shown successful destruction of selenocyanate complex and removal of resulting selenite and selenate species from synthetic wastewater via *reduction* route using EDTA as hole scavenger [37].

2.3.2 Competitive Removal of Phenol

Various studies have explored photocatalytic removal of phenol under varying set of conditions [108-111]. Peral et al. (1989) studied competitive removal of phenol-sulphide and phenol-cyanide systems using ZnO photocatalysis [112]. They observed a decrease in phenol photooxidation in the presence of S^{2-} ions with little effect on the degradation of S^{2-} ion itself, especially at low phenol

concentrations. However, they observed a very strong competition in the phenol-cyanide system. They ascribed such trends to the fact that sulphide is removed via reaction with photo-generated holes while phenol and cyanide are oxidized by reaction with both photo-generated holes and hydroxyl radicals. However, at low concentrations, phenol is preferentially oxidized using hydroxyl radicals. Minero et al. (2000) investigated the effect of various alcohols on photocatalytic degradation of phenol [76]. They found that phenol degradation is affected by the amount of aromatics present in the medium independently from their nature. Lin and Lin (2007) studied the effect of humic substances on 4-chlorophenol [113]. They observed retardation in photocatalytic degradation of phenol in the presence of humic acid and methylene blue as a result of TiO_2 surface deactivation. Kashif and Ouyang (2009) investigated the effect of 4 anions on photocatalytic degradation of phenol [114]. Inhibitory effect of the anions on degradation of phenol follows the order: $Cl^- > SO_4^{2-} > NO_3^- > CO_3^{2-}$. They attributed the above mentioned effect on the ability of the anions to compete with phenol for photo-generated holes and hydroxyl radicals. This inhibitory effect was also observed by Selvam et al. (2007) when they investigated photocatalytic degradation of 4-fluorophenol in the presence of other anions in the order: $CO_3^{2-} > HCO_3^- > Cl^- > NO_3^- > SO_4^{2-}$ [115]. In addition, they observed an increase in photocatalytic degradation of 4-fluorophenol in the presence of Fe^{2+}, Fe^{3+}, and Mg^{2+} due to their high reduction potentials. Tunesi and Anderson (1991) observed an insignificant adsorption of phenol onto TiO_2 ceramic membranes and thus concluded that surface conditions do not appear to influence its degradation kinetics [116]. Therefore, they obtained similar degradation rates at all pH values. The poor adsorption of phenol onto TiO_2 surface was also observed by Robert et al. (2000) and they lead to Ti-phenolate adsorbates [117]. Similarly, Bekkouche et al. (2004) also observed weak adsorption of phenol onto TiO_2 surface [118]. Bekkouche et al. (2012) studied the competitive adsorption of phenol onto TiO_2 surface in the presence of four heavy metals [119].

Though they observed different mechanisms of adsorption between phenol and the cations, competitive adsorption still exists. About 30%, 45% and 60% reduction in phenol adsorption was observed respectively in the presence of zinc/iron, copper and cadmium.

2.3.3 Modelling Selenium Species Adsorption Using Surface Complexation Models

Sorption of selenite and selenate onto various adsorbent have been widely reported. However, few studies utilized surface complexation modelling techniques for modelling selenium species adsorption. Goldberg (1985) studied competitive adsorption of selenite, phosphate, and silicate onto goethite [120]. They observed a decrease in selenite adsorption with an increase in pH between pH 3 and pH 11. Decrease in selenite adsorption was steady below pH 8, with rapid decrease exhibited with an increase in pH starting around pH 8 to 9. The adsorption results were also modelled using the Constant Capacitance Model via FITEQL. The model predicted selenite adsorption trends in single and binary selenite-phosphate binary systems. Though adsorption results were successfully modelled with great accuracy in selenite only systems, selenite adsorption in selenite-phosphate systems was only predicted qualitatively by the model. Discrepancies between experimental and modelled results increases with an increase in phosphate concentration. Inability of the model to predict selenite adsorption in competitive environment was attributed to the assumptions on which Constant Capacitance Model was based.

In another study, Hayes et al. (1987) investigated the mechanism of selenite and selenate adsorption by using the effect of ionic strength and EXAFS data [121]. Selenite adsorption was relatively unaffected by changes in ionic strength suggesting the formation of an inner-sphere type complex between selenite and goethite. Selenate adsorption was however greatly affected by changes in ionic strength which signifies the formation of an outer-sphere complex. They also compared EXAFS

spectra of adsorbed selenite and selenate species to the spectra of their respective sodium salts in aqueous solutions. They did not observe any significant difference between the spectra of adsorbed selenate to that in aqueous solution, which is indicative of lack of scattered iron atoms within approximate 3.5 Å of the selenium atom. This signifies the formation of an outer-sphere complex between selenate and the surface, with water molecule situated between the adsorbate and the adsorbent. Comparison of selenite spectra in adsorbed form to that of aqueous sodium selenite salt shows significant difference. Iron atom was observed in the adsorbed spectra which signifies the formation of an inner-sphere type complex.

Goldberg & Glaubig (1988) investigated the adsorption of selenite and selenate onto an Imperial soil series (fine, montmorillonitic [calcareous], hyperthermic Vertic Torrifluvent) [122]. They did not observe selenate adsorption for either 1.9 mmol/m^3 or 19 mmol/m^3 within the range of pH investigated (pH 2 – 12). They related this to the formation of weakly bonded outer sphere complex. For selenite, maximum sorption was observed at pH 3. Sorption of selenite onto the soil was modelled using constant capacitance model. The model was able to describe selenite sorption till pH 7, but unable to detect sorption plateau between pH 8 and 11. Model prediction improve when they model selenite sorption onto clay minerals. They also investigated the effect of arsenate sorption on selenite adsorption, and they did not observe any significant reduction in selenite adsorption below pH 9. However, above pH 9, reduction of selenite adsorption is more pronounced in the presence of arsenate.

The significance of ionic strength in adsorption studies for the determination of the type of surface complex formed was also investigated by Hayes et al. (1988) [123]. They investigated the effect of changes in the concentration of background electrolyte on the adsorption of selenite and selenate onto goethite and amorphous hydrous ferrous oxide. They found that a change in ionic strength

between 0.005 M and 1 M has little effect on the adsorption of selenite onto the two adsorbents under investigation. On the other hand, they found substantial effect on selenate adsorption onto the two adsorbents when the background concentration was changed. By modelling the adsorption of selenite and selenite in differing ionic strength, they conclude that ions that are weakly bonded are best modelled using ion-pair surface complexes (outer-sphere complexes) while ions that are strongly bonded and are least affected by changes in ionic strength are best modelled using inner-sphere complexes. Balistrieri and Chao (1990) investigated selenite and selenate adsorption onto amorphous iron oxyhydroxide (a neutral to alkaline surface) and manganese dioxide (acidic surface) [57]. The two surfaces were found to have preference for selenite adsorption in relation to selenate. The adsorption of selenite was higher on amorphous iron hydroxide compared to manganese dioxide with no selenate adsorption observed onto manganese dioxide. They found selenite adsorption to be increasing with a decrease in pH and increase in particle concentration. They suggested the formation of an outer-sphere and inner-sphere complexes for selenate and selenite respectively. Adsorption modelling using the Triple Layer Model (TLM) suggest that selenite forms bidentate inner-sphere complexes with amorphous iron oxyhydroxide and monodentate inner-sphere complexes with manganese dioxide while selenate forms monodentate outer-sphere complexes with amorphous iron oxyhydroxide but does not adsorb on the highly acidic manganese dioxide. Model prediction in competitive environment is not very successful because the model did not account for surface site heterogeneity.

Gosh et al (1994) utilized the Triple Layer Model (TLM) for modelling selenite and selenate adsorption onto hydrous alumina satisfactorily [124]. They noted selenate adsorption to be affected by the presence of SO_4^{2-}. Duc et al. (2003) also observed ionic strength effect on selenate adsorption but not on selenite [125]. They observed discrepancies between sorption site densities for selenite and for protons while modelling selenite adsorption onto goethite and hematite using 2-pK and 1-

pK models. In another study, Duc et al. (2006) modelled selenite adsorption onto hematite using 2-pK/Constant Capacitance Model [125]. They fitted adsorption data using both monodentate and bidentate surface complexes. Another study also utilized the constant capacitance model for selenite adsorption modelling. The model prediction was found to be qualitative on one soil type and semi-quantitative on three soil types. Modelling selenite adsorption onto TiO_2 using constant capacitance model has also been reported by Shi et al. (2009) [30]. Constant Capacitance Model was also reported to predict selenite and selenate adsorption onto soil samples from Sao Paulo State, Brazil successfully [126].

Recently, the Diffuse Layer Model has also been utilized for modelling adsorption of selenium ions onto different surfaces. Jordan et al. (2009 a and b) investigated competitive adsorption of selenite and silicic acid onto magnetite and hematite respectively [127, 128]. The model predicted selenite adsorption onto the two surfaces both qualitatively and quantitatively. Kim et al. (2012) also investigated selenite and selenate adsorption onto magnetite [128]. They found selenite adsorption to be decreasing with an increase in pH and decreasing with an increase in carbonate and silicate ions. Selenate adsorption was found to be negligible. Diffuse layer model predicted selenite adsorption using an inner-sphere monodentate surface complex. Nsir et al. (2014) investigated selenite and selenate adsorption onto TiO_2 [129]. A sorption model based on Sips isotherm was used to predict the sorption of selenium oxyanions. Goldberg (2014) investigated the sorption of selenate adsorption on oxides, clay minerals and soils [130]. Selenate adsorption was predicted using Triple Layer Model (TLM) using either two outer-sphere complexes or one outer and one inner-sphere complexes [130]. Comparison of prediction results between DLM and TLM showed better prediction using the TLM model.

OBJECTIVES

It is evidenced from the literature review that though selenite and selenate adsorption onto different surfaces has been modelled using DLM, TLM, and CCM, modelling of selenite onto TiO_2 using diffuse layer model is only reported by Shi et al. (2009) [30]. The study modelled selenite adsorption onto TiO_2 in a single system. No study has modelled either selenate or selenocyanate adsorption onto TiO_2 using diffuse layer model. Likewise, neither competitive adsorption of selenite, selenate, and selenocyanate species onto TiO_2 nor adsorption modelling for the same is reported to the best of our knowledge. Therefore, it is also true that utilization of diffuse layer model for modelling the adsorption of selenite, selenate, and selenocyanate in competitive environment is not explored.

Furthermore, it is also evident from the above given literature review, no study so far has explored the effect of co-pollutants selenite, selenate, thiocyanate, ammonia, cyanide, and phenol (that are typically noted in respective wastewater streams) on to competitive destruction of selenocyanate along with simultaneous removal of respective co-pollutants using the TiO_2 assisted PCD process. However, for practical applications the removal of selenocyanate and the co-pollutants from respective wastewater streams under COMPETITIVE environment must be understood. Furthermore, since adsorption plays an important role in photocatalytic degradation of various pollutants, understanding the competitive adsorption of selenocyanate (and its reaction intermediates: selenite and selenate) is inevitable for successful removal of the said pollutants using photocatalysis. Hence the present study's main objectives are 1) to study the competitive adsorption of selenite, selenate and selenocyanate onto TiO_2 under varying mixed scenarios and 2) to investigate the efficiency of TiO_2 based photocatalytic degradation (PCD) process for the

competitive destruction of selenocyanate complex along with simultaneous removal of co-pollutants ammonia, cyanide, thiocyanate, and phenol from simulated mixed wastewater streams.

We intend to determine the efficiency of PCD process for treatment of said streams under a varying set of conditions and extend fundamental knowledge on subject for possible practical applications. We ntend to investigate use of artificial UV lamp for the treatment of said streams, and also run some selective solar radiation energized experiments for respective photocatalysis work. Furthermore, use of hole scavenger EDTA during the PCD process for enhanced reduction initiated removal of selenite and selenate species (that will result from selenocyanate oxidation) will also be probed. The findings from the present study will be of use to better treat wastewater streams containing selenocyanate and respective co-pollutants under a competitive environment along with knowing the optimum operational conditions for the said respective applications.

The specific objectives include:

1- To investigate competitive adsorption of SeO_3^{2-}, SeO_4^{2-}, and $SeCN^-$ onto TiO_2 surface under varying pH and stoichiometric scenarios.
2- To model the adsorption results obtained under objective 1 employing the diffuse layer model accounting for solid and aqueous speciations and electrostatic forces.
3- To investigate competitive photocatalytic removal of aqueous phase selenocyanate in the presence of inorganic co-pollutants *cyanide, thiocyanate, and ammonia* present in varying mixed state using UV lamp assisted PCD process. The simultaneous removal of respective co-pollutants and formation of selective reaction intermediates will also be monitored.

4- To investigate the competitive removal of aqueous phase selenocyanate in the presence of *phenol* present in varying mixed states using UV lamp assisted PCD process. The simultaneous removal of phenol and formation of selective intermediates will also be monitored.

5- To conduct selective experiments as per objectives 3 and 4 using SOLAR light assisted PCD process.

6- To optimize and probe the mechanistic details of competitive photocatalytic removal of selenocyanate and phenol from aqueous by developing RSM and kinetic models.

RESEARCH METHODOLOGY

4.1 Materials

All chemicals used were of high purity reagent grade quality. The main chemicals included sodium selenite (ALDRICH, U.S.A.), potassium selenate (ALDRICH, U.S.A.), potassium selenocyanate (ALDRICH, U.S.A.), sodium carbonate (BDH, U.K.), sodium bicarbonate (BDH, U.K.), ammonia, cyanide, cyanate, nitrite, nitrate, phenol, hydroquinone, resorcinol, pyrocatechol, benzeneseleninic acid, glacial acetic acid, methanol, and pH calibration standards (FISHER, U.S.A.). The DEGUSSA P25 titanium dioxide/TiO_2 (DEGUSSA, GERMANY) was used for all adsorption studies. The respective TiO_2 was used as is, without any purification or modification. Table 4.1 provides several physico-chemical properties of Degussa P25 TiO_2. The pH adjustments were made using either HCl (SURECHEM, UK) or NaOH (J.T. BAKER, U.S.A) solutions. All glassware used were Pyrex based that were appropriately cleaned, washed, and dried before each use. All sample collection, storage, and processing accessories were also cleaned, washed, and dried before each use.

Table 4.1: TiO_2 surface properties

Property	**Value**
Specific surface area (m^2/g)	55
Surface site density (mmol/g)	0.274
Solid concentration (g/L)	1
pH_{zpc}	6.5
Crystal phase ratio	80% Anatase, 20% Rutile

4.2 Adsorption experiments

Stock solutions (1000 ppm) for selenite/SeO_3^{2-}, selenate/SeO_4^{2-}, and selenocyanate/$SeCN^-$ were prepared using above mentioned reagent grade chemicals and high purity de-ionized water (CORNING Mega Pure™ System), and stored in Pyrex bottles under dark conditions. For the adsorption experiments, the respective selenium-species solutions were prepared using the above-mentioned stock solutions and de-ionized water. A blank sample was first collected after which 1 g/L TiO_2 was added with appropriate mixing to ensure its complete dispersion. This suspension was then transferred to a set of Pyrex glass bottles. Each experiment was conducted in a set of nine bottles by adjusting the pH of the suspensions between 2 and 11 using HCl and/or NaOH solutions. The test solutions were vigorously mixed for about 24 hours and the final suspension pH was measured before sample collection and filtration using 0.2-µm membrane filters (WHATMAN, Germany). The syringe and filter holders were also appropriately washed and dried before each use. The collected samples were then duly stored before being analyzed for the target selenium species.

4.3 Photocatalysis Experimental Details: Using UV Lamp

The UV lamp based PCD experiments were conducted using a batch type (Pyrex glass) reactor with 1000 mL capacity. Fig. 4.1 provides the reactor details. For each experiment, 1.1 L of synthetic mixed wastewater were prepared using high purity water (CORNING Mega Pure^{TM} System) and stock solutions of selenocyanate and co-pollutants (as per Table 4.2). 100 mL of the synthetic wastewater was stored as blank to serve as a reference during analysis. For the initial PCD experiments 1 g TiO_2 was then suspended in the remaining 1 L of synthetic selenocyanate wastewater using a magnetic stirrer setup, after which the initial suspension pH was measured and adjusted to the desired value using HCl or NaOH. The system is then allowed to equilibrate for 20 minutes and another sample was collected to account for any initial substrate adsorption on to TiO_2 at the given initial pH. The synthetic wastewater batch with TiO_2 was then transferred to the PCD reactor and again subjected to continuous stirring using a magnetic stirrer setup (Fig. 4.1). A 15 W near UV light lamp with peak maximum at ~352 nm was then positioned at the centre of the reactor while being separated from the synthetic wastewater batch using a glass sleeve (Fig. 4.1). The UV lamp was turned on and samples were collected at pre-designed. All samples collected were filtered through 0.2-μm membrane filters (WHATMAN, Germany). The syringe and filter holders were also appropriately washed and dried before each use. The collected samples were then stored in dark under 4^0C. For experiments involving hole scavenger, appropriate amount of EDTA was added to the respective experiments after 3 or 5 hours as deemed appropriate.

Table 4.1 Pollutants for adsorption and photocatalysis studies.

Adsorption experiments		**Photocatalysis experiments**	
Species	Concentration (mg/L)	Species	Concentration (mg/L)
Selenocyanate	10 ppm	Selenocyanate	10 ppm
Selenite	10 ppm	Cyanide	5 ppm
Selenate	10 ppm	Thiocyanate	5 ppm
		Ammonia	5 ppm
		Phenol	5 ppm

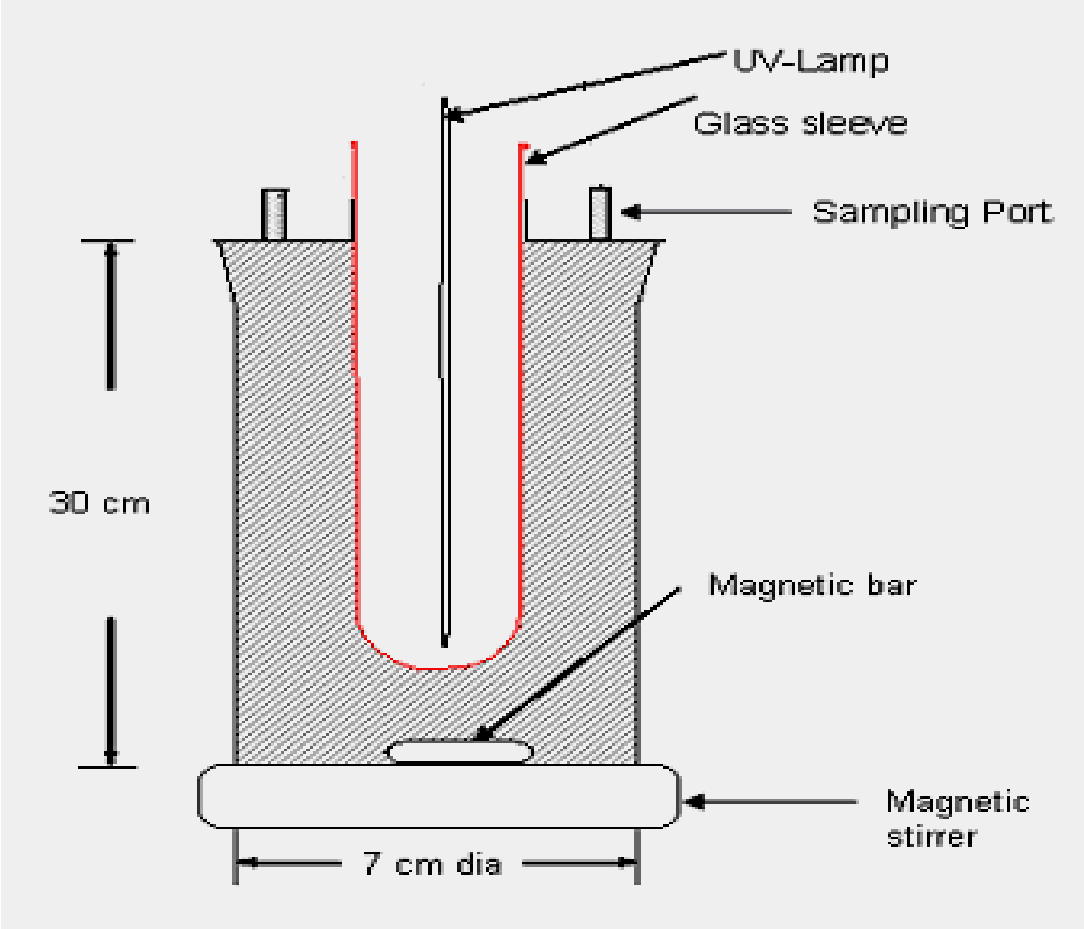

Figure 4.1 The reactor layout/details for UV lamp based photocatalysis experiments.

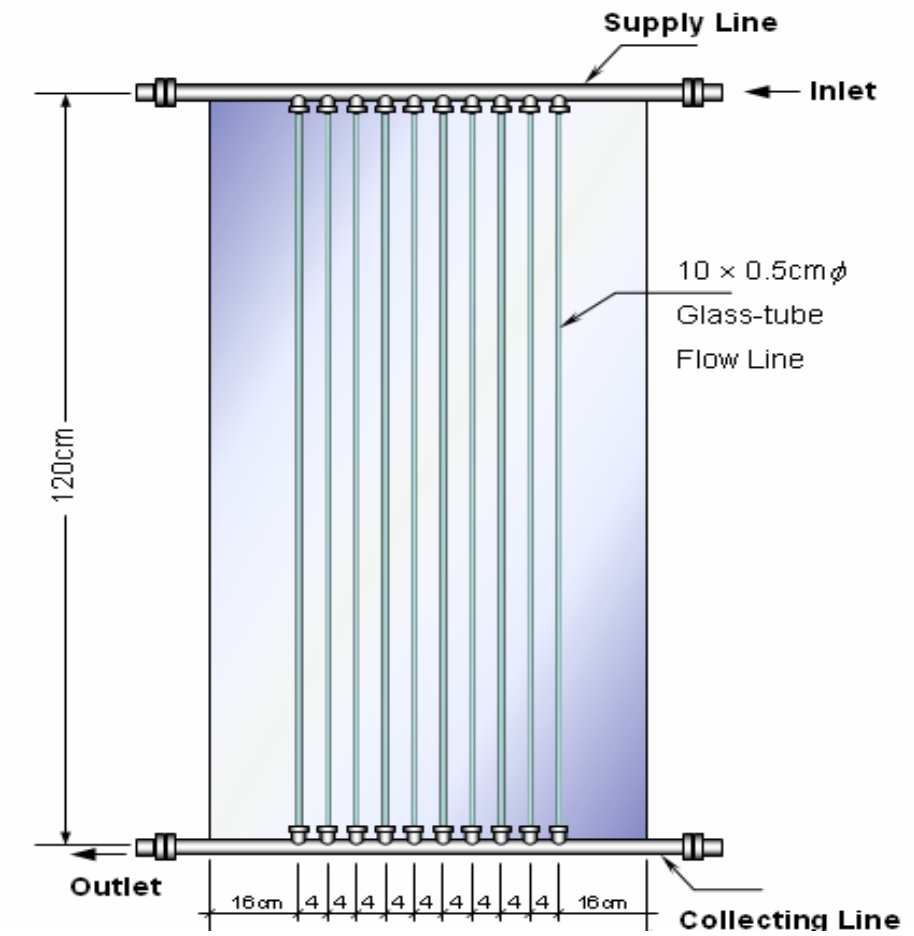

Figure 4.2 Pyrex glass reactor for the solar photocatalysis experiments.

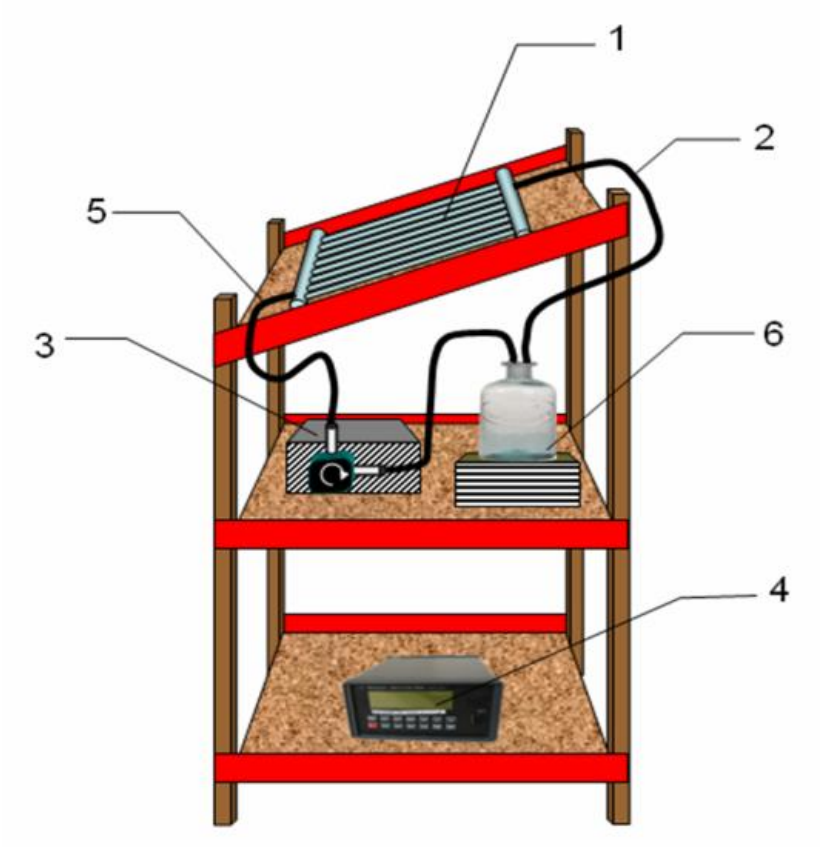

Figure 4.3 Solar photocatalysis reactor and support hardware [1 - Glass Reactor; 2 - Effluent Header; 3 - Pump; 4 - Solar Intensity Meter; 5 - Influent Header; 6 - Storage Tank].

4.4 Photocatalysis Experimental Details: Using Solar Energy

The solar photocatalytic experiments were conducted using a re-circulating one-sun plug flow type reactor. The details of the reactor are reported in Figures 4.2 and 4.3. Batches of test solutions were prepared using high purity water (CORNING Mega Pure^{TM} System) and stock solutions of respective chemicals. Initially a 2 L test solution was prepared in the laboratory for each solar experiment, and a blank sample was collected

before the addition of photocatalyst. After this TiO_2 photocatalyst was added to remaining test solution at 0.25 g/L, and initial pH was adjusted to the desired value using HCl or NaOH solutions. The respective system was mixed using a magnetic stirrer set up and was allowed to equilibrate for 20 min after which a sample was taken. Such a blank accounted for any initial substrate loss because of reasons other than the SPCD initiated reactions. The synthetic wastewater sample containing both the target pollutant and the TiO_2 was then transferred to the experimental site and another blank was also taken before the wastewater was introduced into the solar reactor via the influent header (using pump setup) from where it flows through the solar reactor (Figure 4.2). The third blank is to account for substrate loss while transferring the wastewater from lab to the site. To assure mixing, the wastewater storage tank incorporated a magnetic stirrer setup as well. As the wastewater and TiO_2 flow through the reactor, the aqueous pollutants were exposed to the solar radiation, initiating the degradation of target pollutant. The effluent was returned back to batch tank from where it was again re-circulated to the reactor for further treatment. During the course of solar experiments, several samples were collected at appropriate time intervals, to assess the degree of pollutant species removal.

4.5 Analytical Methods

The filtered sample aliquots were analyzed for SeO_3^{2-}, SeO_4^{2-}, $SeCN^-$, SCN^-, SO_4^{2-}, NO_3^-, NO_2^- OCN^-, and NH_4^+ using an advanced ion chromatograph set-up (Metrohm, Switzerland) equipped with conductivity and amperometric detectors. The eluent composition for anions analysis was 2.7 mM Na_2CO_3/3.0 mM $NaHCO_3$ and column used was anion Dual 2 IC column (6.1006.100, 4.6 mm x 75 mm, Metrohm, Switzerland).

Cations were separated using an eluent composition 5.4 mM nitric acid through Metrosep C3-250/4.0 column (6.1010.430, 150 mm x 4.0 mm). I some cases, selenocyanate, cyanide and cyanate were analysed using an amperometic detector after been separated in an anion Dual 2 IC column (6.1006.100, 4.6 mm x 75 mm, Metrohm, Switzerland) using 100 mM NaOH eluent. Total selenium was analyzed using an atomic absorption spectrophotometer setup (Perkin Elmer, U.S.A) that was equipped with both flame and furnace units. A standard ICP setup (Thermo, U.S.A) was also utilized for total selenium analysis. Phenol, EDTA and their degradation intermediates were analysed using advanced High Performance Liquid Chromatograph, HPLC (Shimadzu, Japan) equipped with a pump and auto sampler setup. 0.7% acetic acid/methanol (60/40) was used as the mobile phase at a flow rate of 1 mL/min while Restek Ultra C18 column was used for separation. All analytes of interest were detected at a wavelength of 254 nm. The solution pH were analyzed using a standard pH electrode-meter setup (AccuTupH$^+$ 13-620-185 electrode, Accumet XL15 pH meter, Singapore). Also, all analytical instruments were regularly calibrated.

Each collected sample will first be filtered through a 0.2 μm 25 mm Ø cellulose nitrate membrane filter (WHATMAN, Germany) and then analyzed for the target pollutants. The concentration of most ionic species including selenocyanate, co-pollutants thiocyanate, and ammonia, and reaction intermediates cyanate, nitrite, nitrate, sselenite, and selenate, will be analyzed using a state of the art Ion Chromatograph system (METROHM, Switzerland). The IC system is equipped with high sensitivity conductivity detector. A metrosep Anion Dual 2 IC column (6.1006.100, 4.6 mm x 75 mm, Metrohm,

Switzerland) will be used for respective analysis.The IC system will be regularly calibrated using appropriate calibration standards prepared using the respective reagent grade chemicals. Ammonia which is also an expected reaction intermediate will be analyzed using an ion specific electrode and a meter setup with mV readings option (Orion, USA). Each respective sample will be transferred into a beaker to which an appropriate amount of 10 M NaOH will be added (in order to increase the pH). The solution will be stirred using a magnetic stirrer, with the ammonia electrode dipped into it. The meter reading (in mV) will be noted after the meter shows a stable-mV value. Cyanide species, will be analyzed using an ion specific electrode and meter setup (Orion, USA) and the rest procedure will be same as reported above for ammonia analysis. The ammonia and cyanide testing setup will be regularly calibrated. The pH analyses will be completed using a pH meter setup (ORION, U.S.A.) that will be regularly calibrated using respective calibration standards. EDTA concentration will be quantified in terms of total organic carbon (TOC). A total organic carbon/TOC setup (SHIMADZU, JAPAN) will be used for TOC analyses, to assess the degree of EDTA and phenol mineralization. Total selenium analysis will be completed using ICP and AAS setup. A UV-light detector setup (and its accessories) will be used to quantify the incoming solar radiation intensity (Newport, U.S.A.). Some other common lab accessories will include high purity gases, Pyrex glass ware, physical balance, pumps, Teflon pipes, pH meter, etc.

4.6 Adsorption Modelling Approach

Visual MINTEQ version 3.1 was employed for all surface complexation modelling exercises. Its extensive database can support the speciation, solubility, and adsorption

modelling of many aqueous phase species of interest. The TiO_2 surface complexation reactions employed for modelling are shown in Table 4.2. The current version of Visual MINTEQ does not have selenocyanate ($SeCN^-$) in its database. However, the Visual MINTEQ allows for specific changes to its database and thus $SeCN^-$ and HSeCN were added to the database as a component and species, respectively (Table 4.3). Also some other aqueous speciation reactions from MINTEQA2 database are also presented in Table 3. Also Figs. 4.4 to 4.6 provide the speciation diagrams (completed using MINTEQ) for TiO_2, selenite, and selenate species; these will be recalled later to elucidate some of the experimental findings.

Table 4.2: TiO_2 surface complexation reactions

S/No.	Reaction	Log K^s_{int}
1	$\underline{\mathbf{Ti}}\mathrm{OH} + \mathrm{H}^+ \rightleftarrows \underline{\mathbf{Ti}}\mathrm{OH}_2^+$	3.9[a]
2	$\underline{\mathbf{Ti}}\mathrm{OH} \rightleftarrows \underline{\mathbf{Ti}}\mathrm{O}^- + \mathrm{H}^+$	-8.7[a]
3	$\underline{\mathbf{Ti}}\mathrm{OH} + \mathrm{HSeO}_3^- \rightleftarrows \underline{\mathbf{Ti}}\mathrm{SeO}_3^- + \mathrm{H}_2\mathrm{O}$	4.6[b]
4	$\underline{\mathbf{Ti}}\mathrm{OH} + \mathrm{SeO}_4^{2-} + \mathrm{H}^+ \rightleftarrows \underline{\mathbf{Ti}} - \mathrm{H}_2\mathrm{O} - \mathrm{SeO}_4^-$	4.8[b]
5	$\underline{\mathbf{Ti}}\mathrm{OH} + \mathrm{SeCN}^- + \mathrm{H}^+ \rightleftarrows \underline{\mathbf{Ti}} - \mathrm{H}_2\mathrm{O} - \mathrm{SeCN}$	6.55[b]

[a][131]

[b]Present study

Table 4.3: Important aqueous speciation reactions employed for adsorption modelling

S/No.	Reaction	Log *K*
1	$CN^- + H^+ \leftrightarrow HCN$	9.21[c]
2	$SeCN^- + H^+ \leftrightarrow HSeCN$	-3.77[d]
3	$SeO_4^{2-} + H^+ \leftrightarrow HSeO_4^-$	1.7[c]
4	$HSeO_3^- \leftrightarrow SeO_3^{2-} + H^+$	-8.4[c]
5	$HSeO_3^- + H^+ \leftrightarrow H_2SeO_3$	2.63[c]
6	$OH^- + H^+ \leftrightarrow H_2O$	-13.997[c]

[c]Visual Minteq Database

[d]From Chemicalize.org

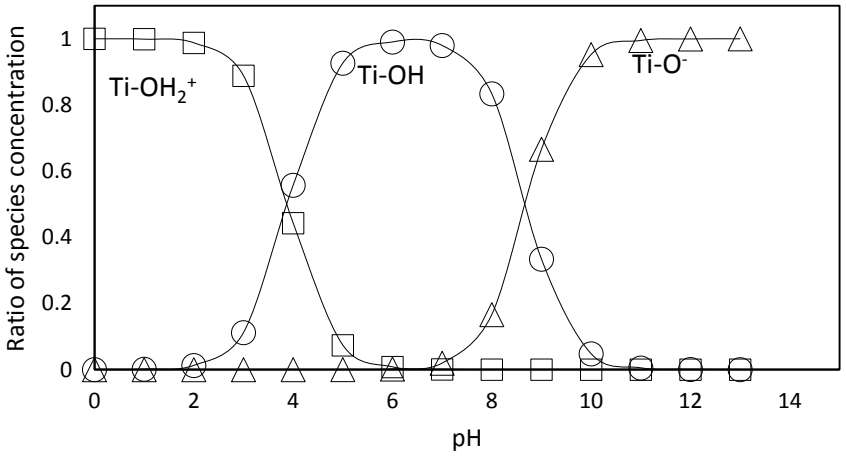

Figure 4.4: TiO_2 speciation diagram as a function of pH (Calculated using MINTEQ software).

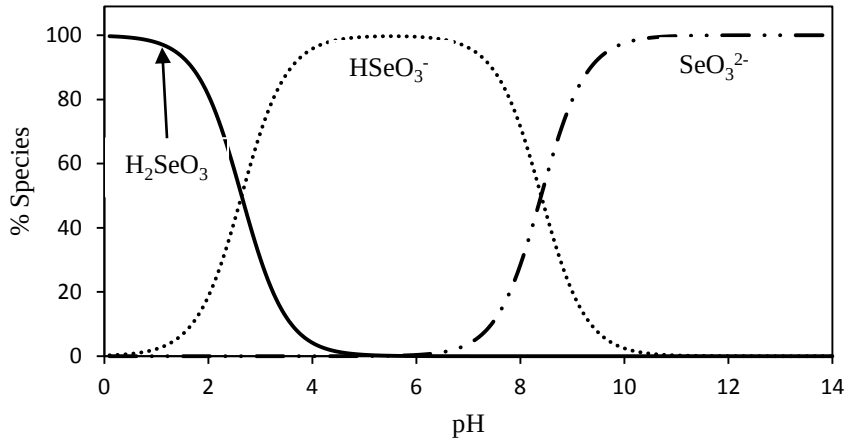

Figure 4.5: Selenite speciation diagram as a function of pH (Calculated using MINTEQ software).

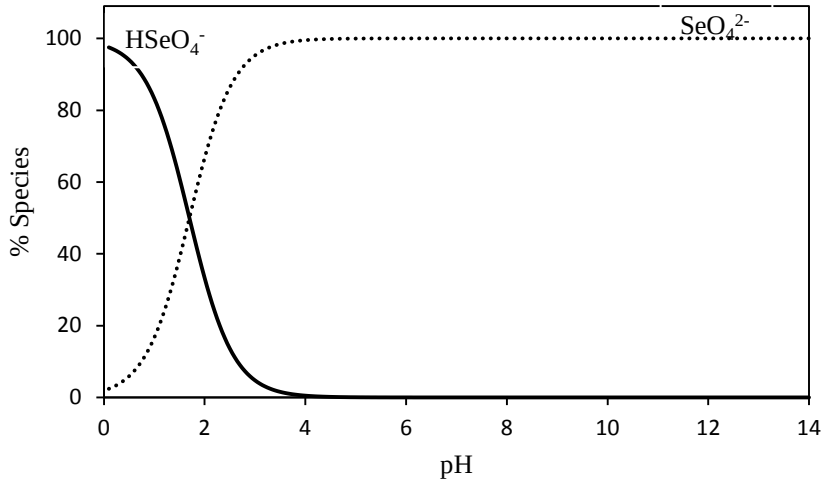

Figure 4.6: Selenate speciation diagram as a function of pH (Calculated using MINTEQ software).

COMPETITIVE ADSORPTION OF SELENITE, SELENATE, AND SELENOCYANATE SPECIES ONTO TiO_2

5.1 Binary Systems

We first studied the adsorption of respective selenium species onto TiO_2 at varying pH and binary solution matrices. The respective experimental and modelling results are discussed in this section. Figures 5.1 to 5.4 provide adsorption results for the binary selenite/selenate systems. Figure 5.1 shows the effect of selenate onto adsorption of selenite. In the absence of selenate, about 89% selenite adsorption transpires at pH 2, which first gradually decreases to 65% till pH 4 and then onwards sharply to 31% till pH 7. The TiO_2 surface speciation (Figure 4.4) shows that $\underline{\mathbf{Ti}}\text{-}OH_2^+$ is the dominant surface species below pH 3.9 and thus interaction between the cationic TiO_2 surface and anionic selenite species yields higher selenite adsorption between pH 2 and 4 (Figure 5.1). However, with an increase in pH to 4, the $\underline{\mathbf{Ti}}\text{-}OH_2^+$ surface species reduces to 50% and then to a very low value at pH 7 (Figure 4.4). The selenite adsorption (Figure 5.1) also shows a similar decreasing trend. Shi *et al.* [30] also report decreasing selenite adsorption onto TiO_2 with an increase in pH. Now adding 5 ppm selenate to the respective single selenite-only system does not cause any signficant change in selenite adsorption and

similar is noted for 10 ppm selenate (Figure 5.1). This fact was supported by results from additional adsorption studies completed at 5 ppm selenite (Figure 5.2) that also show that an increase in selenate from 5 to 10 ppm has no significant effect onto selenite adsorption. This indicates that relative affinity of TiO_2 is higher for selenite compared to selenate species. This might result because of differences in the type of surface complexes that selenite and selenate species form with the TiO_2 surface sites. Balistrieri and Chao [57] who studied the adsorption of selenium species onto amorphous iron oxyhydroxide and manganese dioxide also observed higher surface affinity for selenite relative to selenate. Hence the displacement of surface bound selenite by the aqueous selenate species will be difficult. Vohra (2015) who studied TiO_2 assisted photocatalysis of selenocyanate species also noted albeit slower selenate buildup from oxidation of surface bound selenite species; the resulting selenate species then diffused into bulk aqueous phase as a result of solid-solution equilibrium and also because of comparatively lower selenate affinity for the TiO_2 surface [37]. Tan et al. [31] and Nguyen et al. [29, 47], who report brief selenite/selenate adsorption onto TiO_2 also report somewhat higher selenite adsorption onto TiO_2 compared to selenate species. The authors suggest that different surface complexation mechansims because of different selenite/selenate molecular structures could explain the respective differences in the adsorption trends. Also comparing the results from Figure 5.1 and Figure 5.2, we note a higher percent-based selenite adsorption for the 5 ppm selenite systems as compared to the 10 ppm selenite systems (Figures 5.2 and 5.1, respectively). For example approx. 96%, 94%, and 54%, selenite adsorption was achieved for the 5 ppm selenite/5 ppm selenate system at

pH 2, 4, and 7 respectively (Fig. 5.2), whereas for the 10 ppm selenite/5 ppm selenate, selenite adsorption is 76%, 74%, and 34%, at pH 2, 4, and 7, respectively (Fig. 5.1). However it should be noted that on mass basis the adsorption values are still higher for the 10 ppm selenite system that transpires because of corresponding higher mass transfer driving force across the bulk aqueous and bulk solid phase.

We further employed the diffused layer model (DLM) for surface complexation modelling of above mentioned experimental findings. In that regard, several surface-binding possibilities (for selenite and selenate) were considered and eventually those surface complexes that yielded the best match for most (if not all) experimental adsorption matrices including the tertiary systems (as discussed later) were adopted for the modelling purpose. Table 4.2 provides the respective surface complexation details whereas Table 4.3 provides some of aqueous speciation reactions. For the 10-ppm selenite systems we typically note a good correlation between the experimental results and model estimates (Figure 5.1) except at pH 2 and 3 where the model overestimates selenite adsorption. A similar trend is observed for the 5 ppm selenite systems (Fig. 5.2), albeit with good correlation at all pH values. In general the model delivers better adsorption estimates under a varying set of conditions including pH and selenite/selenate concentrations. Modelling output details shows that for selenite, consideration of **Ti**-SeO_3^- surface complex provides a good model fit, whereas in case of selenate (discussed in detail in the coming section) the **Ti**-H_2O-SeO_4^- was noted to provide better fits. Furthermore for selenite species adsorption, several studies have indicated the formation

of an inner sphere complexe with different surfaces including geo thite [123], and TiO_2 [30]. The evidence for such a complexation comes from sources such as no significant effect of ionic strength on adsorption [123, 132, 133], and use of advanced analytical techniques including XAS and XPS [133-135]. Hayes and Leckie [123] employing EXAFS findings indicate formation of an inner sphere complex between selenite and goethite surface, whereas for selenate they report an outer sphere complex formation; the respective analysis for selenite indicated Se-Fe distance of 3.38 Å. Papelis et al. [133, 136] report similar observations for selenite adsorption onto aluminum oxide surfaces; Papelis et al [133] report Se-Al distance of 3.5 Å that is supportive of an inner sphere complex. Also Gurkan et al. [137] who investigated selenite-doped TiO_2 synthesis noted increased Ti- and O- species binding energies (based on XPS data) attributed to Ti-O-Se bond formation; the Se species in the bond was noted to be selenite as well. We also completed XPS analysis for TiO_2 samples after the adsorption of respective selenium anions and the results are shown in Figure 5.5 that shows that for selenite and selenate adsorbed TiO_2 samples, O 1s and Ti 2p3/2 binding energies are about 530 eV and 458.5 eV respectively. This shows that TiO_2 exist in +4 state as Ti^{4+} respective samples. By fixing the main C 1s binding energy at 248.8 eV, Se 3p3/2 binding energies for selenite and selenate containing samples are found to be 165.6 and 166.2 respectively. The relative difference in the energy level between the TiO_2 samples containing selenite and selenate was found to be 0.6 eV. Sartz et al. [138] who investigated selenium species XPS spectra obtained Se 3p3/2 binding energies of 164.6, 164.1 and 159.1 eV for selenium in +6, +4 and -2 oxidation states with difference in binding energies between +6

and +4 of about 0.5 eV. The similarity (between the present study and above mentioned study) regarding the relative difference in the binding energies for selenite and selenate indicates that selenite and selenate are adsorbed on the TiO_2 surface reaching a thermodynamically stable state [139]. Furthermore the selenate adsorption results from above discussed systems are also summarized here. Figure 5.3 shows the adsorption findings for 10 ppm selenate in the presence of 0 to 10 ppm selenite. For the 10 ppm selenate system without selenite (Figure 5.3), about 71, 52, 34, and 9% selenate adsorption transpires at equilibrium pH of 2, 3, 4 and 5, respectively. A sharp decrease in selenate adsorption is observed with an increase in pH from 2 to 5, with insigniciant adsorptrion observed above pH 5. Selenate speciation (Figure 4.6) shows that near pH 1.7, about 50% of selenate is in the form of $HSeO_4^-$, which reduces to negligible amount at pH 4 and above. Likewise, TiO_2 speciation (Figure 4.4) also shows declining cationic $\underline{\mathbf{Ti}}OH_2^+$ species above pH 4. Therefore, since both anionic $HSeO_4^-$ and cationic $TiOH_2^+$ species decrease with an increase in pH, the electrostatic attraction between the two species also decrease with an increase in pH thus resulting into reduced selenate adsorption. Addition of 5 ppm selenite to 10 ppm selenate system (Fig. 5.3) results into decreased selenate adsorption, i.e., 45, 25, 18, and 0% at pH 2, 3, 4 and 5, respectively. Furthermore at 10 ppm selenite, selenate adsorption decreases further (Fig. 5.3). For example the respective selenate adsorption values at pH 2 are as follows: 71% at 0 ppm selenite, 45% at 5 ppm selenite, and 29% at 10 ppm selenite. Results from 5 ppm selenate (Fig. 5.4) show similar trends, i.e., an increase in selenite from 5 to 10 ppm also decreases selenate adsorption from 69%, 51%, 27%, and 9% to 52%, 31%, 11% and 2%

at pH 2, 3, 4, and 5, respectively. Tan et al. [31] also observed a decrease in selenate adsorption when formate was introduced to the system. In any case these findings indicate the differences in selenite and selenate interactions with the metal oxide surfaces. Also the selenate adsorption results (Figures 5.3 and 5.4) show lower removals compared to respective selenite adsorption results (Figures 5.1 and 5.2). These findings also indicate preferential selenite adsorption on to TiO_2 surface. Comparing results in Figure 5.3 and Figure 5.4, we also observe decrease in percent selenate adsorption when its initial concentration is increased from 5 to 10 ppm. Nevertheless selenate removal on mass basis is still higher for 10 ppm selenate (Fig. 5.3). Figure 5.3 also shows that the diffused layer model reasonably predicts selenate adsorption whereas trends in Figure 5.4 show some underestimations. Also both the experimental and modelling results show adsorption traspiring between a narrow pH range of 2 to 5 (Figs. 5.3-5.4).

To build on above given selenite/selenate adsorption results, we further studied adsorption of selenite/selenocyanate binary systems (Figs. 5.6-5.9). However, unlike the above mentioned selenite/selenate systems, we noticed a pinkish precipitate formation during selenocyanate adsorption work. To ascertain the source of the precipitation, we ran two blank selenocyanate experiments without TiO_2 and the results are presented in Figure 4. About 99%, 66%, 17% and 15% selenium precipitation was observed for 10 ppm selenocyanate at pH 2, 3, 4 and 5 respectively whereas 77% and 24% selenium precipitation was observed at pH 2 and pH 3 for the 5 ppm selenocyanate, respectively.

The precipitation resulted from the breakdown of selenocyanate complex according to equation 1 as suggested by Hamada et al [140]:

$$SeCN^- + H^+ \longrightarrow HCN + Se^0 \qquad 5.1$$

Hence the precipitation results in Figure 5.10 were duly deducted from the respective overall selenocyanate removal before modelling the adsorption of selenocyanate using **Ti**-H_2O-SeCN type surface complex. Similar to selenite/selenate systems (Figs. 5.1-5.2) selenocyanate also shows no significant effect onto selenite adsorption (Figs. 5.6-5.7) that can be explained based on aforementioned discussion on an inner-sphere type selenite complexation. However unlike the suppresive effect of selenite onto selenate removal (Figs. 5.3-5.4) we do not observe any notable effect of selenite onto selenocyanate removal and the respective selenocyanate removal trend lines are somewhat more gradual in their drop from acidic to basic pH range (Figs. 5.8-5.9) as compared to selenate (in selenite/selenate systems) that showed a sharp adsorption edge traspiring between a narrow pH range of 2 till 5 (Figs. 5.3-5.4). Also, the respective selenocyanate removal results above pH 4 are higher in comparison to selenate removal. Hence the selenocyanate removal findings from selenite/selenocyanate binary systems (Figs. 5.8-5.9) are somewhat different from selenate removal from selenite/selenate binary systems (Figs. 5.3-5.4). In general for the binary selenite/selenocyanate systems we can achieve high selenite removals with insignificant selenocyanate effect. The respective selenocyanate modelling results as provided in Fig. 5.6 to 5.9 also show a good match between the experimental and modelling results using an outer sphere type complex.

Nevertheless if selenocyanate also forms an outer sphere type complex then question arises why its removal is not affected by selenite (Figs. 5.8-5.9) unlike the selenate species removal (Figs. 5.3-5.4). This query lead us to conduct another set of experimets for selenate and selenocyanate mixed systems. Results for binary selenate/selenocyanate adsorption results are provided in Figs. 5.11 to 5.14. We observe no effect of selenocyanate onto selenate removal (Figs. 5.11-5.12) that is qualitatively similar to selenite trends in selenite/selenocyanate systems (Figs. 5.6-5.7). Also similar to selenite/selenocyanate results (Figs. 5.8-5.9), no notable selenate effect is observed on selenocyanate removal (Figs. 5.13-5.14). In any case the above results indicate adsorption trends that are important to understand any respective treatment applications. We further extended the work for tertiary systems and the respective results are given below.

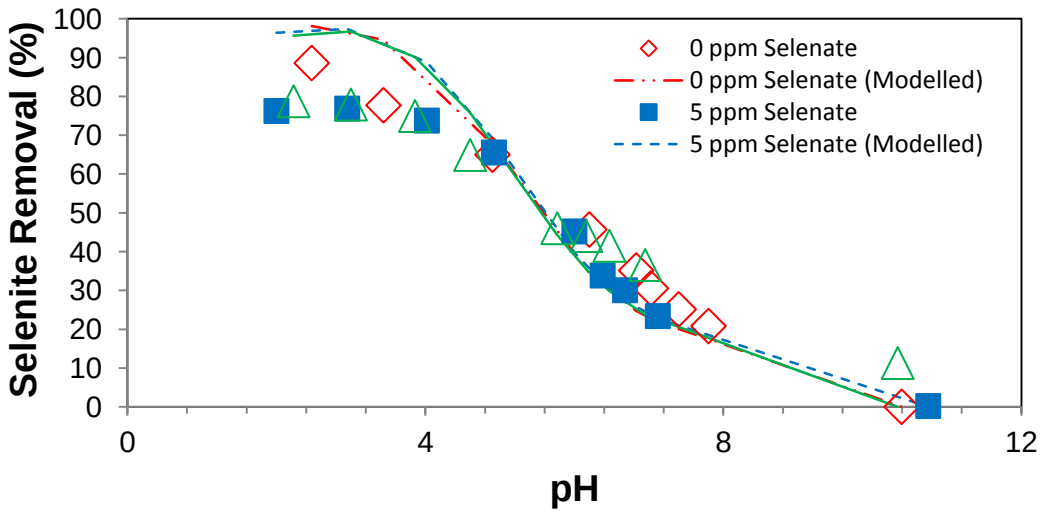

Figure 5.1: Experimental and modelling results for selenite adsorption onto TiO_2 in presence of selenate (1 g/L TiO_2, 10 ppm selenite).

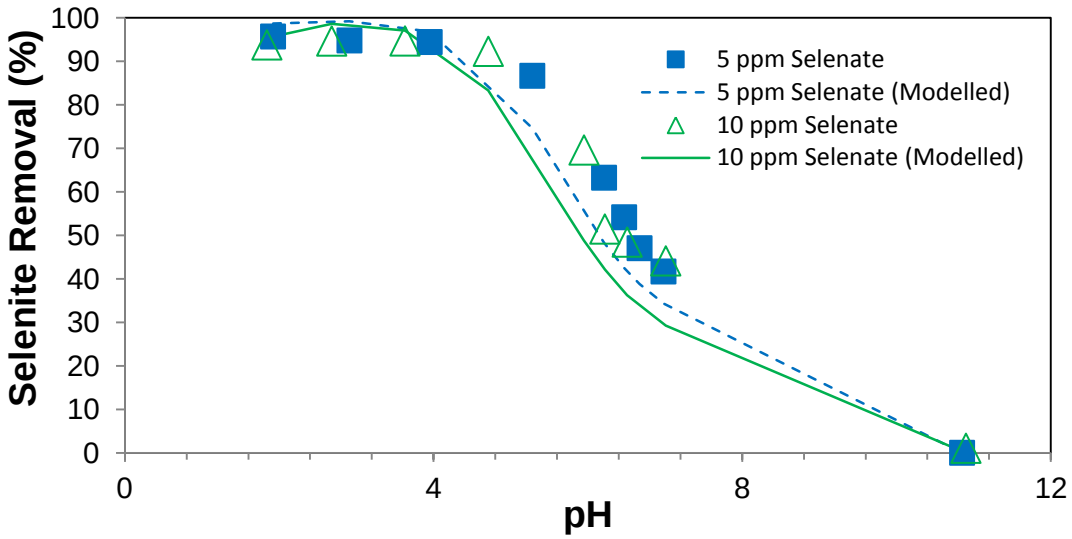

Figure 5.2: Experimental and modelling results for selenite adsorption onto TiO_2 in presence of selenate (1 g/L TiO_2, 5 ppm selenite).

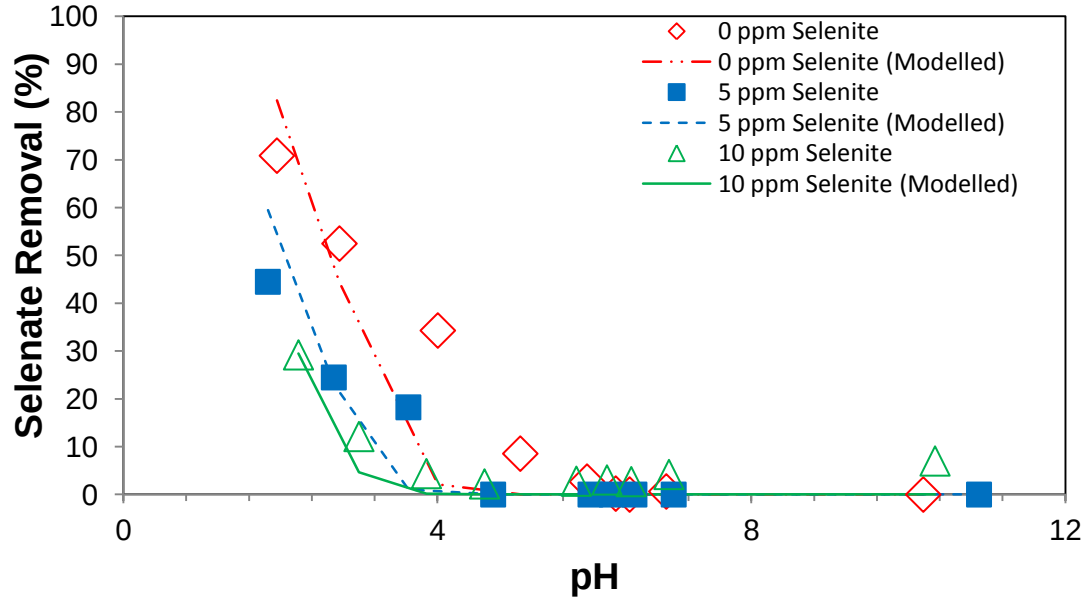

Figure 5.3: Experimental and modelling results for selenate adsorption onto TiO_2 in presence of selenite (1 g/L TiO_2, 10 ppm selenate).

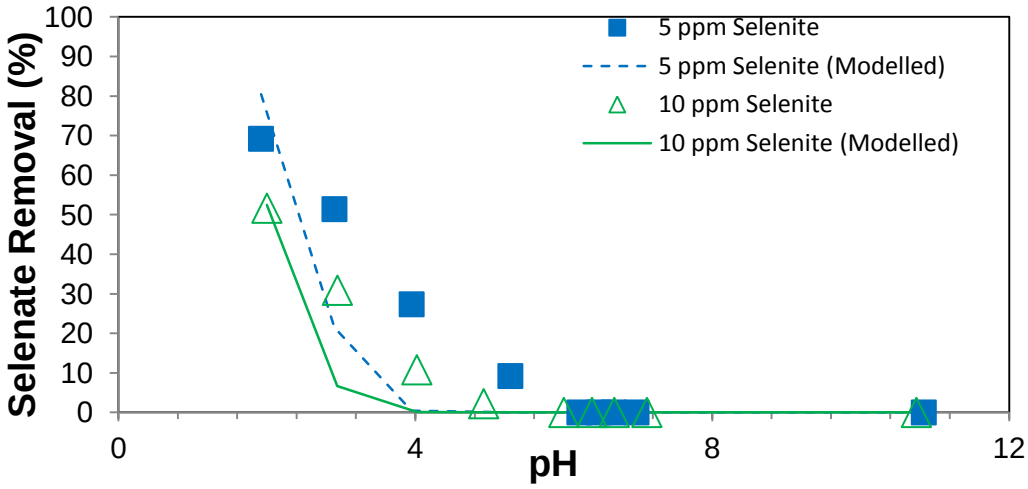

Figure 5.4: Experimental and modelling results for selenate adsorption onto TiO_2 in presence of selenite (1 g/L TiO_2, 5 ppm selenate)

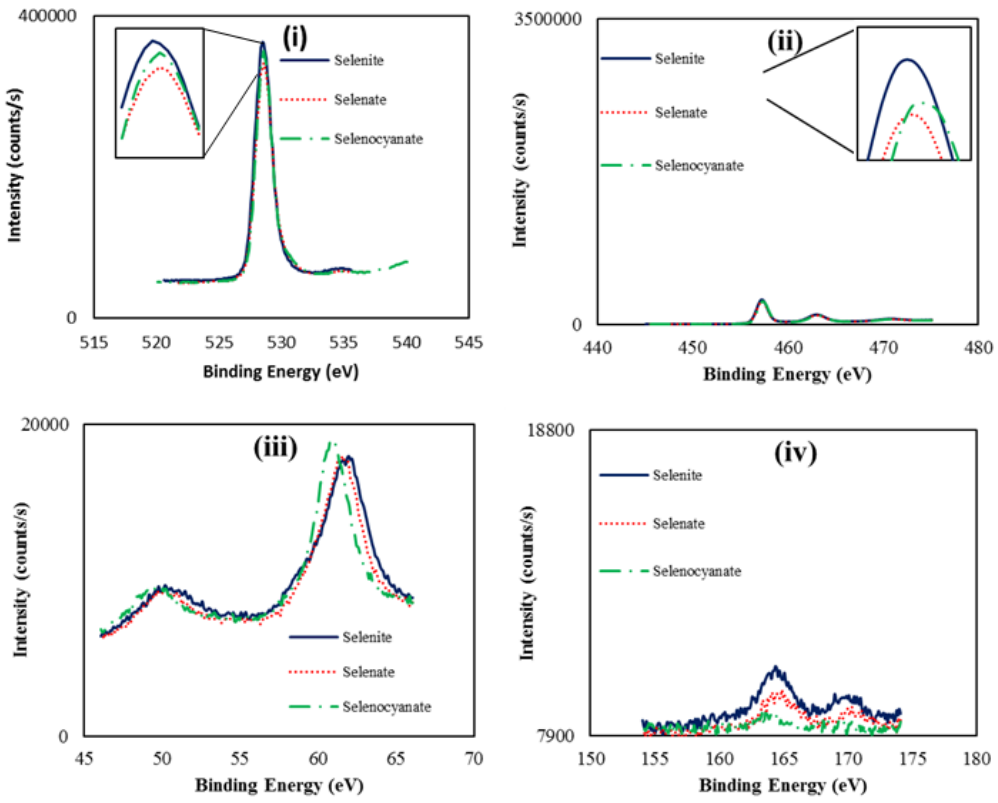

Figure 5.5: X-ray photoelectron spectroscopy (XPS) spectra of TiO_2 samples for the adsorption of selenite, selenate and selenocyanate (i) O 1s, (ii) Ti 2p, (iii) Se 3d, (iv) Se 3p.

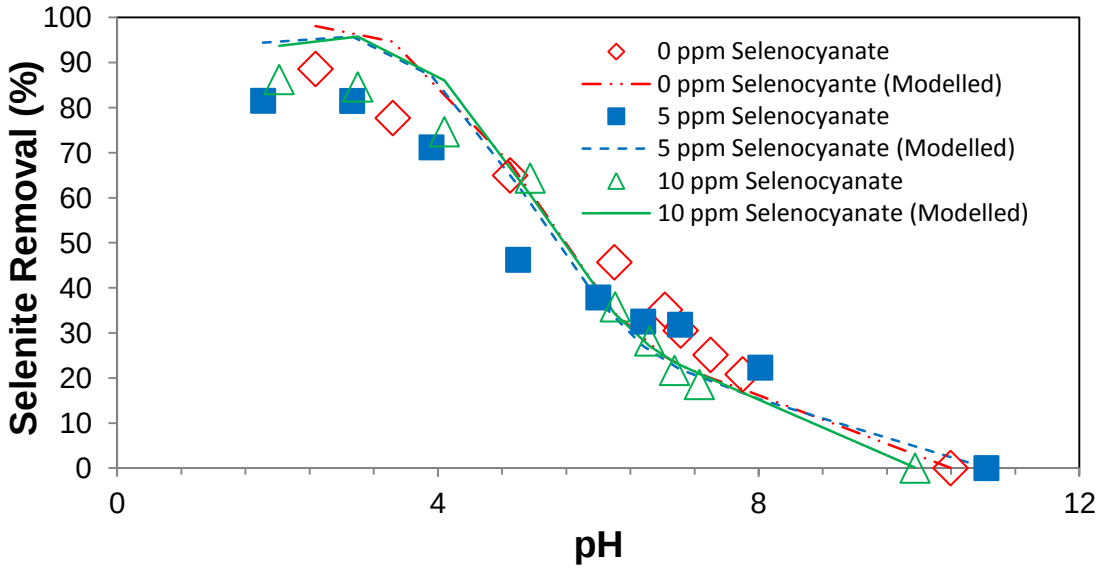

Figure 5.6: Experimental and modelling results for selenite adsorption onto TiO_2 in presence of selenocyanate (1 g/L TiO_2, 10 ppm selenite).

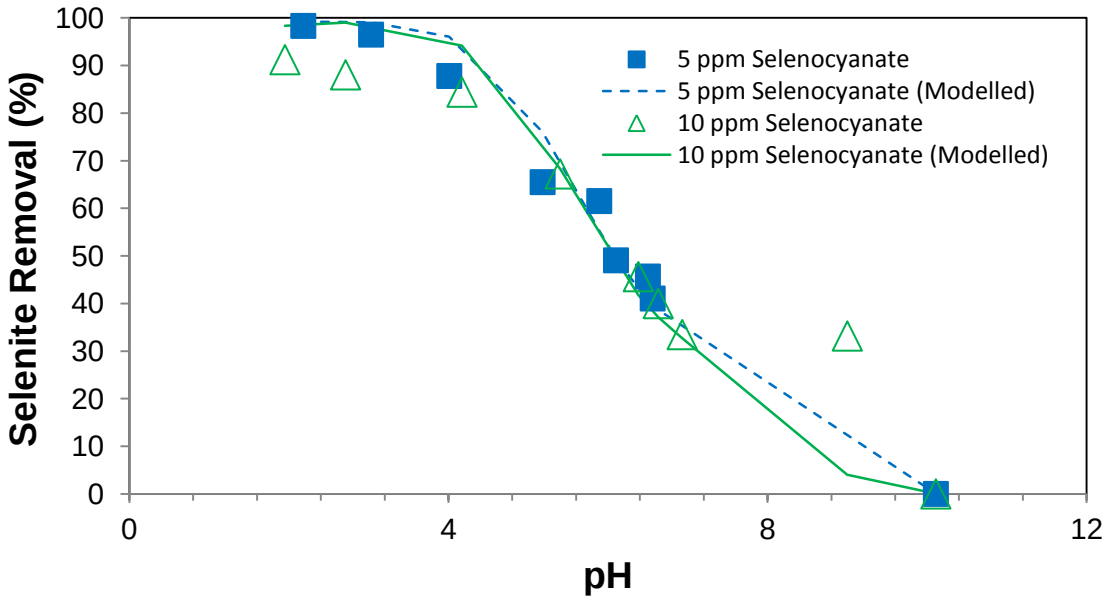

Figure 5.7: Experimental and modelling results for selenite adsorption onto TiO_2 in presence of selenocyanate (1 g/L TiO_2, 5 ppm selenite).

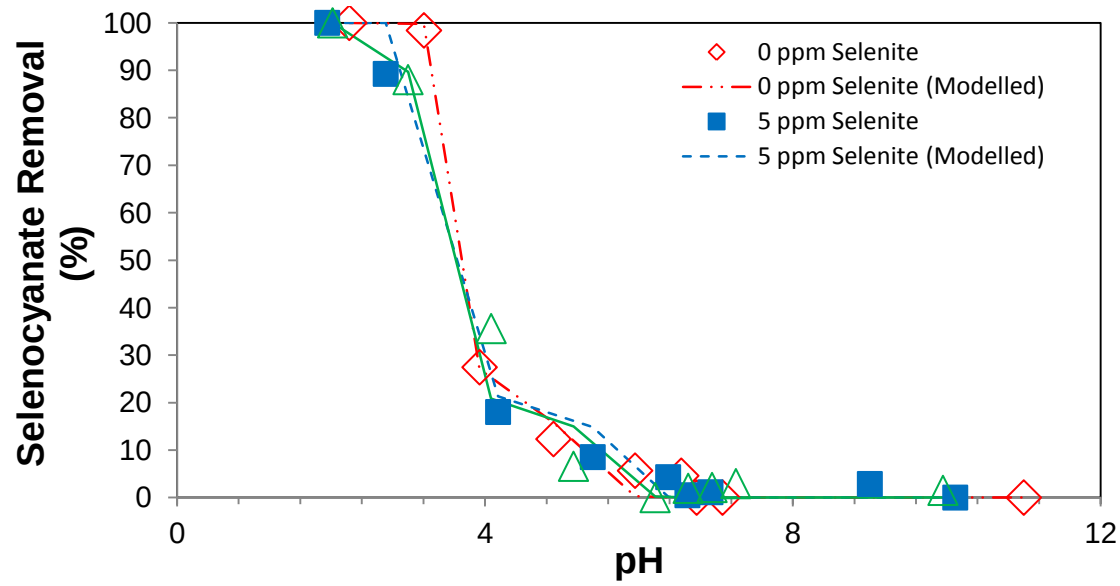

Figure 5.8: Experimental and modelling results for selenocyanate adsorption onto TiO_2 in presence of selenate (1 g/L TiO_2, 10 ppm selenocyanate).

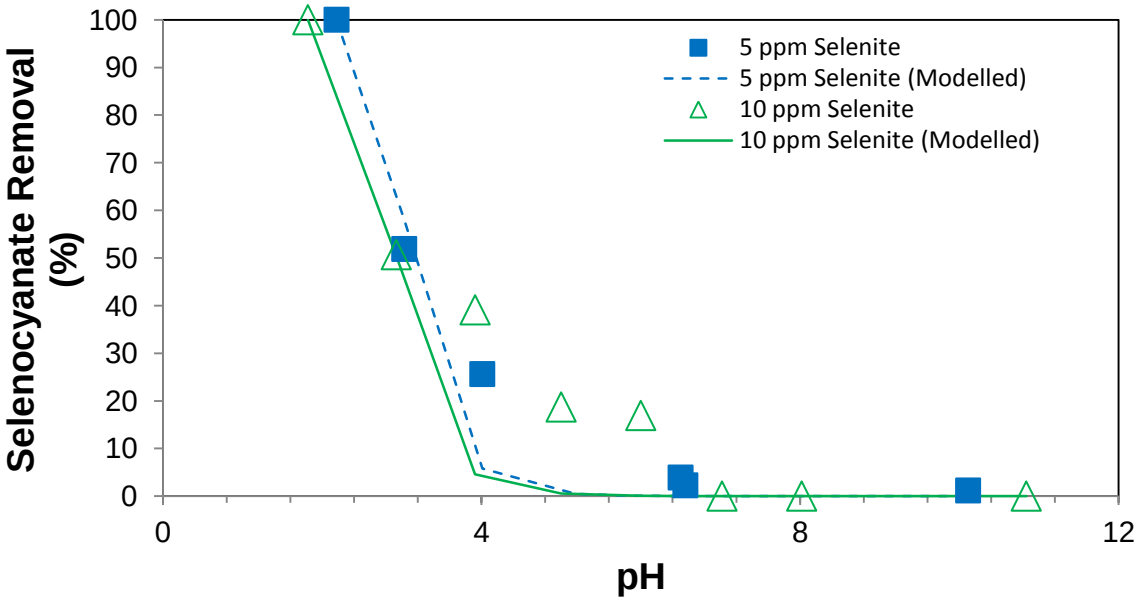

Figure 5.9: Experimental and modelling results for selenocyanate adsorption onto TiO_2 in presence of selenate (1 g/L TiO_2, 5 ppm selenocyanate).

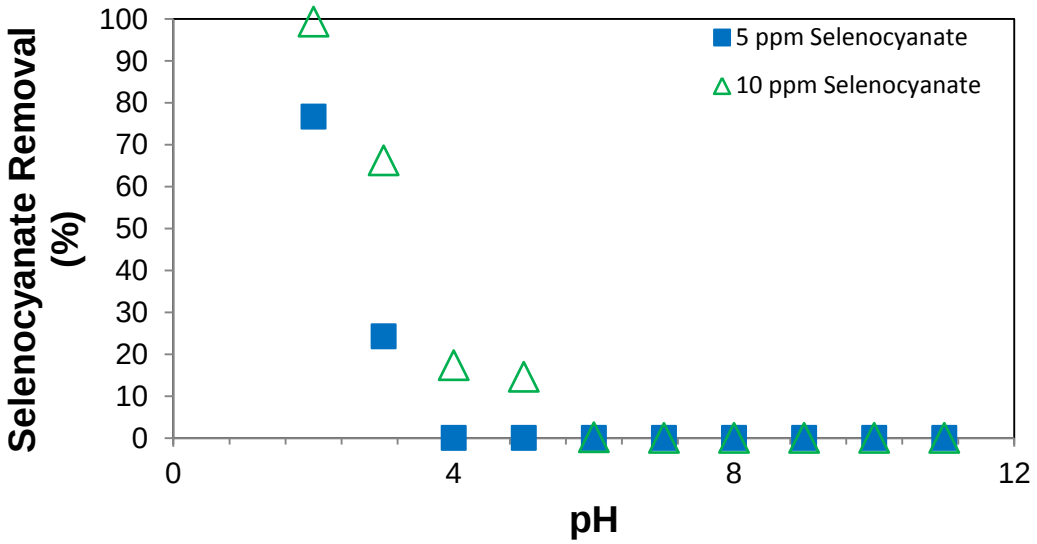

Figure 5.10: Selenocyanate precipitation trends in the absence of TiO_2.

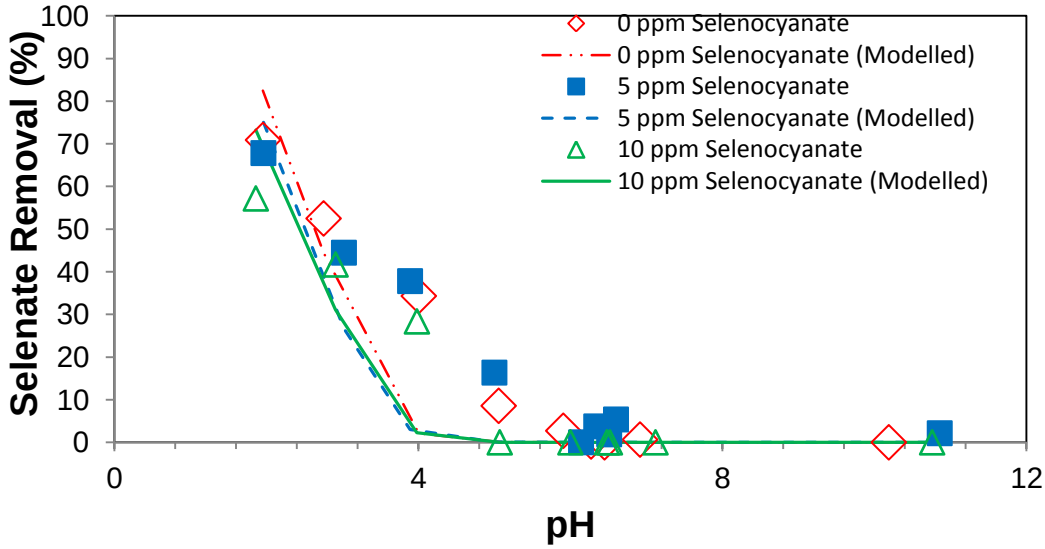

Figure 5.11: Experimental and modelling results for selenate adsorption onto TiO_2 in presence of selenocyanate (1 g/L TiO_2, 10 ppm selenate).

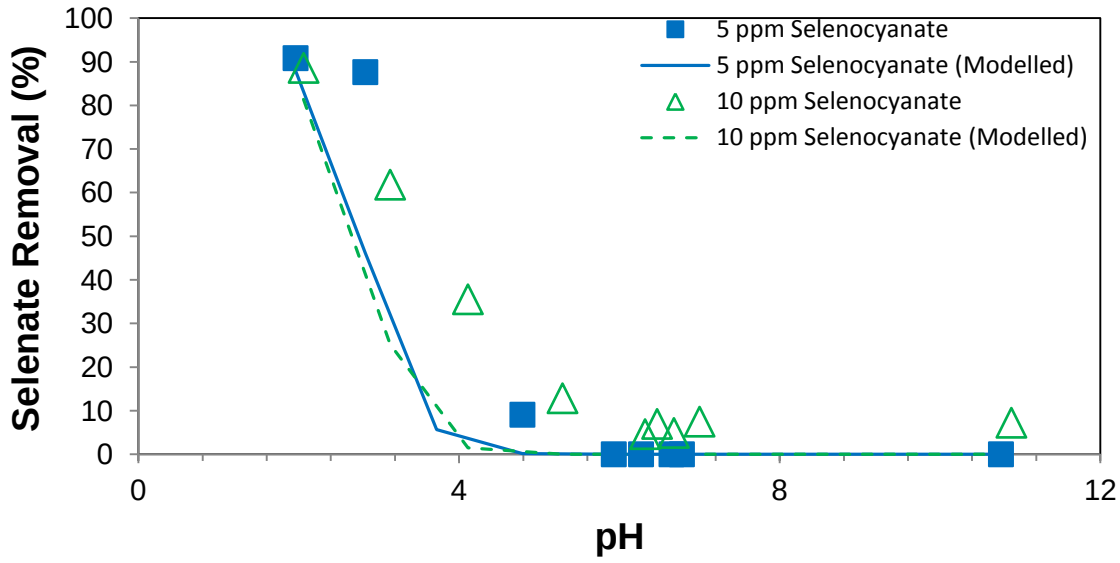

Figure 5.12: Experimental and modelling results for selenate adsorption onto TiO_2 in presence of selenocyanate (1 g/L TiO_2, 5 ppm selenate).

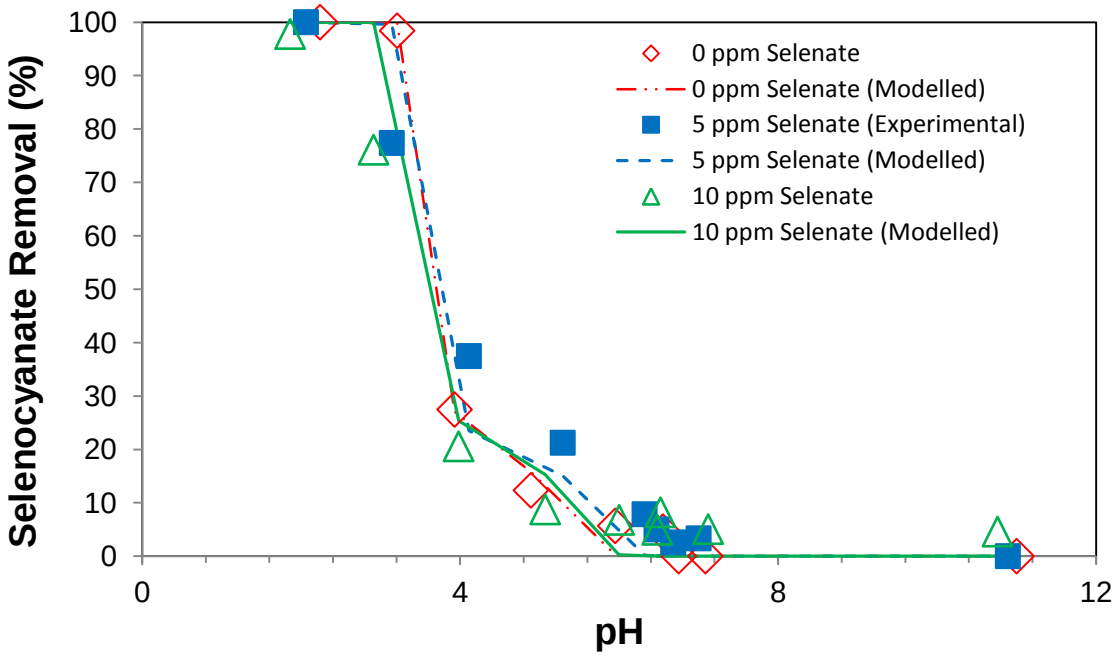

Figure 5.13: Experimental and modelling results for selenocyanate adsorption onto TiO_2 in presence of selenate (1 g/L TiO_2, 10 ppm selenocyanate).

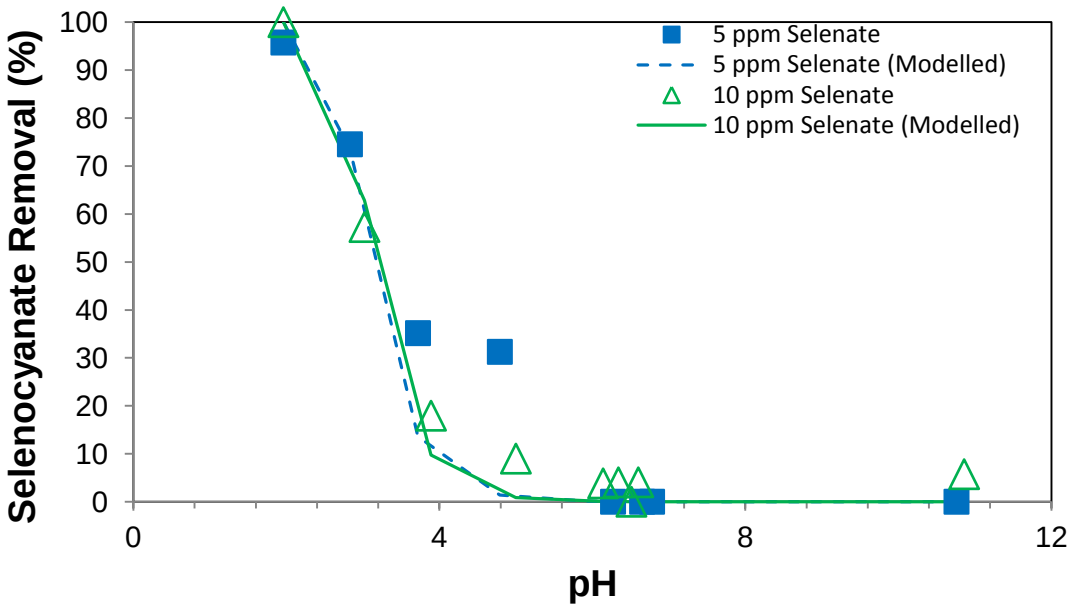

Figure 5.14: Experimental and modelling results for selenocyanate adsorption onto TiO_2 in presence of selenate (1 g/L TiO_2, 5 ppm selenocyanate).

5.2 Tertiary Systems

After completing the above mentioned binary-systems adsorption studies, the present work was extended to investigate selenite, selenate and selenocyante adsorption trends under several tertiary system conditions. In that regard, we studied the adsorption of respective selenium species onto TiO_2 at varying pH values and tertiary solution matrices. The respective experimental and modelling results are given below.

The results for the effect of selenate onto 10 ppm selenite adsorption in the presence of 5 ppm selenocyanate are shown in Figure 5.15. In the absence of selenate, about 82%, 71%, 33% and 0% adsorption values (Figure 5.15) were observed at pH 2, 4, 7 and 11, respectively. An introduction of 5 ppm selenate concentration to the above system shows

no significant change in selenite removal. Also an increase in selenate concentration from 5 ppm to 10 ppm shows a similar trend. We further investigated the effect of selenate concentration on the adsorption of 5 ppm selenite in tertiary system containing 5 ppm selenocyanate (Figure 5.16), that also shows no significant change. Furthermore, the findings in Fig. 5.17 for 10 ppm selenite and 10 ppm selenocyanate though show that an increase in selenate concentration (from 0 to 10 ppm) leads to some decrease in selenite adsorption specifically at low pH values (e.g., at pH 2, 86%, 69%, and 64% selenite adsorption was achieved for the 0 ppm, 5 ppm, and 10 ppm selenate systems respectively), the results above pH 4 show no selenate effect onto selenite removal (Figure 5.17). Also similar to the single and binary systems, a gradual decrease in selenite adsorption for pH 2 to 4, is followed by sharp change between pH 4 and 7. Furthermore, Figures 5.15-5.18 show that a good correlation exists between the model predicted values and experimental results, except for the tertiary systems in Figure 5.17 (5 ppm selenate/10 ppm selenite/10 ppm selenocyanate and 10 ppm selenate/10 ppm selenite/10 ppm selenocyanate) where the model overestimates the adsorption at low pH values. In general we note no significant selenate effect onto selenite removal in presence of selenocyanate that is similar to selenite/selenate binary system findings (Fig. 5.1-5.2). As also mentioned for the binary systems higher percent selenite adsorption was also observed for tertiary system with 5 ppm selenite concentration (Figures 5.16 and 5.18) as compared to 10 ppm selenite concentration (Figures 5.15 and 5.17), nevertheless adsorption on mass basis is still higher for 10 ppm selenite systems possibly due to higher mass transfer driving force across the thin film between the bulk aqueous and bulk solid

phase. Now regarding the effect of selenocyanate on the adsorption of selenite from above discussed tertiary systems we note some decrease in selenite adsorption especially at acidic pH and 10 ppm selenocyanate (Figs. 5.19-5.22). Nevertheless such differences tend to dilute at pH above 4 and trends look to be similar to respective binary system results (Figs. 5.6-5.7). Now looking into the effect of selenite species onto selenate adsorption as summarized in Figure 5.23-5.26, we note for 10 ppm selenate/5 ppm selenocyanate about 68, 44, 38, and 16% selenate adsorption at pH 2, 3, 4 and 5 respectively. As also noted for the earlier mentioned binary selenate/selenite systems (Fig. 5.3 and 5.4), addition of selenite to the selenate/selnocyanate system results into decreased selenate adsorption (Fig. 5.23). The effect of selenite onto 5 ppm selenate removal (in the presence of 5 ppm selenocyanate) as given in Fig. 5.24 indicates decreased selenate adsorption of 24%, 43%, and 9% at pH 2, 3 and 5 respectively, compared to 91%, 88%, and 9% selenate adsorption at pH 2, 3 and 5 respectively in the absence of selenite. A further increase in selenite concentration from 5 ppm to 10 ppm (Figure 5.24) results in a further decrease in selenate adsorption onto TiO_2. Similar effect was observed for the increase in selenite concentration from 0 to 10 ppm in the presence of 10 ppm selenocyante on the adsorption of 10 ppm selenate (Figure 5.25) and 5 ppm selenate (Figure 5.26). The adsorption trends in Figures 8a-d are similar to the binary systems discussed in Figures 5.3 and 5.4 i.e., an increase in both selenite and selenate concentrations causes a decrease in selenate's overall removal. Also except for the 5 ppm selenite/10 ppm selenate/5 ppm selenocyanate system the model underestimates selenate adsorption (Figs. 5.23-5.26). We also looked into the effect of selenocyanate

onto selenate adsorption for the tertiary systems mentioned in Figs. 5.23-5.26. For the 10 ppm selenate and 5 ppm selenite system we noted no significant effect, i.e., at pH 2, 45%, 44% and 47% selenate adsorption was noted for 0, 5 and 10 ppm selenocyanate concentrations respectively and a qualitatively similar trend was noted for 5 ppm selenate. Also the effect of selenocyanate on to selenate adsorption in the presence of 10 ppm selenite showed no significant differences though the overall selenate adsorption was low. These adsorption trends were qualitatively similar to the binary systems discussed in Figures 5.11 and 5.12 that strenghtens our earlier comment that selenate adsorption is not affected by the presence of selenocyanate. This trend was further supported by the outcomes from the combined effect of selenite/selenate species onto selenocyanate removal that also showed no specific trend. In summary the results and observations presented in this work are very important and aforementioned specific adsorption trends should be carefully considered for an effective treatment of respective selenium species using the TiO_2 based processes under competitive conditions.

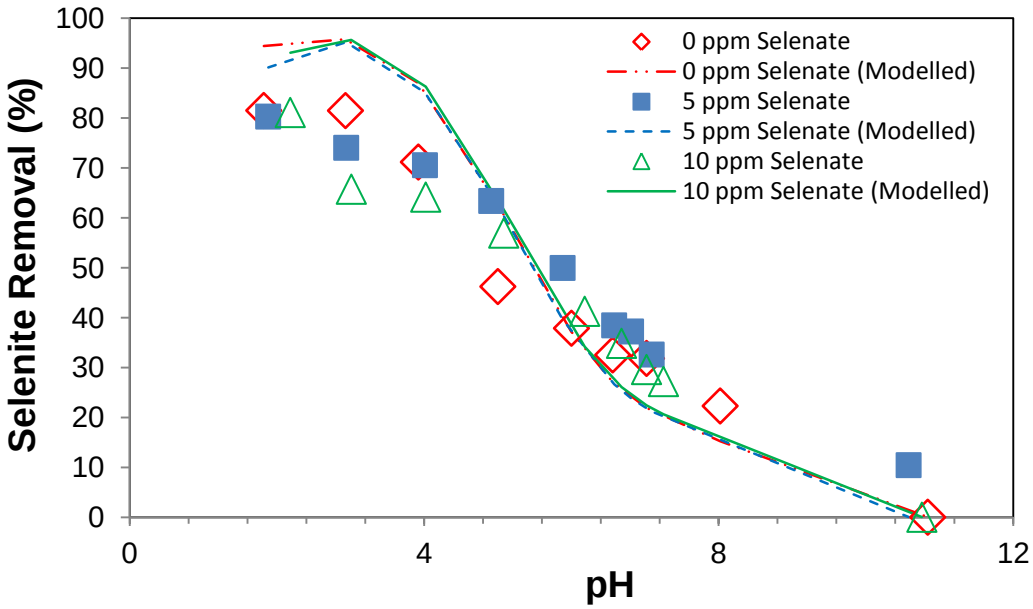

Figure 5.15: Experimental and modelling results for selenite adsorption onto TiO_2 in presence of selenate and selenocyanate (1 g/L TiO_2, 10 ppm selenite, 5 ppm selenocyanate).

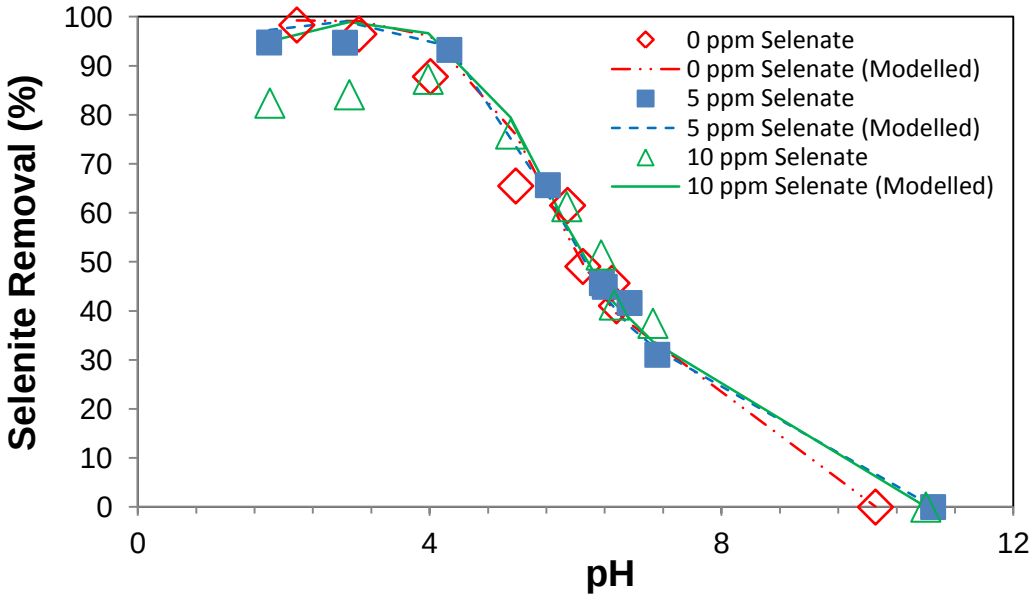

Figure 5.16: Experimental and modelling results for selenite adsorption onto TiO_2 in presence of selenate and selenocyanate (1 g/L TiO_2, 5 ppm selenite, 5 ppm selenocyanate).

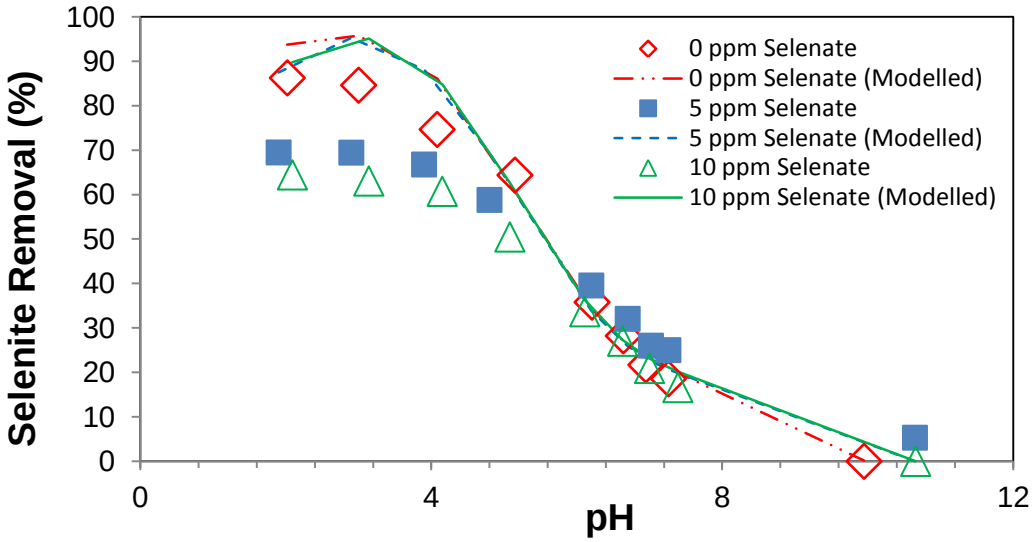

Figure 5.17: Experimental and modelling results for selenite adsorption onto TiO_2 in presence of selenate and selenocyanate (1 g/L TiO_2, 10 ppm selenite, 10 ppm selenocyanate).

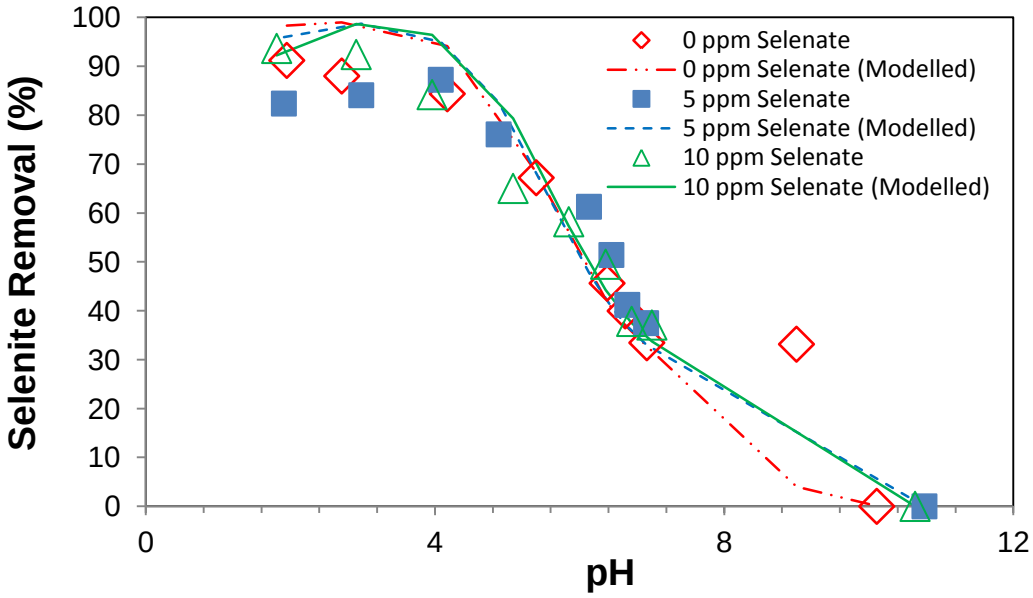

Figure 5.18: Experimental and modelling results for selenite adsorption onto TiO_2 in presence of selenate and selenocyanate (1 g/L TiO_2, 5 ppm selenite, 10 ppm selenocyanate).

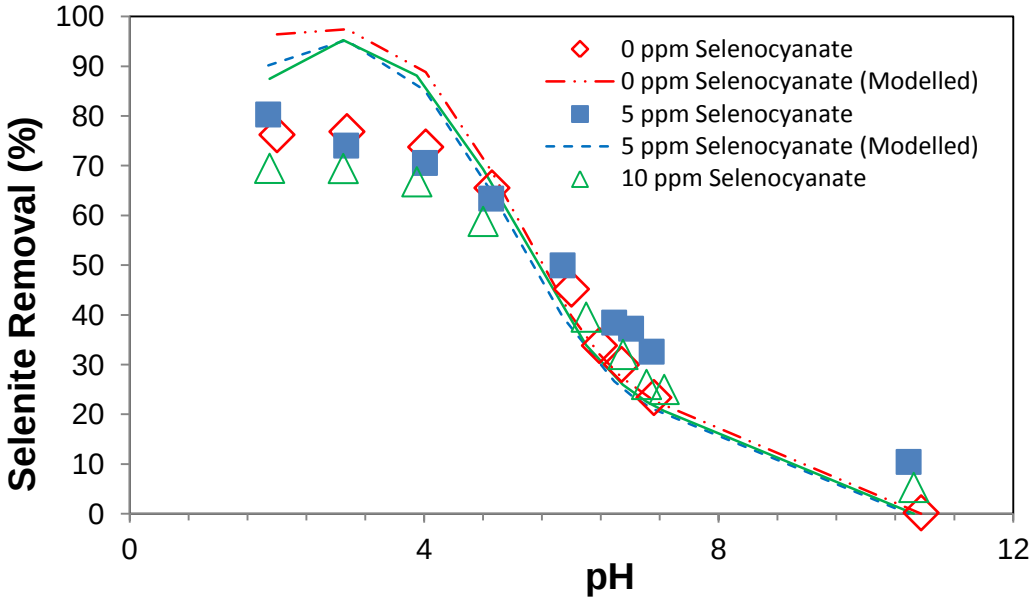

Figure 5.19: Experimental and modelling results for selenite adsorption onto TiO_2 in presence of selenate and selenocyanate (1 g/L TiO_2, 10 ppm selenite, 5 ppm selenate).

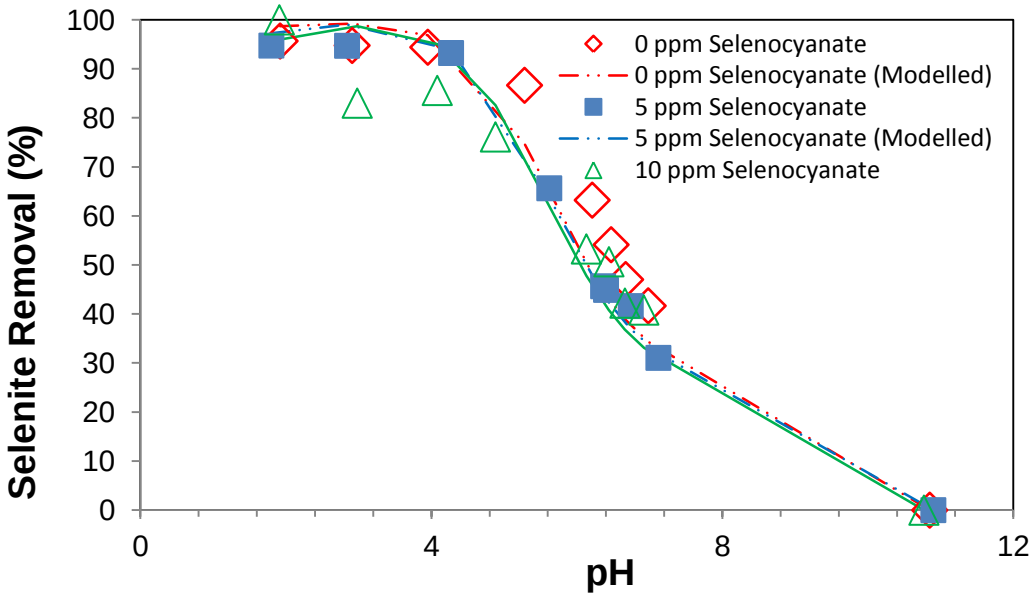

Figure 5.20: Experimental and modelling results for selenite adsorption onto TiO_2 in presence of selenate and selenocyanate (1 g/L TiO_2, 5 ppm selenite, 5 ppm selenate).

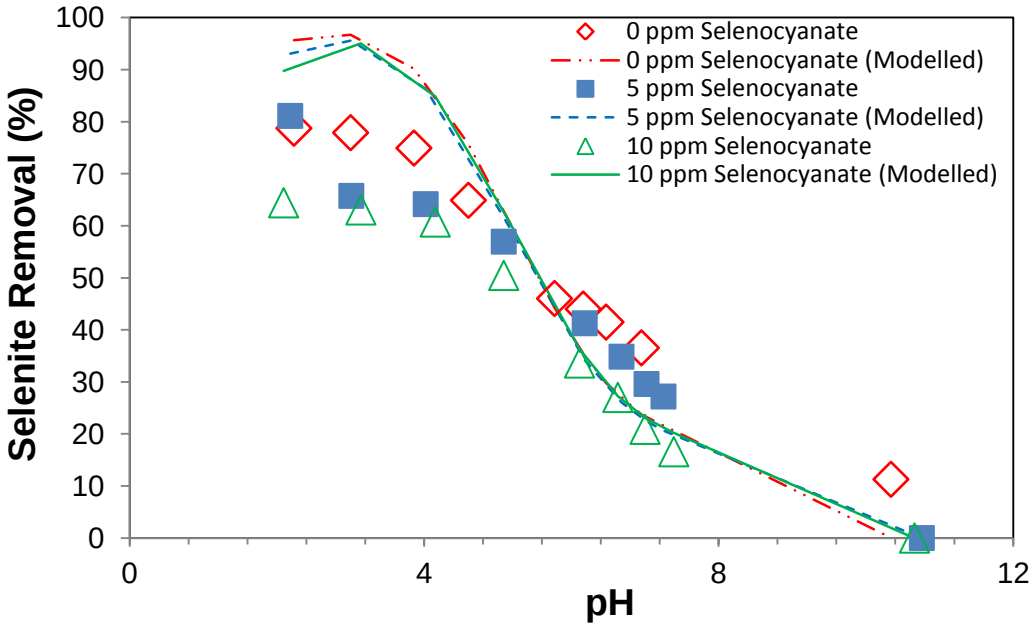

Figure 5.21: Experimental and modelling results for selenite adsorption onto TiO_2 in presence of selenate and selenocyanate (1 g/L TiO_2, 10 ppm selenite, 10 ppm selenate).

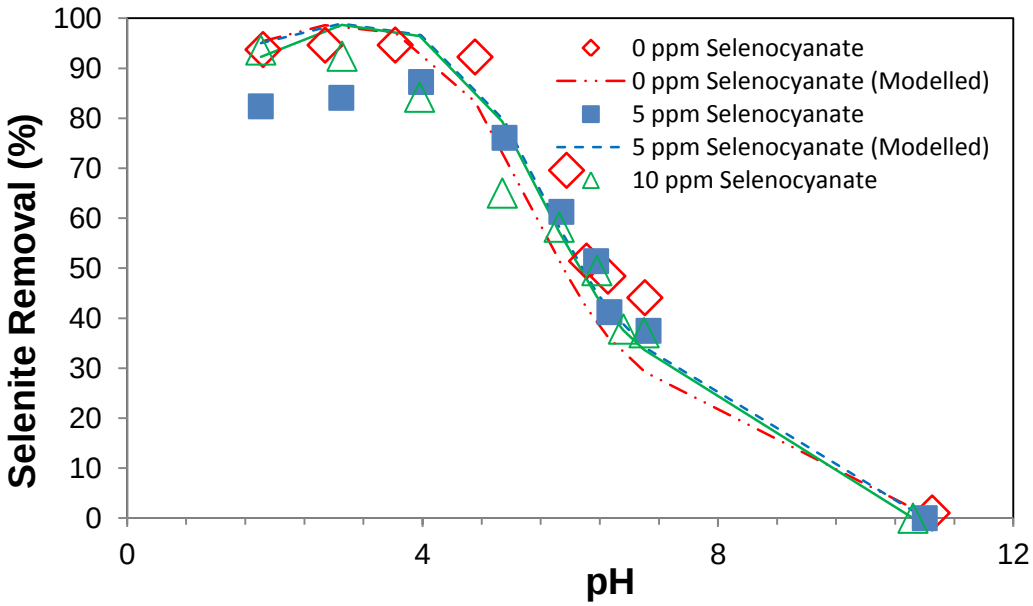

Figure 5.22: Experimental and modelling results for selenite adsorption onto TiO_2 in presence of selenate and selenocyanate (1 g/L TiO_2, 5 ppm selenite, 10 ppm selenate).

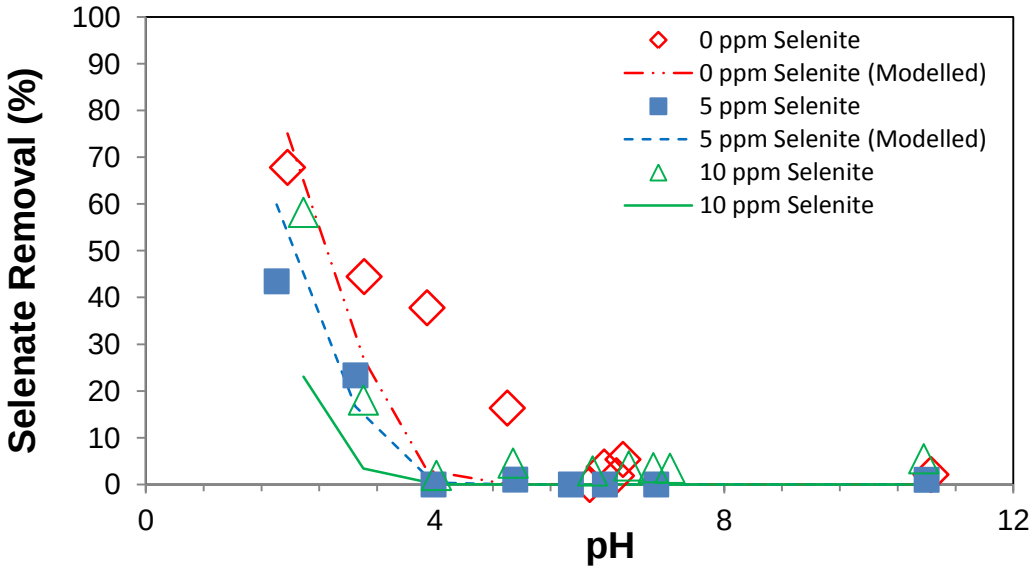

Figure 5.23: Experimental and modelling results for selenate adsorption onto TiO_2 in presence of selenite and selenocyanate (1 g/L TiO_2, 10 ppm selenate, 5 ppm selenocyanate).

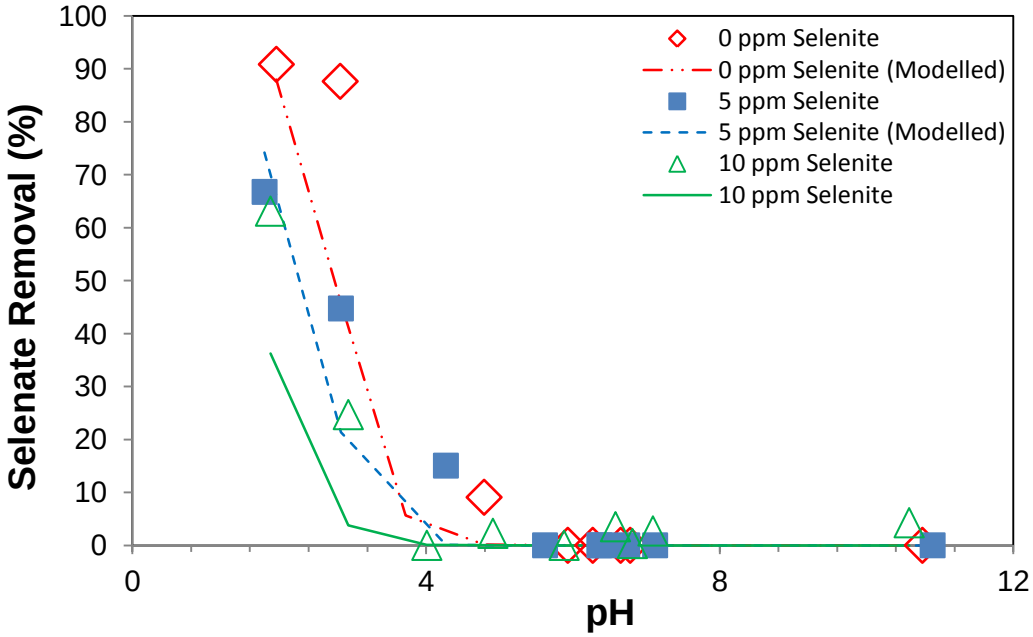

Figure 5.24: Experimental and modelling results for selenate adsorption onto TiO_2 in presence of selenite and selenocyanate (1 g/L TiO_2, 5 ppm selenate, 5 ppm selenocyanate).

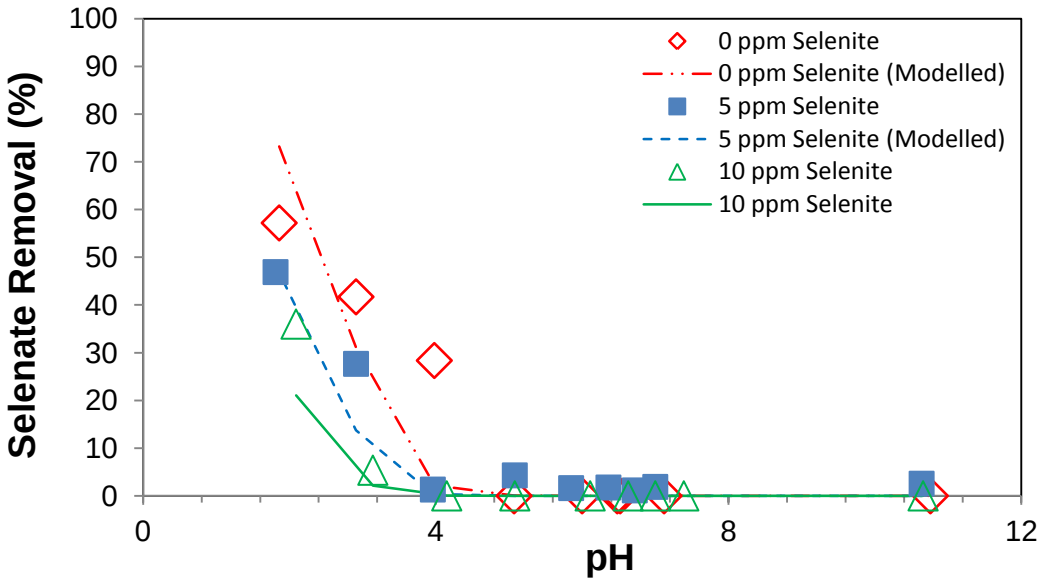

Figure 5.25: Experimental and modelling results for selenate adsorption onto TiO_2 in presence of selenite and selenocyanate (1 g/L TiO_2, 10 ppm selenate, 10 ppm selenocyanate).

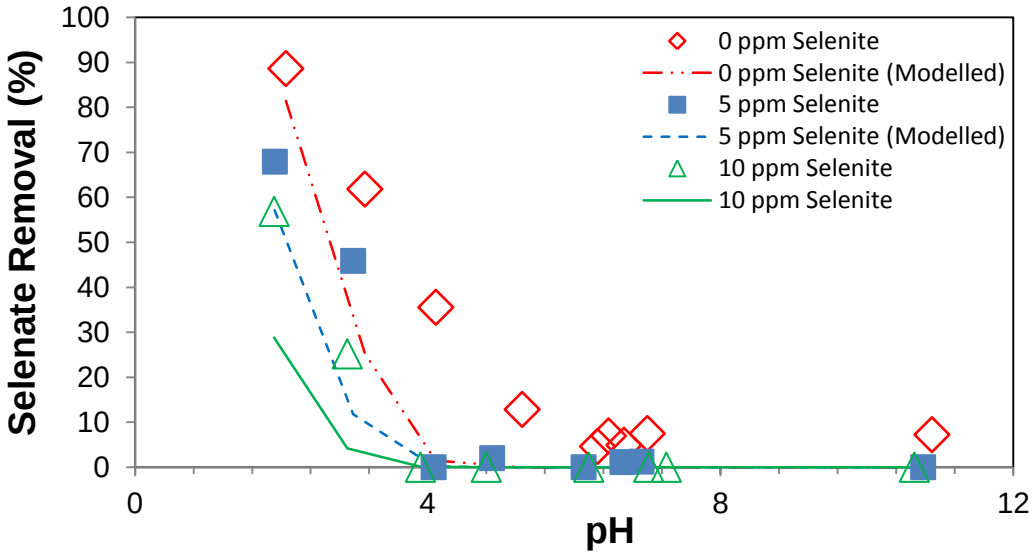

Figure 5.26: Experimental and modelling results for selenate adsorption onto TiO_2 in presence of selenite and selenocyanate (1 g/L TiO_2, 5 ppm selenate, 10 ppm selenocyanate).

REMOVAL OF SELENOCYANATE USING SOLAR ENERGIZED TIO_2 MEDIATED PHOTOCATALYTIC DEGRADATION PROCESS

6.1 Effect of EDTA concentration

The effect of a hole scavenger such as formate on selenate and selenite removal has been reported earlier [31]. Therefore, we first investigated the effect of EDTA concentration on solar light photocatalytic removal of 10 ppm selenocyanate at pH 4. Figure 6.1 shows photocatalysis trend in the absence of EDTA, depicting complete SeCN complex destruction after 180 minutes of irradiation, which is converted to oxidized and toxic forms of selenium i.e., selenite and selenate. Appearance of selenite before selenate shows that SeCN first oxidizes to selenite and then to selenate. Mass balance analysis of species remaining at different time shows negligible loss of total selenium, which suggests that a hole scavenger is indeed required for the reduction of reaction intermediates to elemental selenium. Therefore, EDTA was employed as a hole scavenger in other experiments to improve on photocatalytic removal of selenocyanate. Photocatalysis trends for the removal of 10 ppm selenocyanate at pH 4 and in the presence of 150 ppm, 300 ppm, and 450 ppm EDTA concentrations are shown in Figures 6.2 to 6.4. In the presence of 150 ppm EDTA concentration (Figure 6.2), SeCN

disappeared within 180 minutes of irradiation accompanied by its conversion to selenite and then selenate. At the time of EDTA addition, only selenate was present in the bulk solution. Addition of 150 ppm EDTA concentration (Figure 6.2) resulted in 14% and 7% reduction of selenate to elemental selenium and selenite respectively after 8 hours of irradiation. In the presence of 300 ppm EDTA concentration (Figure 6.3), similar trends were observed before EDTA addition, with selenocyanate disappearing within 180 minutes though with slower conversion rate to selenite and selenate. Similarly, total selenium at 180 minutes is present only in selenate form. Increase in the concentration of EDTA from 150 to 300 ppm lead to an increase in total selenium removal from 14% to about 20%. Faster SeCN conversion to selenite and selenate was achieved in the case of 450 ppm EDTA system after 3 hours of irradiation. Comparing the results in Figure 6.3 and 6.4, increase in total selenium removal from less than 20% to more than 50% via reduction route was achieved within 8 hours due increase in EDTA concentration from 300 to 450 ppm. The increase in SeCN removal with an increase in EDTA concentration might be as a result of an increase in holes depletion by EDTA as its concentration increases, which reduces electron-hole pair recombination. This in turns increases the availability of electrons for the reduction of both selenite and selenate. This is similar to the results obtained by Labaran and Vohra when they investigated the effect of EDTA concentration on photoreduction of selenite and selenate [28].

After completing the effect of EDTA experiments for 10 ppm SeCN, EDTA effect was further investigated for 20 ppm SeCN and trends similar to above were observed. Comparing the results of 300 and 450 ppm EDTA concentration experiments (Figure 6.5

and 6.6), faster conversion of SeCN to selenite and selenate before the addition of EDTA was observed. Lower total selenium values in the case of 300 ppm EDTA system between 30 and 180 minutes might be as a result of higher adsorption of selenite due to its slower conversion rate to selenate. However, in the case of 450 ppm EDTA system, conversion of selenite to selenate was faster (30 to 180 minutes) and this reduces the total amount of selenium adsorbed since adsorption of selenate onto TiO_2 is negligible. Selenite has been reported to have superior adsorption onto TiO_2 in comparison to selenate [28]. Therefore, increase in total selenium in Figure 6.5 at 180 minutes could be because of less adsorbable selenate. About 67% and 75% total selenium removal were achieved via reduction route after 8 hours of irradiation for 300 ppm and 450 ppm EDTA systems respectively. Comparing the solar light intensities for the two systems after the addition of EDTA shows that higher EDTA system receives less radiation. This confirmed that increase in total selenium removal with an increase in EDTA concentration is results from an increase in the trapping of photo-generated holes by EDTA.

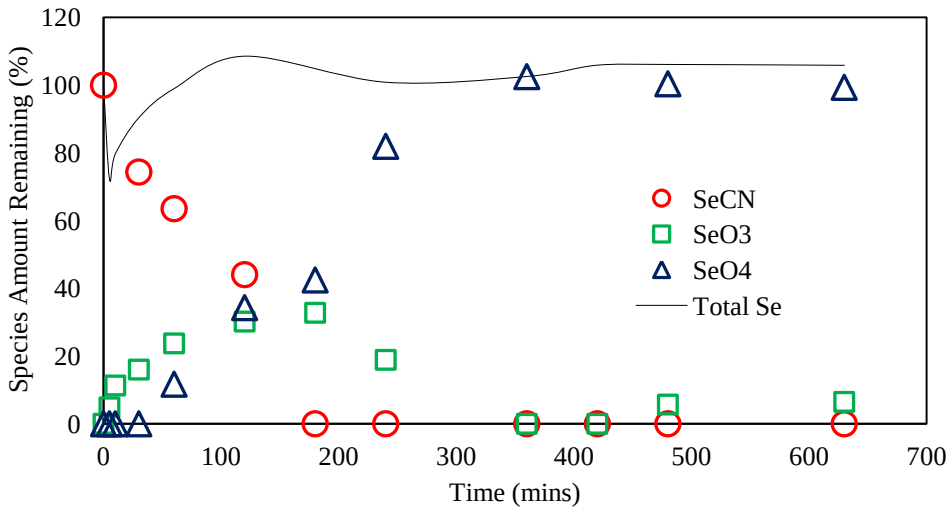

Figure 6.1: Solar light photocatalytic removal of SeCN (10 ppm SeCN, 0 ppm EDTA, pH 4)

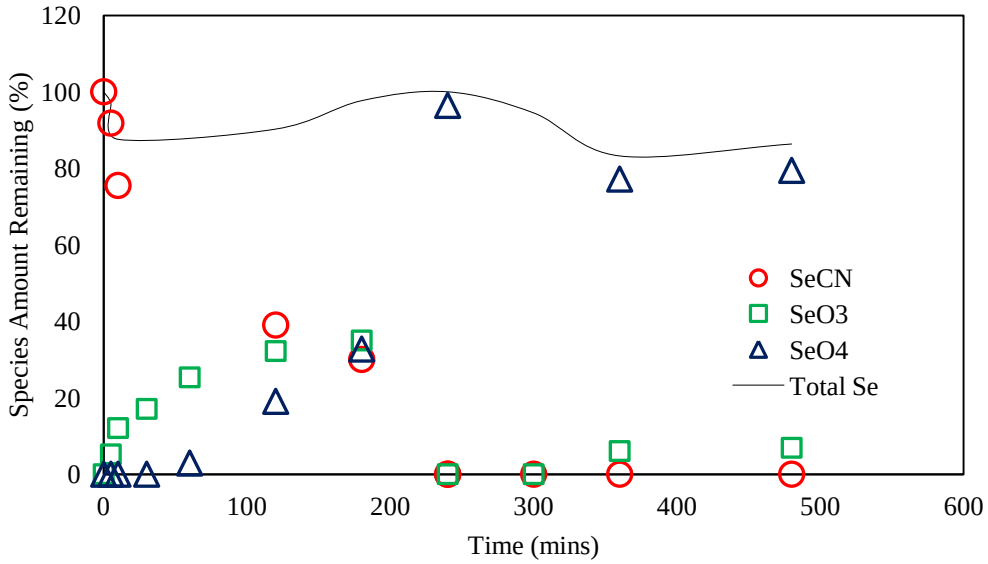

Figure 6.2: Solar light photocatalytic removal of SeCN (10 ppm SeCN, 150 ppm EDTA, pH 4)

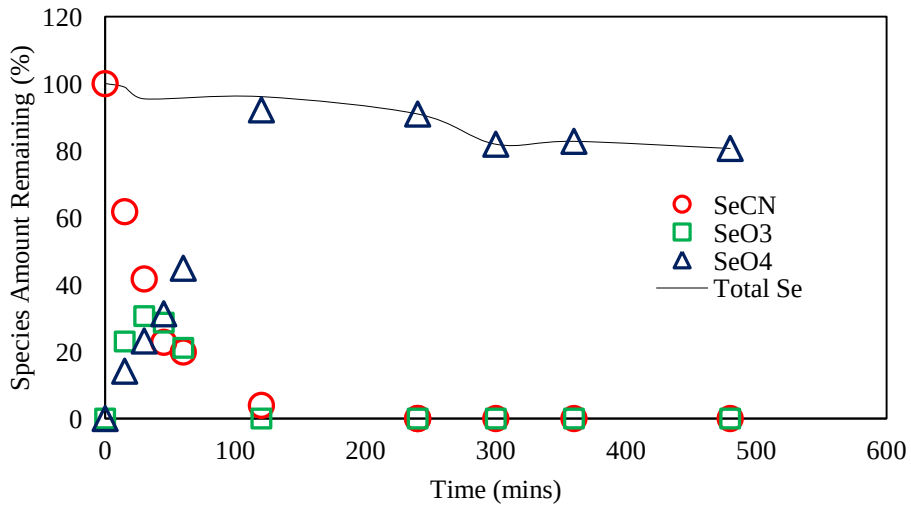

Figure 6.3: Solar light photocatalytic removal of SeCN (10 ppm SeCN, 300 ppm EDTA, pH 4)

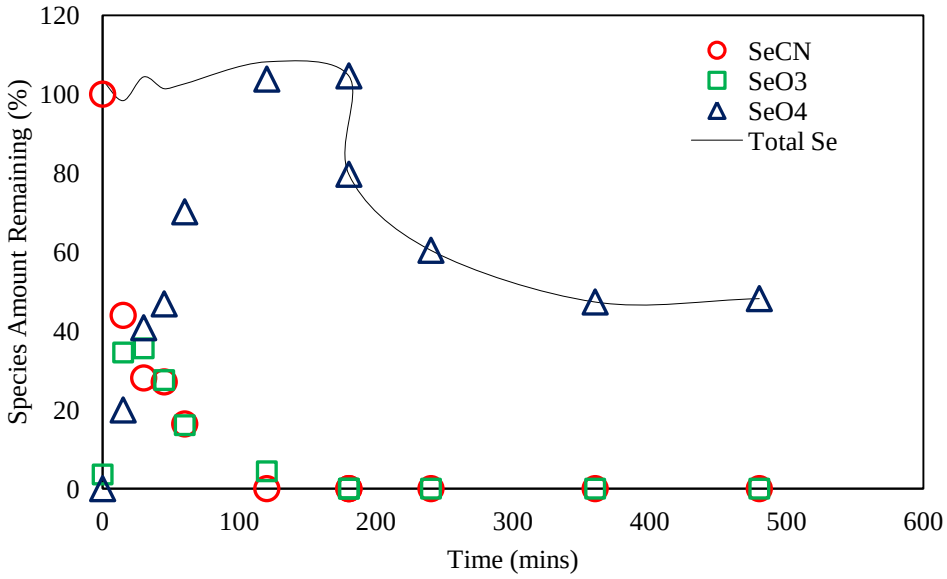

Figure 6.4: Solar light photocatalytic removal of SeCN (10 ppm SeCN, 450 ppm EDTA, pH 4)

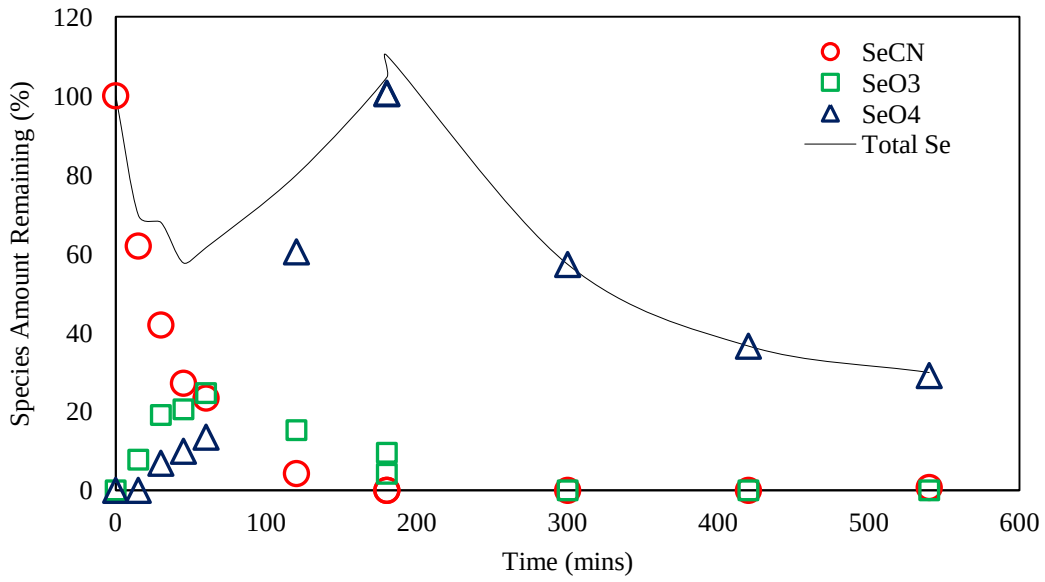

Figure 6.5: Solar light photocatalytic removal of SeCN (20 ppm SeCN, 300 ppm EDTA, pH 4)

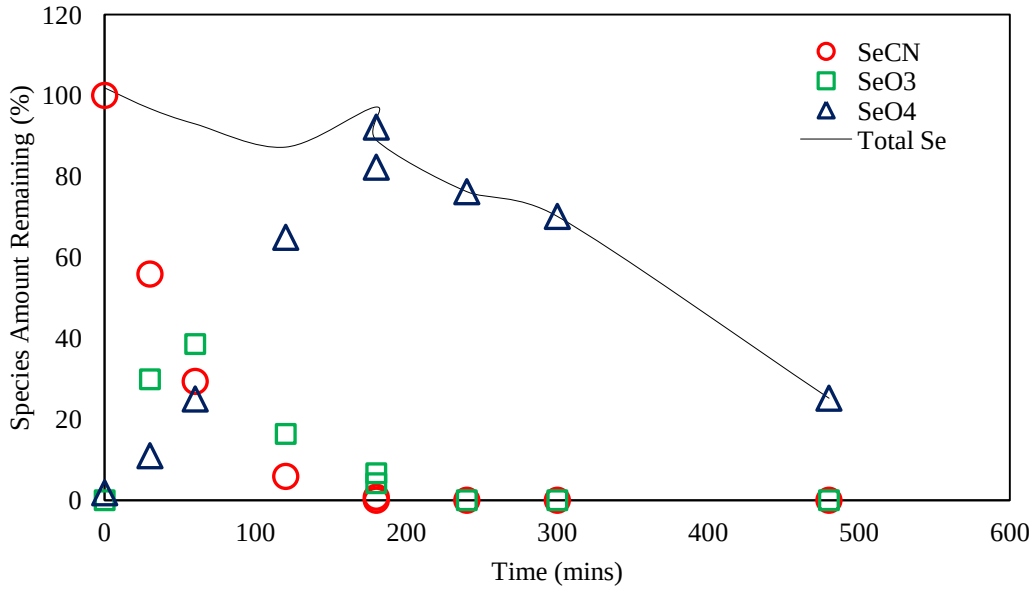

Figure 6.6: Solar light photocatalytic removal of SeCN (20 ppm SeCN, 450 ppm EDTA, pH 4)

6.2 Effect of pH

Figures 6.5, 6.7 and 6.8 show the results of photocatalytic removal of 20 ppm selenocyanate at pH 4, 6 and 8 respectively, in the presence of 300 ppm EDTA concentration. At pH 4 (Figure 6.5), SeCN disappears within 180 minutes accompanied by its conversion to selenite and then selenate. The mass balance between 0 and 180 minutes is low due to higher adsorption of selenite and slower conversion of selenite to selenate. However, at pH 6 and 8, the rate of disappearance of SeCN increases with selenocyanate conversion to selenite and then to selenate also faster. This might be because of increase in OH radicals' formation with pH as a result of increase in OH ions concentration [141]. This shows that selenocyanate complex destruction was not solely by reaction with photo-generated holes, but also by reaction with hydroxyl radical. After addition of EDTA at 180 minutes, approximately 67%, 34% and 17% SeCN removal is observed at 8 hours for pH 4, 6 and 8 respectively. In acidic medium, the surface of TiO_2 is predominantly positive (Equation 2.1 and Figure 4.4) and thus electrostatic attraction exist between TiO_2 and negatively charged ions, a situation that favors selenite, selenate and EDTA adsorption. However, at higher pH values, the surface of TiO_2 is predominantly negative (Equation 2.2 and Figure 4.4), leading to electrostatic repulsion between TiO_2 and anionic species. Increase in the adsorption of selenite/selenate and EDTA anions, increases their chances of reacting respectively with photo-generated electrons and holes. In addition, increased adsorption, reduces the tendency of electron-hole pair recombination. Labaran and Vohra (2014) also reported improved selenite and selenate photo-reduction in acidic medium as a result of increase in electrostatic attraction between selenium oxyanions and TiO_2 particle [28].

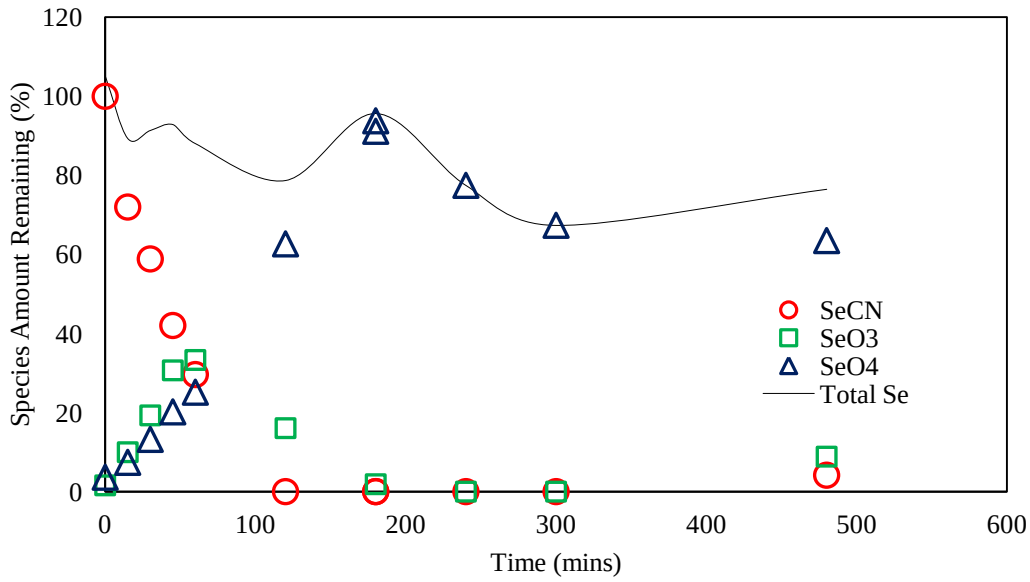

Figure 6.7: Solar light photocatalytic removal of SeCN (20 ppm SeCN, 300 ppm EDTA, pH 6)

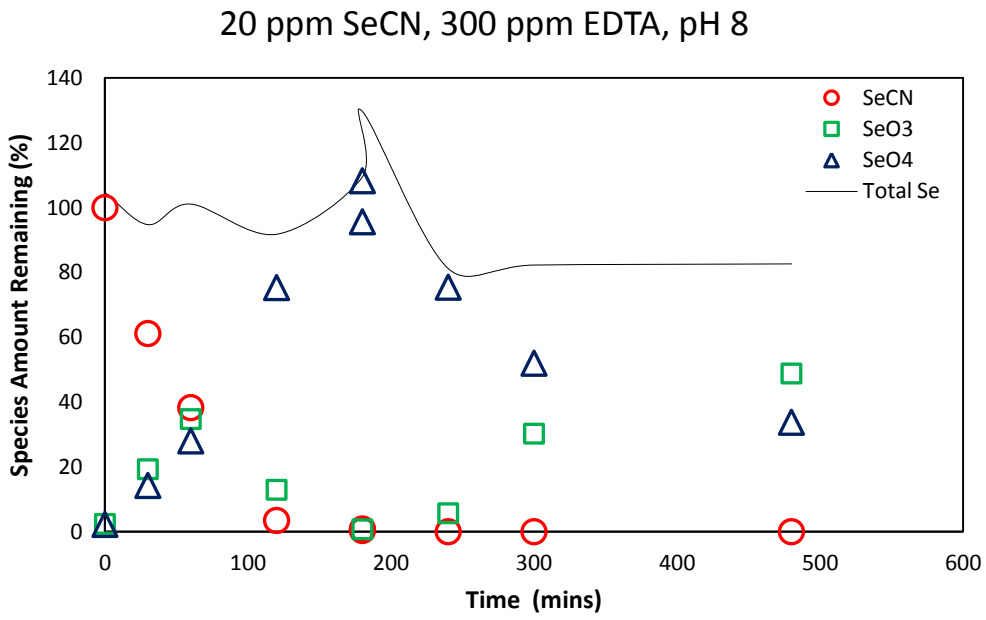

Figure 6.8: Solar light photocatalytic removal of SeCN (20 ppm SeCN, 300 ppm EDTA, pH 8)

6.3 Effect of Selenocyanate Concentration

Figures 6.3 to 6.6 show the effect of initial SeCN concentration on its removal under varying experimental conditions. Solar photocatalysis trends for the removal of SeCN and its reaction intermediates, i.e., selenite and selenate have been discussed in the previous sections. Figures 6.3 and 6.5 show that an increase in initial SeCN concentration from 10 to 20 ppm at pH 4 and in the presence of 300 ppm EDTA concentration lead to an increase in total selenium removal from about 20% to 67% after 8 hours of irradiation. Similar trend was observed in Figures 6.4 and 6.6 when the concentration was increased from 10 to 20 ppm in the presence of 450 ppm EDTA concentration. Approximately 52% and 75% total selenium removal were observed after 8 hours of exposure for 10 and 20 ppm initial SeCN concentrations respectively. This can also be explained based on the increased scavenging of electron-hole pair recombination. As the concentration of SeCN increases, the adsorption of selenite and selenate resulting from the breakdown of SeCN increases which in turn increases their chances of reacting with the photo-generated electrons, thereby hindering the recombination of the electrons and the holes. This trend was observed by Sanuki et al. (2000) when they increased Se(VI) concentration from 50 ppm to 100 ppm [49]. They also attributed this to increased adsorption at 100 ppm Se(VI) concentration. Labaran and Vohra (2014) also observed an increase in photoreduction of selenate when its concentration was increased from 20 ppm to 100 ppm [28].

SOLAR LIGHT ASSISTED PHOTOCATALYTIC REMOVAL OF SELENOCYANATE IN THE PRESENCE OF SELENITE, SELENATE, CYANIDE, THIOCYANATE, AND AMMONIA

Previous studies have shown that despite high efficiency of photocatalysis for the degradation of some pollutants, presence of co-pollutants can be a detriment to the removal of pollutants of interest. For example, Peral *et al.* (1989) observed strong competition between cyanide and phenol during photocatalytic degradation [112]. Furthermore, Vohra *et al.* (2010) have shown that presence of thiocyanate can hinder the removal of thiosulfate especially at high pH values [142]. Therefore, we investigated the effect of various co-pollutants on solar-light assisted photocatalytic removal of SeCN and the results are presented in this chapter. Photocatalytic degradation of selenocyanate (SeCN) in the presence of co-pollutants such as thiocyanate, ammonia and other selenium species has not been investigated to the best of our knowledge. For all experiment, SeCN, SeO_3, SeO_4 are first converted to their selenium equivalence and expressed as

percentages of initial total selenium concentration in the system. Similarly, SCN and its intermediates were converted to their sulfur equivalence and expressed as percentages of initial SCN concentration (as sulfur). Similar was also adopted for nitrogen species and their intermediates.

7.1 Effect of Co-Pollutants

Results from solar photocatalytic degradation of 20 ppm $SeCN^-$ at pH 4 in the presence of 5 ppm selenite are given in Figures 7.1 and 7.2. We do note some selenite adsorption at time zero, followed by its gradual buildup because of selenocyanate degradation (Figure 7.1). This is followed by a decrease in selenite after 1 hour reaction time, with a simultaneous increase in selenate, till 3 hours. We do note lower adsorption of selenate in comparison to selenite, with selenate near equal to total selenium at 3 hours. We also note some selenate and selenocyanate in the aqueous phase at higher reaction time. Selenocyanate seems to re-emerge in the solution phase because of competitive EDTA adsorption. Also, Figure 7.2 shows significant cyanide resulting from selenocyanate destruction followed by its conversion to ammonia.

Figures 7.3 to 7.5 shows the effect of co-pollutant SCN^- on solar photocatalytic degradation of 20 ppm $SeCN^-$. We observed a delay in oxidation of SCN^- to sulfate until a significant portion of $SeCN^-$ is removed (Figure 7.5). Ammonia is the dominant N-intermediate observed as depicted in Figure 7.4. Oxidation of thiocyanate is reported to proceed via formation of some intermediates that quickly converts to ammonia at low pH [143]. This might be the reason some reaction intermediates were not detected. Figures

7.6 and 7.7 shows selenium and nitrogen mass balance for the effect of CN^- on photocatalytic removal of 20 ppm $SeCN^-$ at pH 4. The elemental selenium removals are qualitatively similar to above mentioned thiocyanate effect results with ammonia formation noted later during reaction. Oxidation of cyanide is reported to proceed according to equations 7.1 to 7.3, with ammonia intermediate cyanate converting to ammonia. Nevertheless, quantitatively, we note lesser total selenium removal with cyanide as a co-pollutant (Figure 7.6) compared to thiocyanate experiment (Figure 7.3). This is in spite of the fact that though thiocyanate does show removal via competitive oxidation (Figure 7.5), however no such cyanide removal is noted in Figure 7.7. Furthermore, the maximum selenite formation in case of thiocyanate (Figure 7.3) is also higher than in case of cyanide (Figure 7.6). These contradictory looking trends can be explained as follows: As both selenocyanate and thiocyanate will consume the h^+ species for oxidation, it will leave more e^- species for the reduction of oxidized Se species hence resulting in comparatively higher selenium removal (Figure 7.3).

$$CN^- + 2OH^- + 2h^+ \longrightarrow OCN^- + H_2O \quad (7.1)$$

$$OCN^- + H_2O + +2h^+ \longrightarrow CO_3^{2-} + NH_3 \quad (7.2)$$

$$OCN^- + 2H_2O + 3h^+ \longrightarrow CO_3^{2-} + \frac{1}{2}N_2 + 4H^+ \quad (7.3)$$

The effects of combined co-pollutants $CN^-/SCN^-/NH_4^+$ onto photocatalytic removal of 20 ppm $SeCN^-$ was also investigated and the results are shown in Figures 7.8 to 7.10. We note 65% total selenium removal (Figure 7.8). Results in Figure 7.10 show oxidation of thiocyanate to sulfate after a lag period between 0 and 60 minutes, which is similar to that

noted in Figure 7.5 for SCN only effect, though for the former case we not slower thiocyanate and selenite oxidation that could result from competition for the $h^+/OH^\bullet$ species. Hence preferential $SeCN^-$ removal before SCN^- oxidation should be accounted for during reactor design. Overall SeCN reduction to elemental selenium in the presence of SeO_3^{2-}, SCN^-, CN^-, and $CN^-/SCN^-/NH_4^+$ after 9 hours of irradiation were respectively 78%, 83%, 62% and 65%. In general, $SeCN^-$ reduction to elemental selenium shows the following order $SeO_3^{2-}>SCN^->CN^->CN^-/SCN^-/NH_4^+$. The above results indicate that other than the cyanide, other co-pollutants are also removed from the aqueous mixed stream along with selenocyanate, though longer reaction time may be needed in case of mixed system because of synergistic-competitive effects.

Figures 7.11 and 7.12 shows the effect of combined co-pollutants $CN^-/SCN^-/NH_4^+$ on photocatalytic removal of 10 ppm selenocyanate in the presence of 300 ppm EDTA at pH 4 and 8 respectively. At pH 4 (Figure 7.11), about 61% total selenium removal was observed after 11 hours of irradiation. However, an increase in initial pH from 4 (Figure 7.11) to 8 (Figure 7.12) lead to a decrease in total selenium removal from 61% to 46%. As explained earlier, $TiOH_2^+$ is the most dominant TiO_2 species below pH 3.9 (Equation 2.1 and Figure 4.4), and thus electrostatic attraction exist between the surface and anionic species i.e., selenite, selenate and EDTA. However, between pH 3.9 and 8.7, TiO_2 mostly exist in neutral form (TiOH) and thus electrostatic attraction between the surface and the anionic species reduces, thereby reducing their adsorption. However, decrease in the adsorption of selenite and selenate resulting from the breakdown of SeCN will decrease

their chances of reacting with the photo-generated electrons, thereby reducing their reduction to elemental selenium.

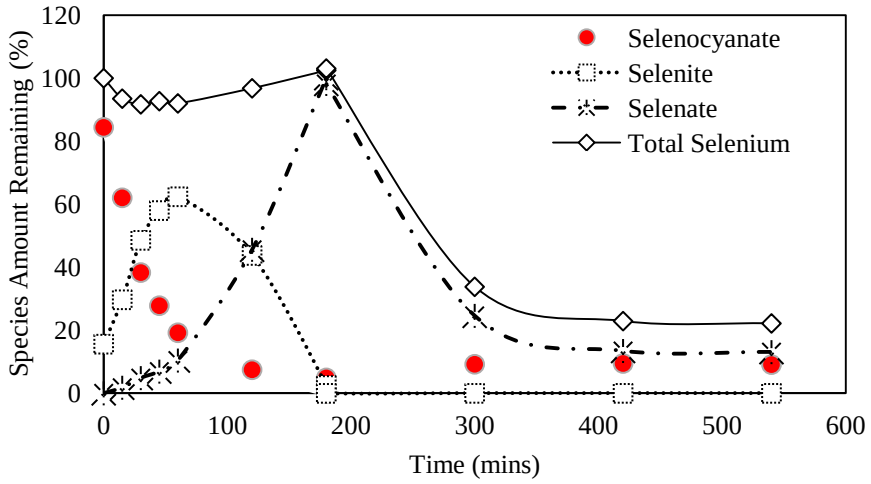

Figure 7.1: Selenium mass balance for solar-light photocatalytic removal of SeCN (20 ppm SeCN, 5 ppm SeO_3^{2-}, 300 ppm EDTA, pH 4)

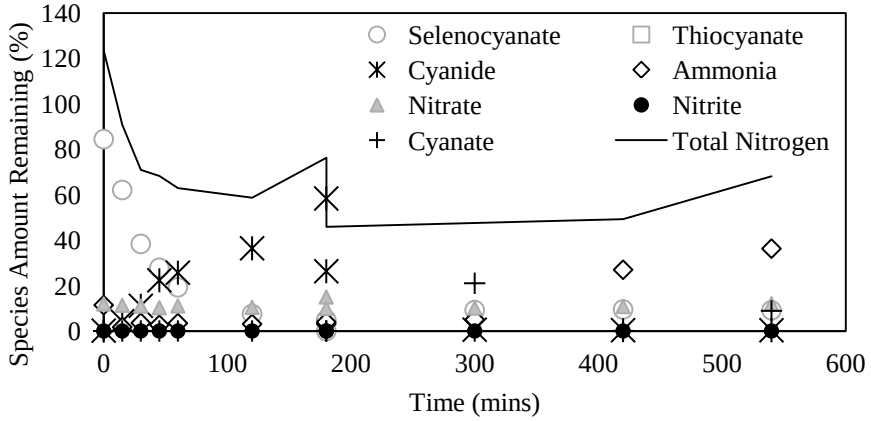

Figure 7.2: Nitrogen mass balance for solar-light photocatalytic removal of SeCN (20 ppm SeCN, 5 ppm SeO_3^{2-}, 300 ppm EDTA, pH 4)

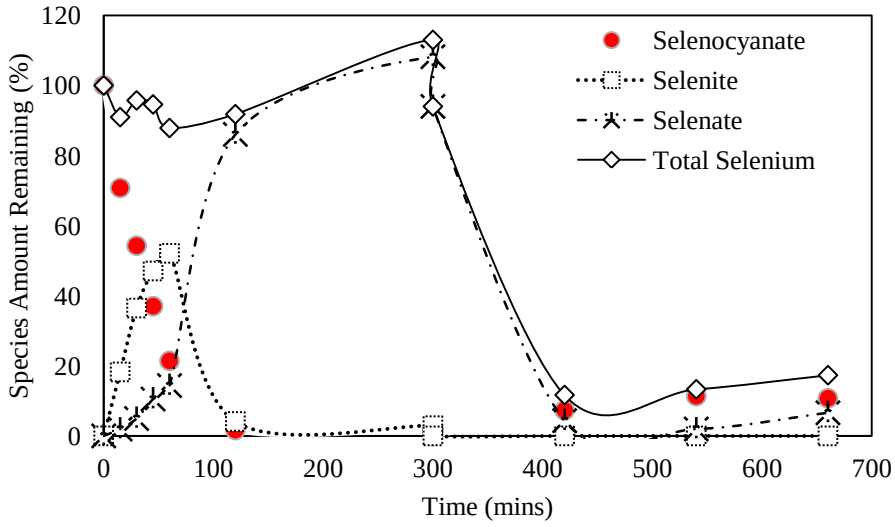

Figure 7.3: Selenium mass balance for solar-light photocatalytic removal of SeCN (20 ppm SeCN, 5 ppm SCN^-, 300 ppm EDTA, pH 4)

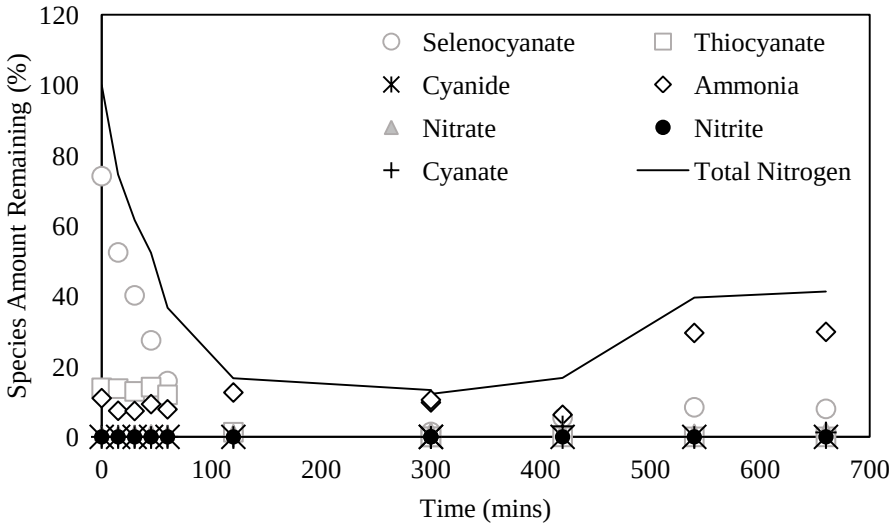

Figure 7.4: Nitrogen mass balance for solar-light photocatalytic removal of SeCN (20 ppm SeCN, 5 ppm SCN^-, 300 ppm EDTA, pH 4)

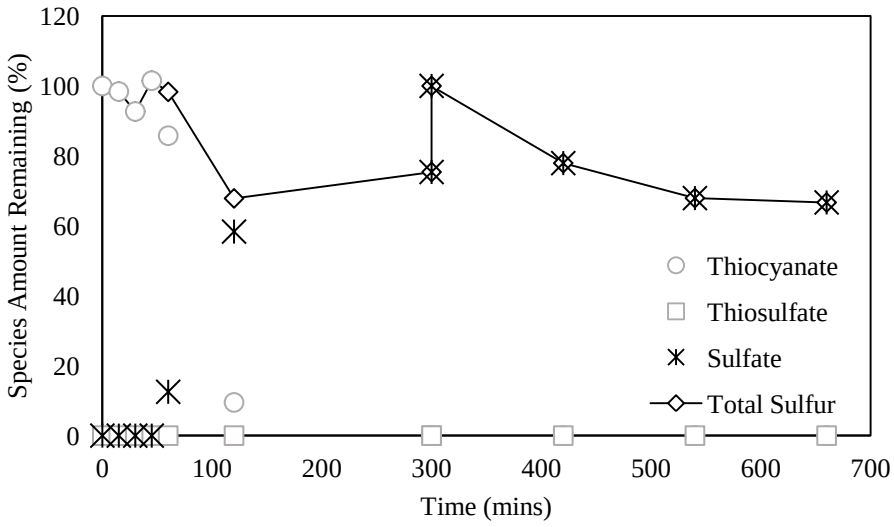

Figure 7.5: Sulfur mass balance for solar-light photocatalytic removal of SeCN (20 ppm SeCN, 5 ppm SCN^-, 300 ppm EDTA, pH 4)

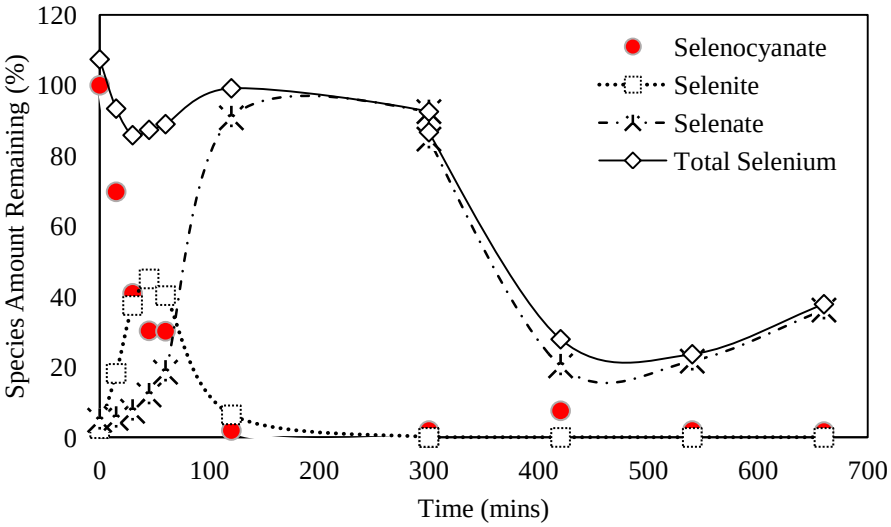

Figure 7.6: Selenium mass balance for solar-light photocatalytic removal of SeCN (20 ppm SeCN, 5 ppm CN^-, 300 ppm EDTA, pH 4)

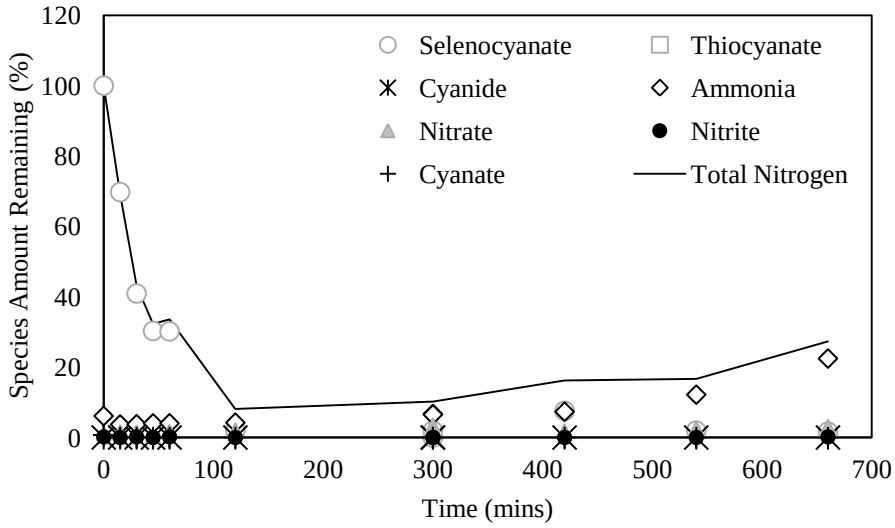

Figure 7.7: Nitrogen mass balance for solar-light photocatalytic removal of SeCN (20 ppm SeCN, 5 ppm CN^-, 300 ppm EDTA, pH 4)

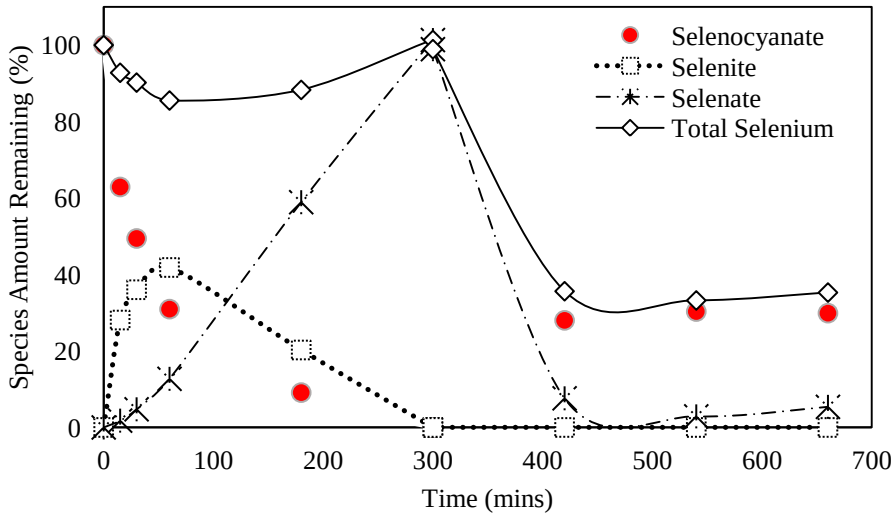

Figure 7.8: Selenium mass balance for solar-light photocatalytic removal of SeCN (20 ppm SeCN, 5 ppm SCN^-, 5 ppm CN^-, 5 ppm NH_4^+,300 ppm EDTA, pH 4)

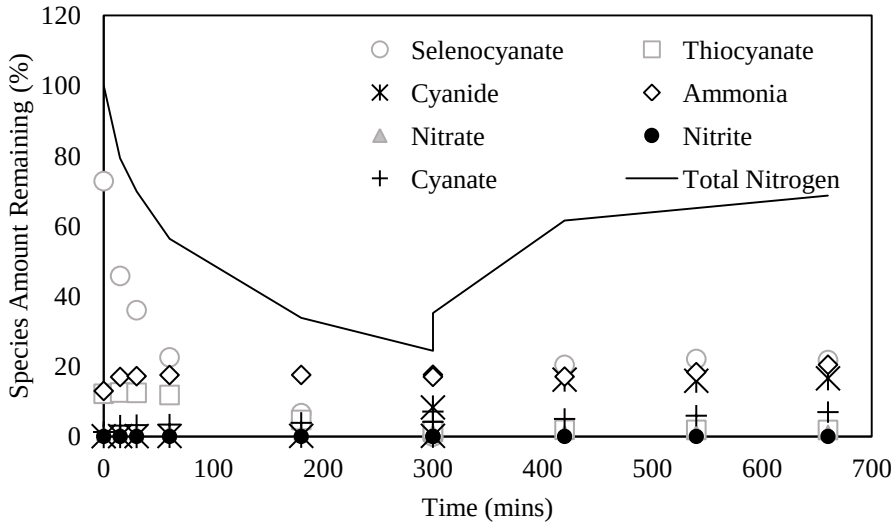

Figure 7.9: Nitrogen mass balance for solar-light photocatalytic removal of SeCN (20 ppm SeCN, 5 ppm SCN^-, 5 ppm CN^-, 5 ppm NH_4^+,300 ppm EDTA, pH 4)

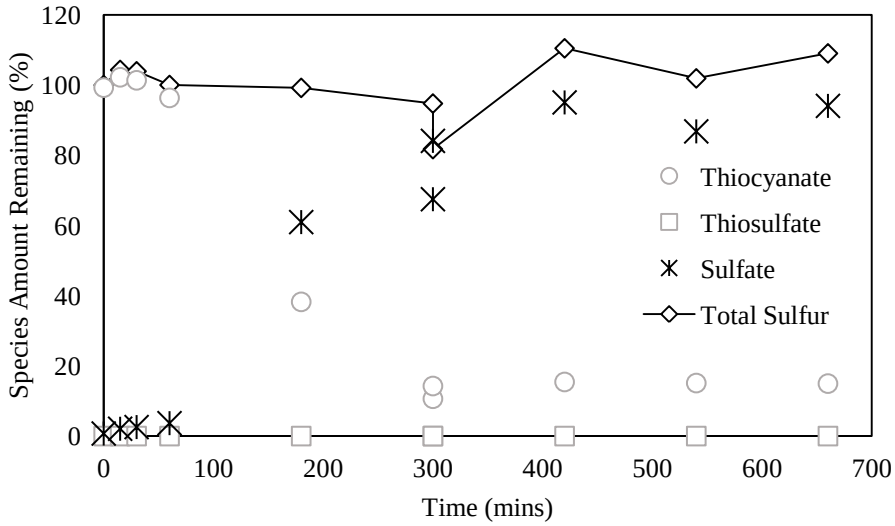

Figure 7.10: Sulfur mass balance for solar-light photocatalytic removal of SeCN (20 ppm SeCN, 5 ppm SCN^-, 5 ppm CN^-, 5 ppm NH_4^+,300 ppm EDTA, pH 4)

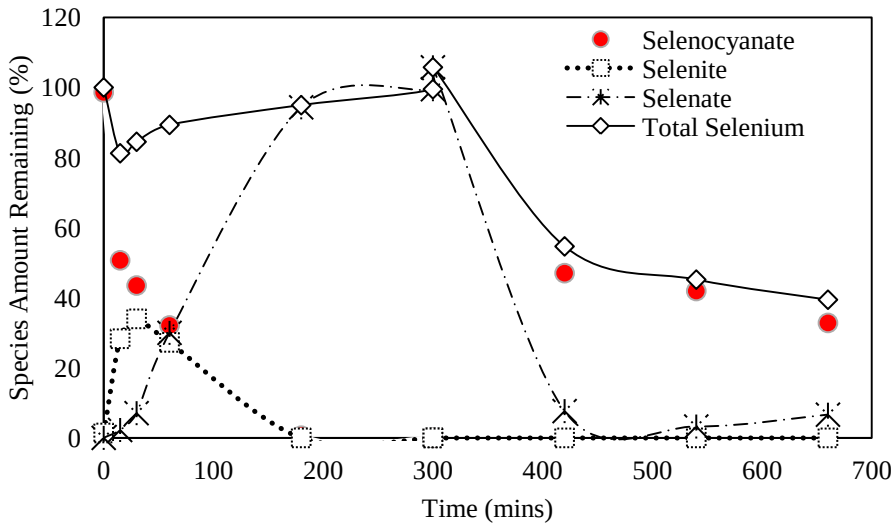

Figure 7.11: Selenium mass balance for solar-light photocatalytic removal of SeCN (10 ppm SeCN, 5 ppm SCN^-, 5 ppm CN^-, 5 ppm NH_4^+,300 ppm EDTA, pH 4)

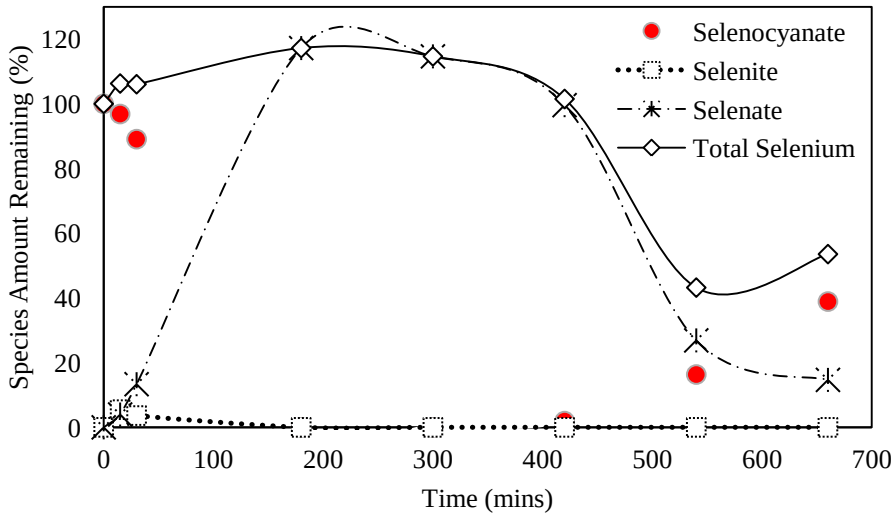

Figure 7.12: Selenium mass balance for solar-light photocatalytic removal of SeCN (10 ppm SeCN, 5 ppm SCN^-, 5 ppm CN^-, 5 ppm NH_4^+,300 ppm EDTA, pH 8)

7.2 Effect of Selenocyanate Concentration

Figures 7.8 and 7.11 shows the combined effect of co-pollutants $CN^-/SCN^-/NH_4^+$ onto photocatalytice removal of 10 ppm and 20 ppm SeCN concentration respectively. The trend of SeCN conversion to selenite and selenate in Figures 7.8 and 7.11 which were obtained in the presence of 300 ppm EDTA concentration at pH 4 have been discussed in the previous sections. An increase in initial SeCN concentration from 10 ppm (Figure 7.11) to 20 ppm (Figure 7.8) at pH 4 and in the presence of 300 ppm EDTA concentration lead to an increase in total selenium removal from about 61% to 65% after 11 hours of irradiation. This can also be explained based on the increased scavenging of electron-hole pair recombination. As the concentration of SeCN increases, the adsorption of selenite and selenate resulting from the breakdown of SeCN increases which in turn increases their chances of reacting with the photo-generated electrons, thereby hindering the recombination of the electrons and the holes. Labaran and Vohra (2014) also observed an increase in photoreduction of selenate when its concentration was increased from 20 ppm to 100 ppm. Sanuki *et al.* 2000 also noted an increase in selenate PCD initiated removal as its concentration was increased from 50 to 100 ppm.

UV LIGHT ASSISTED PHOTOCATALYTIC REMOVAL OF SELENOCYANATE IN THE PRESENCE OF SELENITE, SELENATE, CYANIDE, THIOCYANATE, AND AMMONIA

8.1 Effect of Co-Pollutants

The effect of ammonia on UV-light photocatalytic degradation of 10 ppm SeCN was first investigated at pH 4 and selenium/nitrogen mass balances are shown in Figures 8.1 and 8.2 respectively. Figure 8.1 shows near complete removal of SeCN and its conversion to reaction intermediates (selenite and selenite) within 180 minutes. The appearance of selenite before selenate is a confirmation that SeCN first converts to selenite and then to selenate. Total selenium reduces as SeCN converts to selenite (0 to 60 minutes), which might be as result of the adsorption of species with time. As more selenite is converted to selenate (60 to 180 minutes), total selenium in the system increases as a result of low adsorption of selenate onto TiO_2 as compared to selenite. Labaran and Vohra (2014) have shown that selenite adsorption onto TiO_2 is superior to that of selenate [28]. At 180 minutes, about 100% of total selenium was present in the system after the addition of

EDTA. This might be as a result of competition between selenium species and EDTA for limited adsorption sites on TiO_2 particles. Though, selenium species cannot be reduced to elemental selenium without the presence of a hole scavenger, its presence will limit the oxidation of SeCN bond. Therefore, EDTA was added at 180 minutes at which most of selenium species is converted to selenite and selenate. Reduction of selenate to elemental selenium was observed after the addition of hole scavenger EDTA. About 99% selenium reduction was observed after 420 minutes. Figure 8.2 on the other hand an insignificant change in ammonia concentration. Previous studies have shown that photocatalytic degradation of ammonia is not effective at low pH values. Zhu *et al.* (2005) found that initial ammonia photocatalytic oxidation rates are proportional to the neutral NH_3 form which will be negligible at acidic pH values [144]. Low nitrogen mass balance could result either because of intermediates adsorption or reduction to N_2 as explained by Vohra and co-workers [145]. Furthermore, another experiment that was conducted with addition of EDTA at 300 minutes (Figures 8.3 and 8.4) showed similar trends to the results in Figures 8.1 and 8.2.

We further investigated the effect of selenate added at time zero on photocatalytic degradation of SeCN at pH 4 (Figure 8.5 and 8.6). Faster formation as well as disappearance of selenite is observed (Figure 8.5) in comparison to selenocyanate/ammonia systems (Figure 8.1 and 8.3). However, a lag in the total selenium species removal is observed between 0 and 30 minutes, which results from higher initial concentration of low adsorbing selenate species. However, as selenite concentration increases due to conversion of $SeCN^-$ to selenite, more selenium is

adsorbed between 30 and 60 minutes but reduces again between 60 and 180 minutes as more selenite converts to selenate. Though addition of EDTA at 5 hours results in only 70% total selenium removal, however on mass basis this is close to that achieved in case of selenocyanate/ammonia systems. This shows that the rate of conversion of selenate, which is the only form of selenium remaining at the time of addition of EDTA, is not significantly affected by an increase in its initial concentration. Also, similar to the selenocyanate/ammonia binary systems, a poor nitrogen mass balance is noted.

In continuation, photocatalytic removal of 10 ppm SeCN in the presence of selenite was also conducted (Figure 8.7 and 8.8). As in the two previous cases, SeCN conversion to selenate via selenite was observed. However, due to the presence of additional selenite at the beginning, part of it still remains in the solution at 5 hours reaction time. We also note a jump in selenate concentration after EDTA addition. The only possible explanation is the displacement of selenate from TiO_2 surface by EDTA. As expected, higher total selenium removal (>90%) is observed for selenocyanate/selenite system as compared to selenocyanate/selenate system.

The effect of SCN on photocatalytic removal of 10 ppm $SeCN^-$ was also investigated and the results are displayed in Figures 8.9 to 8.11. Figure 8.9 shows conversion of $SeCN^-$ to selenite and then to selenate. Near complete total selenium removal indicate a non-competitive reaction as SCN^- and $SeCN^-$ species are both oxidized by the $OH^\bullet$ radicals. Near complete conversion of thiocyanate is achieved within one hour. Total sulfur also lowers with time that indicates that sulfate is adsorbed onto TiO_2. However, a delay in the

conversion of SCN to sulfate is observed between 0 and 30 minutes (Figure 8.11) until significant amount of $SeCN^-$ is removed (Figure 8.9). Addition of EDTA at 5 hours results in a sudden increase in sulfate concentration as well as total sulfur which might result from displacement of TiO_2 surface bound sulfate by EDTA. Further decrease in the concentration of sulfate due to adsorption was observed between 5 and 11 hours albeit at a slower rate due to presence of EDTA. Also an increase in the adsorption of sulfate (Figure 8.11) corresponds to the re-appearance of selenocyanate (Figure 8.9) which signifies the displacement of latter by the former from the TiO_2 surface.

Effect of cyanide onto $SeCN^-$ PCD was also investigated and the results are shown in Figures 8.12 and 8.13. Similar to $SeCN^-/SCN^-$ results, re-appearance of $SeCN^-$ is observed after EDTA addition. Figure 8.13 also shows no reduction in cyanide concentration. Also comparing the results from $SeCN^-/SCN^-$ and $SeCN^-/CN^-$ systems, we note that the final $SeCN^-$ concentration for former is lower than in latter, which might result from the presence of more total cyanide in former study.

Photocatalytic removal of $SeCN^-$ in $SeCN^-/CN^-/SCN^-/NH_4^+$ mixed system was also investigated (Figures 8.14 to 8.16). Despite the presence of SCN^- and CN^- species, re-appearance of $SeCN^-$ iss not observed after the addition of EDTA (Figure 8.14), though slower SCN^- degradation is observed for this multi mixed system (Figure 8.16) compared to $SeCN^-/SCN^-$ binary system (Figure 8.11). Also, no significant change iss observed in cyanide and ammonia species (Figure 8.15). Overall, low total selenium and total sulfur

removal were observed in comparison to binary $SeCN^-$/ammonia and $SeCN^-$/thiocyanate systems respectively.

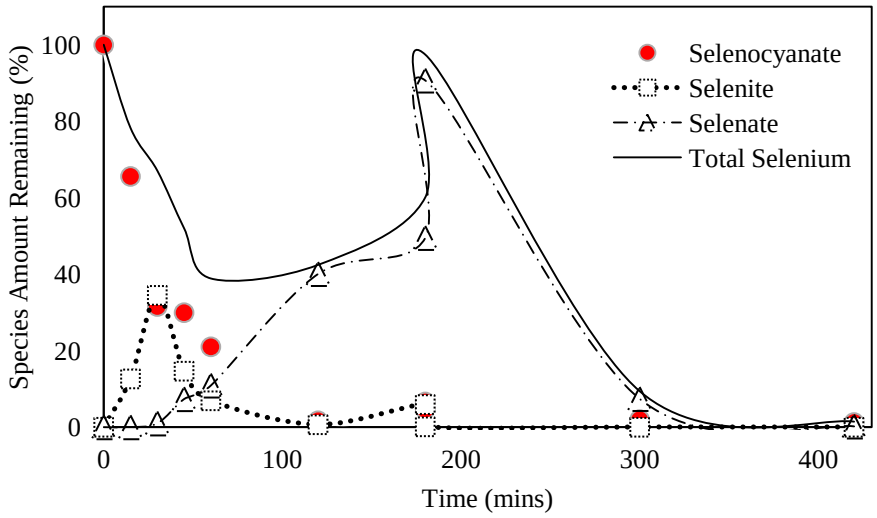

Figure 8.1: Selenium mass balance for UV-light photocatalytic removal of SeCN (10 ppm SeCN, 5 ppm NH_4^+, 300 ppm EDTA, pH 4)

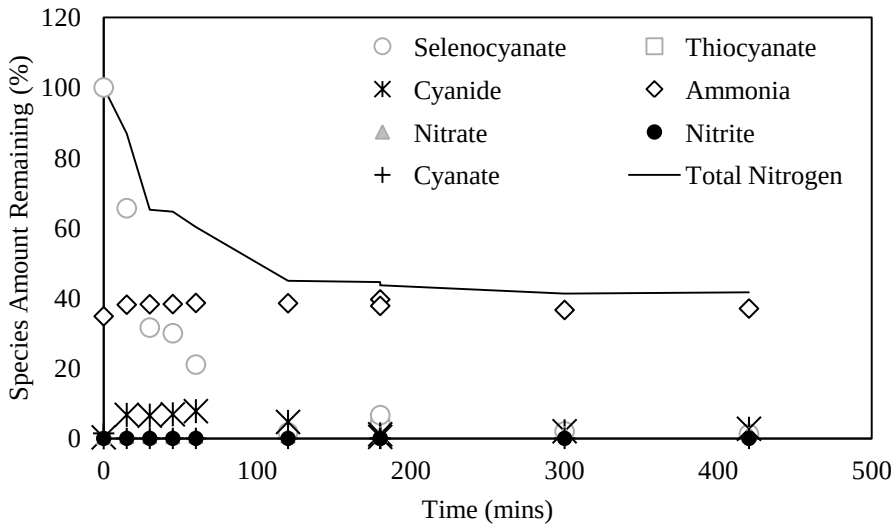

Figure 8.2: Nitrogen mass balance for UV-light photocatalytic removal of SeCN (10 ppm SeCN, 5 ppm NH_4^+, 300 ppm EDTA, pH 4)

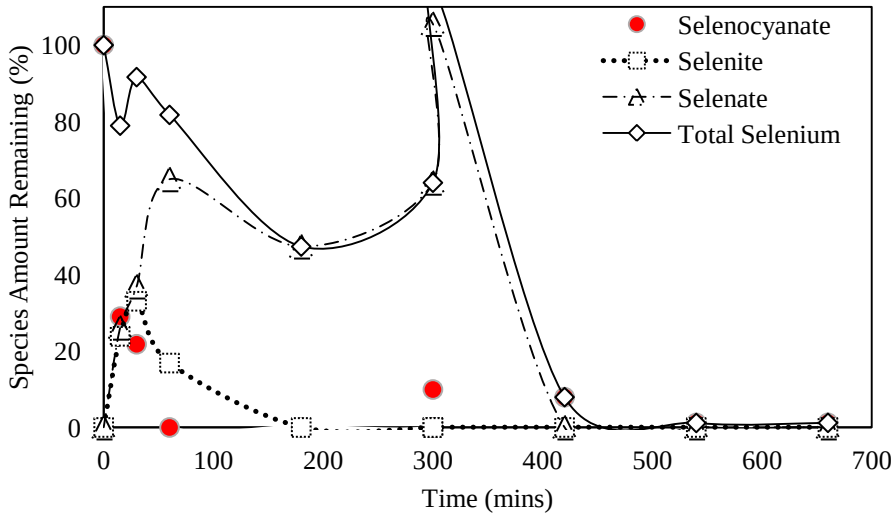

Figure 8.3: Selenium mass balance for UV-light photocatalytic removal of SeCN (10 ppm SeCN, 5 ppm NH_4^+, 300 ppm EDTA added at 300 mins, pH 4)

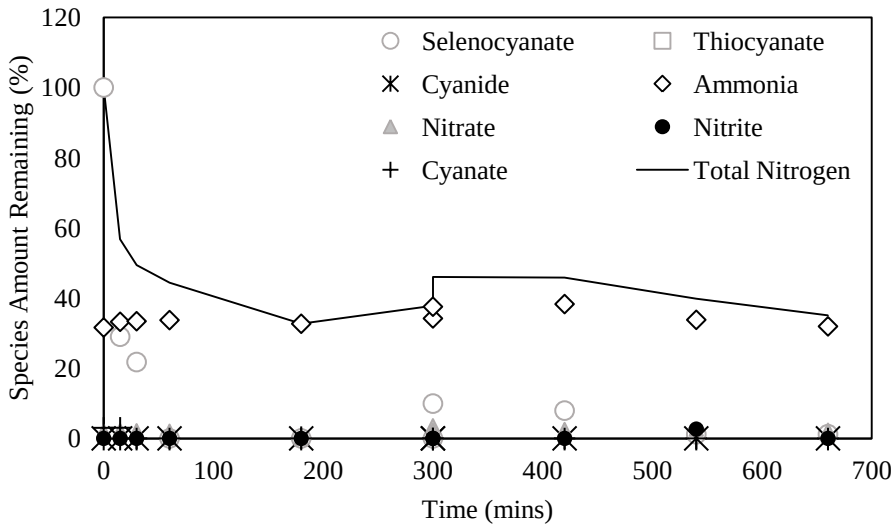

Figure 8.4: Nitrogen mass balance for UV-light photocatalytic removal of SeCN (10 ppm SeCN, 5 ppm NH_4^+, 300 ppm EDTA, pH 4)

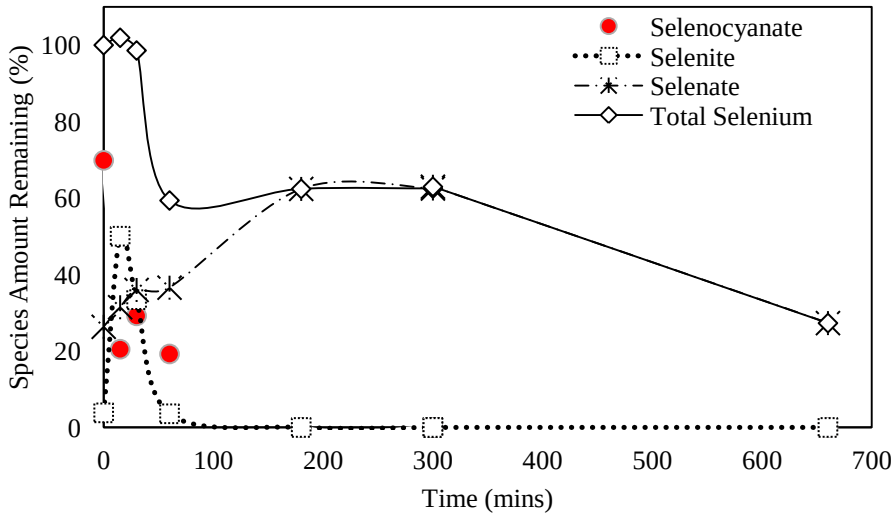

Figure 8.5: Selenium mass balance for UV-light photocatalytic removal of SeCN (10 ppm SeCN, 5 ppm SeO_4^{2-}, 300 ppm EDTA, pH 4)

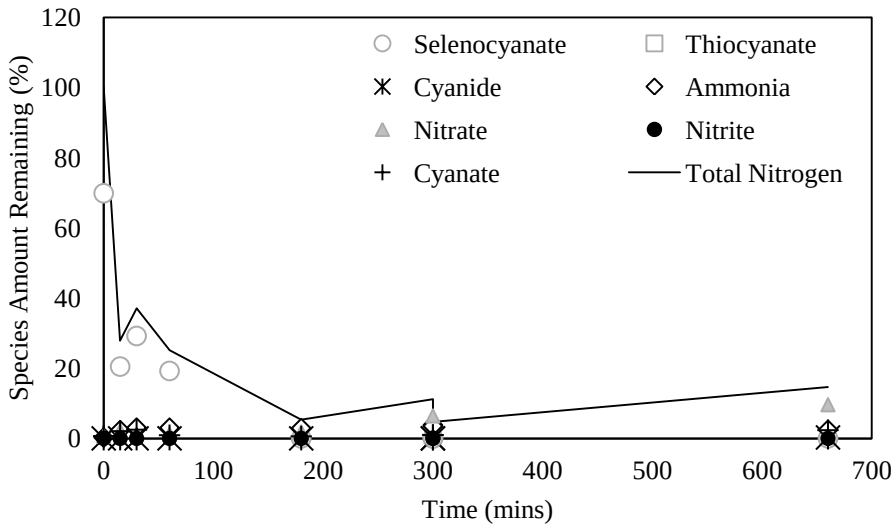

Figure 8.6: Nitrogen mass balance for UV-light photocatalytic removal of SeCN (10 ppm SeCN, 5 ppm SeO_4^{2-}, 300 ppm EDTA, pH 4)

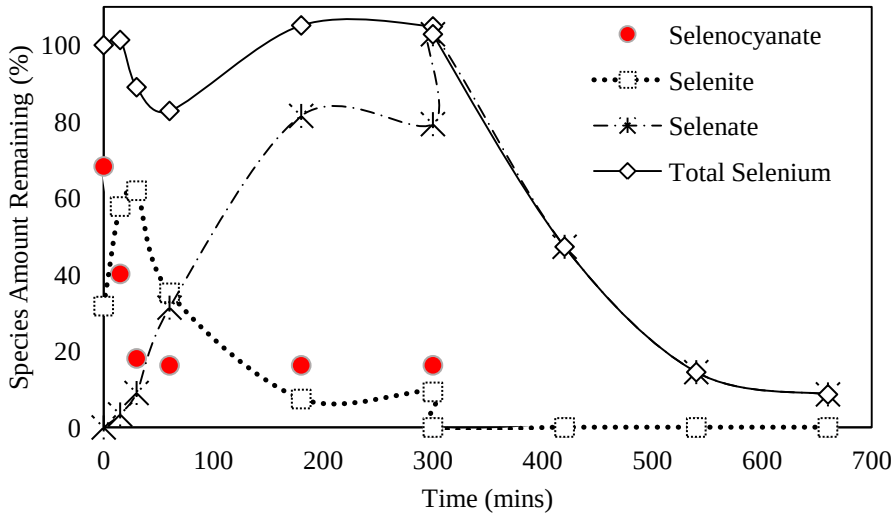

Figure 8.7: Selenium mass balance for UV-light photocatalytic removal of SeCN (10 ppm SeCN, 5 ppm SeO_3^{2-}, 300 ppm EDTA, pH 4)

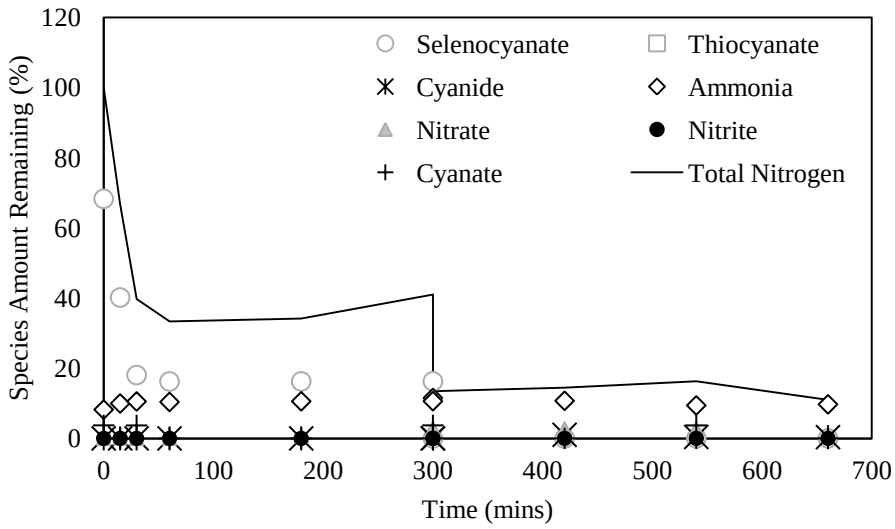

Figure 8.8: Nitrogen mass balance for UV-light photocatalytic removal of SeCN (10 ppm SeCN, 5 ppm SeO_3^{2-}, 300 ppm EDTA, pH 4)

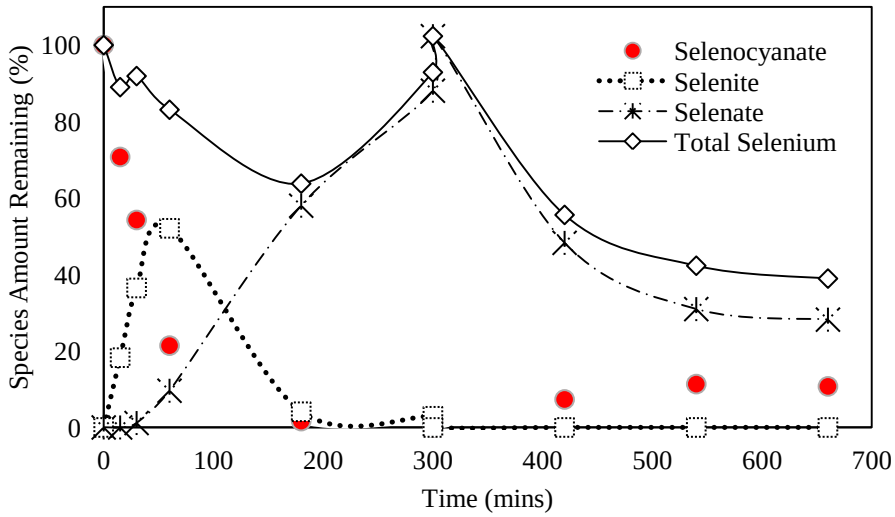

Figure 8.9: Selenium mass balance for UV-light photocatalytic removal of SeCN (10 ppm SeCN, 5 ppm SCN^-, 300 ppm EDTA, pH 4)

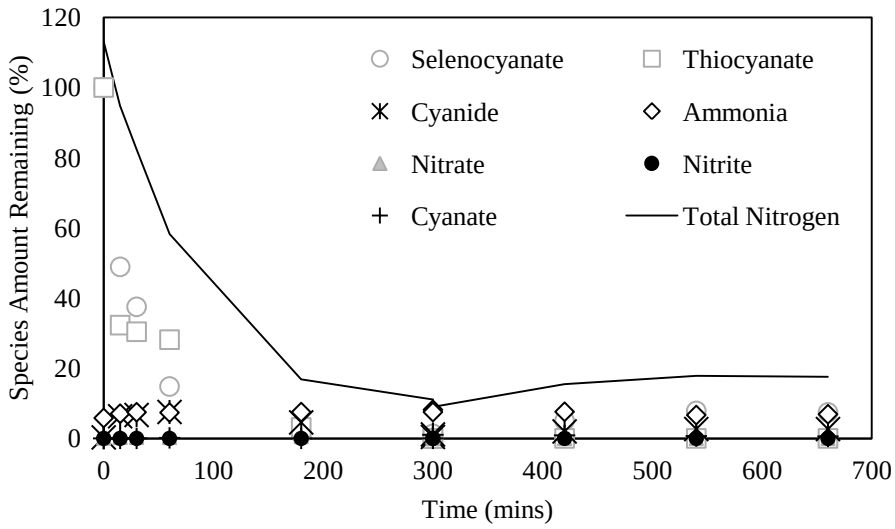

Figure 8.10: Nitrogen mass balance for UV-light photocatalytic removal of SeCN (10 ppm SeCN, 5 ppm SCN^-, 300 ppm EDTA, pH 4)

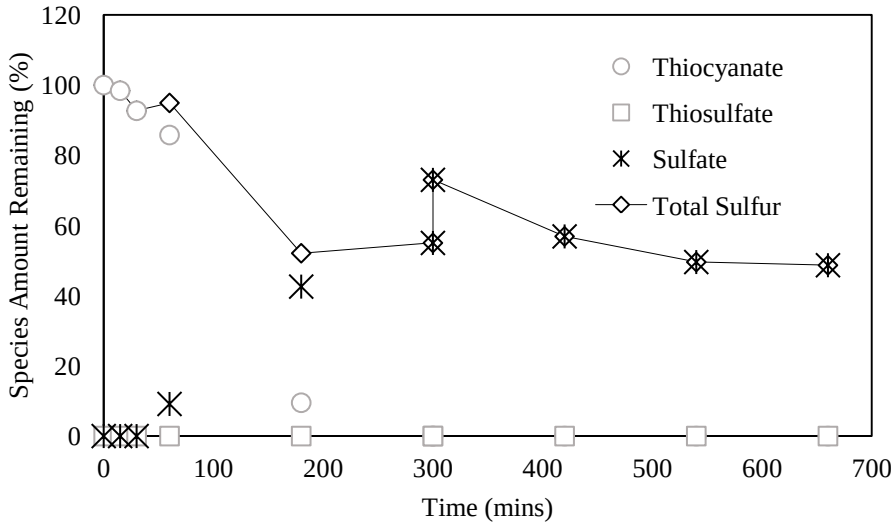

Figure 8.11: Sulfur mass balance for UV-light photocatalytic removal of SeCN (10 ppm SeCN, 5 ppm SCN^-, 300 ppm EDTA, pH 4)

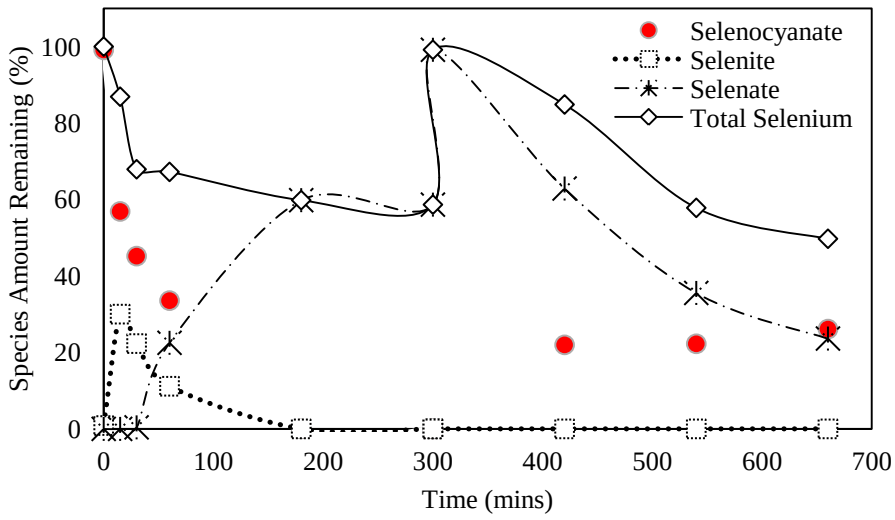

Figure 8.12: Selenium mass balance for UV-light photocatalytic removal of SeCN (10 ppm SeCN, 5 ppm CN^-, 300 ppm EDTA, pH 4)

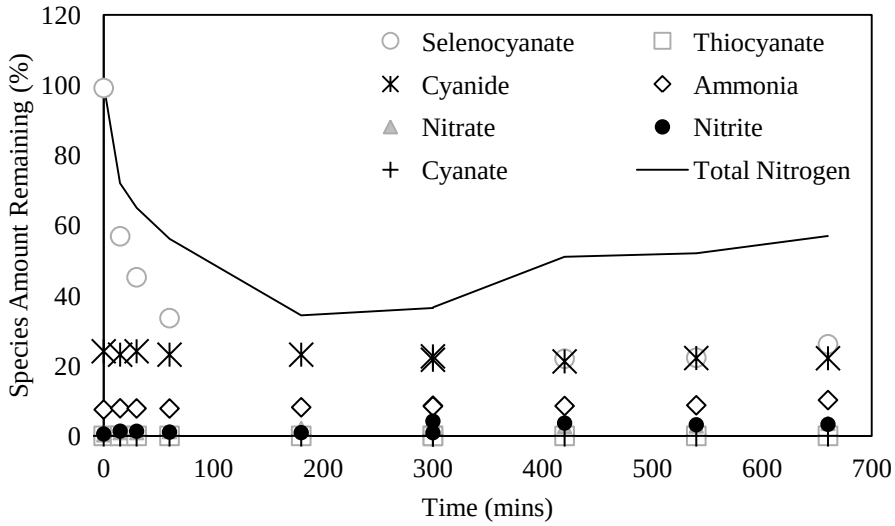

Figure 8.13: Nitrogen mass balance for UV-light photocatalytic removal of SeCN (10 ppm SeCN, 5 ppm CN^-, 300 ppm EDTA, pH 4)

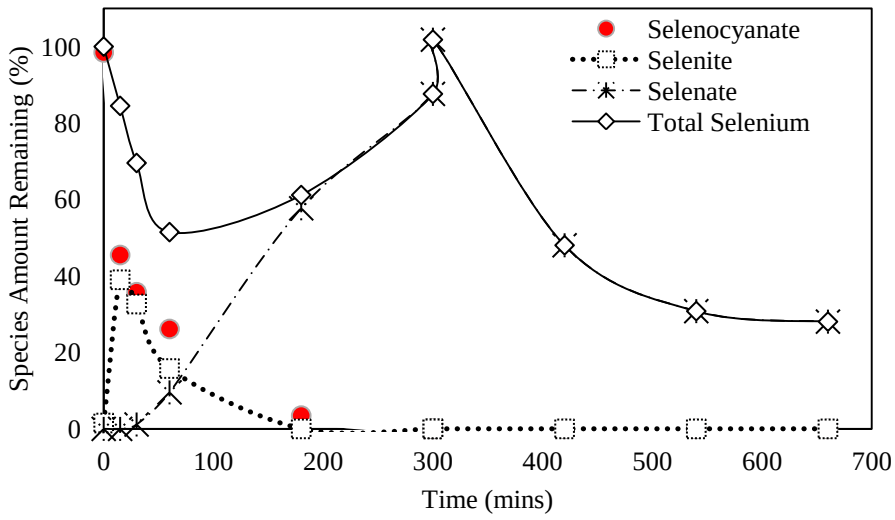

Figure 8.14: Selenium mass balance for UV-light photocatalytic removal of SeCN (10 ppm SeCN, 5 ppm SCN^-, 5 ppm CN^-, 5 ppm NH_4^+,300 ppm EDTA, pH 4)

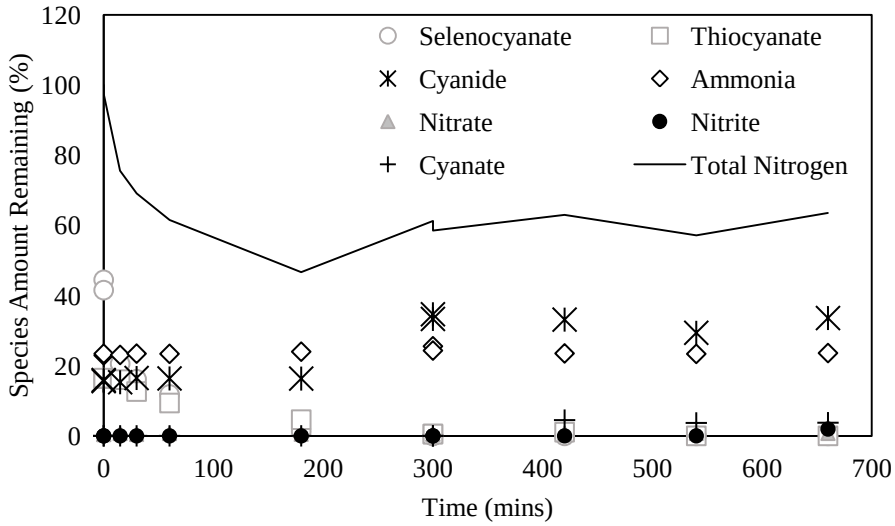

Figure 8.15: Nitrogen mass balance for UV-light photocatalytic removal of SeCN (10 ppm SeCN, 5 ppm SCN^-, 5 ppm CN^-, 5 ppm NH_4^+,300 ppm EDTA, pH 4)

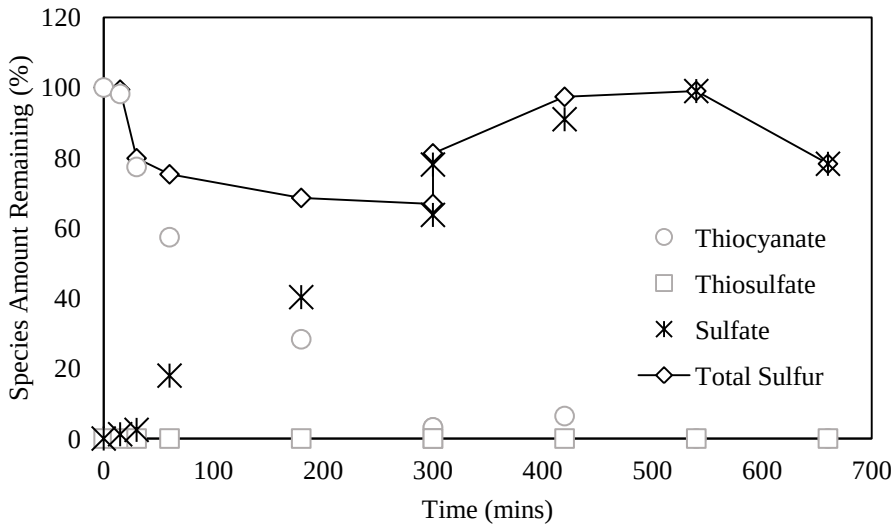

Figure 8.16: Sulfur mass balance for UV-light photocatalytic removal of SeCN (10 ppm SeCN, 5 ppm SCN^-, 5 ppm CN^-, 5 ppm NH_4^+,300 ppm EDTA, pH 4)

8.2 Effect of pH

In this section, the effect of pH on UV-light assisted photocatalytic removal of 10 ppm $SeCN^-$ was investigated for $SeCN/NH_4^+$ and $SeCN^-/CN^-/SCN^-/NH_4^+$ systems. Starting with $SeCN^-/NH_4^+$ systems, an experiment was conducted at pH 10 in the presence of 300 ppm EDTA and the results are shows in Figure 8.17. Comparing the findings in Figure 8.17 with pH 4 results (Figure 8.3), faster selenocyanate degradation was observed here, with near complete $SeCN^-$ disappearance within 1 hour as against 3 hours at pH 10. As explained earlier, this results from electrostatic attraction between positively charged TiO_2 surface and anionic species at low pH values that enhanced adsorption. Higher total selenium increase after 3 hours as a result of displacement of TiO_2 bound selenium ions by EDTA at pH 4 also supports this finding. Also, total selenium removal after 11 hours

of irradiation increases from about 99% at pH 4 (Figure 8.3) to about 54% at pH 10 (Figure 8.17). Similar observations are also noted for $SeCN^-/CN^-/SCN^-/NH_4^+$ systems. Near complete selenocyanate complex destruction was achieved after 3 hours and 5 hours at pH 4 (Figure 8.14) and pH 8 (Figure 8.18) respectively. In addition, decrease in total selenium removal after 11 hours of reaction time is observed due to increase in pH from 4 to 8.

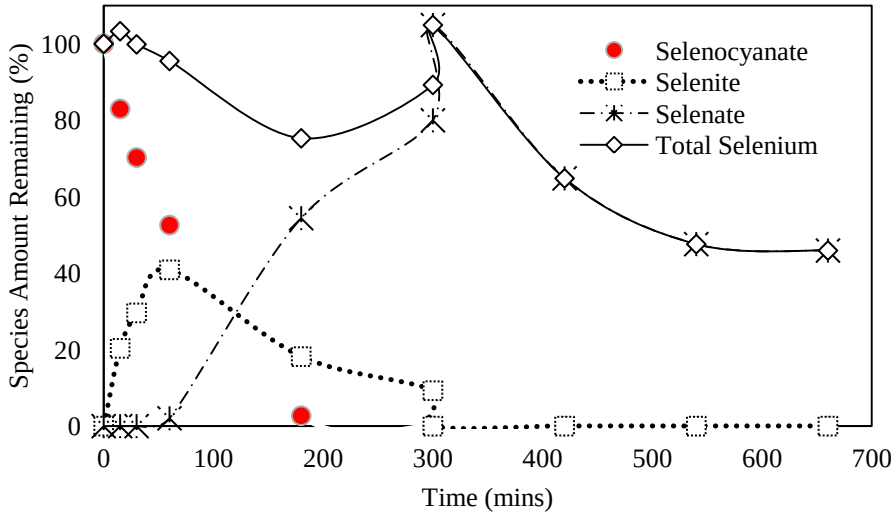

Figure 8.17: Selenium mass balance for UV-light photocatalytic removal of SeCN (10 ppm SeCN,5 ppm NH_4^+,300 ppm EDTA, pH 10)

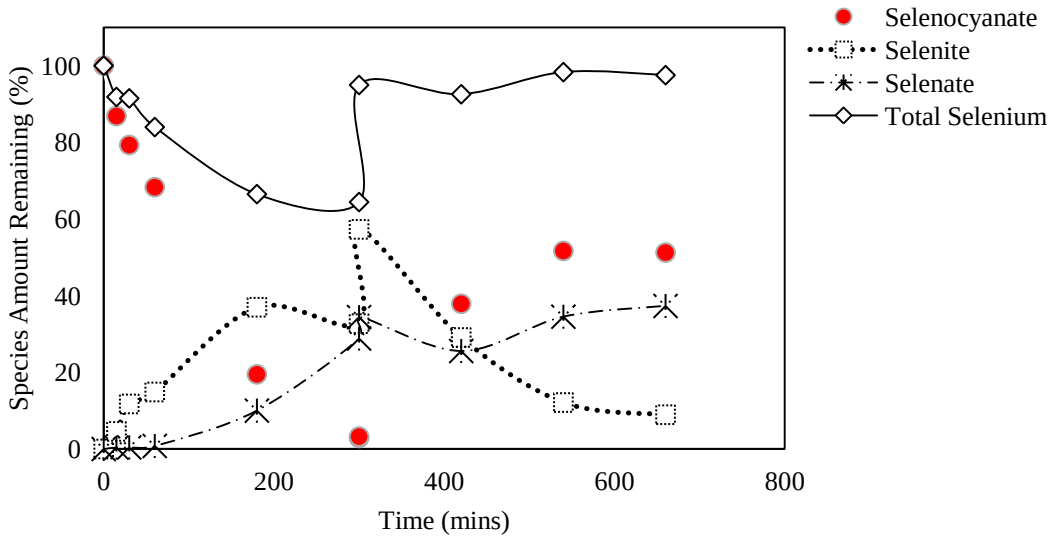

Figure 8.18: Selenium mass balance for UV-light photocatalytic removal of SeCN (10 ppm SeCN, 5 ppm SCN^-, 5 ppm CN^-, 5 ppm NH_4^+,300 ppm EDTA, pH 8)

8.3 Effect of Selenocyanate Concentration

After completing the effect of co-pollutants and pH, we further investigated the effect of initial $SeCN^-$ concentration on its removal. To do that, an experiment was conducted with 20 ppm $SeCN^-$ in the presence of $CN^-/SCN^-/NH_4^+$ using UV-light assisted photocatalysis and the results are presented in Figures 8.19 to 8.21. Comparing $SeCN^-$ photocatalytic reduction to elemental selenium in Figure 8.19 with 10 ppm results displayed in Figure 8.14, increase in $SeCN^-$ removal on mass basis was observed with an increase in initial concentration after 11 hours of irradiation. About 72% (5.5 total selenium as Se) and 62% (9.4 total selenium as Se) SeCN reduction to elemental selenium is achieved for the 10 and 20 ppm respectively. This is similar to the findings of Labaran and Vohra when they investigated the effect of initial selenate concentration on its removal [28]. They

attributed higher selenate reduction to elemental selenium to increased adsorption of the selenate ions. However, a decrease in thiocyanate oxidation to sulfate transpires with an increase in $SeCN^-$ concentration due to increased competition for the photo-generated holes brought by additional $SeCN^-$ in the system.

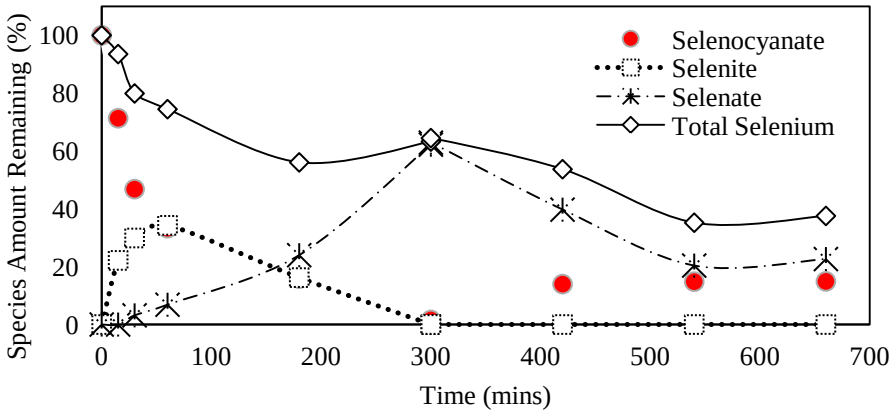

Figure 8.19: Selenium mass balance for UV-light photocatalytic removal of SeCN (20 ppm SeCN, 5 ppm SCN^-, 5 ppm CN^-, 5 ppm NH_4^+,300 ppm EDTA, pH 4

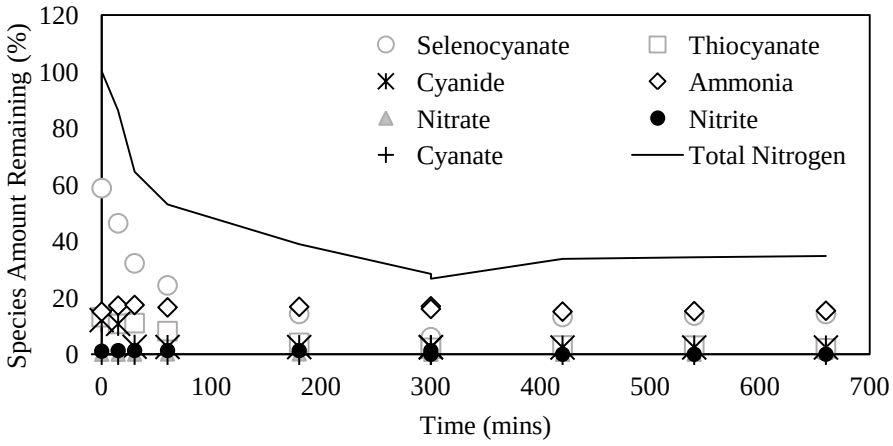

Figure 8.20: Nitrogen mass balance for UV-light photocatalytic removal of SeCN (20 ppm SeCN, 5 ppm SCN^-, 5 ppm CN^-, 5 ppm NH_4^+,300 ppm EDTA, pH 4)

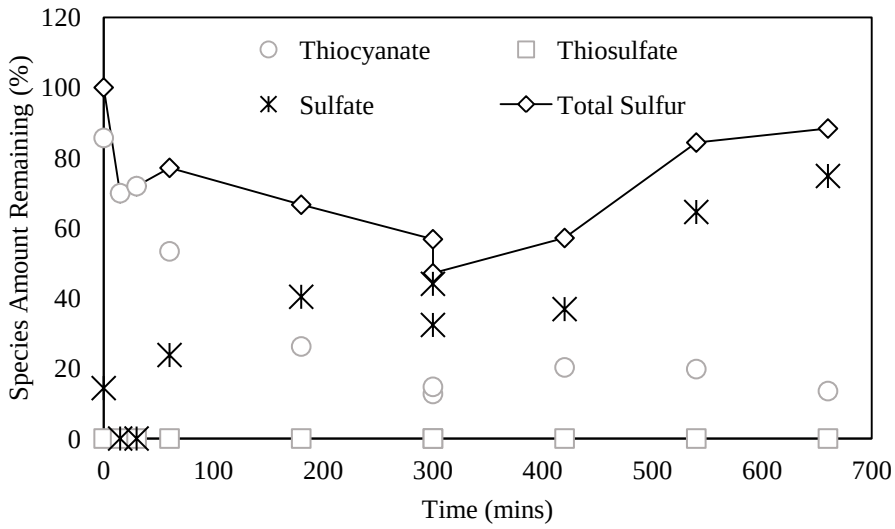

Figure 8.21: Sulfur mass balance for UV-light photocatalytic removal of SeCN (20 ppm SeCN, 5 ppm SCN^-, 5 ppm CN^-, 5 ppm NH_4^+,300 ppm EDTA, pH 4)

UV LIGHT ASSISTED COMPETITIVE PHOTOCATALYTIC REMOVAL OF SELENOCYANATE AND PHENOL

9.1 Effect of pH

9.1.1 10 ppm Selenocyanate Concentration

After looking into the effect of inorganic species SeO_3^{2-}, SeO_4^{2-}, NH_4^+, SCN^- and CN^-, the effect of phenol onto selenocyanate photocatalysis was also investigated. In that regard, several experiments were conducted, at varying process operational conditions as outlined in Table 10.2 as per design of experiment. In that regard, initially, two experiments were conducted at pH 4 and 8 and respective results are shown in Figures 9.2 and 9.4 respectively. Faster selenocyanate destruction is noticed at pH 4 (Figure 9.2), with its near complete removal at 3 hours. As also noted earlier, the appearance of selenite before selenate shows that selenocyanate is first oxidized to selenite and then to selenate. We also noticed a minor benzeneseleninic acid buildup before the appearance of selenate, reaching a maximum of about 2.6% at 45 minute. Selenate was not detected between 0 and 30 mins showing a delay in the conversion of selenite to selenate. This coupled with high selenite adsorption resulted in low total selenium mass balance

between the time frame (0 and 30 mins). However, as selenite converts to selenate, total selenium in aqueous phase also increases, thereby leading to near complete mass balance at 300 mins. This is due to the lower adsorption potential of selenate as compared to selenite. Now looking at the results for the experiment conducted at pH 8 (Figure 9.4), we note negligible benzeneseleninic acid formation, but considerable selenate buildup because of its lower adsorption at pH 8, with overall selenium mass balance noted to be complete between 0 and 5 hours reaction time. Also unlike Figure 9.2 where we note a jump in both selenite and selenate at 300 mins after the addition of EDTA, findings in Figure 9.4 show no such jump, which also indicates that most Se-species are in the aqueous phase at higher pH 8. Furthermore, selenocyanate also reappeared after EDTA addition, but got oxidized later. Nevertheless, the total selenium removal in the presence of phenol is low, i.e., 56% and 50% after 10 hours of irradiation at pH 4 (Figure 9.2) and pH 8 (Figure 9.4) respectively. This indicates that competitive and synergistic effect of phenol and its reaction intermediates onto total selenium removal. We also monitored phenol degradation trends and intermediates formation trends both at pH 4 (Figure 9.3) and pH 8 (Figure 9.5). At pH 4, near complete phenol removal is achieved within 3 hours of irradiation. Comparison of results in Figure 9.3 and 9.5 also shows that an increase in pH lead to faster phenol degradation kinetic, with complete phenol removal achieved within 1 hour at pH 8. The quantitative assessment of some intermediates showed minor formation of hydroquinone and benzeneseleninic acid from the beginning of the experiment, while resorcinol and pyrocatechol were only detected after 30 and 15 mins of irradiation respectively. Hydroquinone concentration increases from about 0.5% at time 0

to a maximum value of about 4% after 1 hour of irradiation. Maximum seleninic acid formation of about 5% was observed at 45 minute reaction time. Neither phenol nor its degradation intermediates were detected after 5 hours of irradiation. Therefore, we suggest mineralization of phenol to carbon dioxide through the formation of during the course of reaction as also suggested decrease in TOC results with time (data not shown). Some of possible reactions occurring during the phenol-$SeCN^-$ photocatalysis are provided in equation 9.1. to 9.8. Phenol oxidation to the three benzenediols proceeds according to equation 9.1. However, oxidation of phenol to benzeneseleninic acid is suggested to proceed either from direct reaction between selenocyanate and phenol to form benzeneseleninic acid (equation 9.2), or reaction between phenol and selenocyanate to form phenyl selenocyanate (equation 9.3), followed by quick oxidation of phenyl selenocyanate to benzeneseleninic acid (equation 9.4). However, since phenyl selenocyanate was not detected, benzeneseleninic acid formation is more likely by equation 9.2. In addition to the primary intermediates mentioned, some small peaks were also detected but not in measurable quantities due to their small concentrations. Other reactions such as oxidation of hydroquinone to maleic acid and acetylene (equation 9.5), oxidation of pyrocatechol to oxalic acid and acetylene (equation 9.6), oxidation of resorcinol to fumaric acid and acetylene (equation 9.7) and reduction of benzeneseleninic acid to dimethyl selenide (equation 9.8) are also possible among other intermediate reactions. Intermediate formations at pH 8 and its comparison with the pH 4 results show that hydroquinone formation increases with an increase in pH while benzeneseleninic

acid decreases with an increase in pH. Faster selenocyanate destruction and higher selenite adsorption at pH 4 favors the formation of benzeneseleninic acid.

$$C_6H_5OH + H_2O \leftrightharpoons C_6H_4(OH)_2 + 2H^+ + 2e^- \quad 9.1$$

$$C_6H_5OH + SeCN^- + H_2O \leftrightharpoons C_6H_5SeO_2H + CN^- + H^+ + e^- \quad 9.2$$

$$C_6H_5OH + SeCN^- + H^+ \leftrightharpoons C_6H_5SeCN + H_2O \quad 9.3$$

$$C_6H_5SeCN + 2H_2O \leftrightharpoons C_6H_5SeO_2H + HCN + 2H^+ + 2e^- \quad 9.4$$

$$C_6H_4(OH)_2 + 2H_2O \rightleftharpoons HO_2CCHCHCO_2H + C_2H_2 + 4H^+ + 4e^- \quad 9.5$$

$$C_6H_4(OH)_2 + 2H_2O \rightleftharpoons HO_2CCO_2H + 2C_2H_2 + 4H^+ + 4e^- \quad 9.6$$

$$C_6H_4(OH)_2 + 2H_2O \rightleftharpoons HO_2CCHCHCO_2H + C_2H_2 + 4H^+ + 4e^- \quad 9.7$$

$$C_6H_5SeO_2H + 8H^+ + 8e^- \leftrightharpoons CH_3SeCH_3 + 2C_2H_2 + 2H_2O \quad 9.8$$

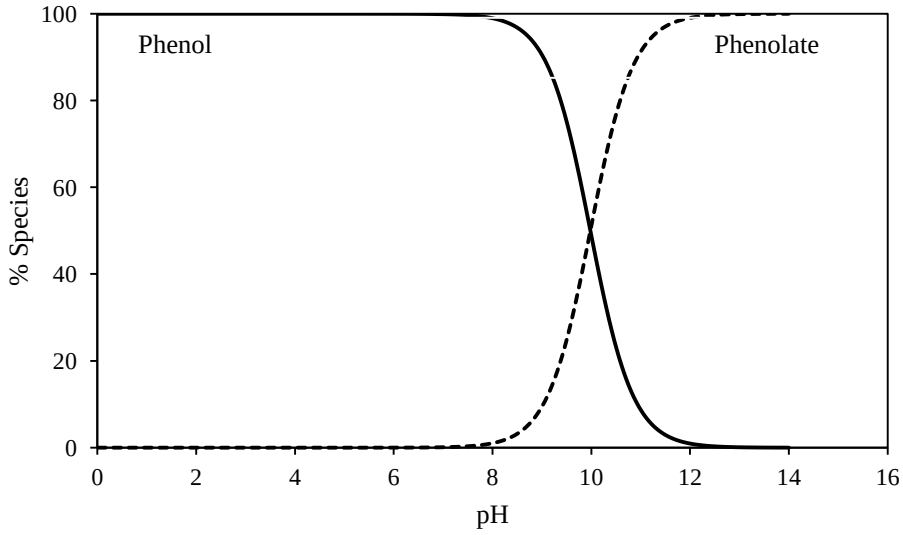

Figure 9.1: Phenol speciation diagram as a function of pH (Calculated using MINTEQ software).

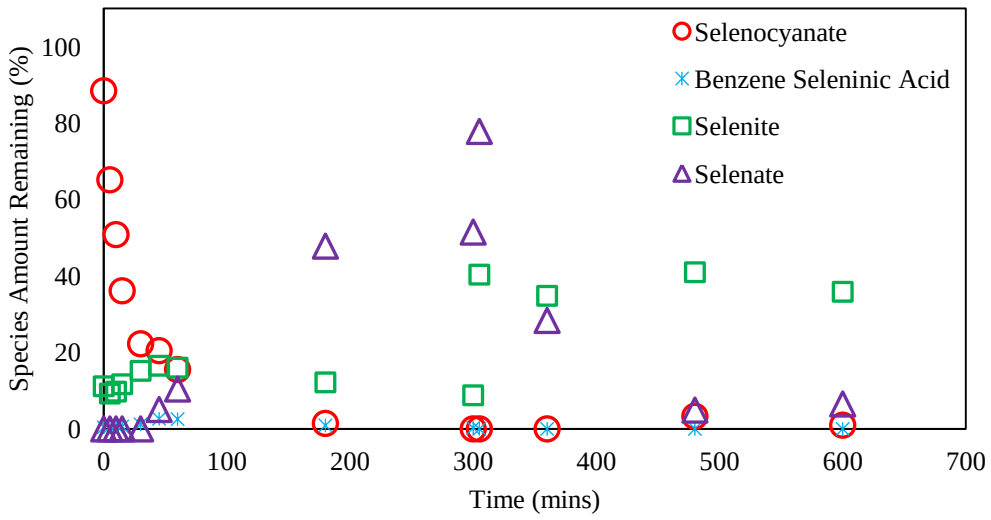

Figure 9.2: Trends from UV light photocatalytic destruction of selenocyanate at pH 4 (10 ppm selenocyanate, 5 ppm phenol, 150 ppm EDTA added at 5 hours).

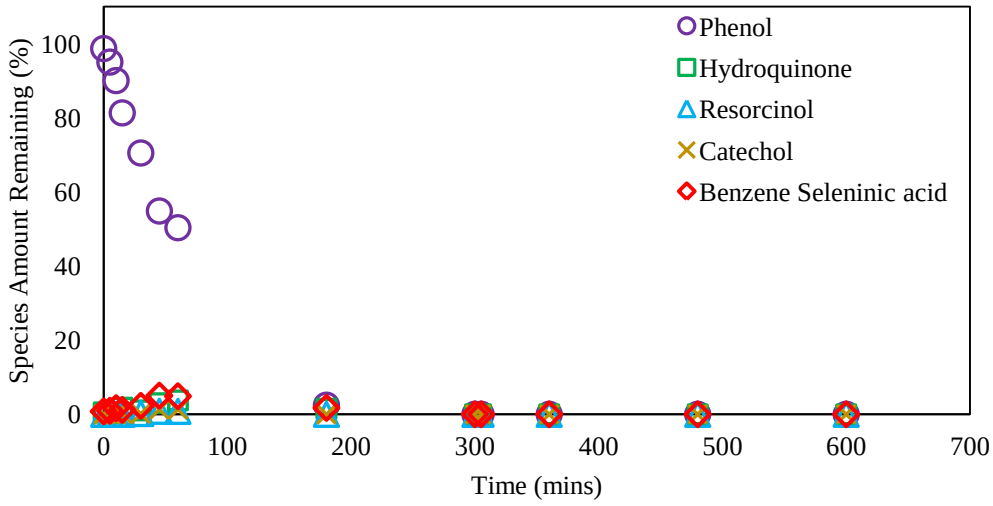

Figure 9.3: Trends from UV light photocatalytic destruction of phenol at pH 4 (10 ppm selenocyanate, 5 ppm phenol, 150 ppm EDTA added at 5 hours).

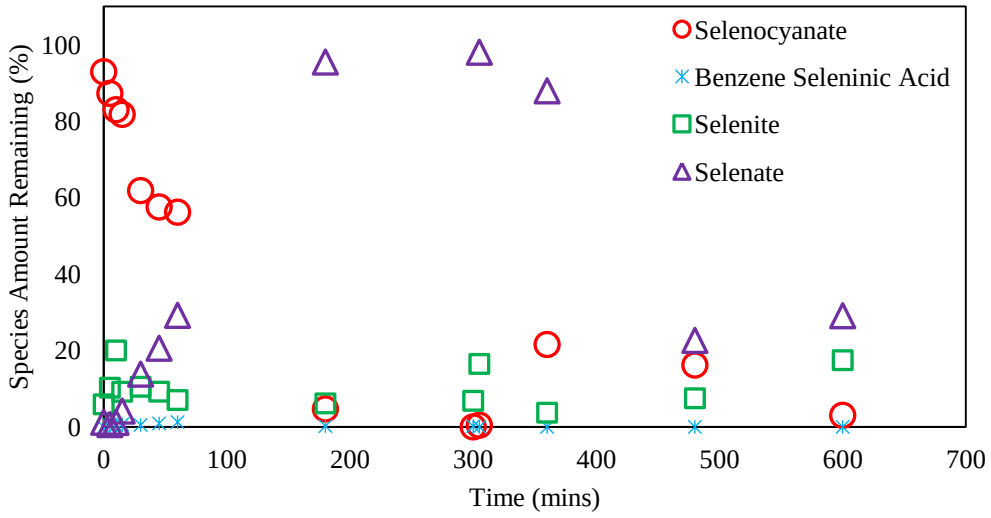

Figure 9.4: Trends from UV light photocatalytic destruction of selenocyanate at pH 8 (10 ppm selenocyanate, 5 ppm phenol, 150 ppm EDTA added at 5 hours).

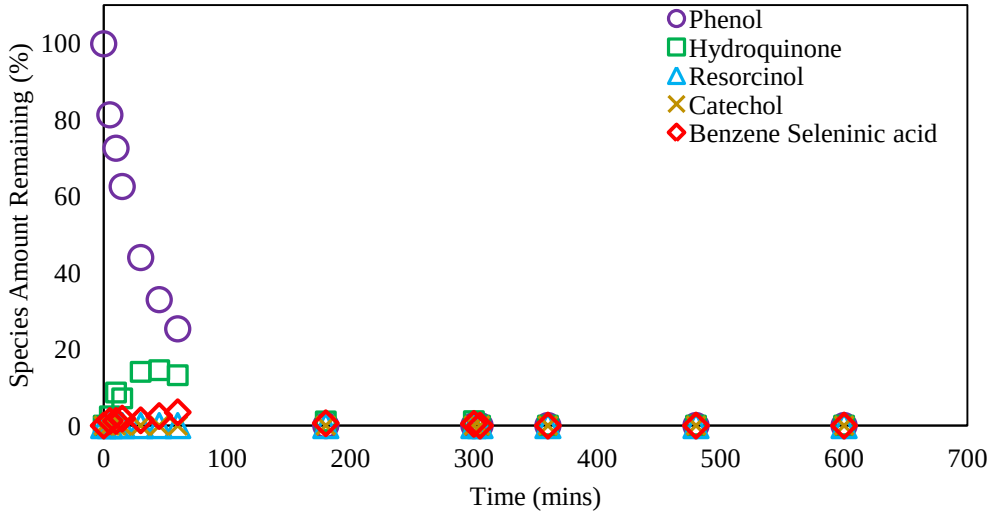

Figure 9.5: Trends from UV light photocatalytic destruction of phenol at pH 8 (10 ppm selenocyanate, 5 ppm phenol, 150 ppm EDTA added at 5 hours).

As noted above that both at pH 4 and 8, the total selenium removal was about 50%, hence we also investigated use of higher 300 ppm EDTA for greater reduction of selenite/selenate to elemental selenium and the respective results at pH 4 as given in Figure 9.6 show comparatively larger total selenium removal. An exponential destruction of selenocyanate with time (Figure 9.6). Also similar to the results presented in Figure 2, conversion of selenite to selenate is delayed. Benzeneseleninic acid formation trends were also similar to those in Figure 2. An almost linear reduction of selenite and selenate is also observed between 5 hours and 6 hours. However, after 7 hours, the rate of selenite reduction decreases accompanied by reappearance of selenocyanate. Formation of selenite and selenate at pH 6 (Figure 9.8) is faster than at pH 4 (Figure 9.6). Benzeneseleninic acid formation was less than 1% throughout the course of reaction, showing a decrease in its formation with an increase in pH. Nevertheless, complete mass balance is noted between 0 and 5 hours. Comparing selenate reduction to elemental selenium after EDTA addition, a decrease is observed when the pH is increased from 4 to 6. Unlike pH 4, no reappearance of selenocyanate is observed at pH 6, however total selenium removal is low with a possible explanation of lower selenate adsorption at pH 6. A somewhat similar trend is also noted at pH 8 (Figure 9.10). Also an increased selenate formation between 0 and 5 hours is observed at pH 8 (Figure 9.10) compared to pH 4 (Figure 9.6) and 6 (Figure 9.8), with an almost linear increase in selenate formation at 5 hour reaction time. Benzeneseleninic acid formation was negligible which then shows a decrease from pH 4 till 8. Now looking at pH 10 results (Figure 9.12), the destruction of selenocyanate is slower with more than 20% selenocyanate remaining in solution after 5

hours of irradiation and before the addition of EDTA. Formation of selenate is also negligible within the above-mentioned duration, with selenite and selenate almost completing the mass balance. However, after EDTA addition, selenocyanate destruction proceeds at a very slow rate due to competitive EDTA oxidation and we also note selenite conversion to selenate. Now comparing the respective phenol degradation and intermediates formation results at pH 4 (Figure 9.7), phenol is completely removed within 3 hours of reaction time accompanied by a minor benzeneseleninic acid, hydroquinone, and catechol formation. Benzeneseleninic acid formation trends show a buildup of about 6% within 10 minutes, which disappeared after 3 hours. Hydroquinone and catechol were detected between 15 minutes and 3 hours. Increase in pH from 4 (Figure 9.7) to 6 (Figure 9.9) lead to an increase in phenol removal at all reaction time. This is however accompanied by a decrease in benzeneseleninic acid formation because of a decrease in selenocyanate degradation rate as explained earlier. Further increase in pH from 6 (Figure 9.9) to 8 (Figure 9.11) also lead to an increase in phenol removal at all reaction time. Benzeneseleninic acid formation is almost negligible, with notable hydroquinone formation observed till 5 hours. Hydroquinone formation at pH 8 is the highest. Nevertheless, a further increase in initial pH from 8 (Figure 9.11) to 10 (Figure 9.13) lead to a decrease in phenol removal. This might be attributed to electrostatic repulsion between the negatively charged TiO_2 particle and phenol speciation to phenolate (Figure 9.1). Though at pH 10, phenol will still be dominant species considering a pKa value of 9.9 [146-151] with some phenolate, however TiO^- will be the most dominant TiO_2 species. O'Sea and Cardona (1995) reported an increase in phenol

initial degradation rates between pH 1 and pH 7, and a decrease between pH 7 and 11, with near complete phenol removal was achieved after 8 hour reaction time [152].

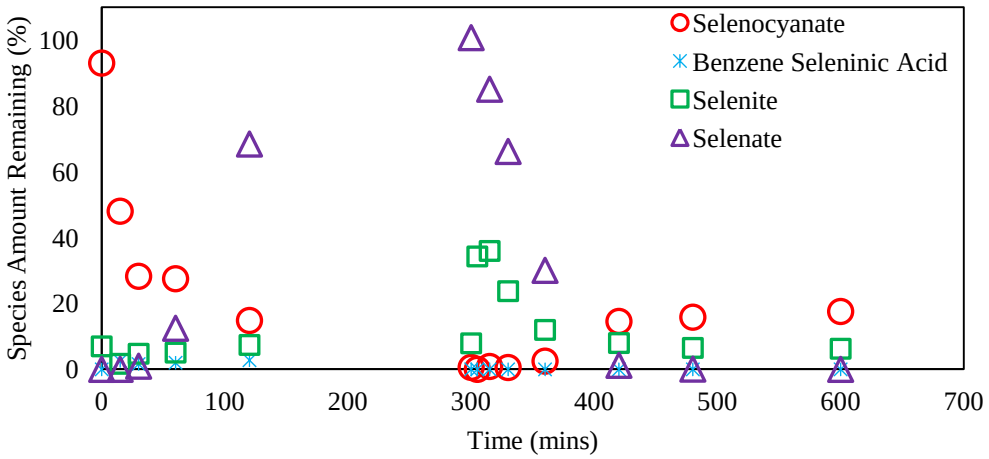

Figure 9.6: Trends from UV light photocatalytic destruction of selenocyanate at pH 4 (10 ppm selenocyanate, 5 ppm phenol, 300 ppm EDTA added at 5 hours).

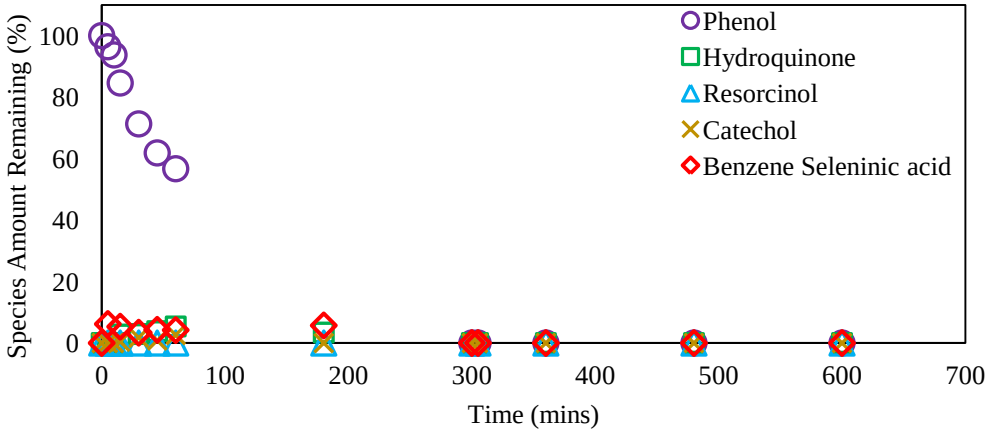

Figure 9.7: Trends from UV light photocatalytic destruction of phenol at pH 4 (10 ppm selenocyanate, 5 ppm phenol, 300 ppm EDTA added at 5 hours).

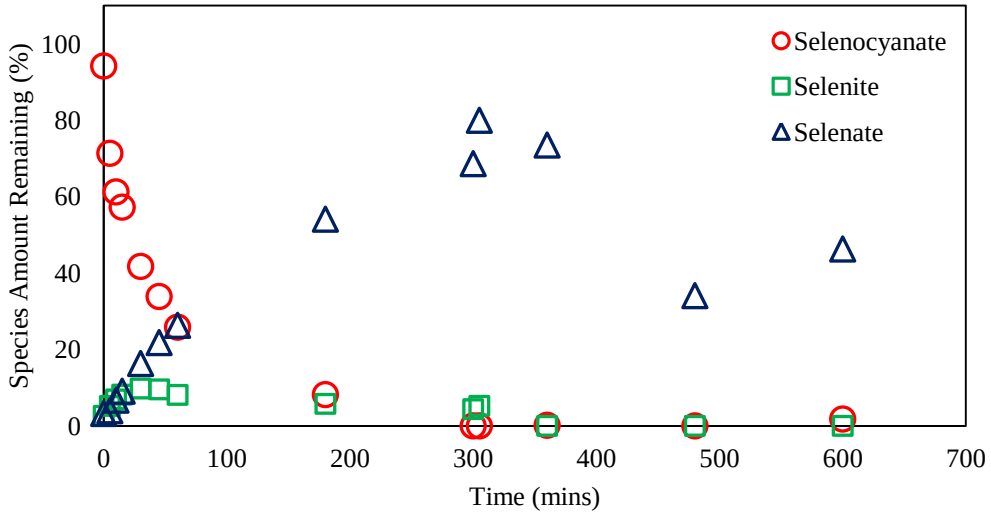

Figure 9.8: Trends from UV light photocatalytic destruction of selenocyanate at pH 6 (10 ppm selenocyanate, 5 ppm phenol, 300 ppm EDTA added at 5 hours).

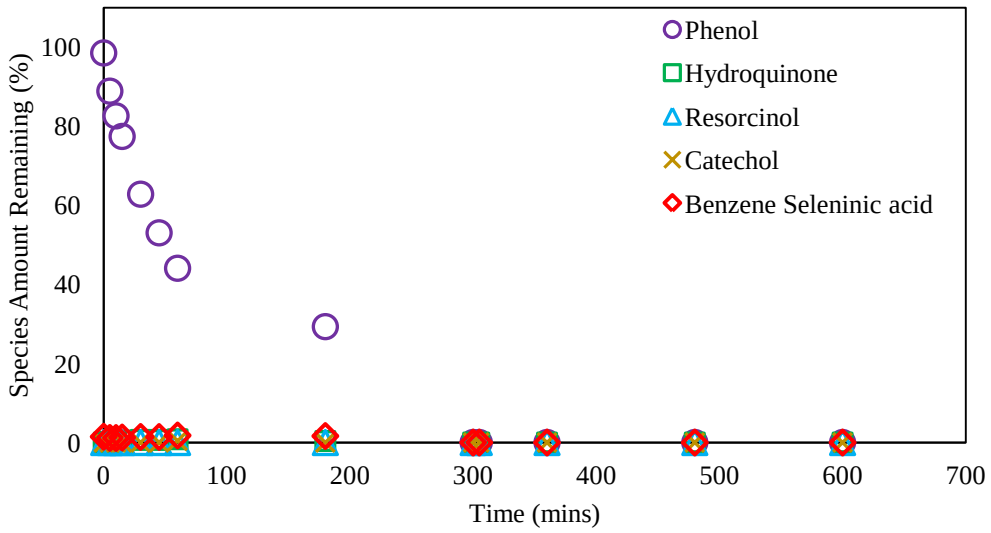

Figure 9.9: Trends from UV light photocatalytic destruction of phenol at pH 6 (10 ppm selenocyanate, 5 ppm phenol, 300 ppm EDTA added at 5 hours).

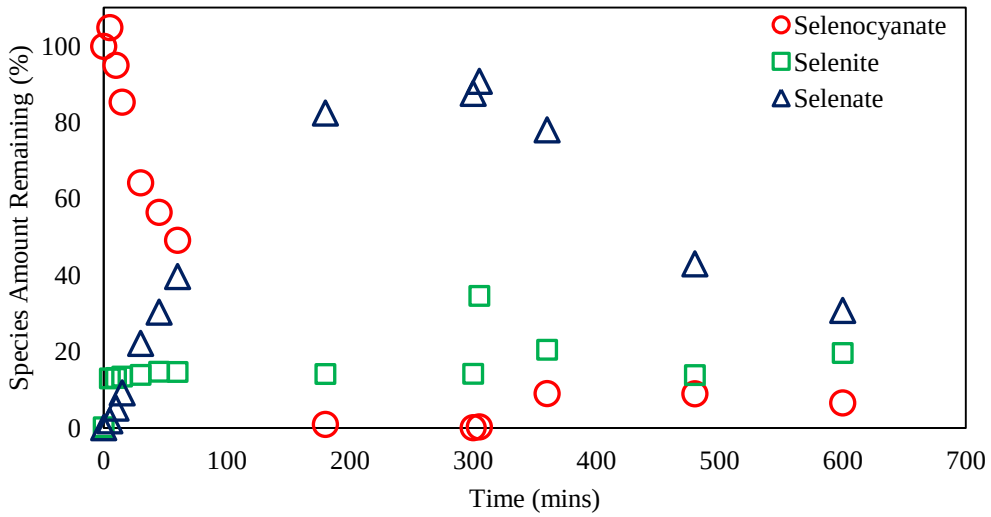

Figure 9.10: Trends from UV light photocatalytic destruction of selenocyanate at pH 8 (10 ppm selenocyanate, 5 ppm phenol, 300 ppm EDTA added at 5 hours).

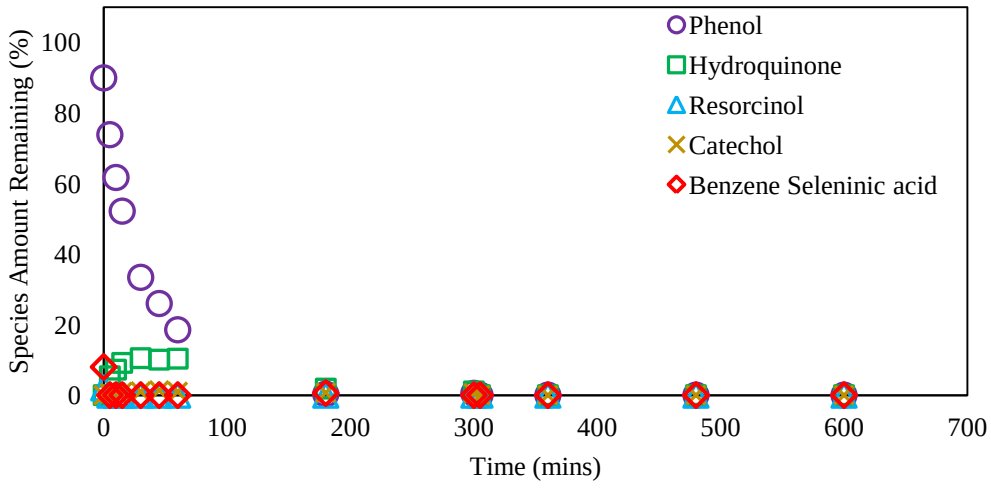

Figure 9.11: Trends from UV light photocatalytic destruction of phenol at pH 8 (10 ppm selenocyanate, 5 ppm phenol, 300 ppm EDTA added at 5 hours).

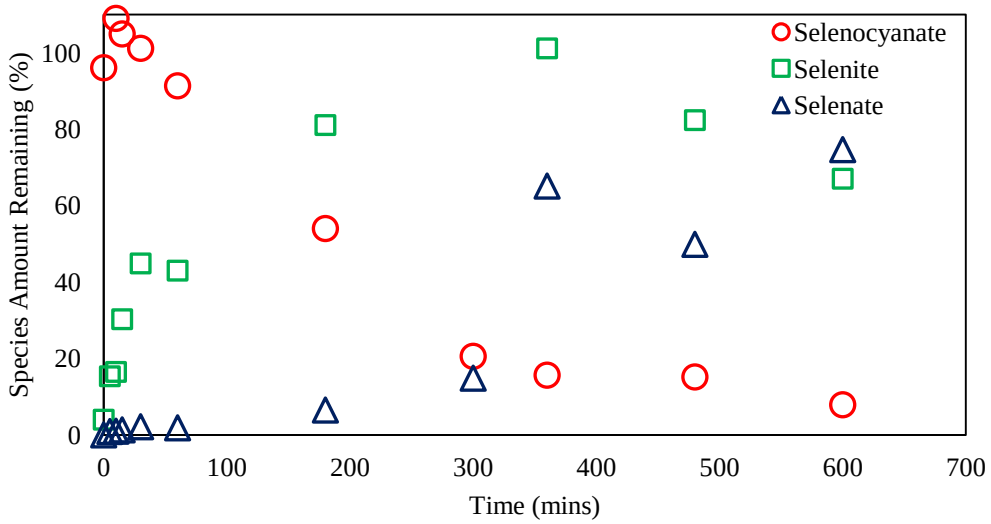

Figure 9.12: Trends from UV light photocatalytic destruction of selenocyanate at pH 10 (10 ppm selenocyanate, 5 ppm phenol, 300 ppm EDTA added at 5 hours).

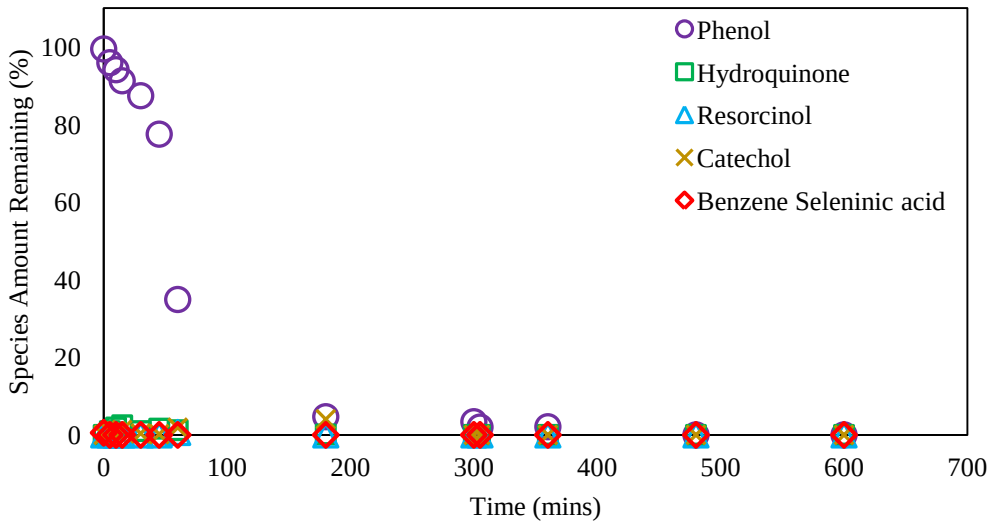

Figure 9.13: Trends from UV light photocatalytic destruction of at pH 10 (10 ppm selenocyanate, 5 ppm phenol, 300 ppm EDTA added at 5 hours).

The above mentioned incomplete total selenium removal even at low pH 4 and employing 300 ppm EDTA, prompted to try a higher concentration of the hole/h^+ scavenging agent EDTA, i.e., 450 ppm, to achieve near complete total selenium removal. The respective results at pH 4 are provided in Figure 9.14. Similar to the results in Figures 9.2 and 9.6, faster selenocyanate destruction was also observed at pH 4 in the presence of 450 ppm EDTA concentration (Figure 9.14). At pH 4, the destruction of selenocyanate is almost complete after 5 hours of irradiation. Selenocyanate is first converted to selenite and then to selenate as observed in the previous results with negligible organic selenium formation as compared to inorganic selenium. As observed for previous pH 4 results (Figures 9.2 and 9.6), selenate formation in Figure 9.14 is also delayed, with selenate appearing in the solution only after 1 hour of irradiation time. Total selenium decreases with time because of selenate and selenite reduction after EDTA addition. The total selenium removal is higher than reported in Figure 9.2 and 9.6 due to higher amount of EDTA which causes decreased recombination of photo-generated holes and electrons and hence higher availability of later for selenite and selenate reduction. Increase in the pH from 4 (Figure 9.14) to pH 8 (Figure 9.15) results in decreased rate of selenocyanate destruction and an increase in the rate of selenate formation. After EDTA addition, increase in selenite and selenate concentrations is observed because of desorption as caused by EDTA adsorption. The selenite and selenate are then reduced to elemental selenium. While selenite reduction is almost complete after 8 hour of irradiation, selenate reduction proceeds linearly even at 10 hours. About 20% selenate concentration remains at 10 hours which might be as a result of partial reduction of selenate due to decrease in EDTA concentration. Overall total selenium removal after 10 hours of irradiation stood at about 87% and 55% at pH 4 and pH 8 respectively.

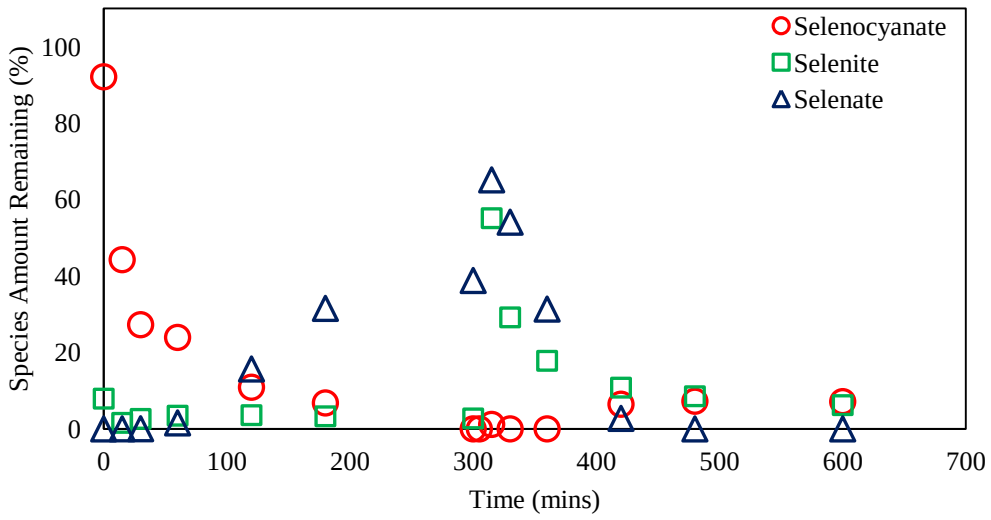

Figure 9.14: Trends from UV light photocatalytic destruction selenocyanate at pH 4 (10 ppm selenocyanate, 5 ppm phenol, 450 ppm EDTA added at 5 hours).

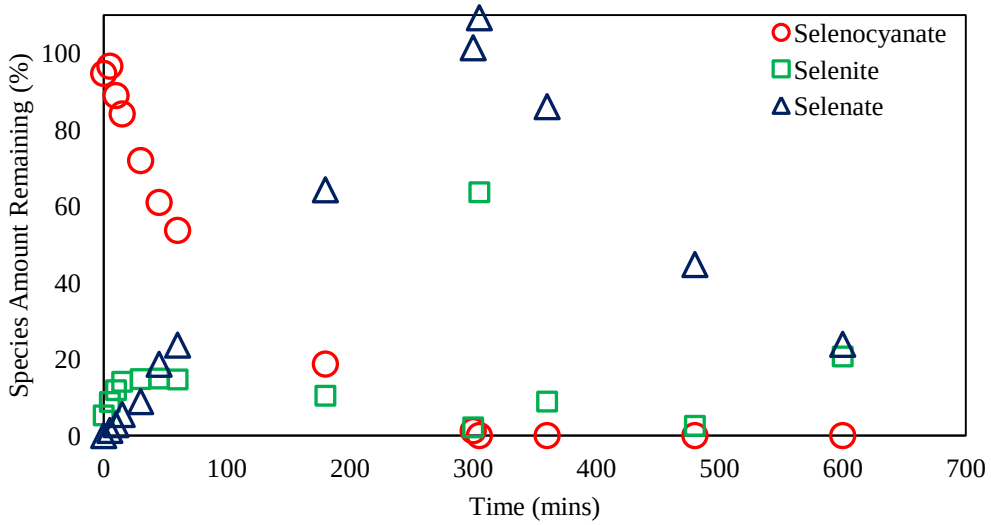

Figure 9.15: Trends from UV light photocatalytic destruction of selenocyanate at pH 8 (10 ppm selenocyanate, 5 ppm phenol, 450 ppm EDTA added at 5 hours).

After successful investigating the effect of pH on photocatalytic removal of 10 ppm selenocyanate and 5 ppm phenol under varying EDTA concentrations, we then investigated the respective systems at higher phenol concentration of 15 ppm. Figures 9.16 and 9.18 shows experimental trend for the removal of 10 ppm selenocyanate in the presence of 15 ppm phenol and 150 ppm EDTA. For pH 4 results (Figure 9.16), the general trends for selenocyanate destruction and intermediates (selenite and selenate) formation are similar to those in Figures 9.2, 9.6 and 9.14; A total selenium removal of about 51% is achieved after 10 hours of irradiation is lower due to higher phenol concentration (15 ppm) and also because of lower 150 ppm EDTA amount. High phenol concentration results in competitive oxidation between selenocyanate and phenol, whereas as the low EDTA is sufficient to minimize electrons and holes recombination, which in turn decreases photocatalytic reduction efficiency of both selenite and selenate. Trends in Figure 9.18 showing results at pH 8 are somewhat different from the other respective systems at pH 8 discussed earlier (Figures 9.4, 9.10 and 9.15). Results in Figure 9.18 shows a delay in selenate formation similar to that observed at pH 4 (but not at pH 8) in the presence of 5 ppm phenol. This might be as a result of an increase in competitive adsorption and oxidation between the added phenol and selenocyanate. Overall total selenium removal after 10 hours of irradiation decreases from 51% at pH 4 (Figure 9.16) to 41% at pH 8 (Figure 9.18). Phenol degradation and intermediates formation for the experiments discussed above are presented in Figures 17 and 19. About 99% phenol was observed at pH 4. Overall phenol removal increases with an increase in pH from 4 to 8 at all reaction time. For example, 4%, 10%, and 14% increase in phenol

removal was observed at 10, 30 and 60 minutes respectively when initial pH was increased from 4 to 8. Similar to most of the results at pH 4, minor amounts of benzeneseleninic acid and hydroquinone were detected before pyrocatechol and resorcinol. Peak intermediates formation is in the order hydroquinone > pyrocatechol > benzeneseleninic acid > resorcinol. Results in Figure 19 obtained at pH 8 also show complete phenol removal with a decrease noted in benzeneseleninic acid formation and increase in hydroquinone formation compared to pH 4 results (9.17).

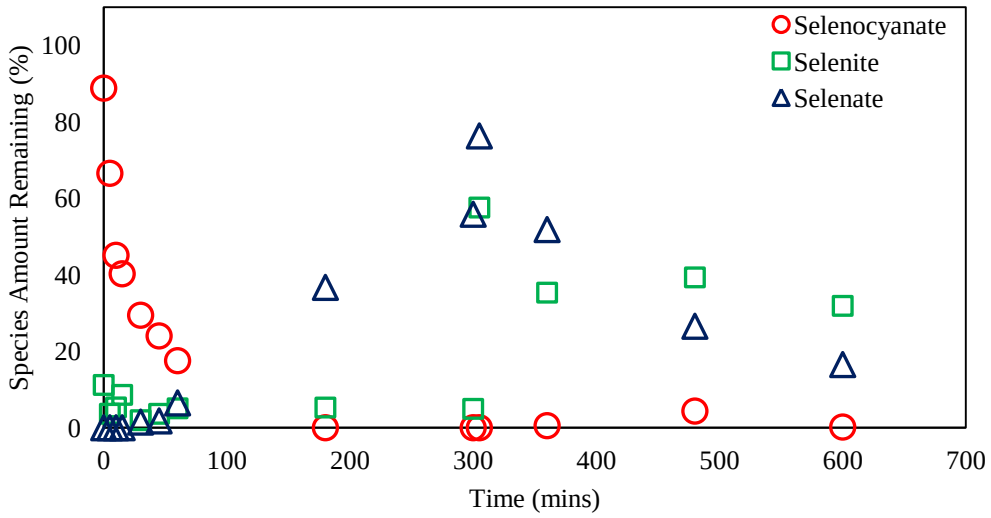

Figure 9.16: Trends from UV light photocatalytic destruction of selenocyanate at pH 4 (10 ppm selenocyanate, 15 ppm phenol, 150 ppm EDTA added at 5 hours).

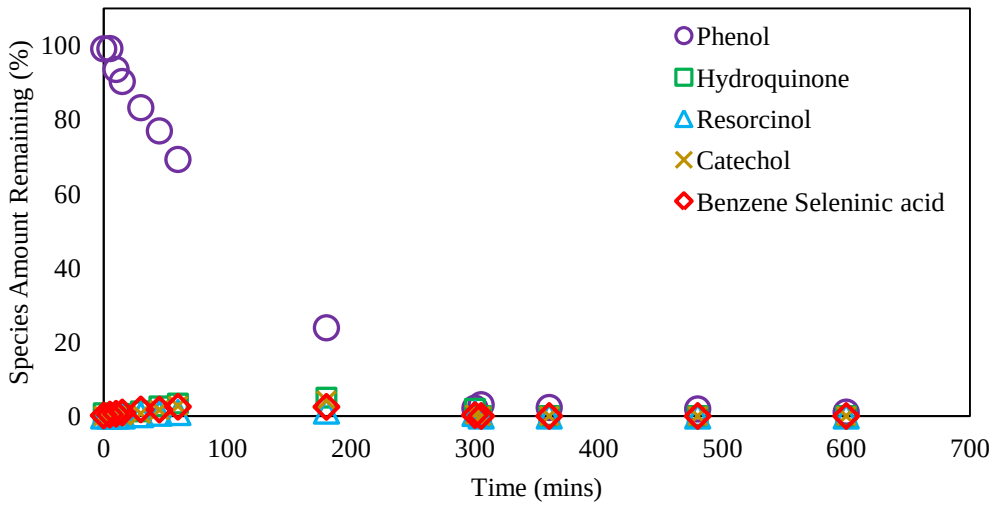

Figure 9.17: Trends from UV light photocatalytic destruction of phenol at pH 4 (10 ppm selenocyanate, 15 ppm phenol, 150 ppm EDTA added at 5 hours).

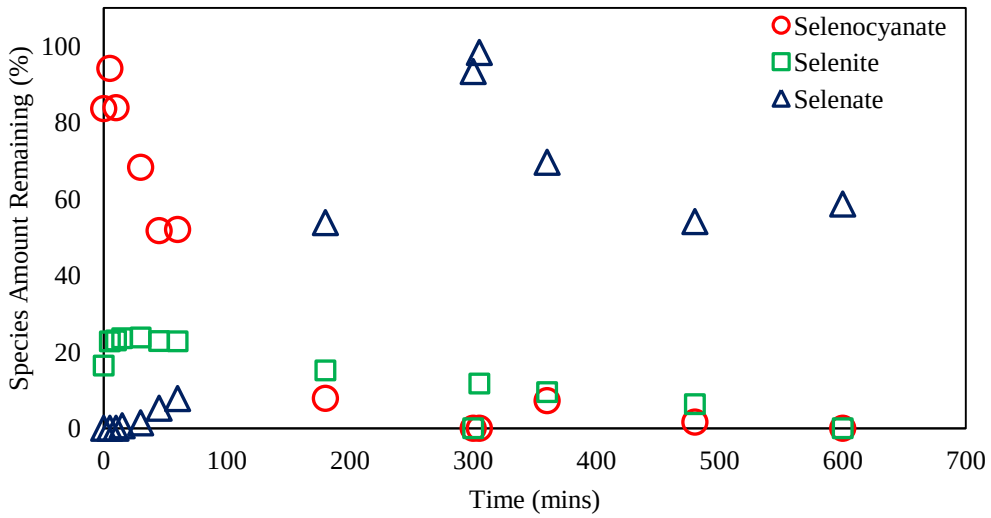

Figure 9.18: Trends from UV light photocatalytic destruction of selenocyanate phenol at pH 8 (10 ppm selenocyanate, 15 ppm phenol, 150 ppm EDTA added at 5 hours).

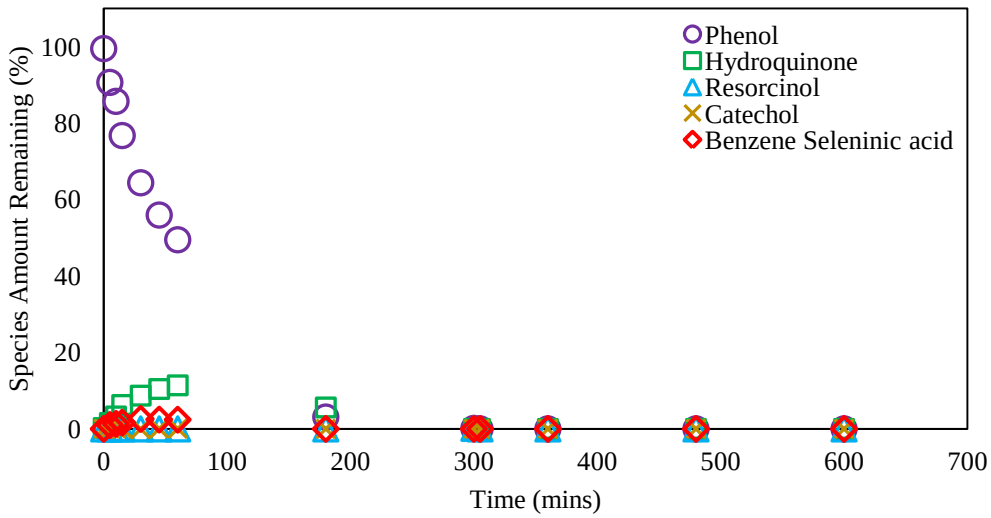

Figure 9.19: Trends from UV light photocatalytic destruction of phenol at pH 8 (10 ppm selenocyanate, 15 ppm phenol, 150 ppm EDTA added at 5 hours).

Like the earlier reported lower total selenium removal at low EDTA, we further investigated photocatalytic removal of 10 ppm selenocyanate in presence of 15 ppm phenol using 450 ppm EDTA, with respective results shown in Figures 9.20 and 9.21. Comparing the results at pH 4 (Figure 9.20) with those at pH 8 (Figure 9.21), faster selenocyanate removal iss observed at pH 4. After 10 hours of irradiation, total selenium present at pH 4 as selenite, selenate, and selenocyanate are 8%, 39%, and 0% and 8%, 16%, 29% at pH 8, respectively. Total selenium removal was thus 53% at pH 4 and 47% at pH 8. This confirms our earlier observation that an increase in pH results in a decrease in total selenium removal. Also important to note is that comparing Figure 9.14 and 9.20, we not that total selenium removal even using 450 ppm EDTA, decreases significantly with an increase in phenol concentration. However, the intriguing questions that should

be asked are 1) most phenol is removed at an earlier stage, and 2) like EDTA, phenol or its intermediates should also scavenge h^+ species (either directly or indirectly) that should in turn leave more e^- species for selenite/selenate reduction. Then why an increase in phenol from 5 ppm (Figure 9.14) to 15 ppm (Figure 9.20) causes a notable decrease in the total selenium removal. One possible explanation is that the reaction intermediates resulting from phenol degradation may adsorb onto TiO_2 surface thus reducing interaction of remaining selenate species with the TiO_2 surface for effective reduction or a simple poising of TiO_2 surface (from same) could also decrease photoactivity.

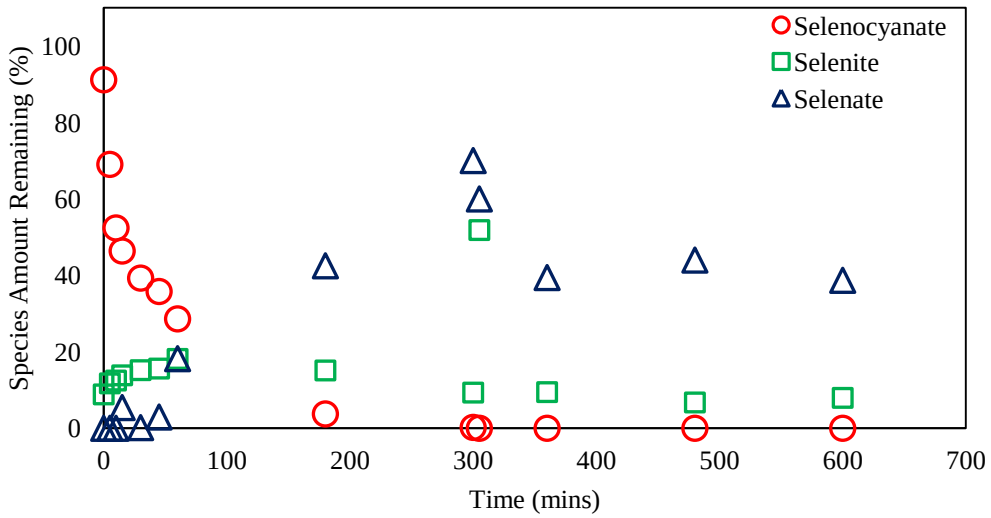

Figure 9.20: Trends from UV light photocatalytic destruction of selenocyanate at pH 4 (10 ppm selenocyanate, 15 ppm phenol, 450 ppm EDTA added at 5 hours).

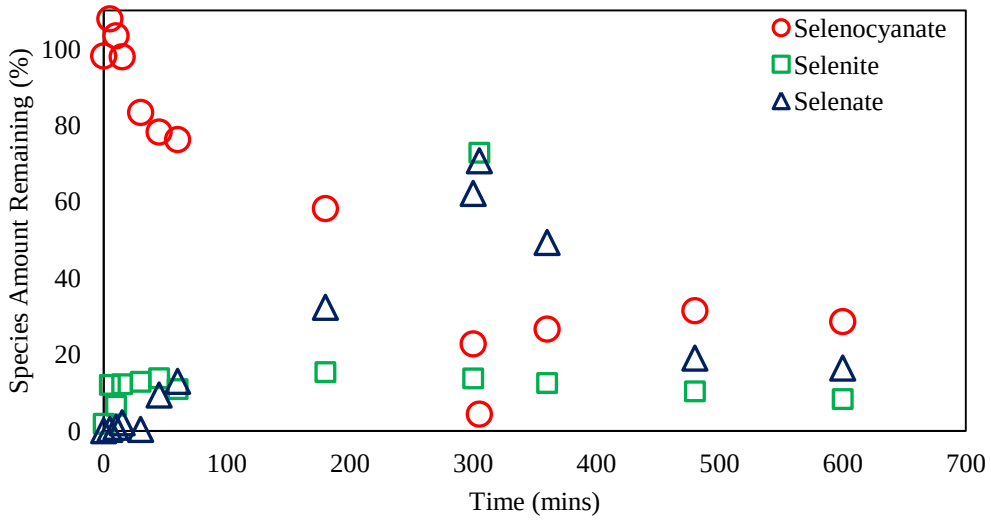

Figure 9.21: Trends from UV light photocatalytic destruction of selenocyanate at pH 8 (10 ppm selenocyanate, 15 ppm phenol, 450 ppm EDTA added at 5 hours).

9.1.2 20 ppm Selenocyanate Concentration

To build on the results discussed for photocatalytic removal of 20 ppm selenocyanate, we conducted three experiments at pH 4, 6 and 8 at 20 ppm selenocyanate and fixed phenol concentration of 10 ppm and EDTA concentration of 300 ppm; the respective results are presented in Figures 9.22, 9.24 and 9.26 respectively. Unlike experiments completed for 10 ppm selenocyanate concentration (Figures 9.2 to 9.21) where selenocyanate is almost completely removed within 5 hours, results in Figures 9.22, 9.24, and 9.24 show that significant amount of selenocyanate remains even after 5 hours of irradiation. For example, selenocyanate remaining after 5 hours of reaction time is 12, 28, and 34% at pH 4, 6 and 8 respectively. It should however be noted that though the selenocyanate % based removal decreases with an increase in its concentration, the mass based removal is

still higher at elevated concentration. Therefore, the rate of selenocyanate destruction increases with an increase in selenocyanate concentration. Selenite formation increases with time at pH 4 (Figure 9.22) until it reaches about 13% at 45 minutes followed by some few decrease and then a constant trend till 5 hour reaction time. Addition of EDTA lead to an abrupt increase in selenite due to displacement of adsorbed selenite from the surface by EDTA adsorption. Also comparing the respective jump in selenite aqueous phase concentration in Figures 9.22, 9.24 and 9.24, we note a relative decrease as pH is increased from 4 to 8, which is because of reduced selenite adsorbed amount at higher pH. Nevertheless, selenate with insignificant adsorption, also shoe insignificant jump upon EDTA addition. Also after EDTA addition, both selenite and selenate concentrations decreased with time accompanied by a slight increase in selenocyanate concentration. Also important to note is that the results in Figures 9.24 and 9.26 show very negligible initial aqueous phase selenite between 0 and 5 hours. Though and as also mentioned above that selenite does show higher adsorption at low pH values, however a qualitative comparison between present pH 8 selenite trends (Figure 9.26) with others, e.g. (Figure 9.10, 10 ppm SeCN), shows comparatively lower selenite in the aqueous phase. One explanation for this different trend is comparatively lower SeCN degradation as noted in Figures 9.22, 9.24 and 9.26. Furthermore, on mass basis the amount of Se-species adsorbed will be higher and thus considering a limited number of TiO_2 surface sites may eventually yield lower adsorption. Furthermore, a delay in selenate formation is also observed at all pH values that can also be attributed to slower SeCN degradation and eventually slower Se-intermediates formation. Similar to the results in Figures 9.2 to 9.21

where an increase in total selenium removal was observed with a decrease in pH, total selenium removal decreased from 42% at pH 4 to 36% at pH 6 for 20 ppm selenocyanate. A further increase in pH from 6 to 8 lead to a further decrease in total selenium removal from 36% to 26%, respectively.

We also investigated the effect of pH on photocatalytic removal of phenol for 20 ppm selenocyanate/10 ppm phenol systems in the presence of 300 ppm EDTA concentration and the results at pH 4, 6, and 8 are shown in Figures 9.23, 9.25, and 9.27. Overall removal after 10 hours irradiation is about 87, 92, and 97% at pH 4, 6, and 8 respectively. Furthermore, results displayed in Figure 9.23 show an increase in phenol removal with time, with the increase been more pronounced before the addition of EDTA. Hydroquinone and benzeneseleninic acid concentrations increased to about 4% at 3 and 5 hours, respectively. Pyrocatechol and resorcinol were also detected intermittently between 0 and 5 hours. An increase in pH from 4 (Figure 9.23) to 6 (Figure 9.25) lead to an increase in phenol removal vs time. However, we noticed a decrease of about 4% in benzeneseleninic acid formation due to an increase in pH from 4 to 6, whereas hydroquinone formation at pH 6 almost double than that at pH 4. Similar observations were made when the initial pH was further increased from pH 6 to pH 8 (Figure 9.27).

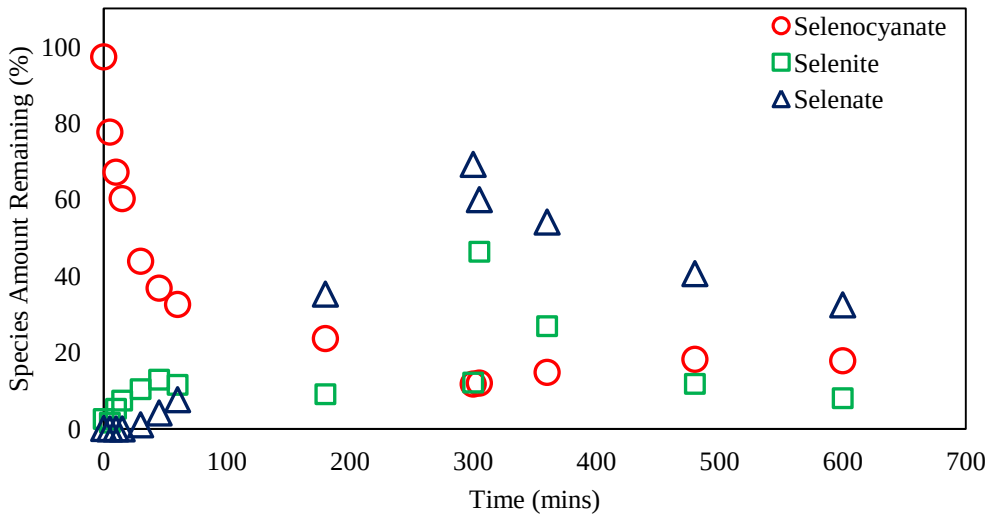

Figure 9.22: Trends from UV light photocatalytic destruction of selenocyanate at pH 4 (20 ppm selenocyanate, 10 ppm phenol, 300 ppm EDTA added at 5 hours).

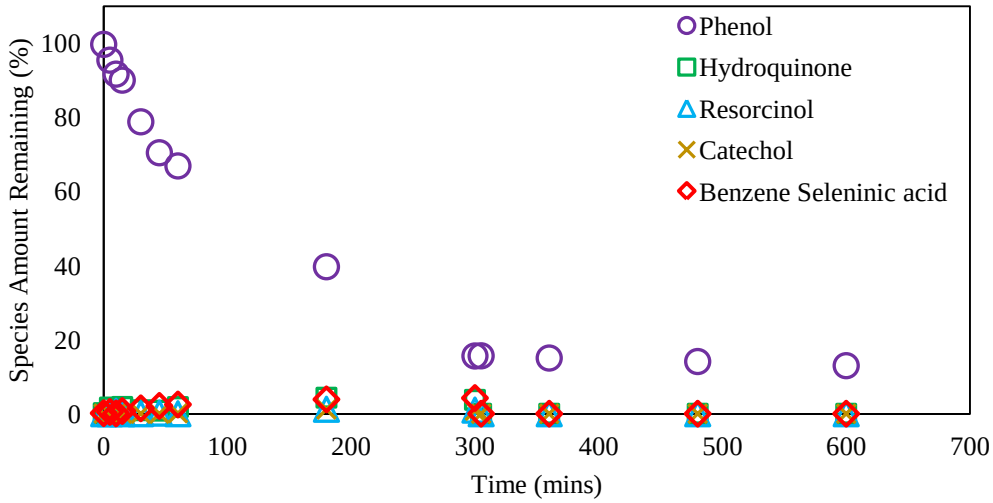

Figure 9.23: Trends from UV light photocatalytic destruction of [b] phenol at pH 4 (20 ppm selenocyanate, 10 ppm phenol, 300 ppm EDTA added at 5 hours).

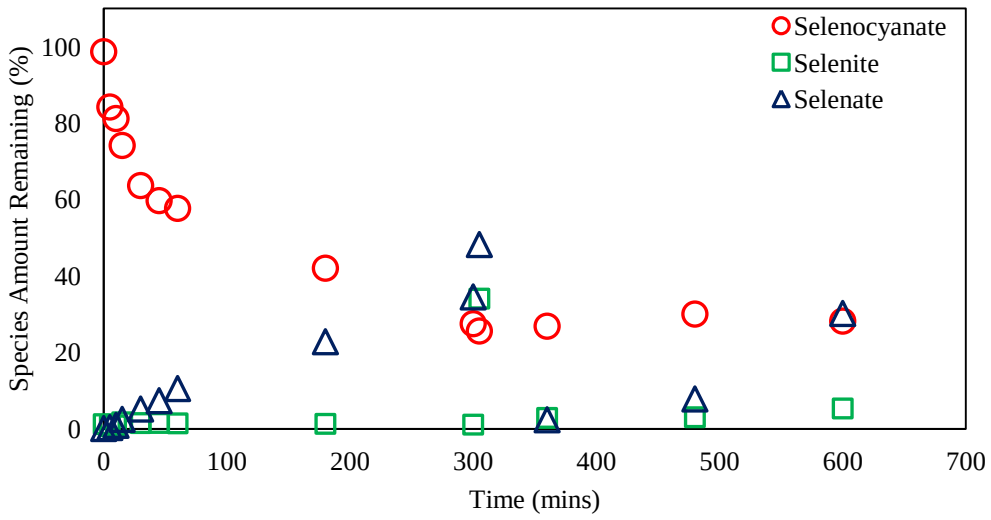

Figure 9.24: Trends from UV light photocatalytic destruction of selenocyanate at pH 6 (20 ppm selenocyanate, 10 ppm phenol, 300 ppm EDTA added at 5 hours).

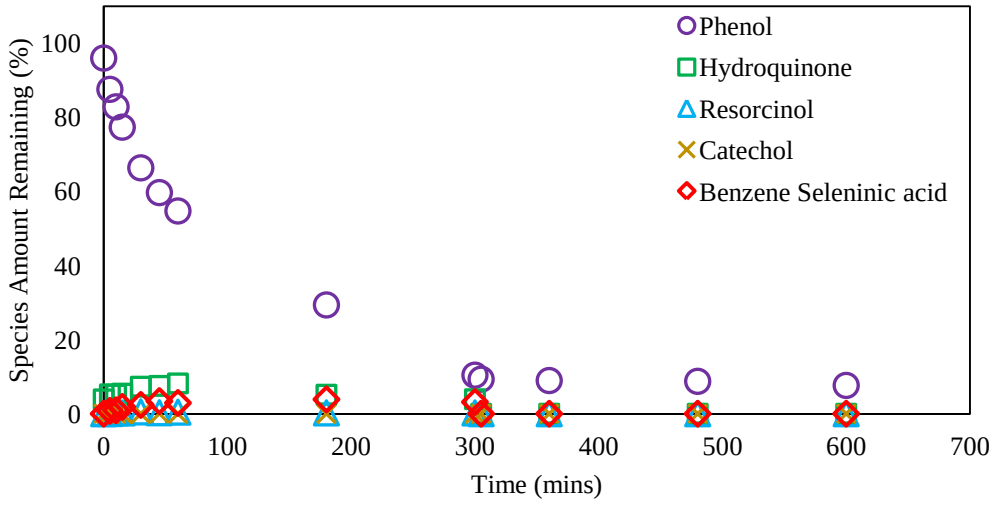

Figure 9.25: Trends from UV light photocatalytic destruction of phenol at pH 6 (20 ppm selenocyanate, 10 ppm phenol, 300 ppm EDTA added at 5 hours).

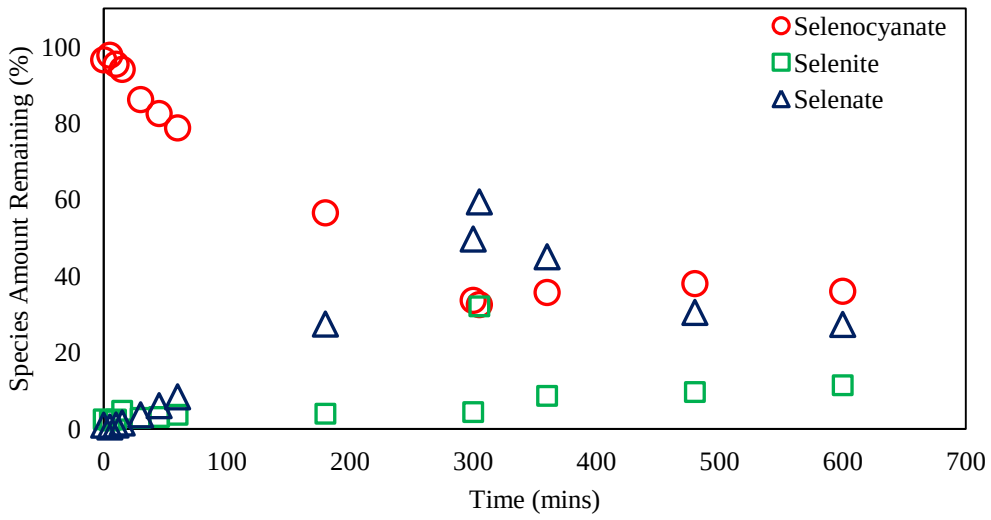

Figure 9.26: Trends from UV light photocatalytic destruction of selenocyanate at pH 8 (20 ppm selenocyanate, 10 ppm phenol, 300 ppm EDTA added at 5 hours).

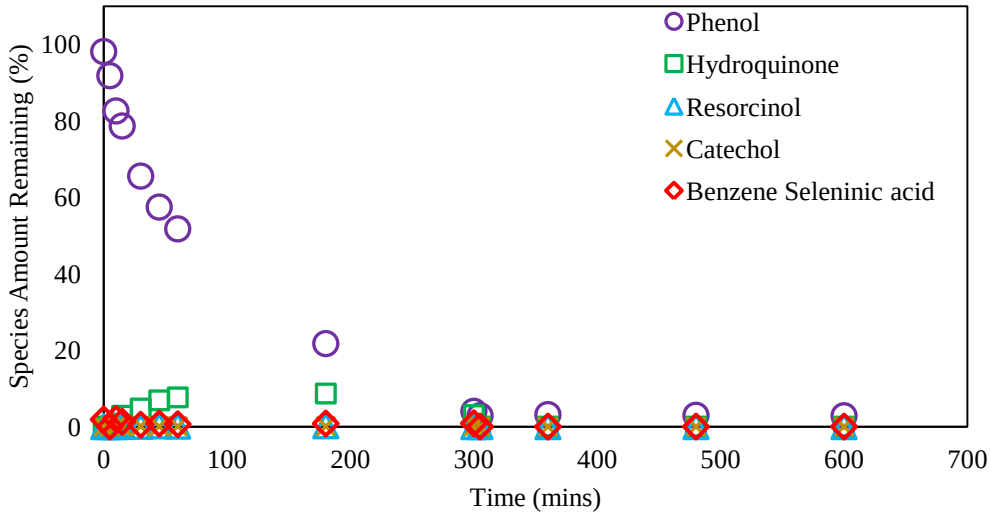

Figure 9.27: Trends from UV light photocatalytic destruction of phenol at pH 8 (20 ppm selenocyanate, 10 ppm phenol, 300 ppm EDTA added at 5 hours).

9.1.3 30 ppm Selenocyanate Concentration

We further investigated the selenocyanate/phenol mixed system at 30 ppm selenocyanate concentration under a varying set of conditions. We first conducted experiments for 30 ppm selenocyanate in the presence of 5 ppm phenol and 150 ppm EDTA and respective results are presented in Figures 9.28 and 9.30. Results in Figure 9.28 show a notable increase in aqueous phase selenite as compared to previously mentioned results for 10 and 20 ppm selenocyanate. Selenite formation increases to almost 34% after 3 hours, followed by a drop to about 25% after 5 hours. Addition of EDTA lead to an increase in its concentration to 31% because of its desorption stated earlier. A decrease in selenite and selenate concentrations is however observed after EDTA addition with somewhat increase in the selenocyanate concentration. Though significant decrease in selenite concentration is noted, however, notable selenate amount remains even 10 hours reaction time. Comparing the results at pH 4 (Figure 9.28) and 8 (Figure 9.30), a decrease in selenocyanate destruction rate is observed with an increase in pH, with difference more noticeable within the first one hour, e.g., selenocyanate remaining at pH 8 is almost double than that at pH4. However, at pH 8 (Figure 9.30), low selenite formation is noted between 0 and 5 hours, whereas and selenate formation is significant. This is explained based upon the noted slower selenocyanate degradation which in turn will also produce lower selenite species. The produced selenite will adsorb and get oxidized to selenate that because of its lower adsorption shows higher aqueous phase presence. Selenite and selenate reduction trends after EDTA addition are similar at both pH 4 and 8. The overall total selenium removal at pH 4 and 8 are around 22%. Such a lower decrease in total

selenium removal is noted both because of a higher initial total selenium and lower EDTA addition. This point will be further revisited in the coming section to explore removal of total selenium at a higher EDTA addition.

Now comparing phenol degradation results at pH 4 (Figure 9.29) and 8 (Figure 9.31), we not an increase in phenol removal due to an increase in pH as also noted in the earlier sections. About 81%, and 100% phenol removal is observed just before EDTA addition at pH 4 and 8 respectively.

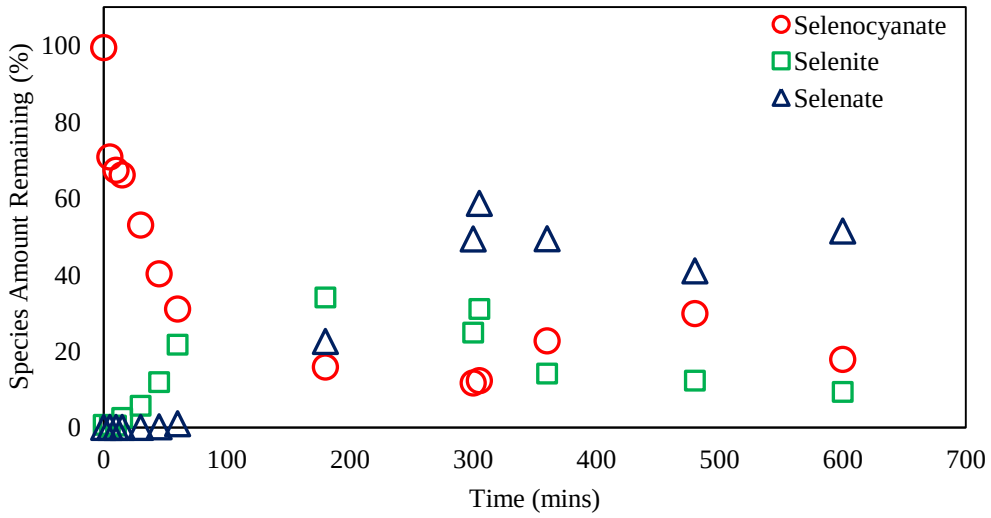

Figure 9.28: Trends from UV light photocatalytic destruction of selenocyanate at pH 4 (30 ppm selenocyanate, 5 ppm phenol, 150 ppm EDTA added at 5 hours).

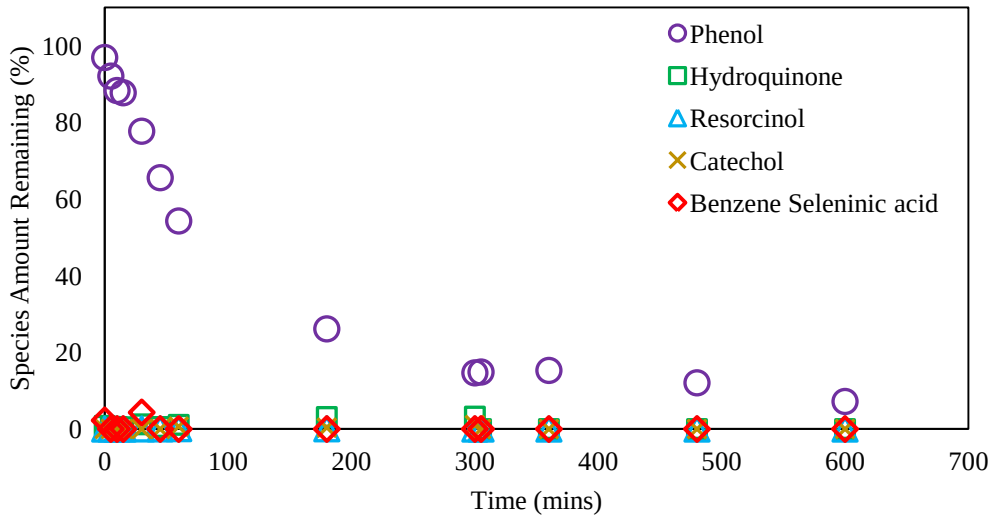

Figure 9.29: Trends from UV light photocatalytic destruction of phenol at pH 4 (30 ppm selenocyanate, 5 ppm phenol, 150 ppm EDTA added at 5 hours).

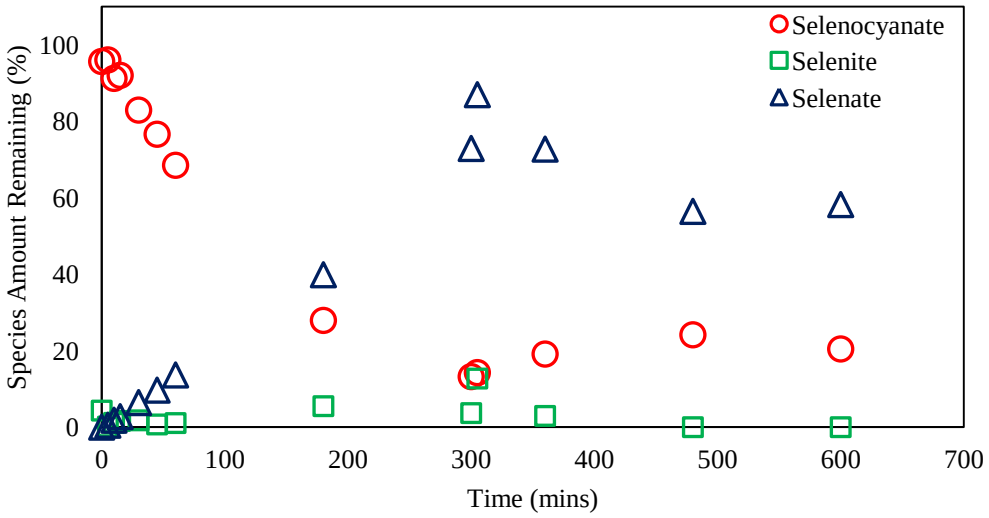

Figure 9.30: Trends from UV light photocatalytic destruction of selenocyanate at pH 8 (30 ppm selenocyanate, 5 ppm phenol, 150 ppm EDTA added at 5 hours).

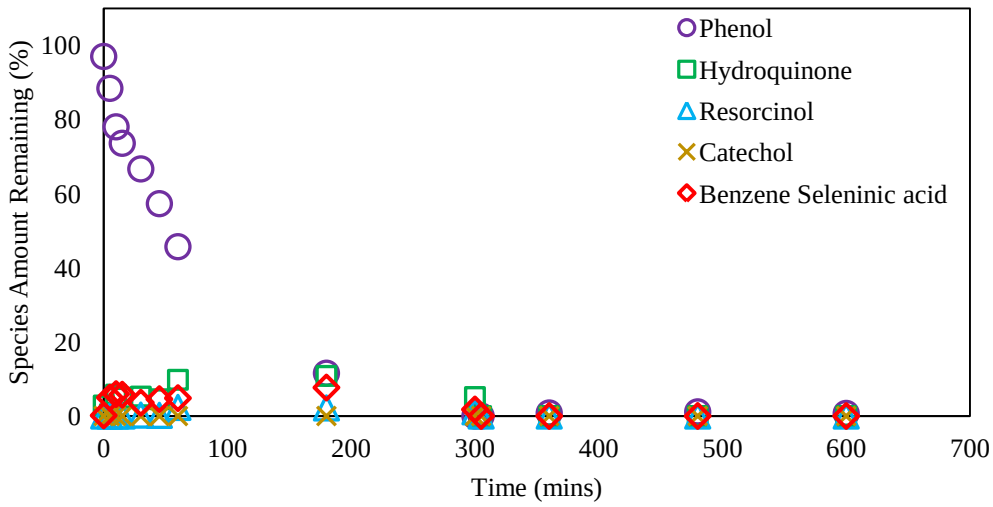

Figure 9.31: Trends from UV light photocatalytic destruction of [a] selenocyanate and [b] phenol at pH 8 (30 ppm selenocyanate, 5 ppm phenol, 150 ppm EDTA added at 5 hours).

To gain more insight into above mentioned photocatalytic removal of 30 ppm selenocyanate, we repeated the respective experiments in the presence of 5 ppm phenol, but adding 450 ppm EDTA after 5 hours. Figures 9.32 and 9.33 show the results for pH 4 and 8 respectively. We indeed note enhanced total selenium removal, e.g., at pH 4 about 58% total selenium is noted that is comparatively higher to 21% in Figure 9.28. Though higher total selenium still remains, however the total mass-basis selenium removal is still higher considering 30 ppm initial selenocyanate.

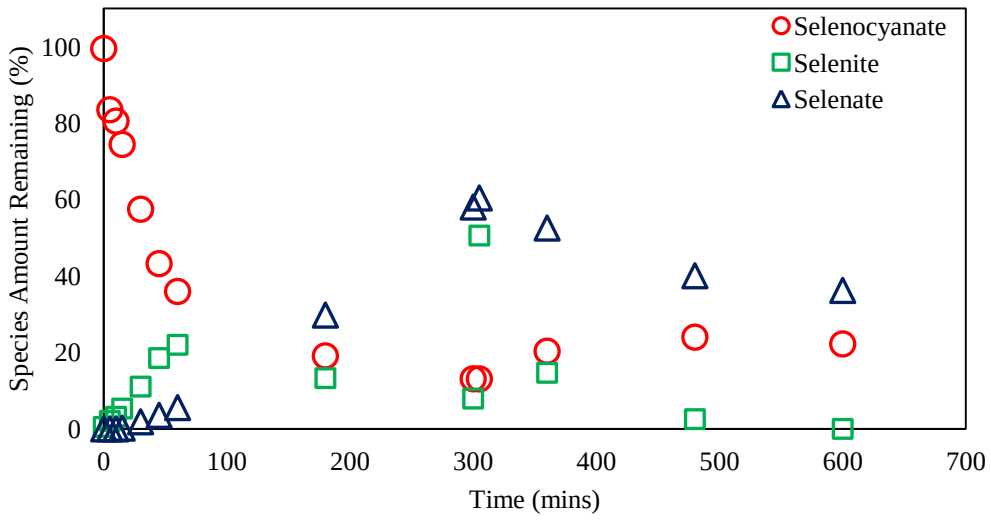

Figure 9.32: Trends from UV light photocatalytic destruction of selenocyanate at pH 4 (30 ppm selenocyanate, 5 ppm phenol, 450 ppm EDTA added at 5 hours).

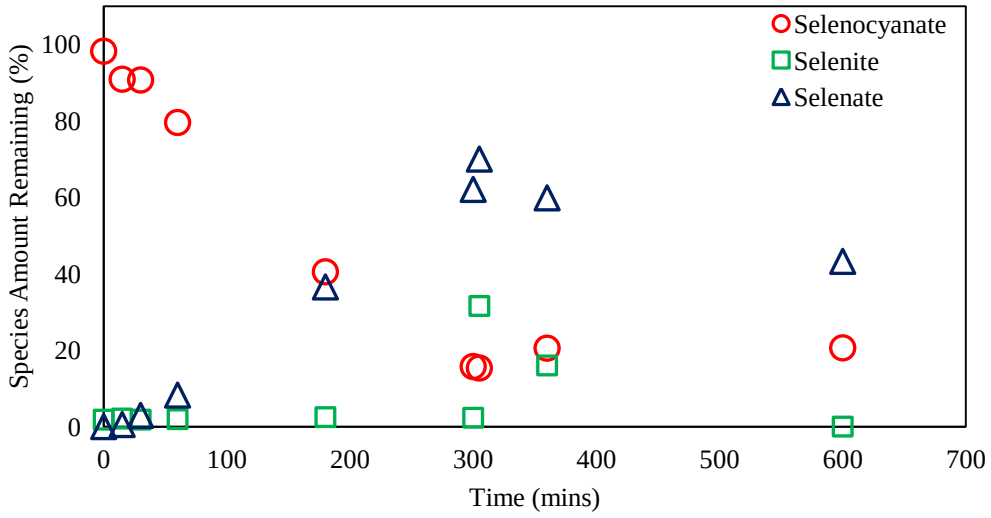

Figure 9.33: Trends from UV light photocatalytic destruction of selenocyanate at pH 8 (30 ppm selenocyanate, 5 ppm phenol, 450 ppm EDTA added at 5 hours).

The above discussion was further expanded by conducting similar experiments at 15 ppm phenol and the respective results are given in Figures 9.34 to 9.39. For the respective 150 ppm EDTA systems, an increase in phenol from 5 to 15 ppm indeed cause reduced SeCN removal at both pH 4 and 8 (Figures 9.28, 9.30, 9.34 and 9.36). For example, about 27% and 59% selenocyanate remains just before EDTA addition at pH 4 and pH 8 (Figures 9.34 and 9.36), showing a decrease in selenocyanate destruction compared to results from experiments conducted at 5 ppm phenol (Figures 9.28 and 9.30). Similarly, Figures 9.38 and 9.39 show about 23% and 56% SeCN remaining respectively at 5 h reaction time that is lower than that noted in Figures 9.32 and 9.33 with value of 58% and 64%, respectively. This shows that increase in both phenol and pH have a negative effect on the destruction of selenocyanate. Despite that, the removal is still higher at pH 4 than at pH 8 which might be because of higher selenite and selenate adsorption at pH 4. Total selenium removal at the end of the experiment was about 26% at pH 4 and 21% at pH 8.

We also investigated the effect of pH on 15 ppm phenol removal in the presence of 30 ppm selenocyanate and respective results are shown in Figures 9.35 and 9.37. Increase in phenol removal from about 71% at pH 4 to about 84% at pH 8 iss observed. Increase in phenol degradation at pH 8 is as a result of increased reaction with hydroxyl radicals. We also observed an increase in hydroquinone, resorcinol, and pyrocatechol formation with an increase in pH.

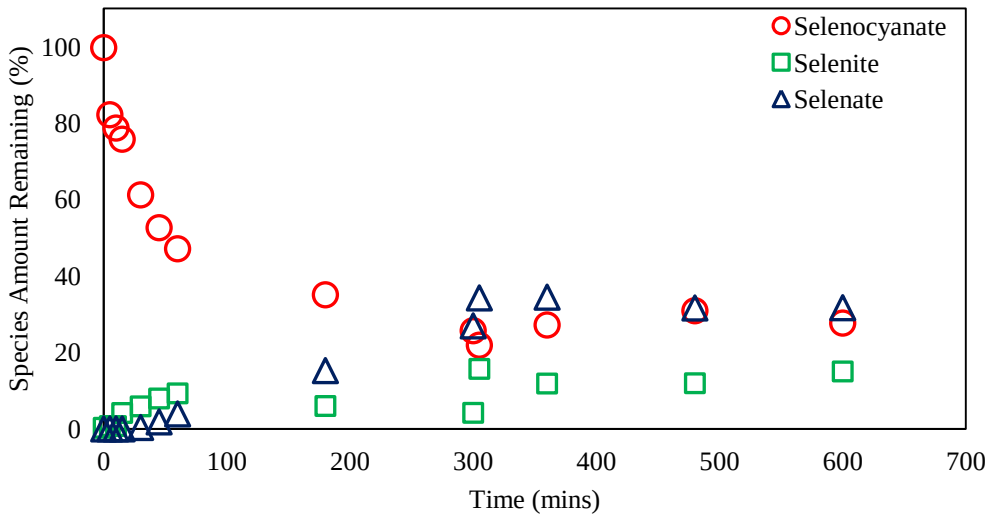

Figure 9.34: Trends from UV light photocatalytic destruction of selenocyanate at pH 4 (30 ppm selenocyanate, 15 ppm phenol, 150 ppm EDTA added at 5 hours).

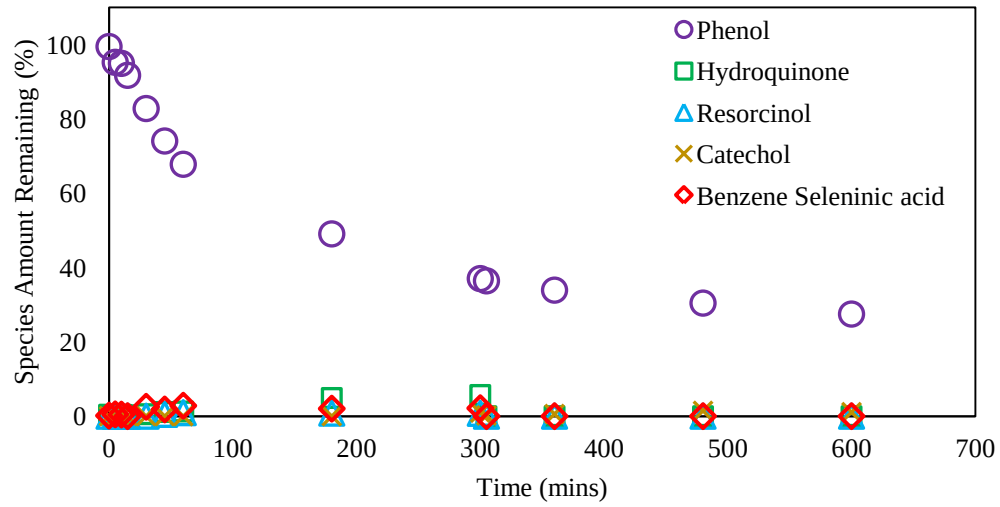

Figure 9.35: Trends from UV light photocatalytic destruction of phenol at pH 4 (30 ppm selenocyanate, 15 ppm phenol, 150 ppm EDTA added at 5 hours).

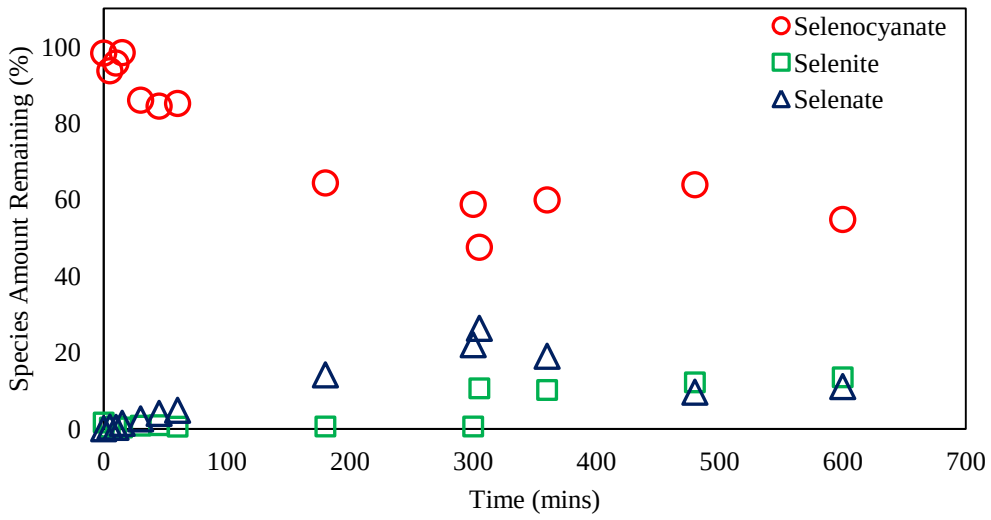

Figure 9.36: Trends from UV light photocatalytic destruction of selenocyanate at pH 8 (30 ppm selenocyanate, 15 ppm phenol, 150 ppm EDTA added at 5 hours).

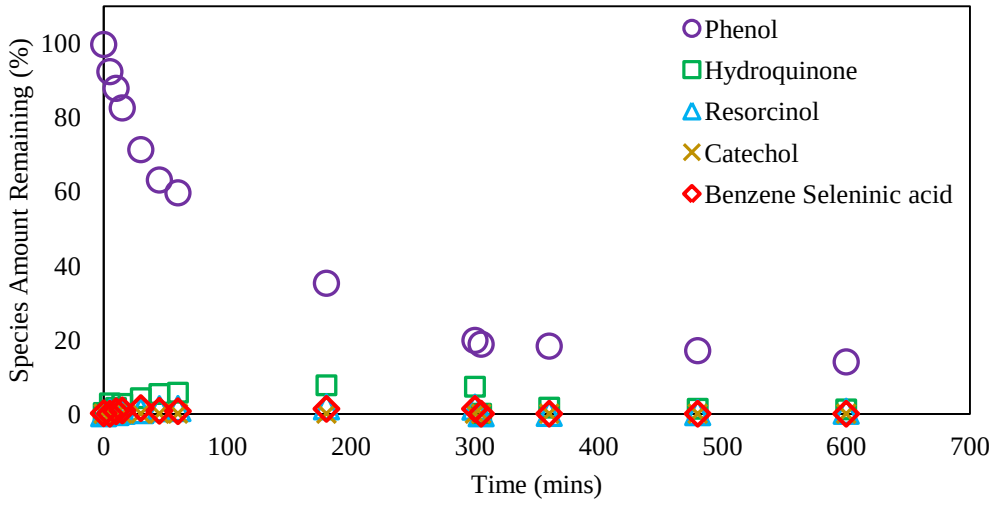

Figure 9.37: Trends from UV light photocatalytic destruction of phenol at pH 8 (30 ppm selenocyanate, 15 ppm phenol, 150 ppm EDTA added at 5 hours).

Also for higher phenol and EDTA studies (Figures 9.38 and 9.39), complete destruction of selenocyanate is not achieved even after EDTA addition. Increased competition for both limited TiO_2 adsorption sites and photo-generated holes/OH radicals for the oxidation of SeCN at higher concentration causes its lower destruction. Percent selenocyanate remaining after 5 hours at pH 4 and 8 are 23% and 56%, respectively. Unlike previous results in the presence of 150 ppm EDTA where reduction to elemental selenium was small after EDTA addition, significant reduction of selenite and selenate is achieved in the presence of 450 ppm especially at pH 4 (Figure 9.38).

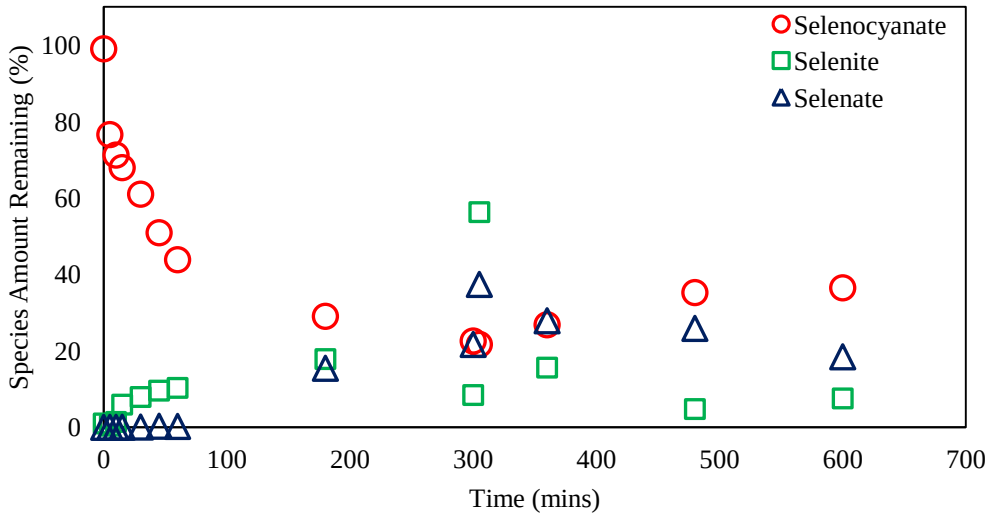

Figure 9.38: Trends from UV light photocatalytic destruction of selenocyanate at pH 4 (30 ppm selenocyanate, 15 ppm phenol, 450 ppm EDTA added at 5 hours).

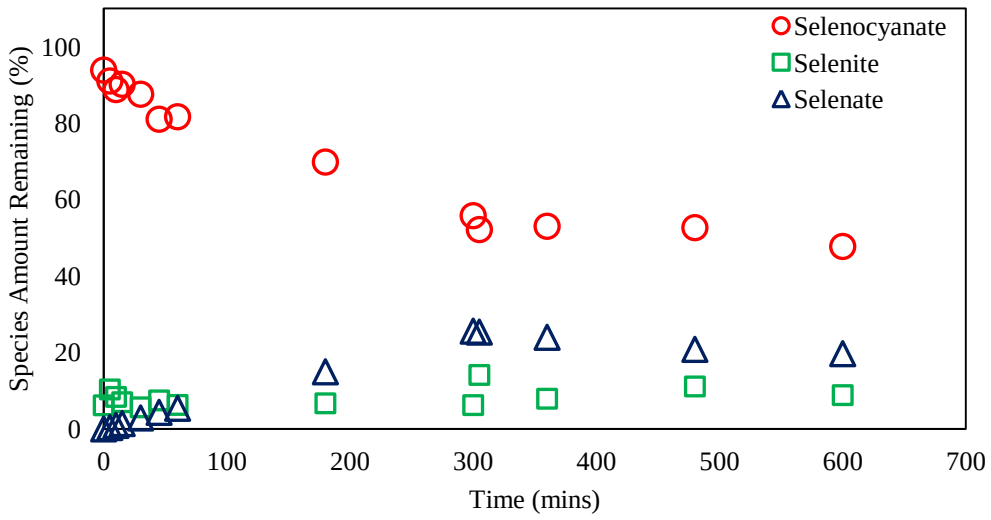

Figure 9.39: Trends from UV light photocatalytic destruction of selenocyanate at pH 8 (30 ppm selenocyanate, 15 ppm phenol, 450 ppm EDTA added at 5 hours).

9.2 Effect of EDTA Concentration

9.2.1 10 ppm Selenocyanate Concentration

Previous studies have shown the significance of hole scavengers on photocatalytic removal of selenite and selenate from aqueous phase. Recently, Vohra (2015) also highlighted the importance of hole scavenger EDTA for photocatalytic reduction of selenite and selenate resulting from oxidation of selenocyanate [37]. For this study, we also investigated the possibility of phenol acting as a hole scavenger by conducting an experiment without adding EDTA. Figure 9.40 shows experimental trends for photocatalytic removal of 10 ppm selenocyanate at pH 4 in the presence of 5 ppm phenol. Oxidation of selenocyanate to selenite and then to selenate is observed. However, lowering in total selenium is not observed during the experiment that may have indicated

photocatalytic reduction of selenite and selenate to elemental selenium. Inability of phenol to act as a hole scavenger in this case can be attributed to low concentration of phenol in the solution which limits its ability to scavenge holes to effectively reduce e^-/h^+ recombination that in turn would have left enough e^- species for selenite/selenate reduction. Labaran and Vohra (2014) noted a similar while exploring use of tiocyanate as a possible hole scavenger [28]. Vohra (2015) has shown that any meaningful removal of selenocyanate should be preceded by complete destruction of selenocyanate followed by subsequent formation and removal of selenite and selenate via reduction route, a condition that is not met here since complete phenol degradation come first before complete selenocyanate destruction [37]. We also summarize here the already mentioned SeCN/phenol findings to gain an overall summarized insight into respective removal trends. Looking at the results for the photocatalytic removal of 10 ppm selenocyanate in the presence of 5 ppm phenol and 150 ppm EDTA at pH 4, reduction of selenate to elemental selenium was observed after EDTA addition (Figure 9.2). Selenite concentration however remains almost constant after the addition of EDTA probably due to limited amount of EDTA for scavenging action. An increase in EDTA concentration to 300 ppm (Figure 9.6) lead to an increase in total selenium removal. A decrease in both selenite and selenate concentrations was observed, which showed that despite incomplete oxidation of selenite to selenate, the presence of right amount of hole scavenger can result in significant photoreduction of both selenite and selenate. A further increase in EDTA concentration from 300 ppm (Figure 9.6) to 450 ppm (Figure 9.14) resulted into reduction of both selenite and selenate to elemental selenium albeit at a higher rate. Total

selenium removal after 10 hours of irradiation in the presence of 150 ppm, 300 ppm, and 450 ppm EDTA concentrations were 56, 76, and 87% respectively. In the event of EDTA addition, simultaneous oxidation of EDTA and reduction of selenite and selenate will prevail. We now summarize the effect of EDTA concentration on photocatalytic removal of 10 ppm selenocyanate at pH 8 and in the presence of 5 ppm phenol and the results in the presence of 150 ppm, 300 ppm, and 450 ppm EDTA as presented in Figures 9.4, 9.10 and 9.15 respectively. Increase in the rate of selenite and selenate reduction to elemental selenium was observed when EDTA concentration was increased from 150 ppm (Figure 9.4). Regarding the effect of EDTA concentration on the removal of 10 ppm selenocyanate in the presence of 15 ppm phenol at both pH4 and pH 8 and the results were displayed in Figures 9.18 to 9.21. At pH 4, increase in EDTA concentration from 150 ppm (Figure 9.16) to 300 ppm (Figure 9.20) lead to about 2% increase in total selenium removal. Likewise, similar increase in EDTA concentration at pH 8 resulted in about 5% increase in total selenium removal (Figures 9.18 and 9.21).

Furthermore, Figure 9.41 shows photocatalysis trends for phenol removal and reaction intermediates formation for 10 ppm selenocyanate and 5 ppm phenol system at pH 4. Complete phenol removal was achieved within 5 hours with maximum benzeneseleninic acid and hydroquinone formations of about 5% and 4% respectively. Now comparing phenol removal trends in Figure 9.41, with those in the presence of 150, 300, and 450 ppm EDTA, no significant difference was observed for phenol removal after 5 hours.

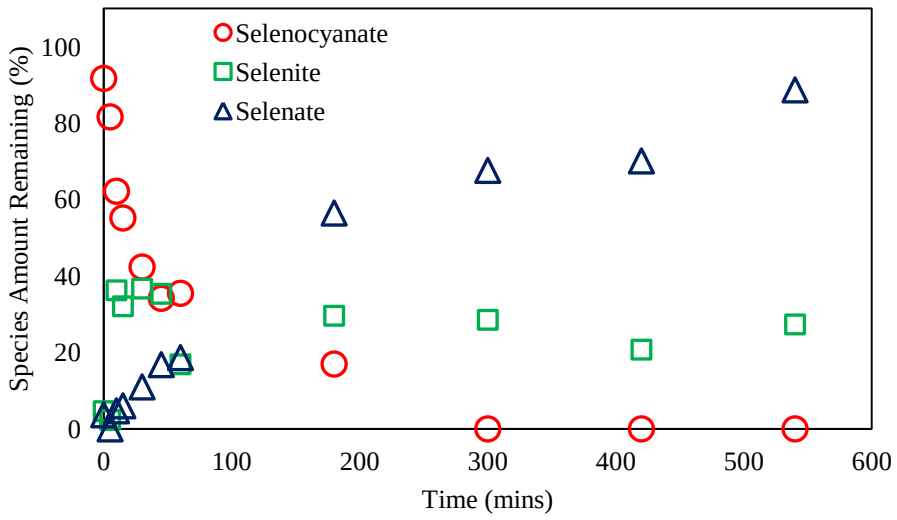

Figure 9.40: Trends from UV light photocatalytic destruction of selenocyanate at pH 4 (10 ppm selenocyanate, 5 ppm phenol, no EDTA).

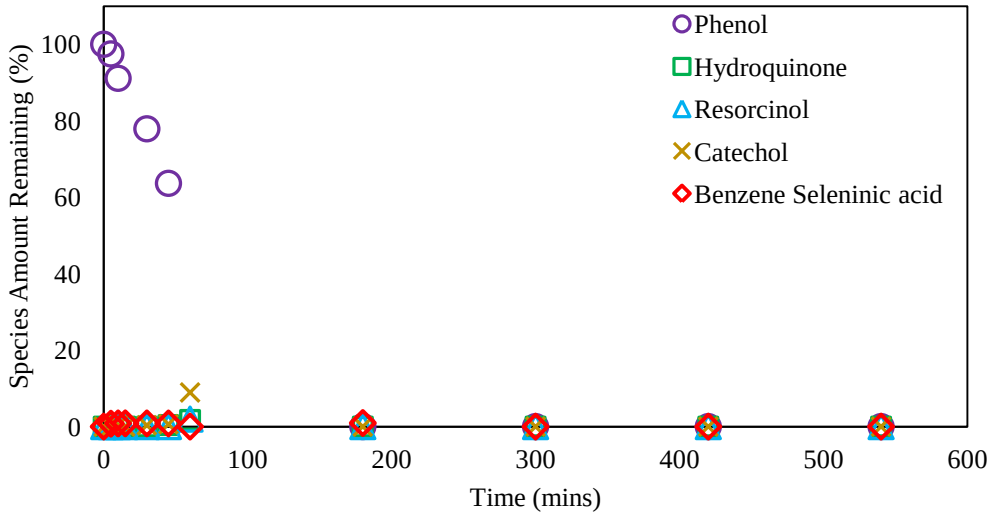

Figure 9.41: Trends from UV light photocatalytic destruction of phenol at pH 4 (10 ppm selenocyanate, 5 ppm phenol, no EDTA).

RSM AND KINETIC MODELING

10.1 RSM MODELING USING FACE-CENTERED CENTRAL COMPOSITE DESIGN

Conventional optimization techniques where only one variable is dependent and other variables fixed is becoming infamous for various disadvantages. Firstly, it requires large number of experiments to estimate the effect of factors which makes it tiresome and resource consuming. Secondly, this once-factor-at-a-time experimental design hardly provide the necessary information for estimating interactions between the dependent variables. This opens the door for statistical optimization techniques or design of experiments also known as DOE such as response surface methodology (RSM). A response surface methodology is nothing but a collection of statistical and mathematical techniques to develop, improve and optimize processes. By employing the modern design of experiments, we can maximize the accuracy of the information we get from experiments. In addition, number of experiments necessary for obtaining the required information can also be reduced without compromising on the accuracy of estimating some physical characteristics that are the objectives of the experiment. Finally, the capability of a model to predict the performance of other designs can be maximized by creating a response surface. Therefore, the main objective of response surface methodology is the determination of optimal points of a process [153]. Central

Composite Design are the most widely used response surface technique and is considered one of the most reliable for the determination of optimum points [154]. Though most of the response surface techniques has the capability of predicting single effects and interactions, central composite design has an added advantage of estimating curvature because of their efficiency in determining the coefficients of second order polynomials [155, 156]. Central composite designs contain an embedded factorial or fractional factorial design that is augmented by adding center points and axial or star points [157]. Therefore, a central composite design consists of three type of points i.e., fractional factorial points, axial points that are located at equal distances α from the center of the design and the center points with all coordinates equal to zero [158]. The function of the star points is to allow for accurate estimate of curvature. There are three types of central composite design, circumscribed central composite (CCC), inscribed central composite (ICC), and face-centered central composite (FCC) [158]. While the first two require five level for their design, FCC can be designed with only three levels. For this type of design, the axial points are located at the center of each face of the factorial space. We thus employed face-centered central composite for optimizing photocatalytic degradation process for the removal of selenocyanate and phenol in competitive environment. Table 10.1 shows experimental levels for the four factors under consideration, i.e., pH (A), selenocyanate concentration (B), phenol concentration (C), and EDTA concentration (D). factors combination for face-centered central composite design.

Table 10.1: Factors and their levels

Factors	Level -1	Level 0	Level +1
A = pH	4	6	8
B = selenocyanate concentration (ppm)	10	20	30
C = phenol concentration (ppm)	5	10	15
D = EDTA concentration (ppm)	150	300	450

10.1.1 Response Surface Model

UV light photocatalysis results discussed in chapter 9 were employed for response surface modeling to determine the optimum conditions for the removal of selenocyanate and phenol. Using the factor levels in table 10.1, we design an experiment using face-centered central composite design with a single center point. Factors combination and the corresponding responses for the 25 runs conducted according to the experimental design are presented in Table 10.2. Total selenium removal and phenol removal responses were fitted to linear model (equation 10.1) and two factor interaction i.e., 2FI model (equation 10.2) respectively by design expert version 10. P-values for model and significant model terms based on 5% level of significance are presented in Table 10.3. Though higher-order (quadratic and cubic) models produced better fit in terms of R^2 value, the above lower-

order models were suggested by the software because of their higher adjusted and predicted R-squared values compared to the higher-order models. R^2 value is often bias since addition of model terms to the model will always increase its value regardless of significance of those model terms. Adjusted R-squared is a modified version of the R^2 that is adjusted for the number of terms in the model and it increases with an addition of a new term only if that term improves the model more than would be expected by chance. Predicted R-squared on the other hand is a measure of how a model predicts new responses for new observations. Both adjusted and predicted R-squared are always less than R-squared and are said to agree with each other if their difference is less than 0.2. The difference is less than 0.035 for the two models as depicted by the adjusted and predicted R-squared values in table 10.4 Box and Cox (1964) developed a plot for the determination of power (Lambda) by which dependent variable will be raised in order to improve normality [159]. Lambda of 0 and 1 were obtained from Box-Cox plots for total selenium removal (Figure 10.1) and phenol removal (Figure 10.2) respectively. A lambda of 0 signifies that a Log transform is required. Therefore, Natural Log transformation was applied to the total selenium removal model as shown in equation 10.1 and Table 10.4. The effects of pH, selenocyanate concentration, phenol concentration, and EDTA concentration as predicted by the model are shown in Figures 10.3 to 10.6. Figure 10.3 shows that an increase in initial pH and selenocyanate concentration decreases percent-based total selenium removal. Figure 10.4 shows the effect of phenol and EDTA concentrations on photocatalytic removal of total selenium. A decrease in total selenium removal is observed with an increase in phenol concentrations, whereas EDTA

concentration increases total selenium removal. The effect of pH and selenocyanate concentration on phenol removal are shown in Figure 10.5. While an increase in phenol removal is observed with an increase in pH, a decrease is observed with an increase selenocyanate concentration. Furthermore, phenol and EDTA concentrations decreases phenol removal as depicted in Figure 10.6. These effects are in agreement with our discussions in chapter 9.

To further validate these models, we employed normal probability plots of residuals. One of the assumptions of a linear regression model is that the error terms are normally distributed. For this to be true, normal probability plot of residuals should be linear. The error terms plots (Figures 10.7 and 10.8) almost falls on a straight line, suggesting a good linearity between residuals and predicted values. Furthermore, normal probability plots are also used as diagnostic tools for finding some elements that differ from others [160]. The linearity of the plots suggest that the model elements are not significantly different from each other. Another important diagnostic tool is the plot of studentized residuals versus predicted values shown in Figures 10.9 and 10.10 for total selenium and phenol removal respectively. It is a scatter plot of studentized residuals on y axis versus predicted responses on x axis that is used to detect non-linearity, unequal error variances, and outliers. The residuals are scattered randomly around the “0” line which suggests the assumption of linearity is reasonable. Also, all the studentized residuals falls within -4 and +4, and thus none of the points can be considered as an outlier assuming that the data follows a t-distribution. Figure 10.11 and 10.12 show plots of studentized residuals versus run that is used to detect a time trend in the responses. A continuous increase or

decrease in residuals with run will signify a serial correlation. The residuals are randomly scattered around the "0" line without any definite pattern which eliminates time correlation. Another simple way of evaluating models is through a plot of predicted versus actual plots (Figure 10.13 and 10.14) [161]. For a good fit, the plot should pass through 0 at 45 angle, with points very close to the line. Points that are far away from the line adversely affects the model fit by either pulling the model towards the point or becoming outliers. Figure 10.13 and 10.14 show a very good fit between the predicted and the actual responses, with all data points almost falling on the line. To determine the relative significance of the model terms, a Pertubation for total selenium removal (Figure 10.15) and phenol removal (Figure 10.16) were plotted. The relative significance of the model terms follows the order selenocyanate concentration > pH > EDTA concentration > phenol concentration and phenol concentration > selenocyanate concentration > pH > EDTA concentration for total selenium and phenol models respectively.

$$\text{Ln(Selenocyanate Removal)} = 3.64 - 0.14*A - 0.32*B - 0.11*C+0.12*D \quad (10.1)$$

$$\text{Phenol Removal} = 92.38 + 2.90*A - 6.02*B - 6.21*C - 1.79*D + 2.72*AB - 3.93*BC - 1.79*CD \quad (10.2)$$

Table 10.2: Factors combination and responses

Run	A: pH	B: Selenocyanate concentration (ppm)	C: Phenol Concentration (ppm)	D: EDTA concentration (ppm)	Response 1: Total selenium removal (%)	Response 2: Phenol removal (%)
1	8	20	10	300	25.8884	97.171
2	6	30	10	300	25.1991	88.3796
3	4	30	15	150	25.6446	71.4424
4	6	10	10	300	47.7649	99.7061
5	6	20	15	300	32.8255	90.1285
6	8	10	15	150	41.3556	100
7	8	30	15	150	20.7151	84.1915
8	4	10	15	150	51.5348	98.952
9	4	10	5	450	86.6552	100
10	6	20	5	300	42.6386	98.2039
11	8	10	15	450	46.7593	89.4432
12	8	30	5	150	21.3356	99.2992
13	4	30	5	450	41.5587	90.9726
14	6	20	10	300	36.2643	92.3628
15	4	30	5	150	21.871	92.8101
16	6	20	10	150	35.5022	97.7028
17	4	20	10	300	41.7476	87.038
18	4	10	5	150	56.6481	100
19	8	30	5	450	36.4757	99.8711
20	8	10	5	150	50.4431	100
21	4	10	15	450	53.347	91.2155
22	6	20	10	450	43.5684	96.6477
23	8	30	15	450	23.6947	79.3278
24	4	30	15	450	37.6494	64.7216
25	8	10	5	450	55.48	100

Table 10.3: Significant level of models and model terms

	Significance of model and model terms							
Responses	Model	A	B	C	D	AB	BC	CD
ln(Total selenium removal)	< 0.0001	0.0007	< 0.0001	0.0091	0.0002			
Phenol removal	< 0.0001	0.0003	< 0.0001	< 0.0001	0.0129	0.0010	< 0.0001	0.0180

Table 10.4: Salient characteristics of the model

Responses	Transformation	Adequate Precision	R^2	Adjusted R^2	Predicted R^2
Total selenium removal	Natural Log	27.700	0.9140	0.8967	0.8630
Phenol removal	none	22.702	0.9395	0.9146	0.8798

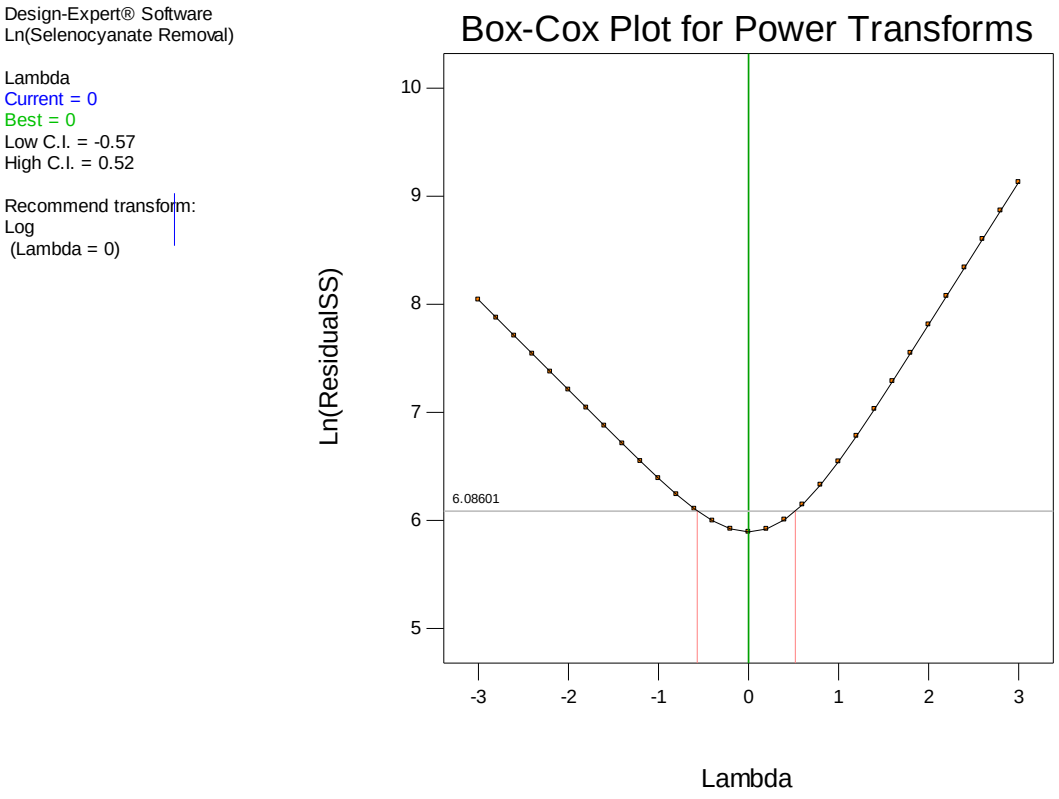

Figure 10.1: Box-Cox plot for total selenium removal model

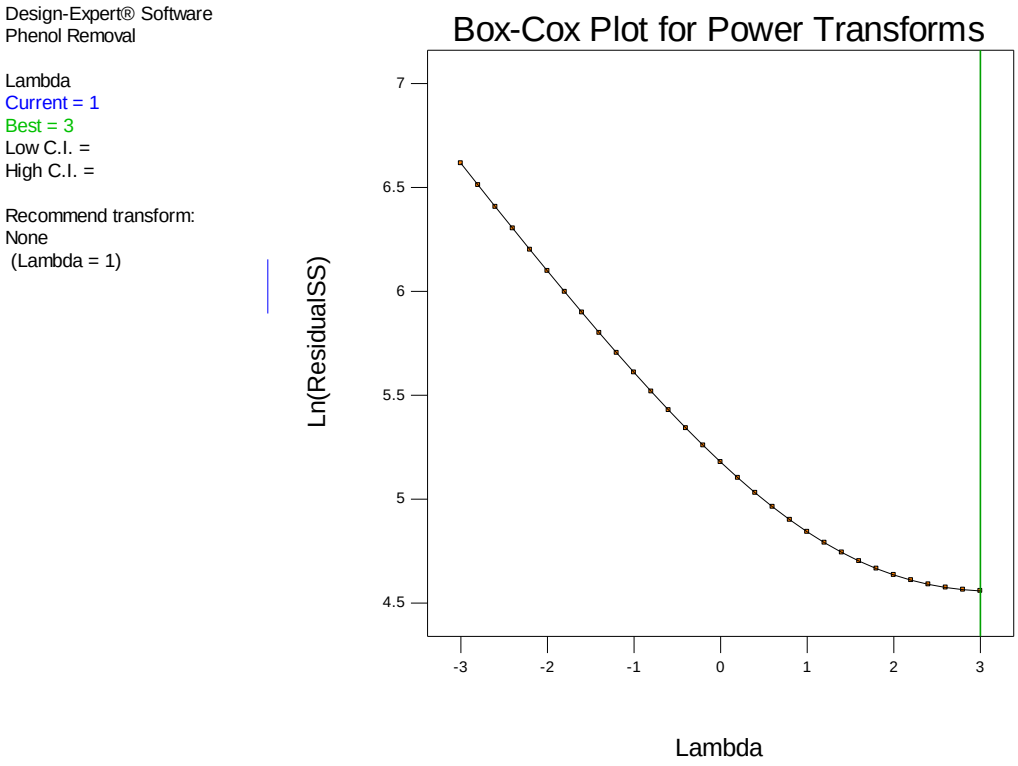

Figure 10.2: Box-Cox plot for phenol removal model

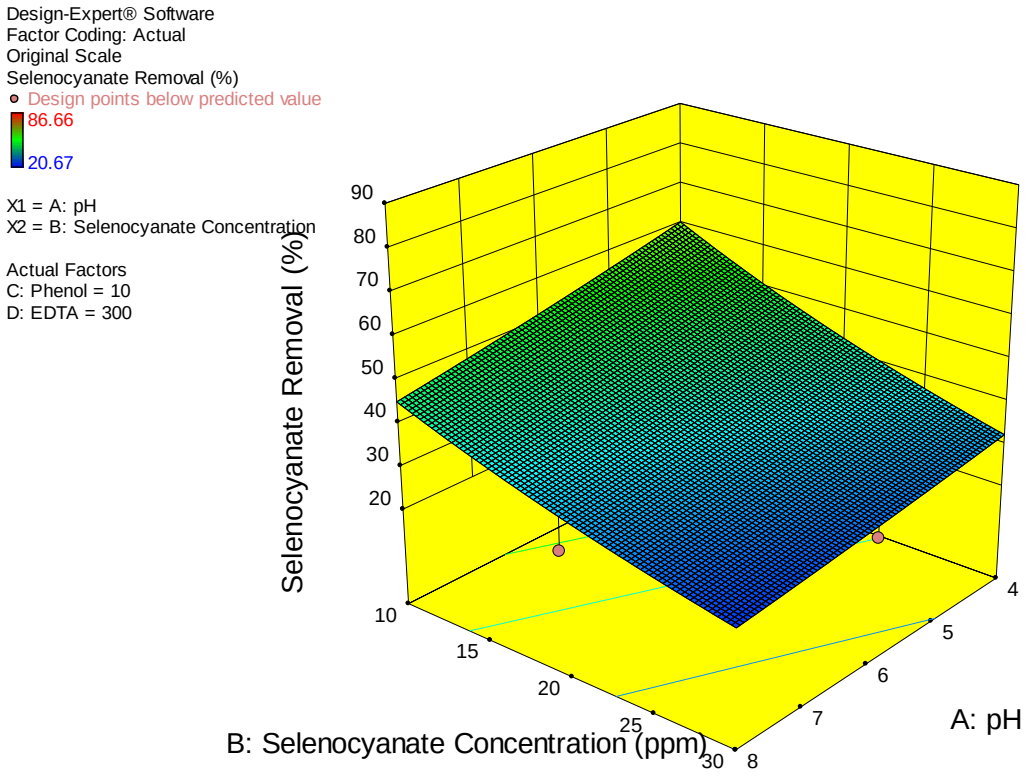

Figure 10.3: Effect of pH and selenocyanate concentration on total selenium removal

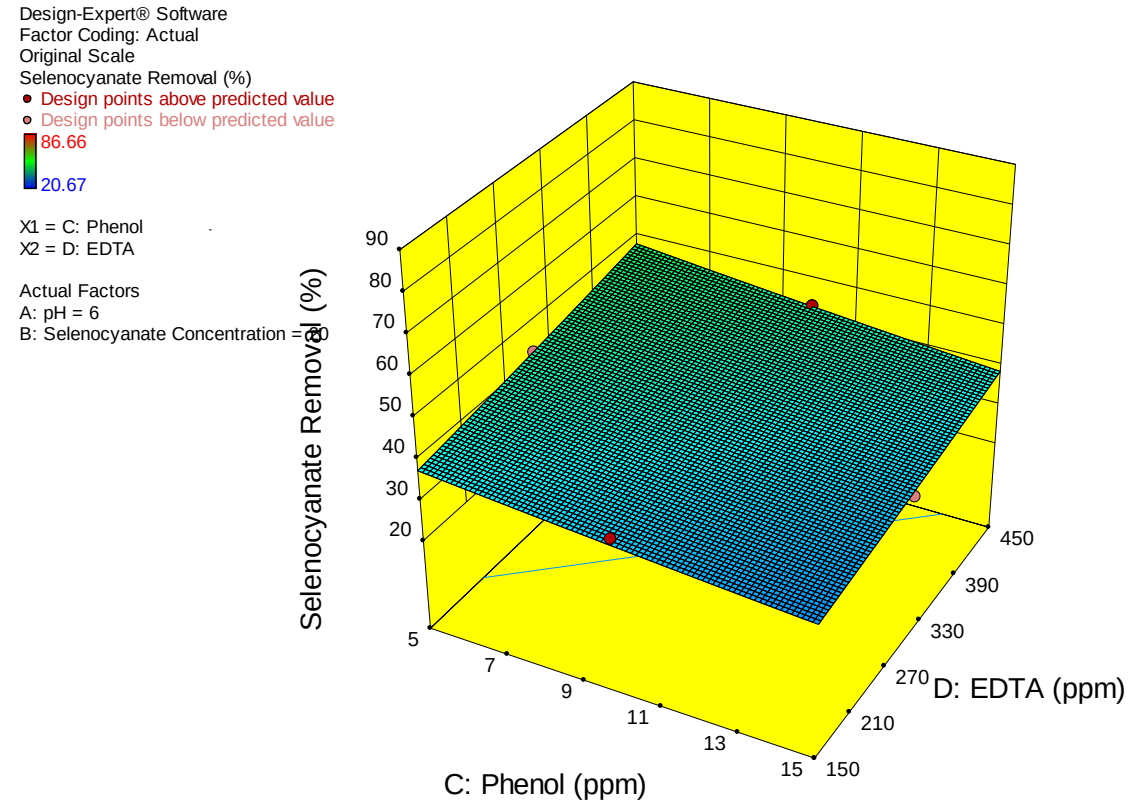

Figure 10.4: Effect of phenol and EDTA concentrations on total selenium removal

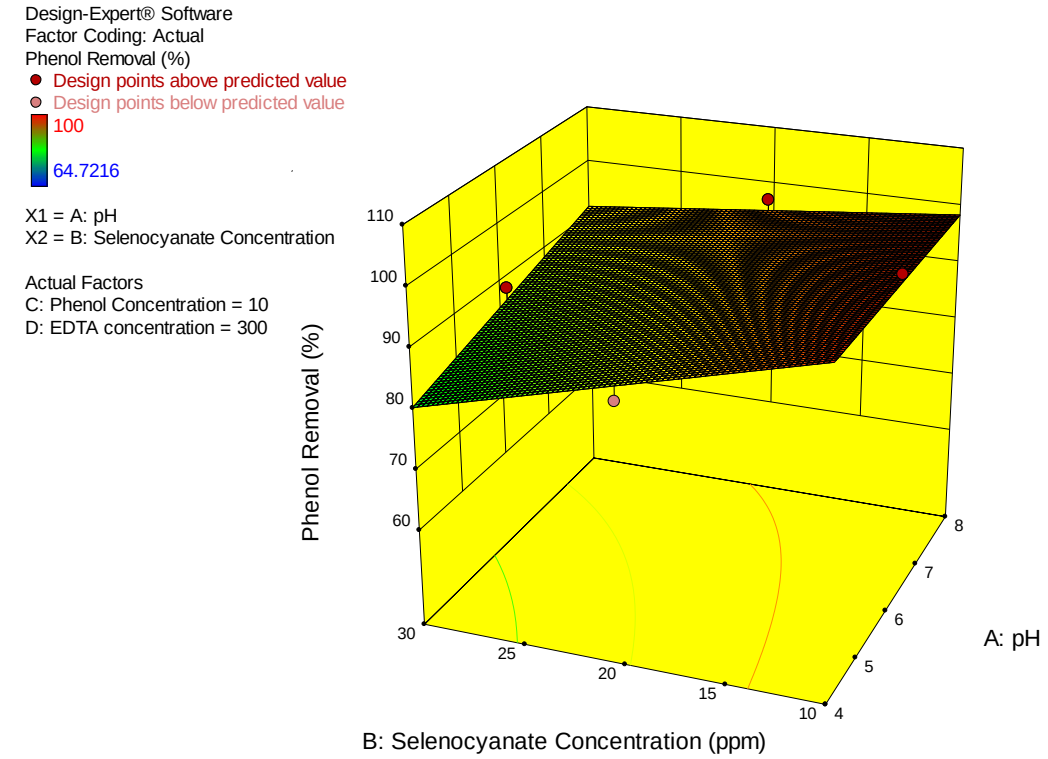

Figure 10.5: Effect of pH and selenocyanate concentration on total phenol removal

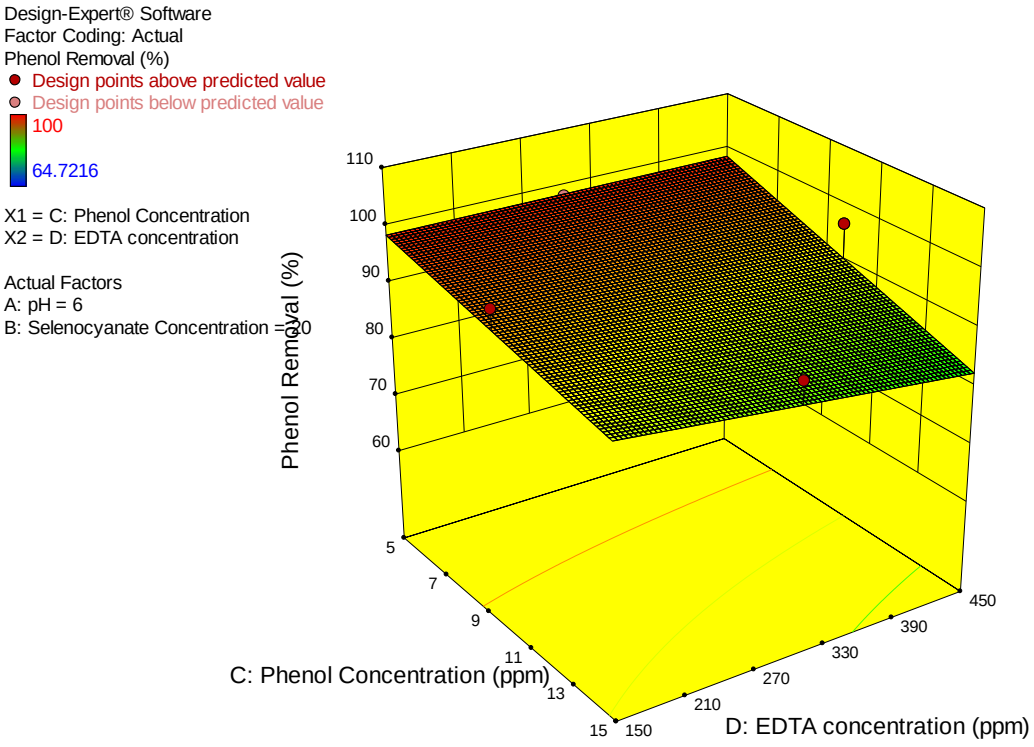

Figure 10.6: Effect of phenol and EDTA concentrations on phenol removal

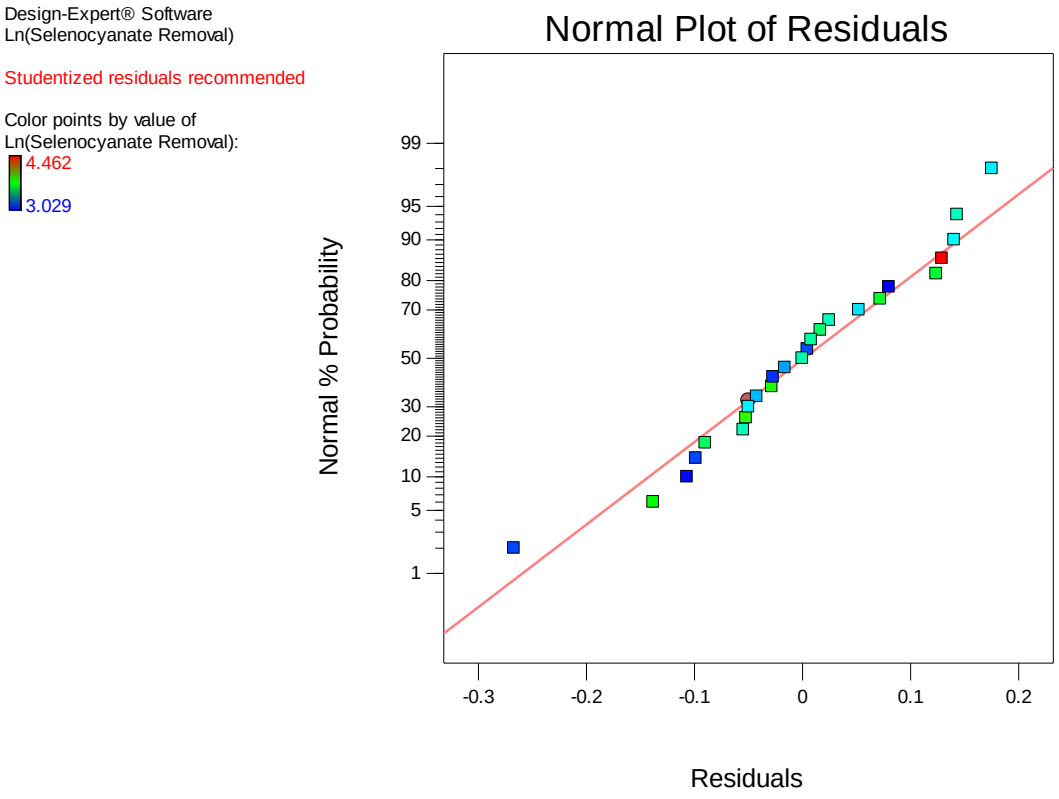

Figure 10.7: Normal plot of residuals for total selenium removal

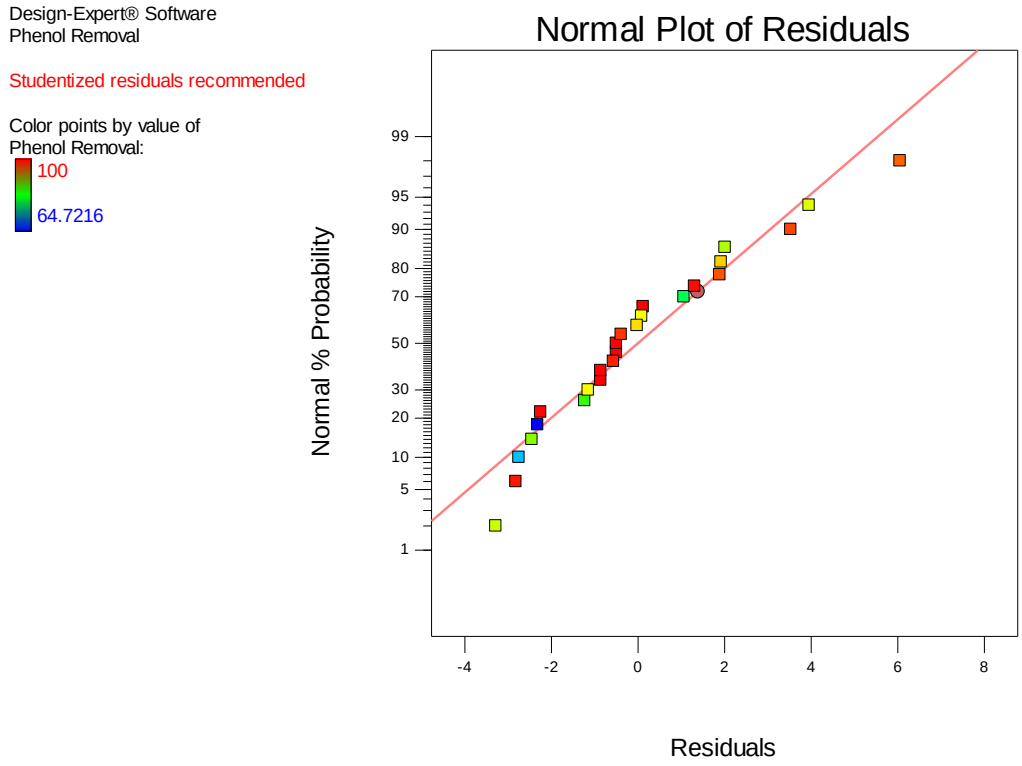

Figure 10.8: Normal plot of residuals for phenol removal

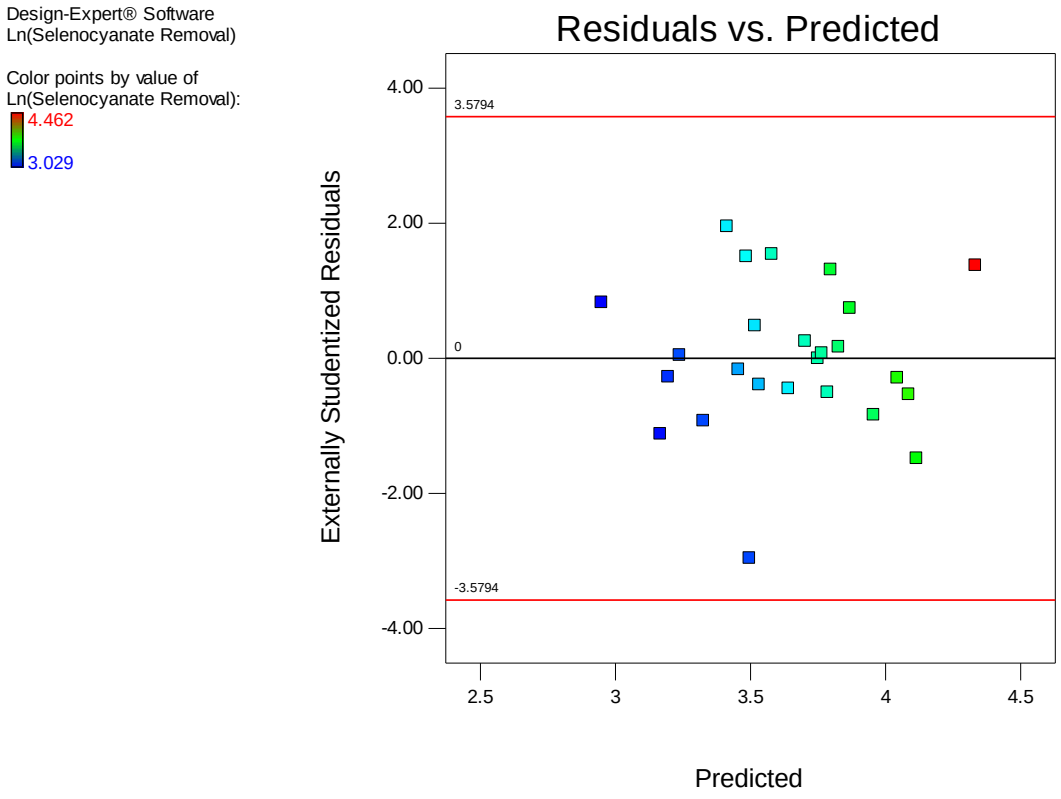

Figure 10.9: Externally studentized residuals versus predicted plot for total selenium removal

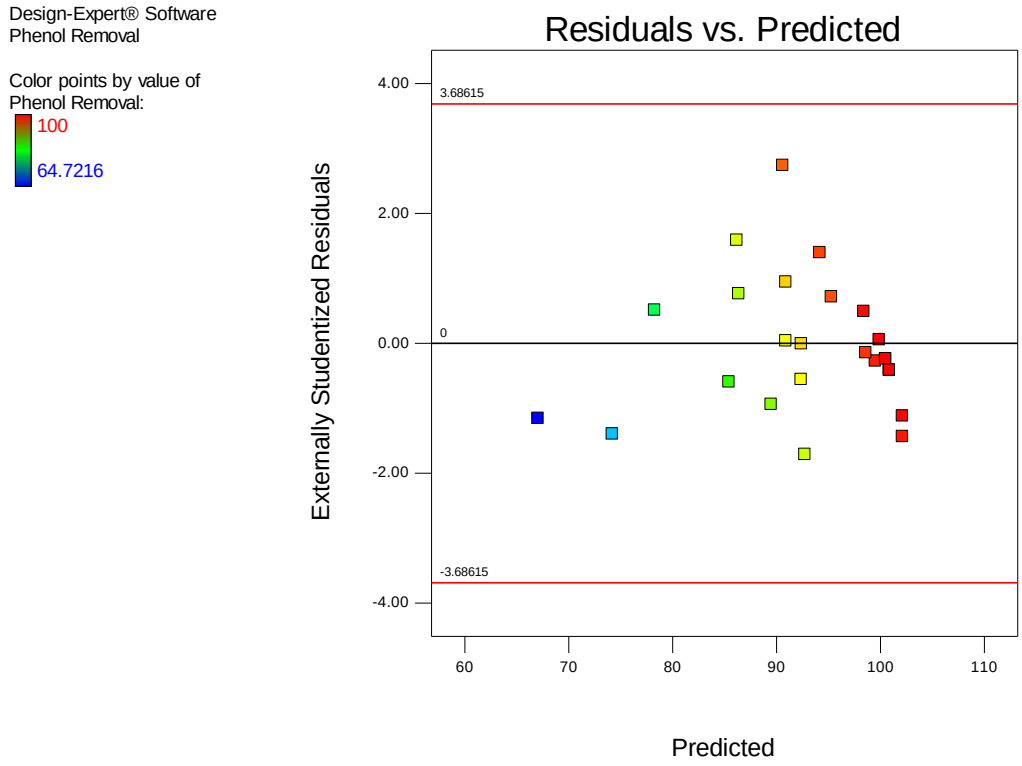

Figure 10.10: Externally studentized residuals versus predicted plot for phenol removal

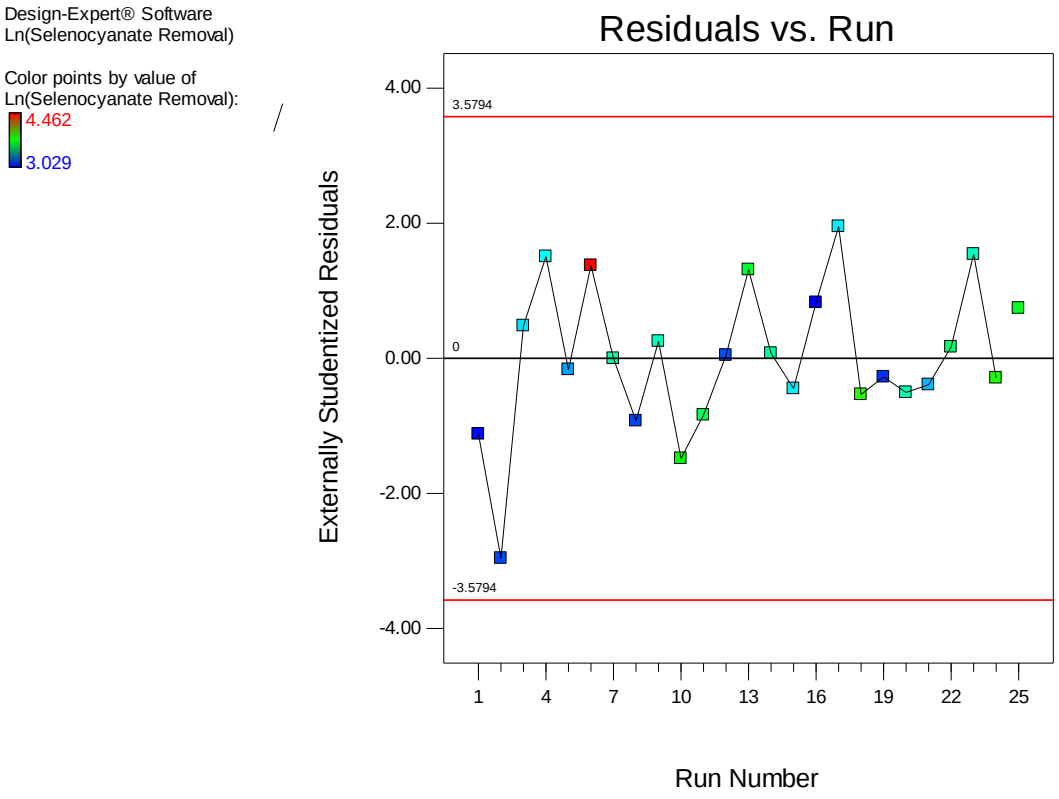

Figure 10.11: Externally studentized residuals versus run plot for total selenium removal

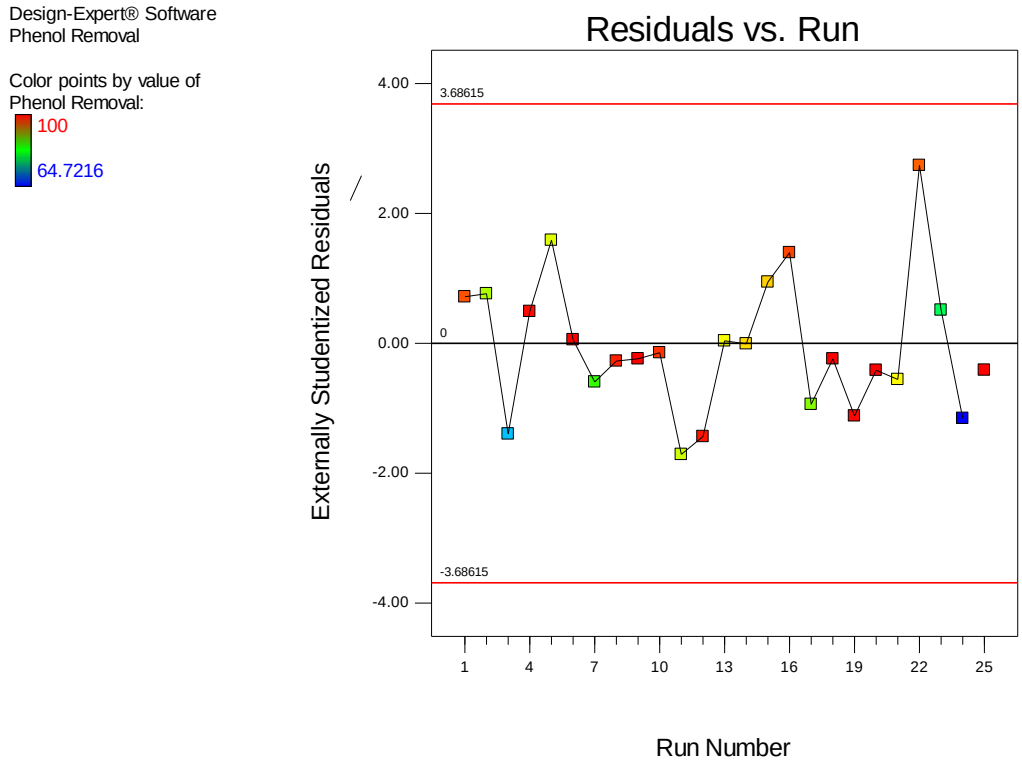

Figure 10.12: Externally studentized residuals versus run plot for phenol removal

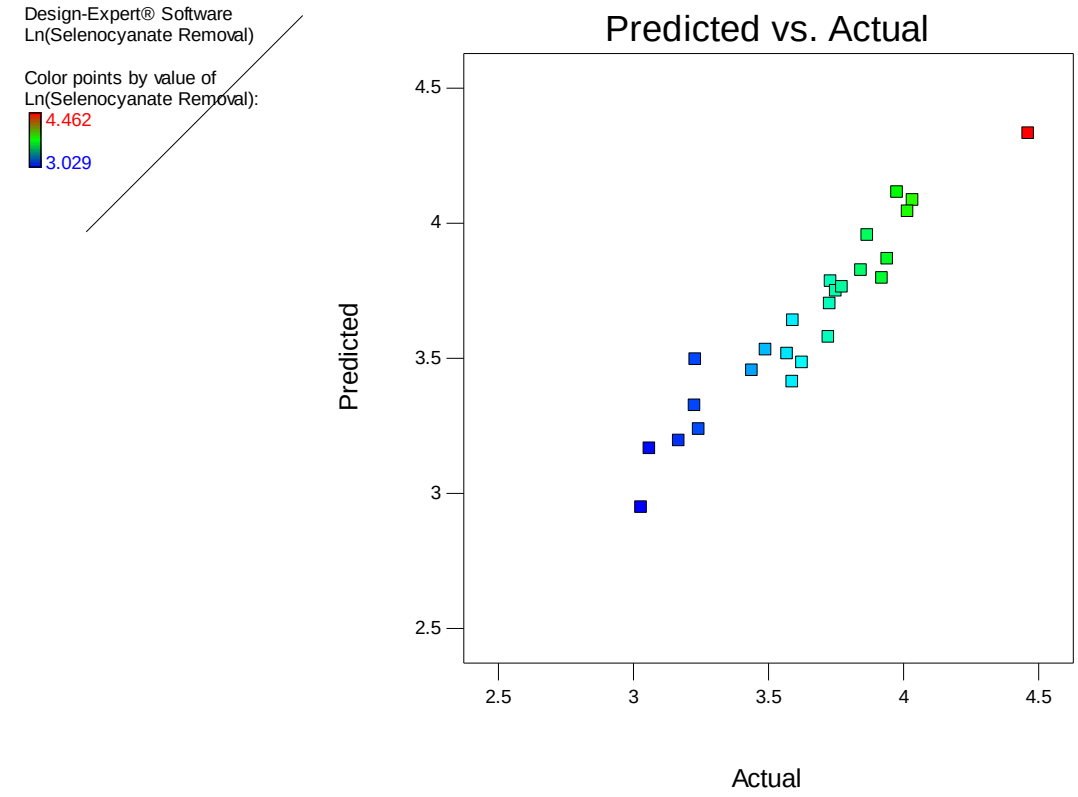

Figure 10.13: Predicted responses versus actual responses for total selenium removal

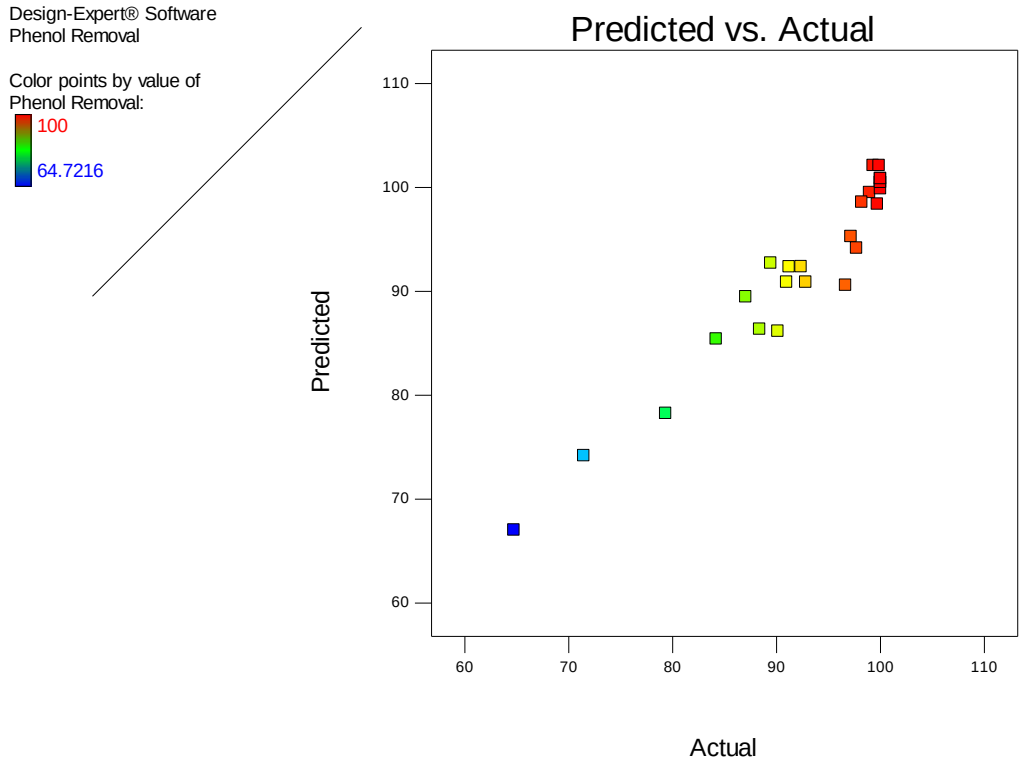

Figure 10.14: Predicted responses versus actual responses for phenol responses

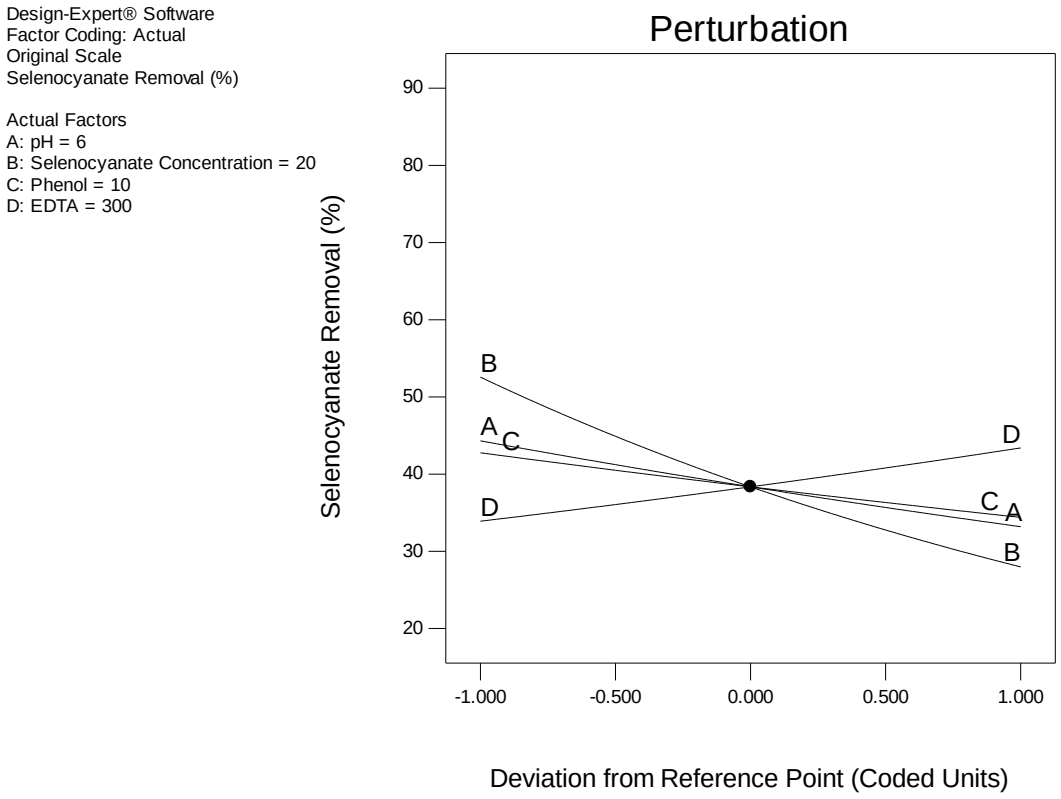

Figure 10.15: Pertubation plots for total selenium removal

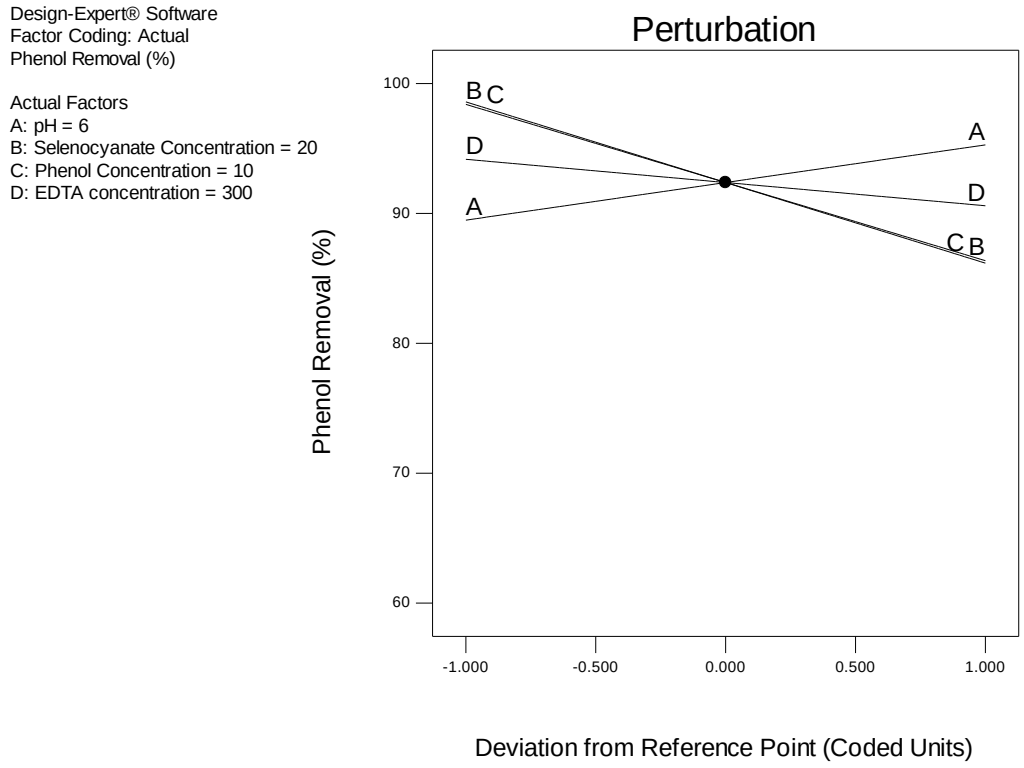

Figure 10.16: Pertubation plots for phenol removal

10.1.2 Models Validation

In order to validate the models obtained and diagnosed in section 10.1.1, four set of experiments were conducted using factor levels that are within the domain of the design of experiment, but not part of the design points. Factor levels, actual responses, predicted responses calculated with equations 10.1 and 10.2, and percent errors were presented in Table 10.5. A good agreement is observed between the experimental and predicted values. For total selenium removal, absolute value of percent errors between predicted

and actual responses fall between 11.1606 and 12.1669, showing a very good prediction. The model prediction was even better for phenol removal model where percent error as low as -0.5 was obtained. The maximum error was -7.0153 showing as excellent ability of the model to predict responses within the domain of the experimental design.

Table 10.5: Actual and predicted responses for model validation

					SeCN Removal			Phenol Removal (%)		
S/No.	pH	SeCN	Phenol	EDTA	Actual (%)	Predicted (%)	Error (%)	Actual (%)	Predicted (%)	Error (%)
1	4	10	5	300	76.1704	67.3565	11.5713	100	100.5	-0.5
2	6	10	5	300	52.2052	58.5570	-12.1669	100	100.68	-0.68
3	4	20	5	450	48.9308	55.1469	-12.7037	89.3870	95.69	-7.0513
4	8	10	5	300	45.7959	50.9070	-11.1606	100	100.86	-0.86

10.1.3 Models Optimization

Numerical optimization is usually the last step in response surface where sets of factor levels that optimizes the response based on predefined constraints are obtained. These constraints are termed goals and are combined in order to come up with an overall desirability ($1 \geq$ desirability ≥ 0). This step simply maximizes or minimizes a response by systematically choosing independent variables within an allowed set. The goals for the optimization process are outlined in Table The higher the desirability, the better the

solution and vice versa. Since optimization is a multi-model, i.e., it possesses various good solutions, we present the best 10 possible solutions for the optimization of photocatalytic removal of selenocyanate and phenol in competitive environment in Table 10.7. Case 1 has the highest desirability of 0.921 and thus it represents the optimum conditions for competitive photocatalytic removal of selenocyanate and phenol. The optimum factors are pH4, 10 ppm selenocyanate concentration, 5 ppm phenol and 450 ppm EDTA concentration.

Table 10.6: Constraints for model optimizations

Name	Goal	Lower Limit	Upper Limit	Lower Weight	Upper Weight	Importance
A:pH	is in range	4	8	1	1	3
B:Selenocyanate Concentration	is in range	10	30	1	1	3
C:Phenol Concentration	is in range	5	15	1	1	3
D:EDTA concentration	is in range	150	450	1	1	3
Total Selenium Removal	maximize	20.6692	86.6552	1	1	3
Phenol Removal	maximize	64.7216	100	1	1	3

Table 10.7: Optimized factor levels and corresponding responses and desirabilities

Number	pH	Selenocyanate Concentration	Phenol Concentration	EDTA concentration	Total Selenium Removal	Phenol Removal	Desirability	
1	4.000	10.000	5.000	450.000	76.631	100.497	0.921	Selected
2	4.000	10.000	5.058	450.000	76.533	100.449	0.920	
3	4.023	10.013	5.000	450.000	76.471	100.492	0.920	
4	4.000	10.092	5.000	449.997	76.408	100.452	0.919	
5	4.027	10.000	5.106	450.000	76.307	100.413	0.918	
6	4.004	10.000	5.000	445.064	76.301	100.497	0.918	
7	4.075	10.001	5.000	449.999	76.217	100.503	0.918	
8	4.000	10.000	5.265	449.997	76.189	100.281	0.917	
9	4.000	10.000	5.325	449.882	76.084	100.233	0.916	
10	4.000	10.246	5.000	449.999	76.038	100.378	0.916	

10.2 KINETIC MODELING

Kinetic modeling is a very important issue in photocatalysis as it helps engineers and scientists to know how fast a certain reaction can go. Chemical kinetics is based on the relationship between quantity of a substance and time, otherwise known as reaction rates. Chemical kinetics is different from chemical equilibrium and chemical thermodynamics where the reactants and the products are in balance [162]. Therefore, chemical kinetics is concerned about chemical rates that also helps us to understand the mechanisms of product(s) formation from reactant(s) through pathways. Considering this, we model the kinetic of competitive photocatalytic removal of selenocyanate and phenol to understand the mechanisms of their removal. Modeling the disappearance of a reactant without considering the formation and disappearance of reaction intermediates is simple as it only requires fitting experimental data to nth order model. Various photocatalytic decay processes has been represented by these simple models [162]. However, such models do not give us the required information to probe the mechanistic details of the chemical processes. However, for stepwise, composite, or complex reactions where more than once steps in involved, individual elementary steps must be incorporated in the models. Experimental results in chapter has shown that competitive photocatalytic removal of selenocyanate and phenol proceeds via multiple and parallel steps. The proposed mechanism for the degradation of phenol and selenocyanate is presented in table 10.8. In the proposed scheme, pyrocatechol, resorcinol, and hydroquinone are lumped into a single pseudo specie and named benzenediols for simplification of the model. It is also worth noting that other reaction intermediates detected at very small concentrations were

considered to be kinetically insignificant and thus dropped. For example, acetic acid and formic acid were detected qualitatively and thus were not considered part of the modeling process. Degradation of parent compounds and intermediates was assumed to be as a result of photocatalytic reactions on the TiO_2 surface. Considering first order reaction kinetic and principles of mass balance and mass transfer, differential equations (DF) were setup according to rates in Table 10.8 (Equations 10.3 to 10.8). The differential equations represent the rate of change of selenocyanate, selenite, selenate, phenol, benzeneseleninic acid, and benzenediols respectively.

The differential equations were solved via Wolfram Mathematica 10 using *ParametricNDSolve* command. The models were fitted to the experimental data using Nonlinear regression analysis. Apparent reaction rate constants for the developed reaction mechanisms under varying experimental conditions as well as adjusted R^2 values are presented in Table 10.9. A good correlation between the experimental and modelled results is observed with maximum, minimum, and mean adjusted R^2 values of 0.9990, 0.7787, 0.9694. Table 10.9 shows that out of 34 sets of experimental results modelled, only two were not fitted well by the model (adjusted R^2 values of 0.7787 and 0.8993). However, for the remaining 32 experiments, a very good to excellent fit was achieved. Experimental and model fits for the reported rate constants are shown in Figures 10.17 to 10.50. Cross correlation matrices close to ±1 indicate a high correlation between the kinetic constants used in optimization as observed in correlation matrices (not shown here). On a general note, no significant difference in k_1 is observed across different pH values investigated, with significant decrease in k_3 observed when pH is increased (Table

10.9). This suggests that increase in photocatalytic degradation of selenocyanate with decrease in pH is because of increased formation of benzeneseleninic acid. Furthermore, increase in k_5 (conversion of phenol to benzenediols) with an increase in pH is also observed because of increase in OH ions and radicals' concentrations with increase in pH. However, increase in k_5 has more effect on k_3 as compared to k_1 probably due to higher selenocyanate/phenol mole ratio in most of the experiments. The preferred pathway for the removal of phenol is therefore through the formation of benzene seleniunic acid and benzenediols at low pH and high pH values respectively. Furthermore, the rate of selenocyanate conversion to selenite also decreases with an increase in initial selenocyanate and phenol concentrations as highlighted by lower k_1 values at elevated selenocyanate and phenol concentrations. This is also true for phenol degradation, where higher degradation rate constants (k_5) were observed for lower phenol and selenocyanate concentrations. Model fits in Figures 10.17 to 10.50 shows that an excellent fit is achieved in single systems with either selenocyanate or phenol only (Figure 10.45 and 10.50 respectively) as a result of cross correlation that exists between model parameters in mixed systems. Furthermore, a better fit is observed generally for the reactants in comparison to the intermediates probably due to contribution of other intermediates not considered in the model. However, despite some limitations in the model, the fit was still very good supporting the mechanisms proposed in this research.

$$\frac{d[SeCN^-]}{dt} = -k_1[\mathrm{SeCN^-}]\text{-}k_3[\mathrm{SeCN^-}][C_6H_5OH] \quad 10.3$$

$$\frac{d[SeO_3^{2-}]}{dt} = k_1[\mathrm{SeCN^-}] - k_2[SeO_3^{2-}] \quad 10.4$$

$$\frac{d[\mathrm{SeO_4^{2-}}]}{dt} = k_2[SeO_3^{2-}] \quad 10.5$$

$$\frac{d[C_6H_5OH]}{dt} = -k_3[\mathrm{SeCN^-}][C_6H_5OH] - k_4[C_6H_5OH] \quad 10.6$$

$$\frac{d[C_6H_5SeO_2H]}{dt} = k_3[\mathrm{SeCN^-}][C_6H_5OH] - k_6[C_6H_5SeO_2H] \quad 10.7$$

$$\frac{d[C_6H_4(OH)_2]}{dt} = k_4[C_6H_5OH] - k_5[C_6H_4(OH)_2] \quad 10.8$$

Table 10.8: Proposed reaction scheme for the degradation of phenol and selenocyanate

Reaction	Rate
$Se\mathrm{CN^-} + 3\mathrm{H_2O} \xrightarrow{\mathrm{TiO_2}} SeO_3^{2-} + HCN + 5\mathrm{H^+} + 4e^-$	$k_1[\mathrm{SeCN^-}]$
$SeO_3^{2-} + \mathrm{H_2O} \xrightarrow{\mathrm{TiO_2}} SeO_4^{2-} + 2\mathrm{H^+} + 2e^-$	$k_2[SeO_3^{2-}]$
$C_6H_5OH + SeCN^- + H_2O \xrightarrow{\mathrm{TiO_2}} C_6H_5SeO_2H + CN^- + \mathrm{H^+} + \mathrm{e^-}$	$k_3[\mathrm{SeCN^-}][C_6H_5OH]$
$C_6H_5OH + H_2O \xrightarrow{\mathrm{TiO_2}} C_6H_4(OH)_2 + 2H^+ + 2e^-$	$k_4[C_6H_5OH]$
$C_6H_4(OH)_2 \xrightarrow{\mathrm{TiO_2}} 2CO_2 + 2C_2H_2 + 2\mathrm{H^+} + 2e^-$	$k_5[C_6H_4(OH)_2]$
$C_6H_5SeO_2H \xrightarrow{\mathrm{TiO_2}} \mathrm{Se^0} + 2CO_2 + 2C_2H_2 + 2\mathrm{H^+} + 2e^-$	$k_6[C_6H_5SeO_2H]$

Table 10.9: Estimated parameters for competitive photocatalytic removal of selenocyanate and phenol under different experimental conditions using reaction schemes in equations 10.3 to 10.8

	Experimental Conditions				Apparent Rate Constants						
S/No.	pH	SeCN	Phenol	EDTA	k_1	k_2	k_3	k_4	k_5	k_6	R^2
1	4	10	5	150	0.0124	0.0137	0.4219	0.0013	0.0139	0.9460	0.9322
2	8	10	5	150	0.0113	0.0465	<0.0001	0.0255	0.1013	0.4892	0.9806
3	4	10	5	300	0.0120	0.0320	0.2666	0.0010	0.0035	0.9835	0.9219
4	6	10	5	300	0.0124	0.0415	0.2718	<0.0001	0.0089	0.8263	0.9796
5	8	10	5	300	0.0133	0.0530	<0.0001	0.0305	0.1334	0.3899	0.9883
6	10	10	5	300	0.0124	0.0471	0.1892	0.0185	0.0566	0.5628	0.9865
7	4	10	5	450	0.0120	0.0195	0.4814	0.0010	0.0061	0.9855	0.8993
8	8	10	5	450	0.0089	0.0286	<0.0001	0.0351	0.3872	0.1911	0.9924
9	4	10	15	150	0.0127	0.0230	0.0911	0.0047	0.0509	0.7981	0.9715
10	8	10	15	150	0.0085	0.0134	0.0649	0.0097	0.0553	0.2056	0.9847
11	4	10	15	450	0.0116	0.0134	0.0511	0.0042	0.0758	0.6759	0.9858
12	8	10	15	450	0.0038	0.0151	0.0182	0.0077	0.0809	0.2799	0.9869
13	4	20	10	300	0.0090	0.0150	0.0989	0.0004	<0.0001	0.4276	0.9552
14	6	20	10	300	0.0024	0.0973	0.0902	0.0000	<0.0001	0.5955	0.9867
15	8	20	10	300	0.0025	0.0309	0.0144	0.0086	0.2708	2.2779	0.9969
16	4	30	5	150	0.0089	0.0055	0.4136	<0.0001	<0.0001	0.9206	0.9248
17	8	30	5	150	0.0044	0.0540	0.0438	0.0010	0.0014	0.2783	0.9896
18	4	30	5	450	0.0082	0.0100	0.2191	<0.0001	0.0007	0.6651	0.9681
19	8	30	5	450	0.0070	0.0192	0.0121	0.0110	0.0656	0.3574	0.9530
20	4	30	15	150	0.0033	0.0105	0.0437	<0.0001	0.0701	0.4670	0.9703
21	8	30	15	150	0.0009	0.0963	0.0136	0.0038	0.0171	0.4635	0.9973
22	4	30	15	450	0.0045	0.0059	0.0474	<0.0001	0.0864	0.5873	0.9518
23	8	30	15	450	0.0011	0.0129	0.0085	0.0042	0.0216	0.5222	0.9979

24	4	10	5	0	0.0140	0.0099	0.1367	0.0043	0.0557	0.9140	0.9544
25	6	20	10	450	0.0026	0.0366	0.0547	0.0022	0.0183	0.4621	0.9966
26	6	20	10	150	0.0055	0.0341	0.0209	0.0078	0.0956	0.3784	0.9908
27	4	10	50	0	0.0082	0.0092	0.0186	0.0009	0.1515	0.6191	0.9990
28	6	10	10	300	0.0058	0.0568	0.0782	0.0058	0.0479	0.6952	0.9903
29	6	20	0	300	0.0141	0.0161					0.9814
30	6	20	5	300	0.0070	0.0457	0.0917	0.0035	0.3968	0.2011	0.9758
31	6	20	15	300	0.0021	0.3241	0.0224	0.0034	0.0181	0.5243	0.9955
32	4	20	5	450	0.0119	0.0071	0.1000	<0.0001	0.2424	0.1000	0.7787
33	6	30	10	300	0.0020	0.1057	0.0245	0.0039	0.0465	0.2837	0.9975
34	4	0	5	0				0.0313	1.6462		0.9988

CONCLUSIONS AND RECOMMENDATIONS

11.1 CONCLUSIONS

TiO_2 based adsorption and photocatalysis were studied for the removal of aqueous phase selenocyanate species. Firstly, we studied competitive adsorption of aqueous phase selenite, selenate and selenocyanate species onto titanium dioxide (TiO_2) under a varying set of conditions and respective details on both experimental and modelling findings are reported. Studies completed under binary selenite & selenate mixed conditions indicated that selenite adsorption is not affected by selenate species with high selenite removal noted specifically at acidic pH values. However, selenate adsorption was suppressed by selenite species. This indicated that relative affinity of TiO_2 surface sites is higher for selenite compared to selenate species. However, findings from selenite/selenocyanate and selenate/selenocyanate mixed systems showed no competitive effect. These findings indicate that both selenite and selenocyanate species adsorption is not affected in the respective binary systems whereas selenate removal is suppressed by selenite species. Similar adsorption trends were also noted for the tertiary mixed systems having selenite, selenate, and selenocyanate species under a varying set of mixed conditions. Also, the overall percent based adsorption at pH above 4 indicated the following trend: selenite > selenocyanate > selenate. We also completed an extensive modelling exercise employing the diffuse layer model. The respective surface complexation species included an inner sphere type complex for selenite, i.e., **Ti**-SeO_3^- whereas for selenate and selenocyanate

species outer sphere complexes were considered, i.e., **Ti**-H_2O-SeO_4^- and **Ti**-H_2O-SeCN. These findings were supported by good to reasonable adsorption estimations for respective selenium species onto TiO_2 over a wide range of conditions. After the adsorption studies, solar photocatalytic removal of selenocyanate only was investigated, followed by comprehensive investigation on the efficiency of UV and solar light assisted TiO_2 based photocatalytic degradation (PCD) processes for the competitive destruction of selenocyanate complex along with simultaneous removal of co-pollutants ammonia, cyanide, thiocyanate, and phenol from simulated mixed wastewater streams. Higher solar photocatalytic removal of selenium species transpired at pH 4 and it increased with an increase in both initial selenium and initial EDTA concentrations. The mechanism for selenocyanate removal is via SeCN complex destruction followed by stepwise oxidation to selenite and then to selenate, which in turn are reduced to elemental selenium using hole scavenger EDTA. While co-pollutants selenite, selenate, and ammonia do not significantly affect selenocyanate removal, photocatalytic removal of selenocyanate is suppressed in the presence of phenol, cyanide and thiocyanate. It is worth noting that while selenium and thiocyanate species were converted to elemental selenium and sulfate respectively, no significant removal of ammonia and cyanide was noted. The mechanism of phenol removal in the presence of selenocyanate involves the formation of benzeneseleninic acid, hydroquinone, resorcinol, and pyrocatechol as primary intermediates. Secondary intermediates include maleic acid, formic acid and fumaric acid among others.

Design of experiment (DOE) using face-centered central composite design was employed for modelling photocatalytic removal of selenocyanate and phenol under competitive environment via design expert version 10. Natural log transformed Linear and non-transformed two factor interaction mathematical models were developed for selenocyanate and phenol removal with R^2 values of 0.9140 and 0.9395 respectively. The difference between adjusted R^2 and predicted R^2 values was less than 0.2, showing a good agreement between the two. The models were validated using various statistical, diagnostic tools, and experimental validation. By setting maximum selenocyanate and phenol removal as optimal goals, optimal process conditions of pH 4, 10 ppm selenocyanate, 5 ppm phenol and 450 ppm EDTA concentrations were established by design expert with desirability of 0.921. RSM modelling prove to be an economical way for the removal of selenocyanate and phenol from aqueous phase using the optimization techniques.

Lastly, kinetic models for photocatalytic removal of selenocyanate and phenol under varying experimental conditions were developed by considering degradation of reactants and the formation and disappearance of reaction intermediates. First order reaction kinetics, and mass law were considered in solving differential equations representing the rate of change of each reactant using Mathematica to obtain reaction rate constants. *ParametricNDSolve* and *NonlinearModelFit* command were utilized for solving the differential equation and fitting the experimental data to the model respectively. A good correlation between the experimental and modelled results is observed with maximum, minimum, and mean adjusted R^2 values of 0.9990, 0.7787, and 0.9694. Findings from

kinetic studies suggest selenocyanate removal via oxidation to selenite and then selenate and reaction of selenocyanate and phenol to form benzeneseleninic acid especially at low pH values. Formation of benzenediols and benzeneseleninic acid were the dominant mechanisms for phenol removal at high and low pH values respectively. These findings from kinetic modelling proves to be vital for controlling the process conditions for selecting preferable pathway for the degradation of selenocyanate and phenol using TiO_2 based photocatalysis.

11.2 RECOMMENDTIONS

Based on the results from this research, we recommend further research in the following areas:

- Application of surface complexation modelling using other advanced models such as charge distribution multi-site complexation (**CD-MUSIC**) model and Triple layer model can also be explored.
- Photocatalytic degradation of selenocyanate in mixed condition with co-pollutants should be investigated using improved photocatalysts that will improve light absorbance and hence photocatalytic degradation.
- Kinetic modelling for competitive photocatalytic removal of selenocyanate in the presence of co-pollutants selenite, selenate, thiocyanate, cyanide and ammonia should also be investigated.
- The current research modelled the kinetic of selenocyanate and phenol removal using apparent rate constants, a more complex model utilizing adsorption constants and various pathway will add to the current knowledge.
- Comparison of various RSM models such as Box-Behnken, full factorial, and other central composite designs for the removal of selenocyanate in the presence of various co-pollutants is also a promising research area.

Appendix A: Kinetic model fits for competitive removal of selenocyanate and phenol using UV lamp assisted photocatalysis

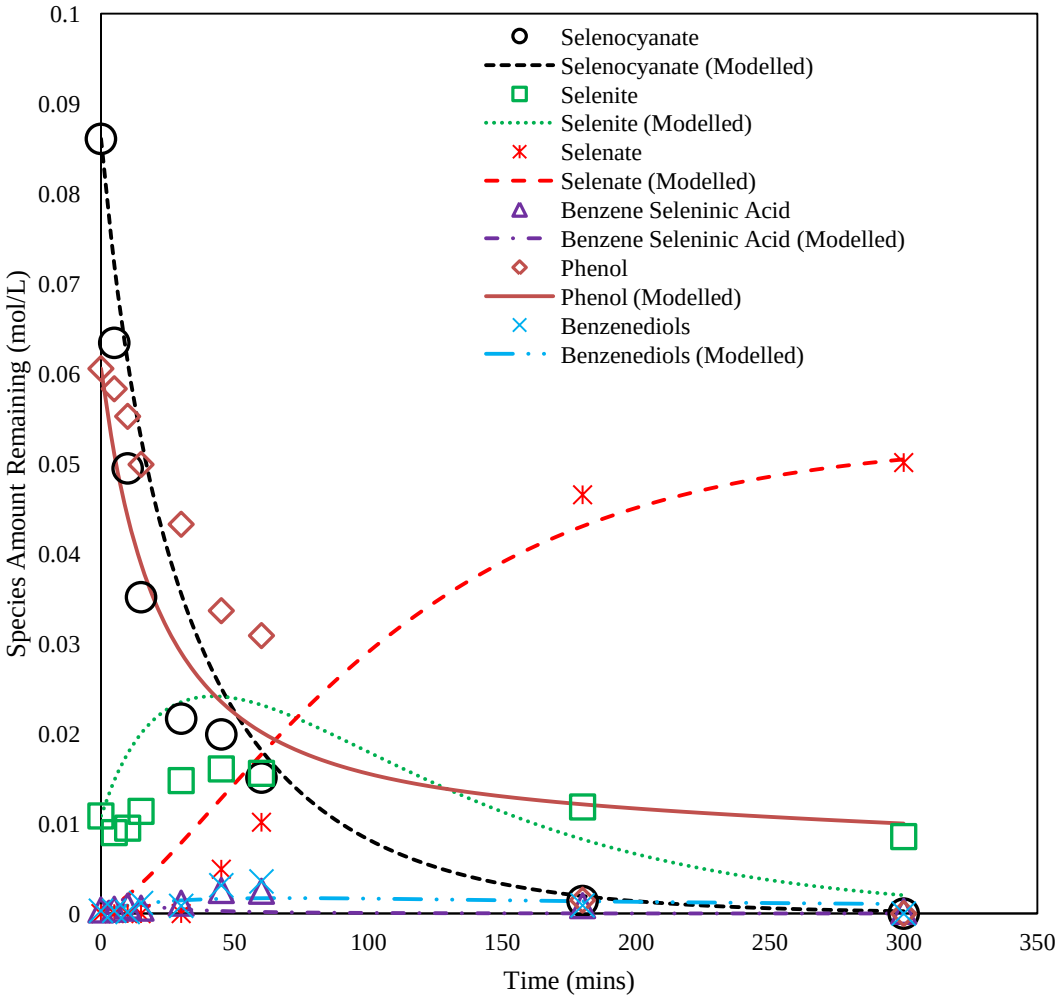

Figure A. 1: Experimental and kinetic modelling results for UV light competitive photocatalytic removal of selenocyanate and phenol at pH 4 (10 ppm selenocyanate, 5 ppm phenol, 150 ppm EDTA added at 5 hours).

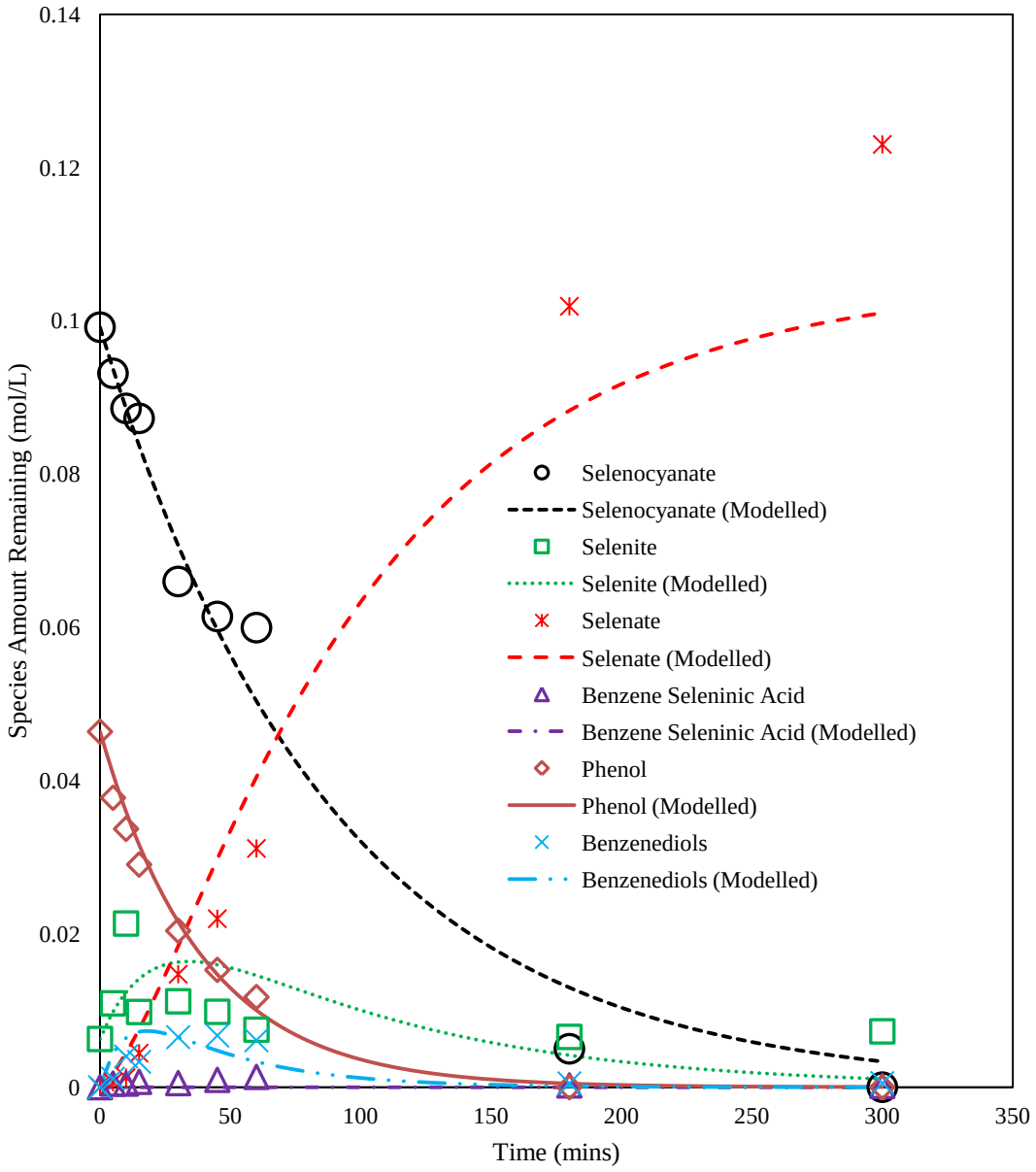

Figure A. 2: Experimental and kinetic modelling results for UV light competitive photocatalytic removal of selenocyanate and phenol at pH 8 (10 ppm selenocyanate, 5 ppm phenol, 150 ppm EDTA added at 5 hours).

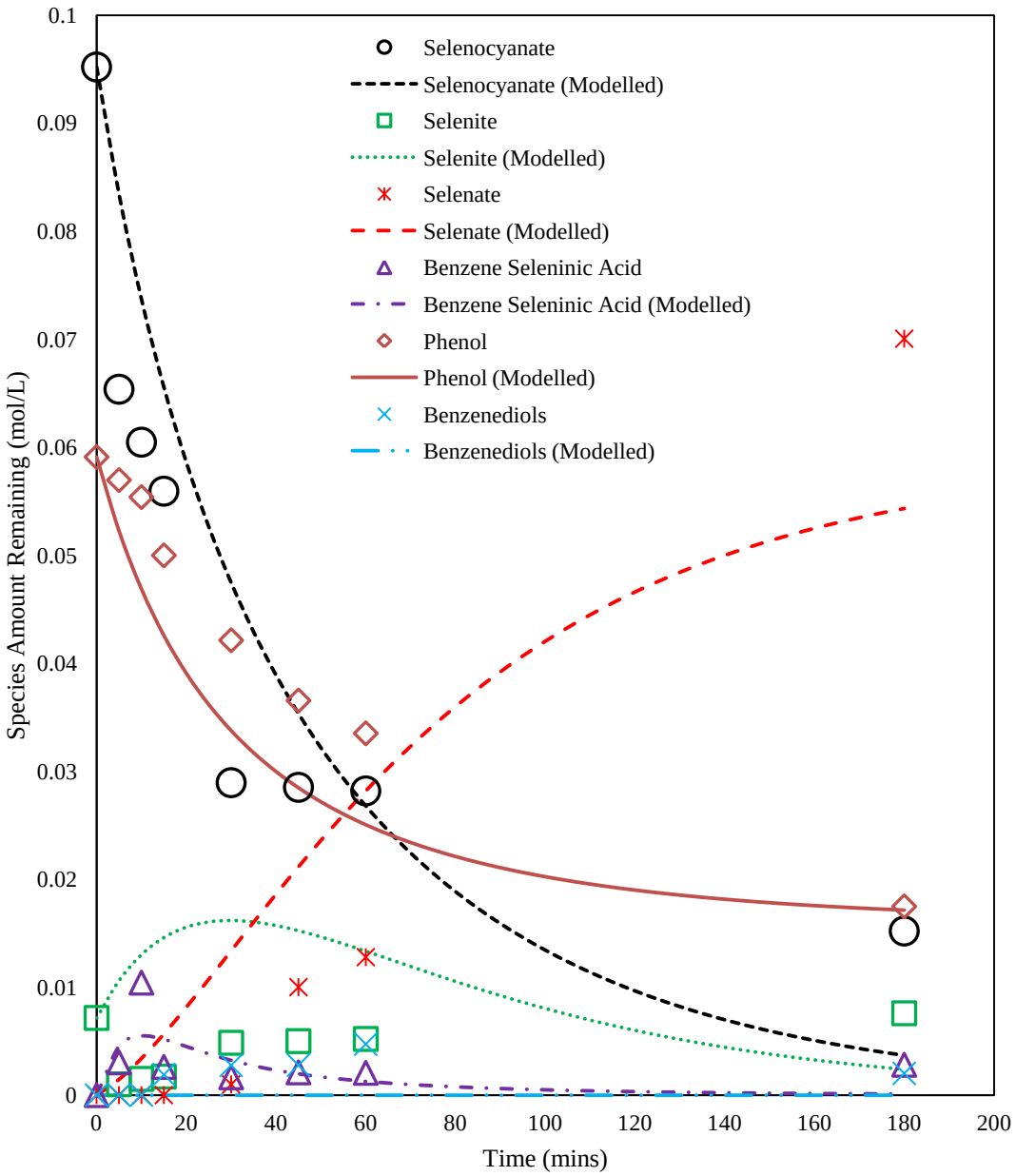

Figure A. 3: Experimental and kinetic modelling results for UV light competitive photocatalytic removal of selenocyanate and phenol at pH 4 (10 ppm selenocyanate, 5 ppm phenol, 300 ppm EDTA added at 5 hours).

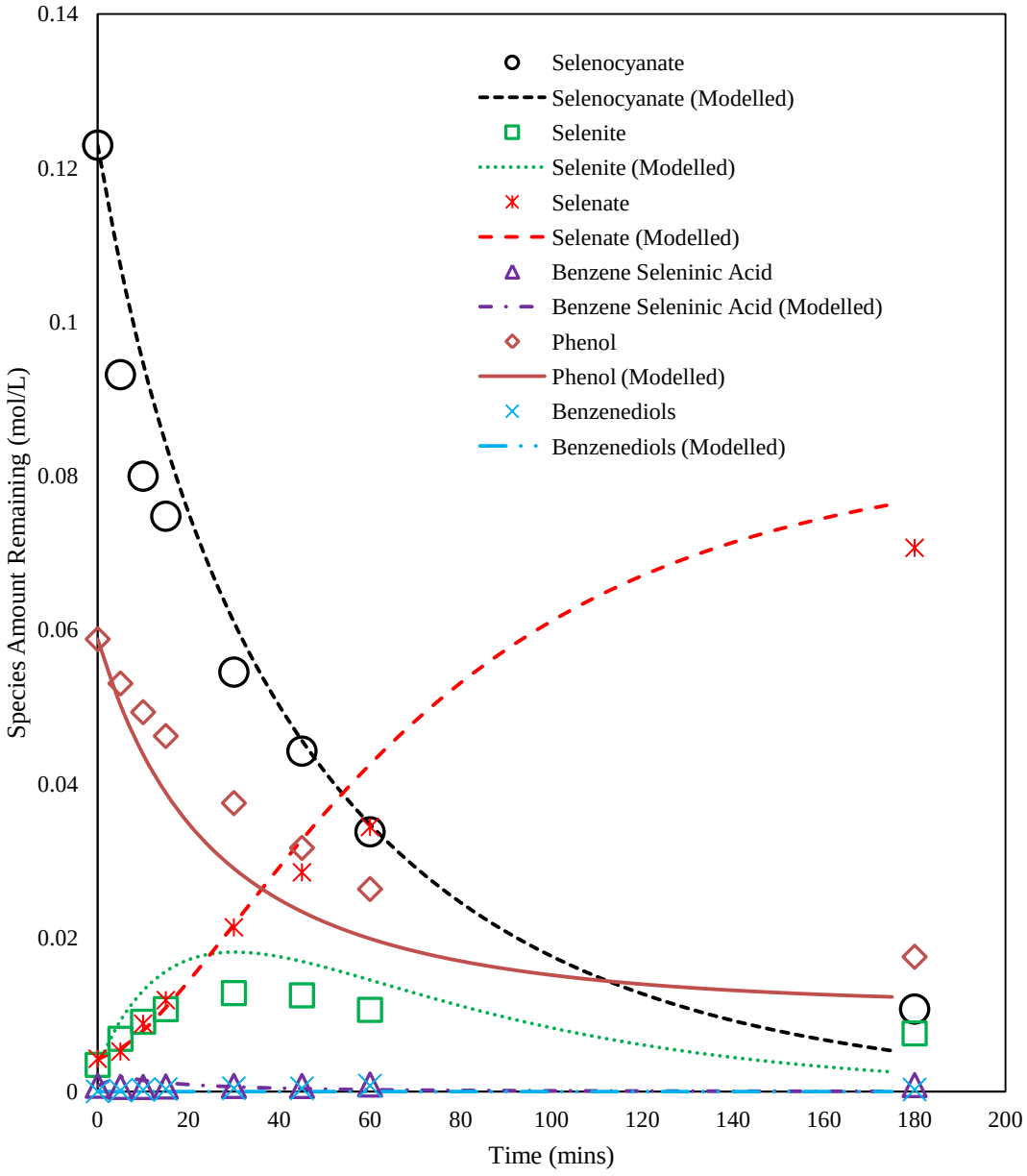

Figure A. 4: Experimental and kinetic modelling results for UV light competitive photocatalytic removal of selenocyanate and phenol at pH 6 (10 ppm selenocyanate, 5 ppm phenol, 300 ppm EDTA added at 5 hours).

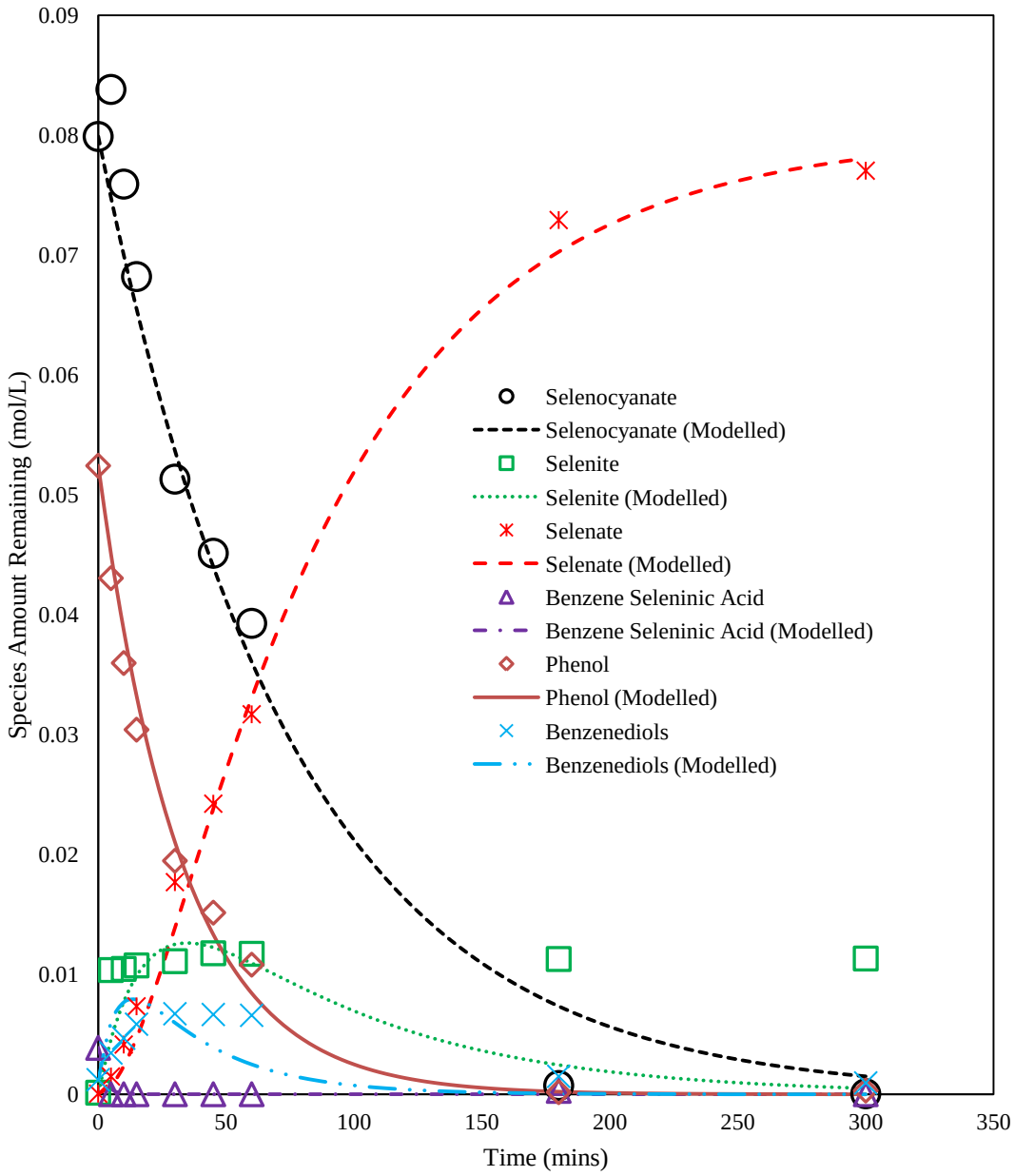

Figure A. 5: Experimental and kinetic modelling results for UV light competitive photocatalytic removal of selenocyanate and phenol at pH 8 (10 ppm selenocyanate, 5 ppm phenol, 300 ppm EDTA added at 5 hours).

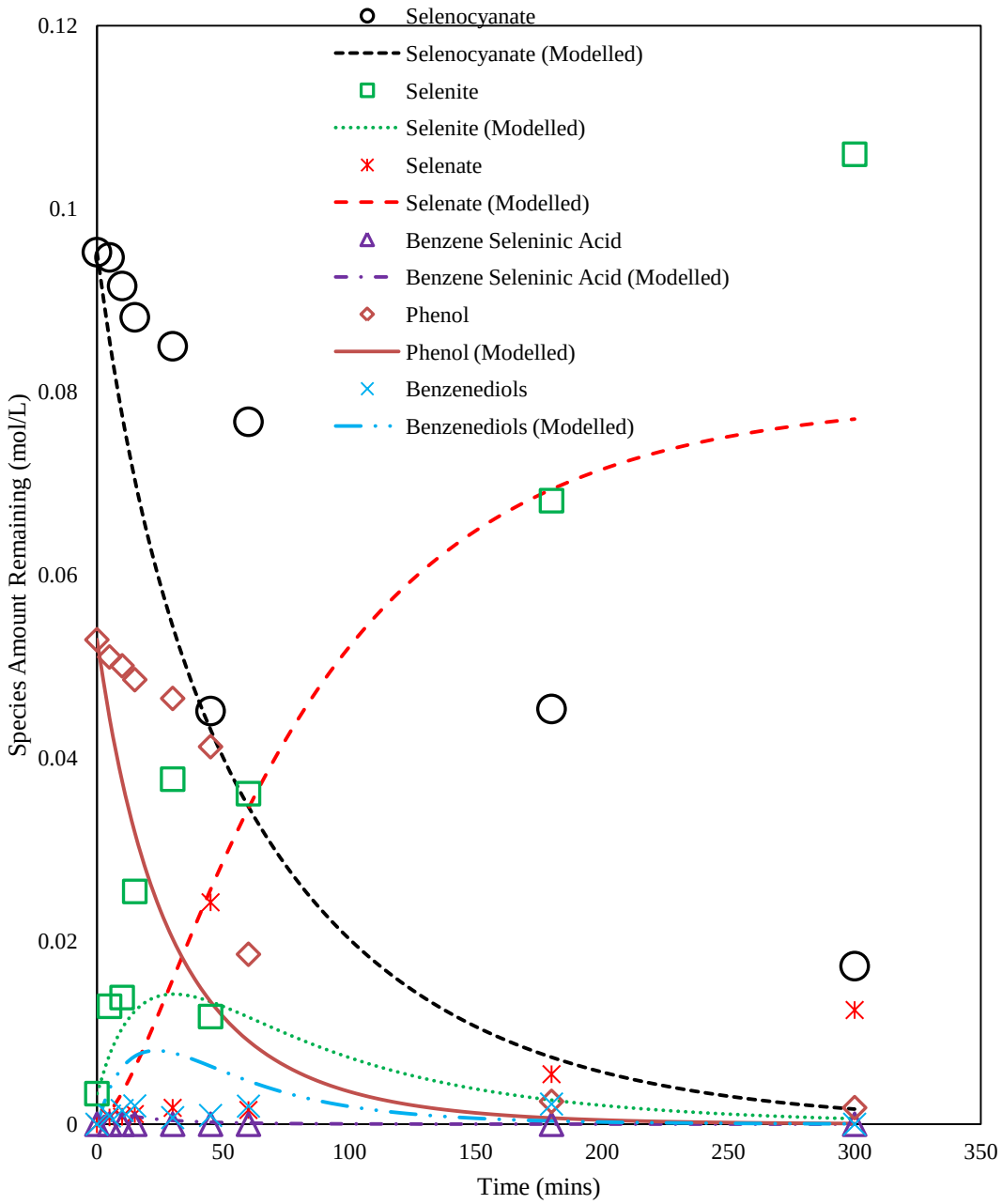

Figure A. 6: Experimental and kinetic modelling results for UV light competitive photocatalytic removal of selenocyanate and phenol at pH 10 (10 ppm selenocyanate, 5 ppm phenol, 300 ppm EDTA added at 5 hours).

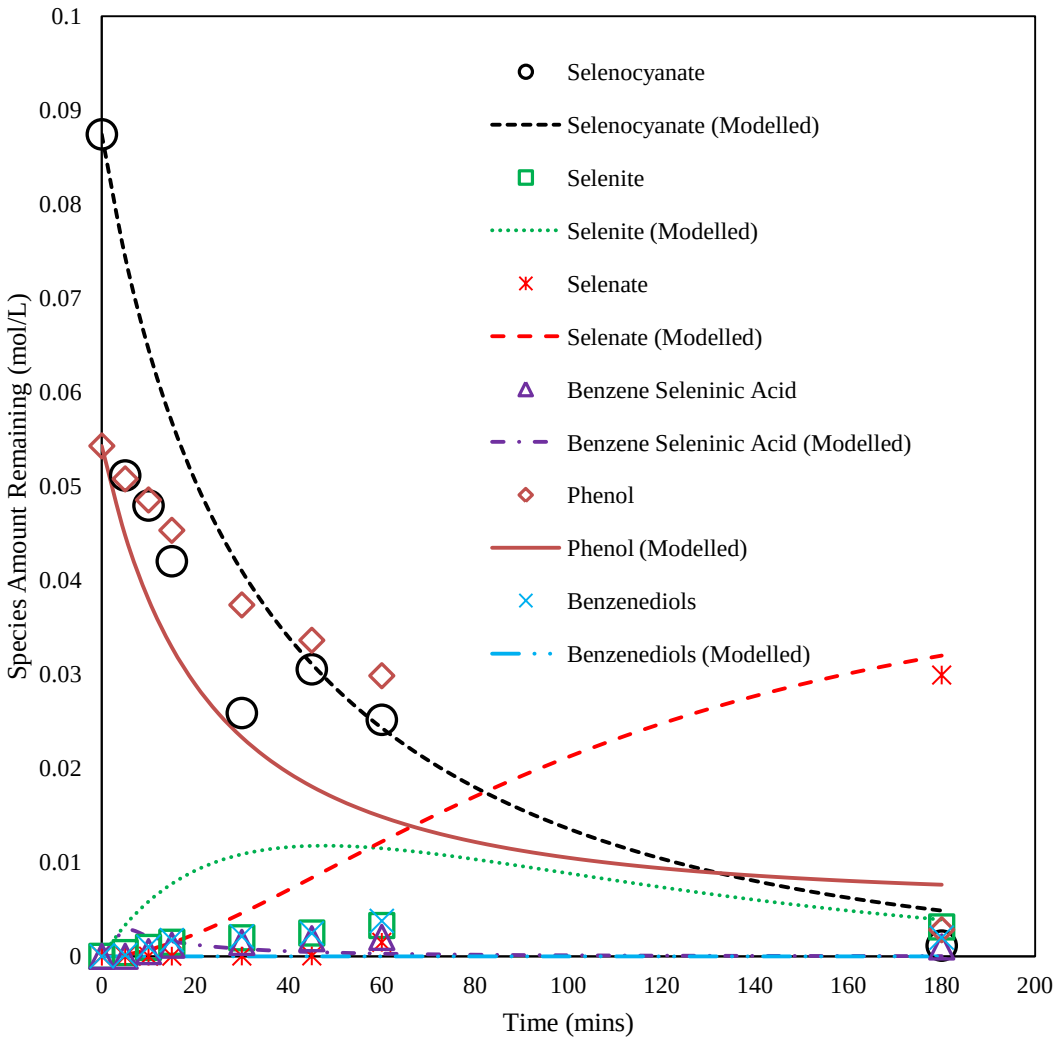

Figure A. 7: Experimental and kinetic modelling results for UV light competitive photocatalytic removal of selenocyanate and phenol at pH 4 (10 ppm selenocyanate, 5 ppm phenol, 450 ppm EDTA added at 5 hours).

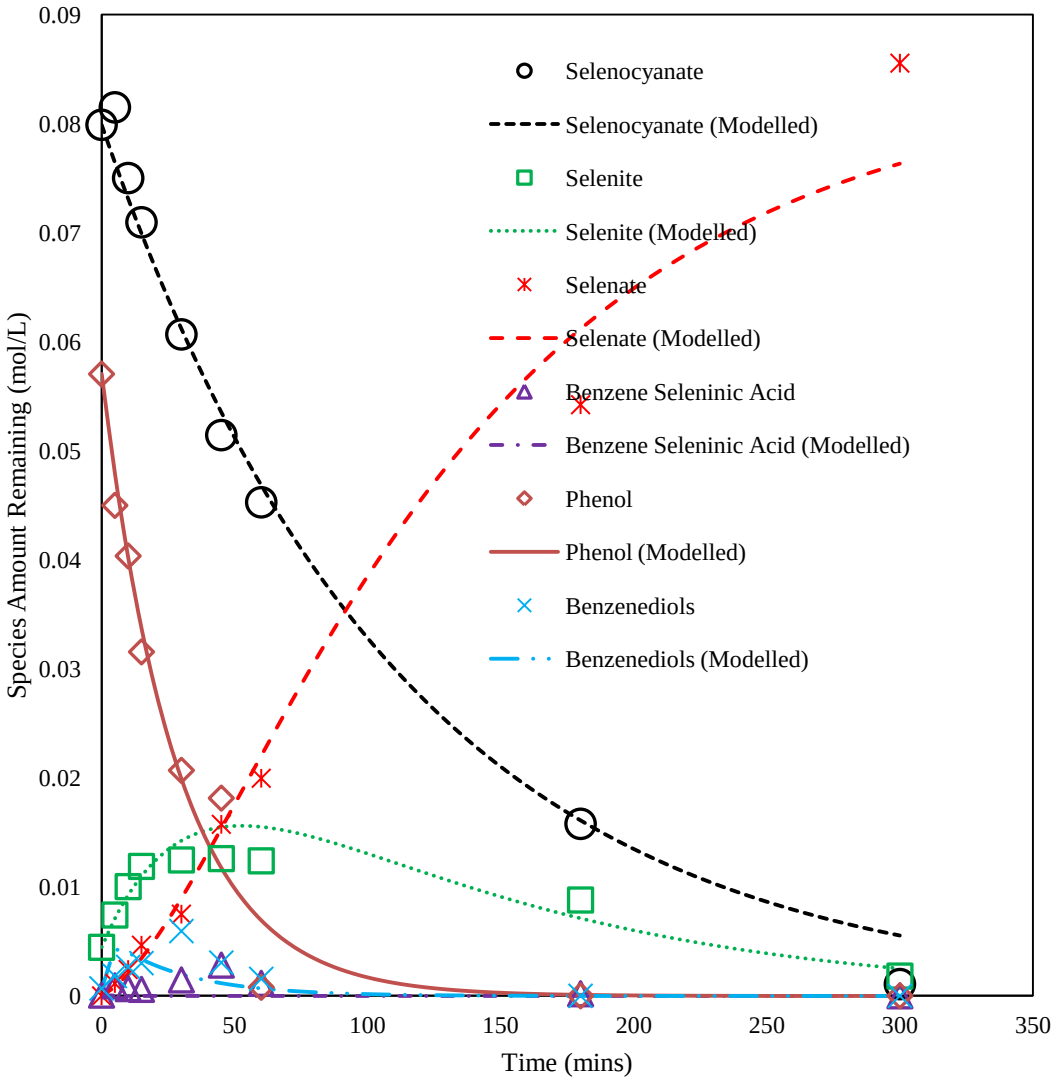

Figure A. 8: Experimental and kinetic modelling results for UV light competitive photocatalytic removal of selenocyanate and phenol at pH 8 (10 ppm selenocyanate, 5 ppm phenol, 450 ppm EDTA added at 5 hours).

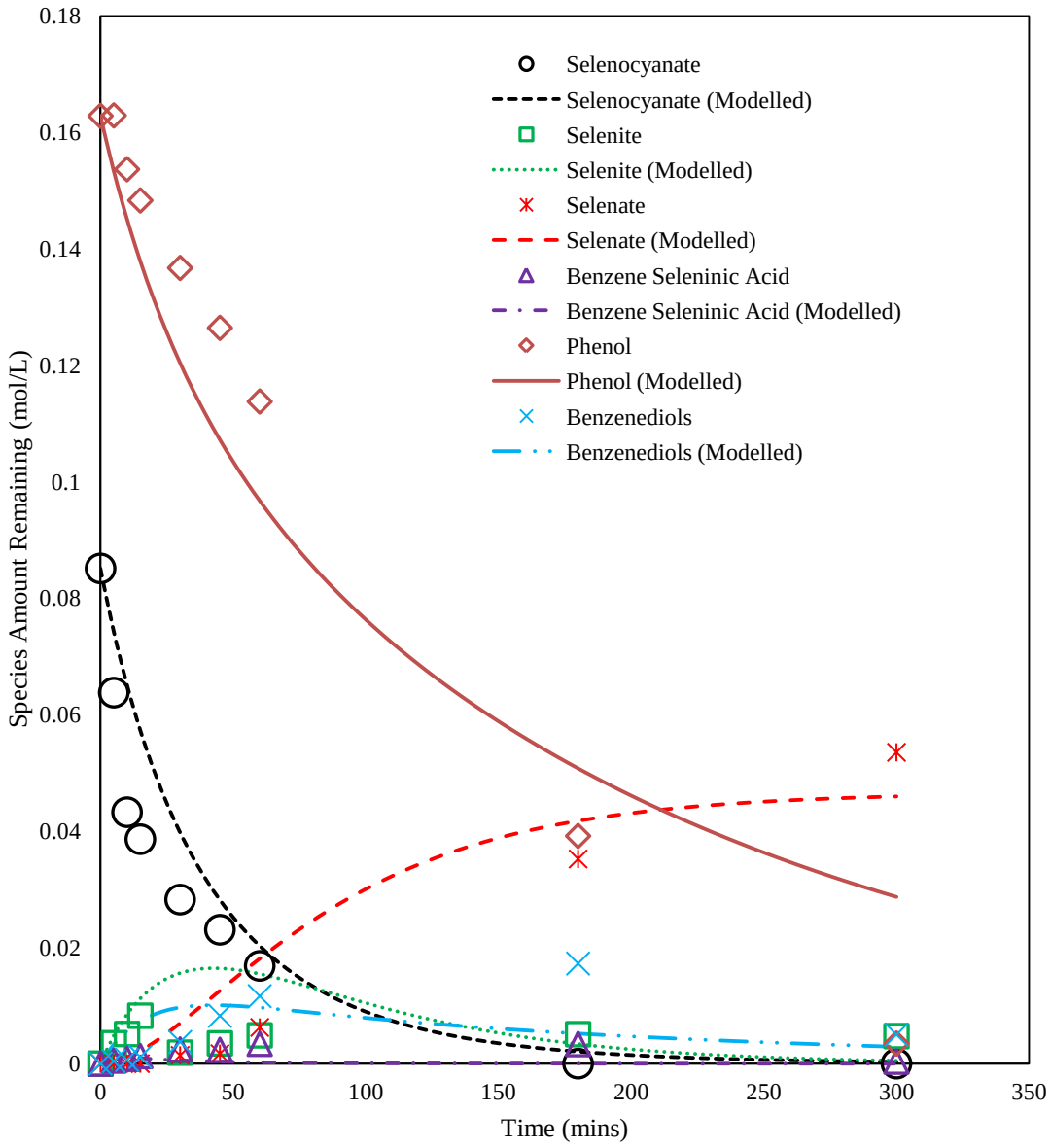

Figure A. 9: Experimental and kinetic modelling results for UV light competitive photocatalytic removal of selenocyanate and phenol at pH 4 (10 ppm selenocyanate, 15 ppm phenol, 150 ppm EDTA added at 5 hours).

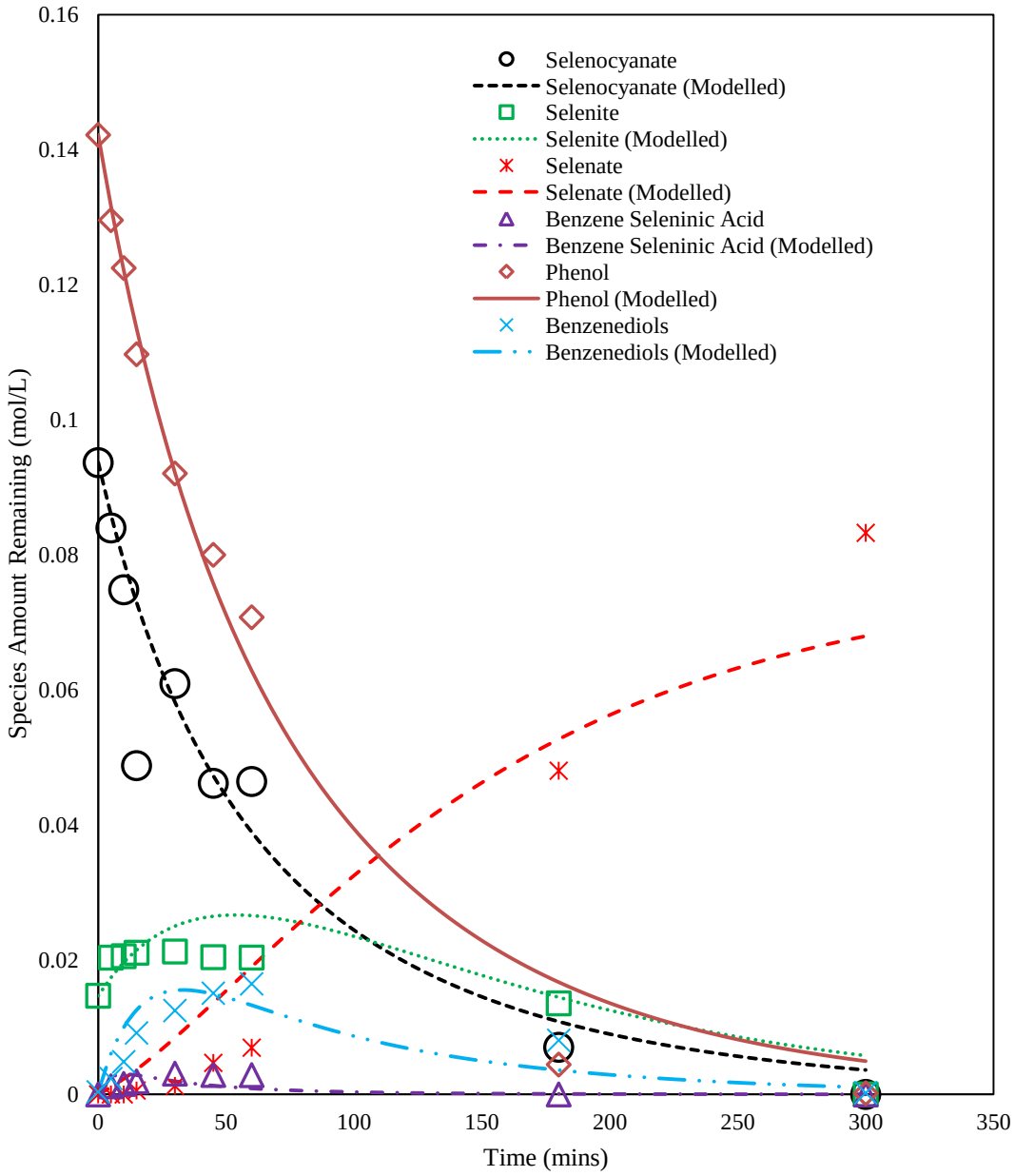

Figure A. 10: Experimental and kinetic modelling results for UV light competitive photocatalytic removal of selenocyanate and phenol at pH 8 (10 ppm selenocyanate, 15 ppm phenol, 150 ppm EDTA added at 5 hours).

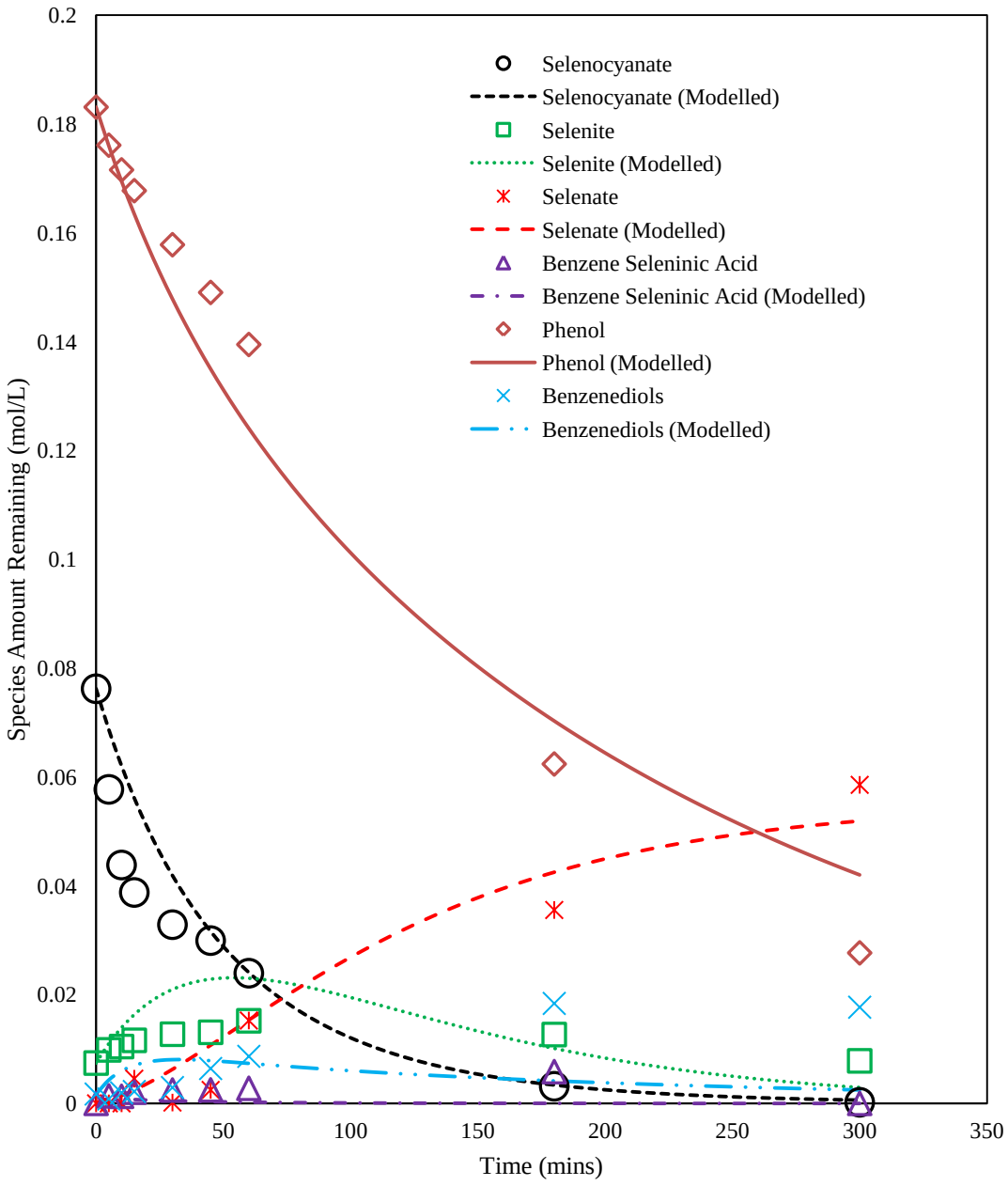

Figure A. 11: Experimental and kinetic modelling results for UV light competitive photocatalytic removal of selenocyanate and phenol at pH 4 (10 ppm selenocyanate, 15 ppm phenol, 450 ppm EDTA added at 5 hours).

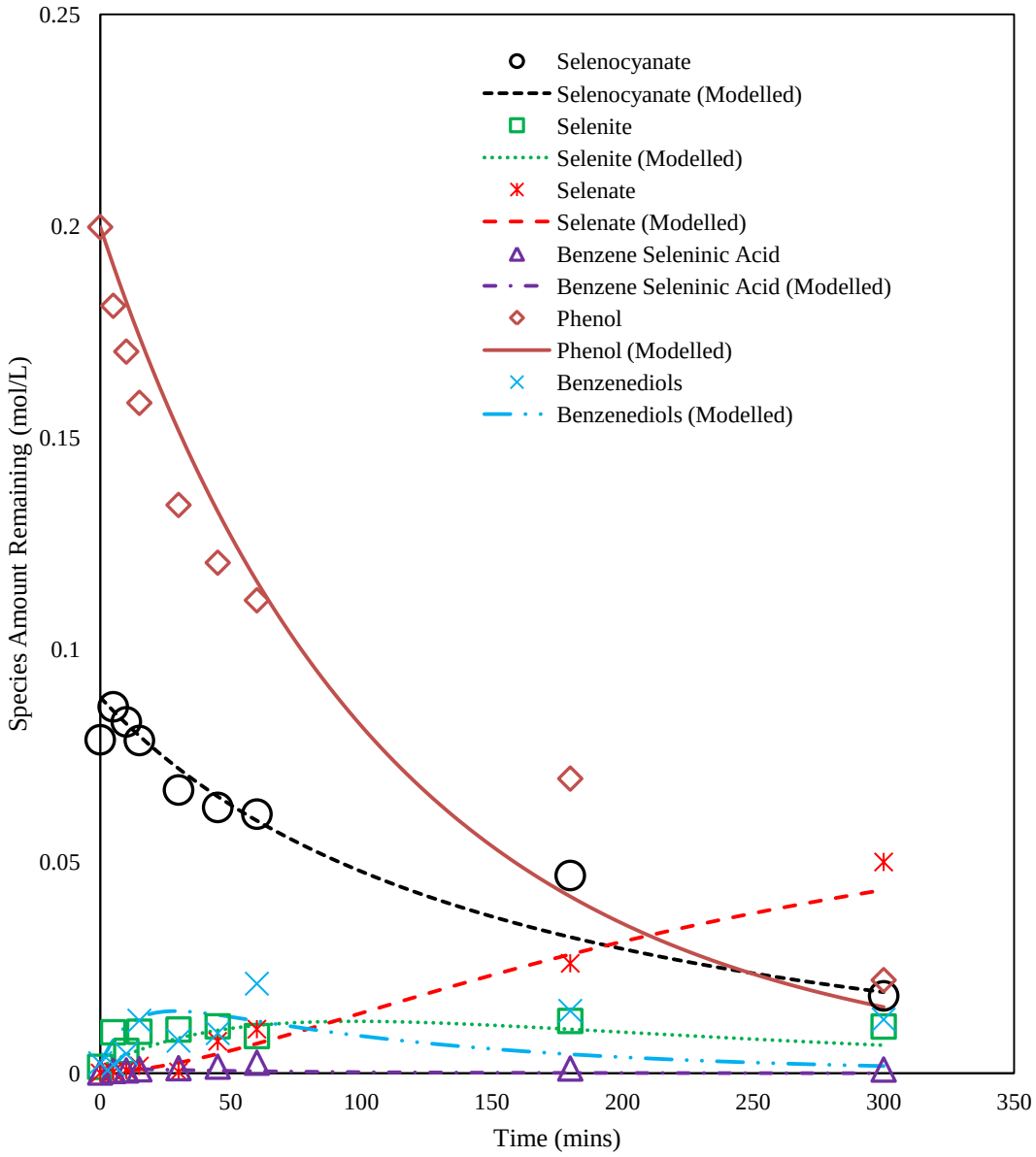

Figure A. 12: Experimental and kinetic modelling results for UV light competitive photocatalytic removal of selenocyanate and phenol at pH 8 (10 ppm selenocyanate, 15 ppm phenol, 450 ppm EDTA added at 5 hours).

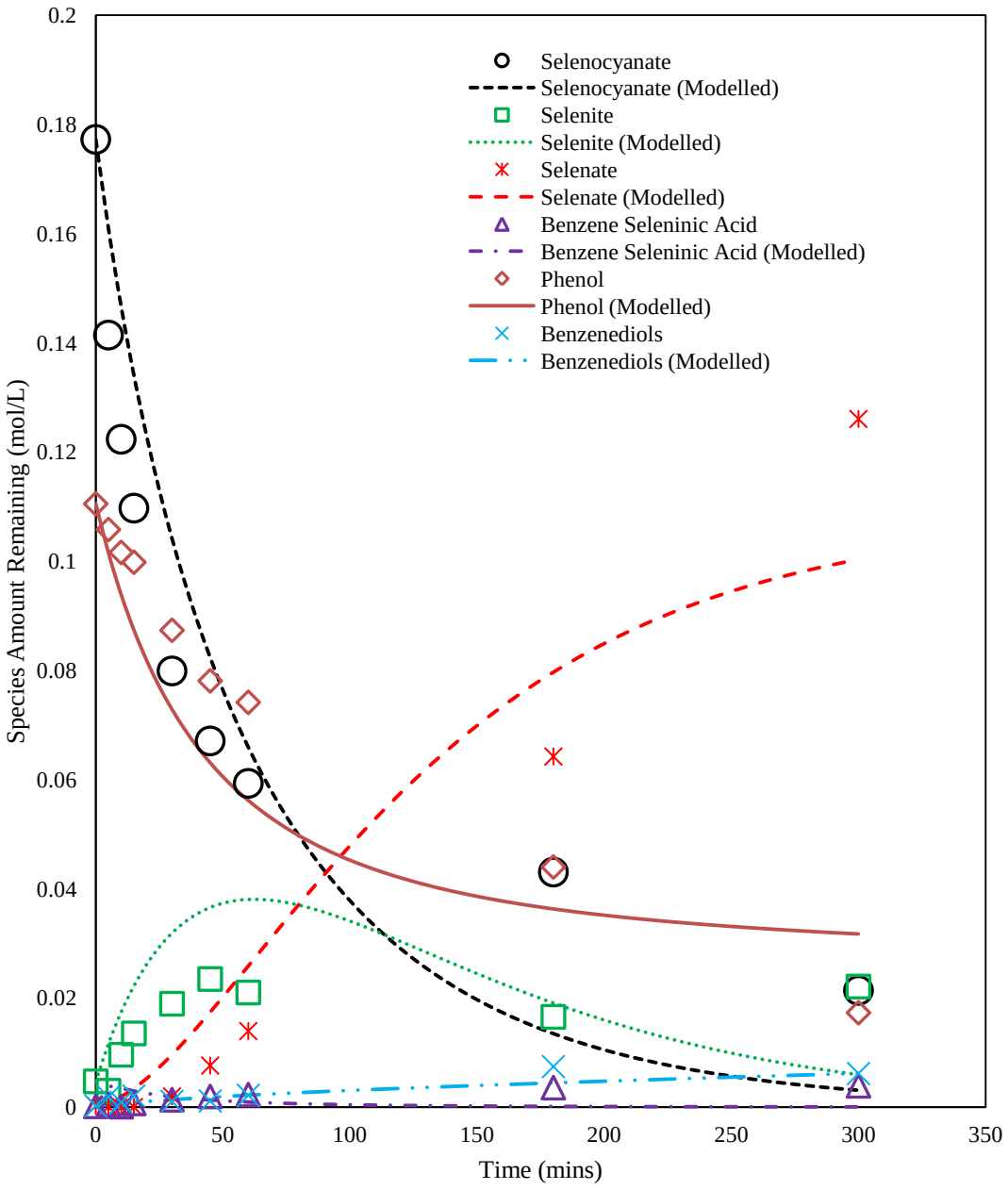

Figure A. 13: Experimental and kinetic modelling results for UV light competitive photocatalytic removal of selenocyanate and phenol at pH 4 (20 ppm selenocyanate, 10 ppm phenol, 300 ppm EDTA added at 5 hours).

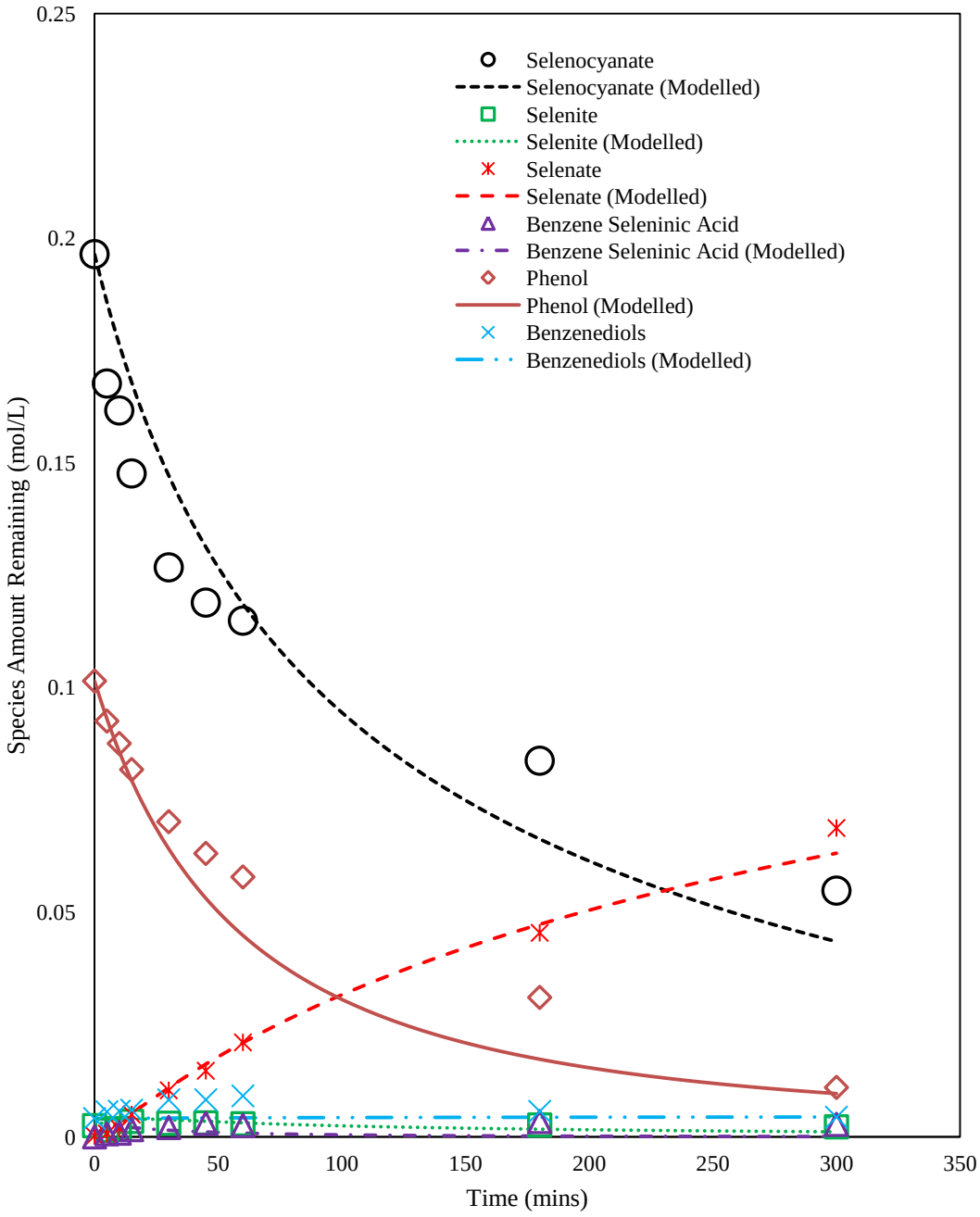

Figure A. 14: Experimental and kinetic modelling results for UV light competitive photocatalytic removal of selenocyanate and phenol at pH 6 (20 ppm selenocyanate, 10 ppm phenol, 300 ppm EDTA added at 5 hours).

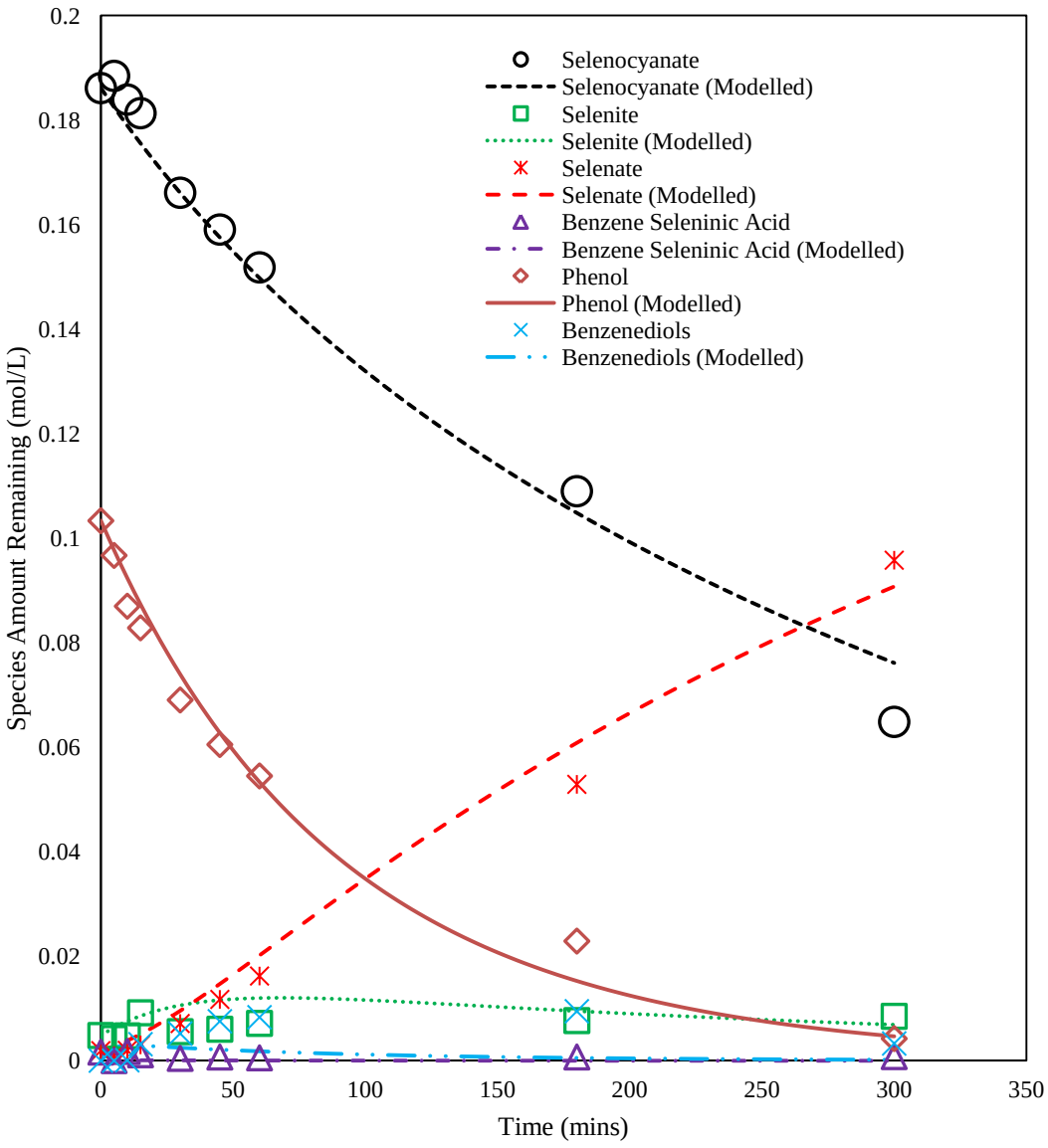

Figure A. 15: Experimental and kinetic modelling results for UV light competitive photocatalytic removal of selenocyanate and phenol at pH 8 (20 ppm selenocyanate, 10 ppm phenol, 300 ppm EDTA added at 5 hours).

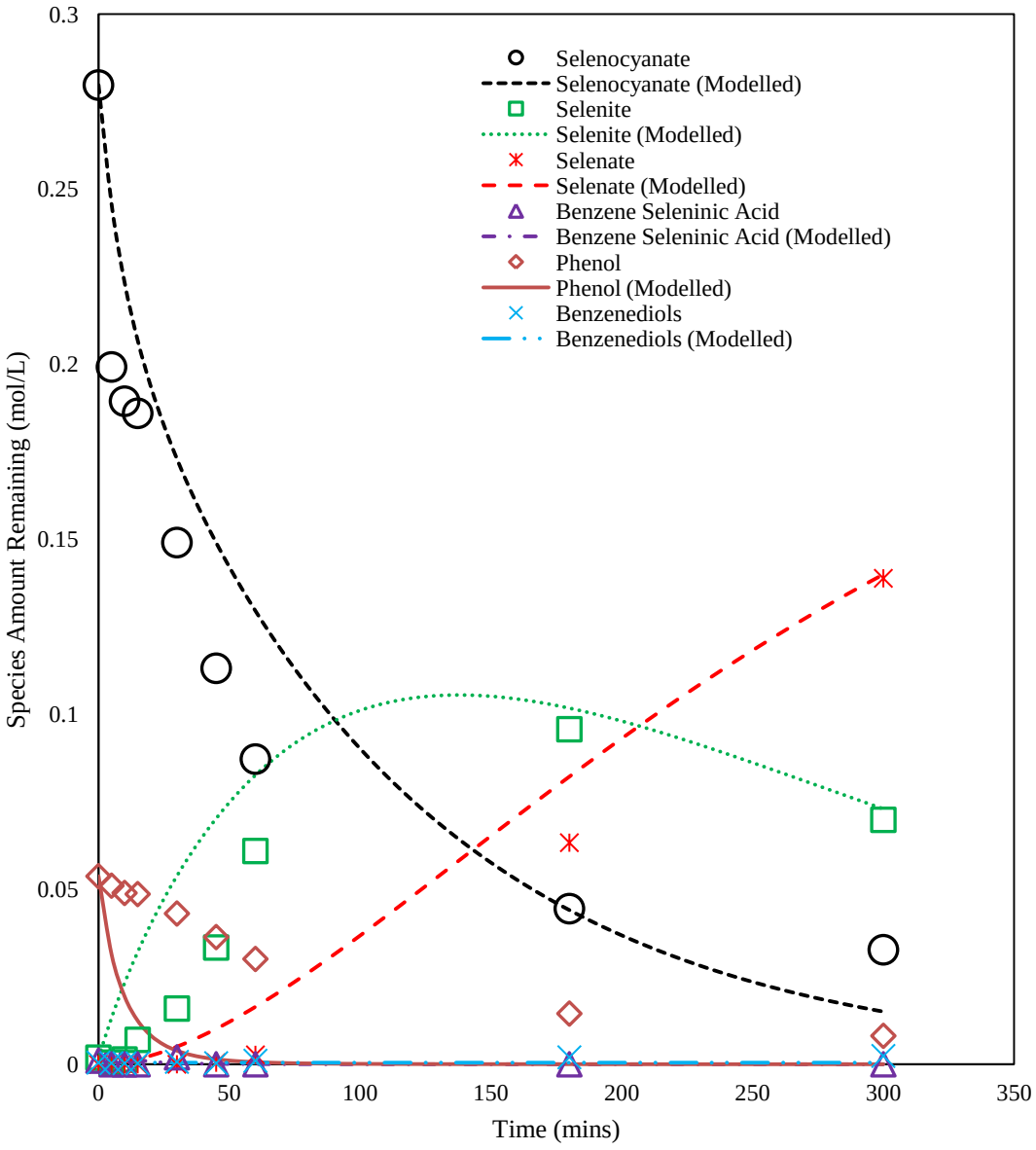

Figure A. 16: Experimental and kinetic modelling results for UV light competitive photocatalytic removal of selenocyanate and phenol at pH 4 (30 ppm selenocyanate, 5 ppm phenol, 150 ppm EDTA added at 5 hours).

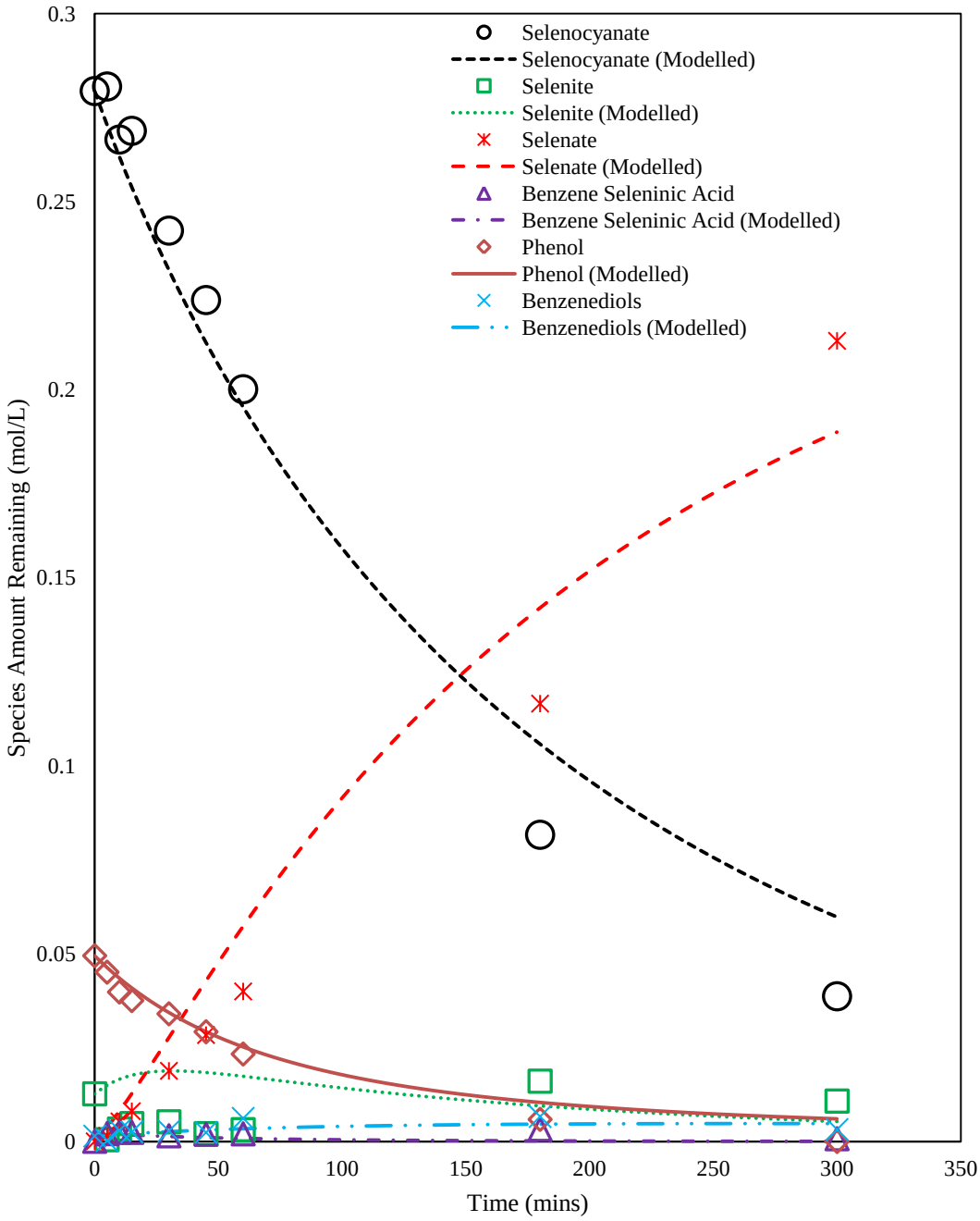

Figure A. 17: Experimental and kinetic modelling results for UV light competitive photocatalytic removal of selenocyanate and phenol at pH 8 (30 ppm selenocyanate, 5 ppm phenol, 150 ppm EDTA added at 5 hours).

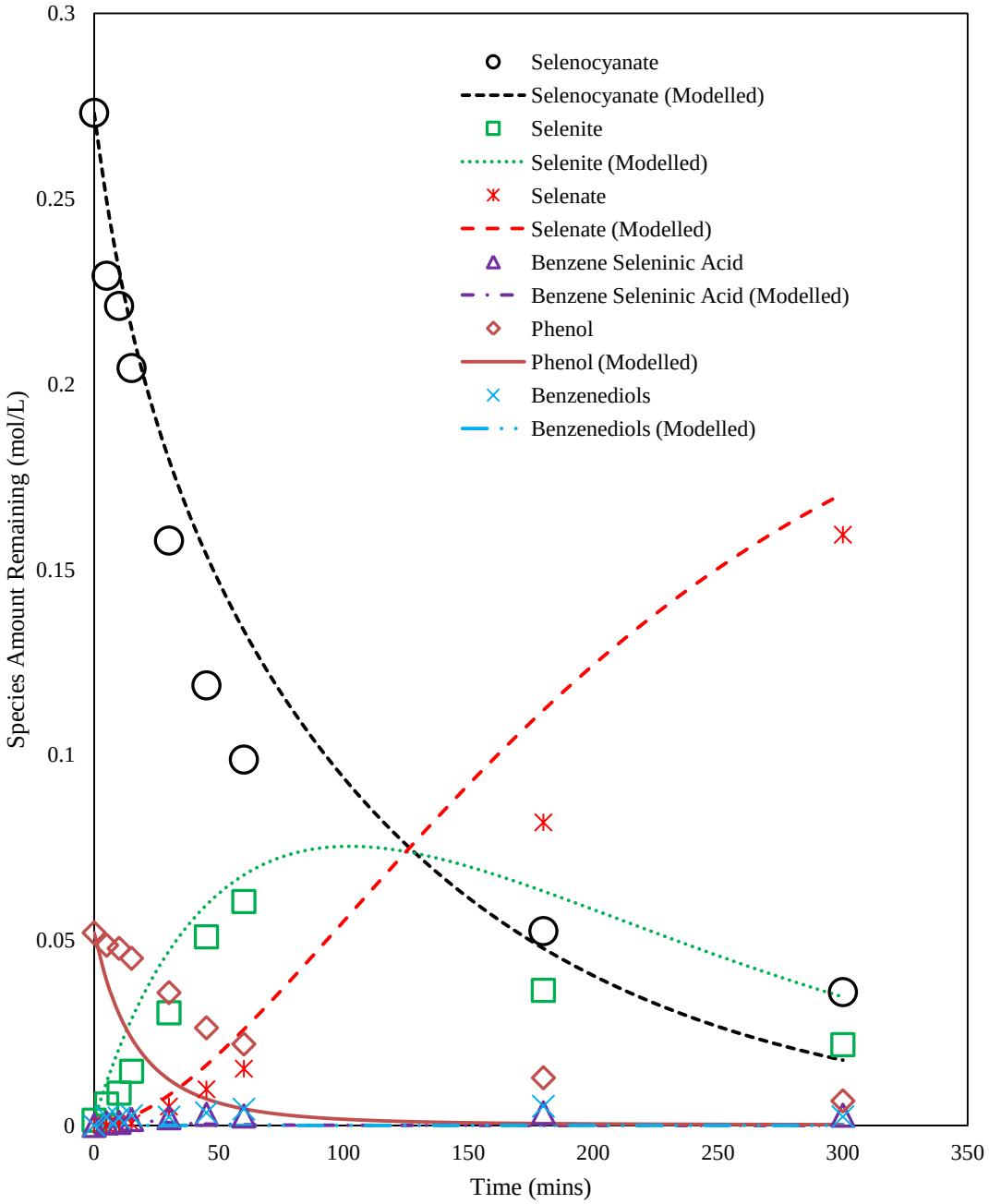

Figure A. 18: Experimental and kinetic modelling results for UV light competitive photocatalytic removal of selenocyanate and phenol at pH 4 (30 ppm selenocyanate, 5 ppm phenol, 450 ppm EDTA added at 5 hours).

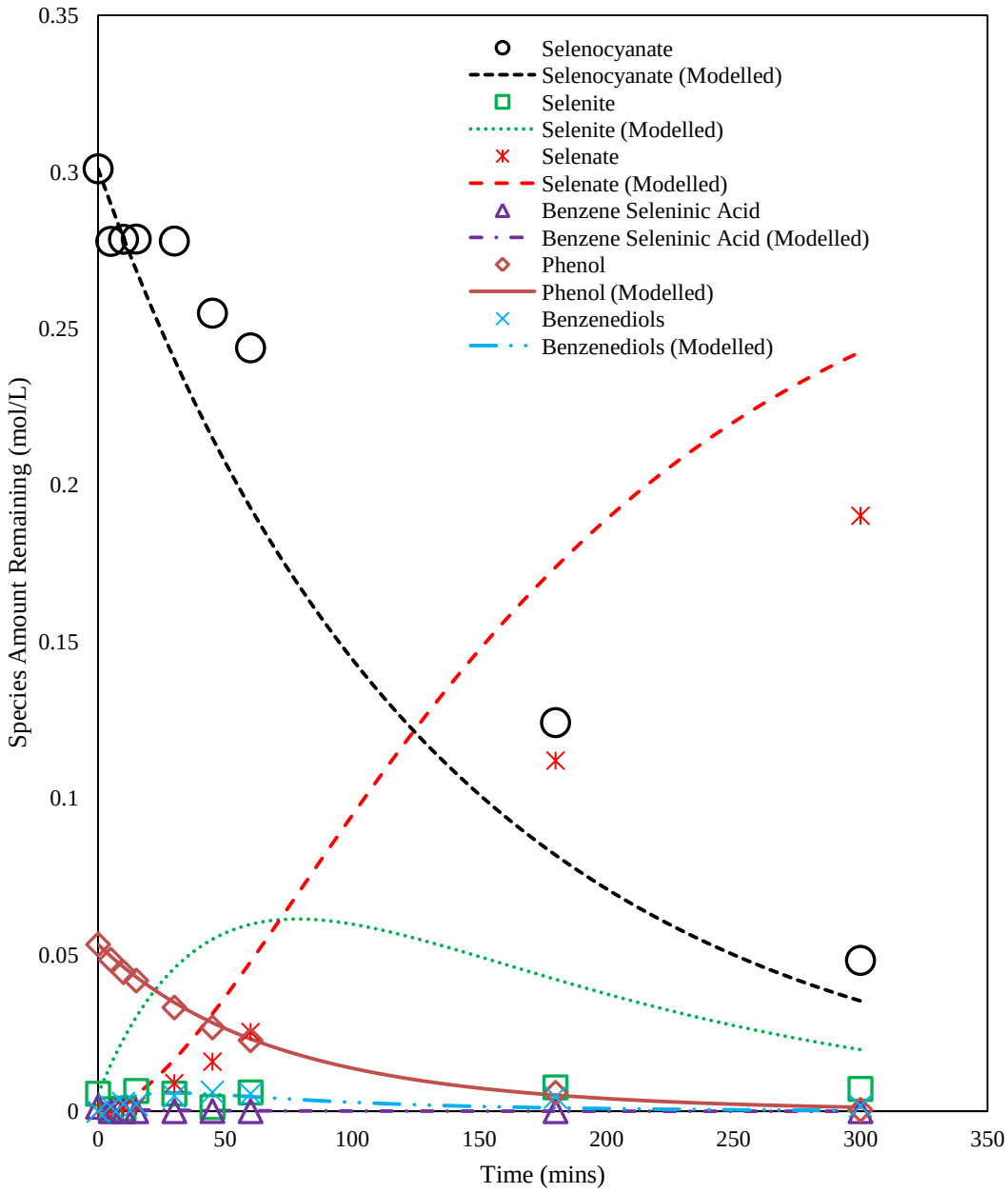

Figure A. 19: Experimental and kinetic modelling results for UV light competitive photocatalytic removal of selenocyanate and phenol at pH 8 (30 ppm selenocyanate, 5 ppm phenol, 450 ppm EDTA added at 5 hours).

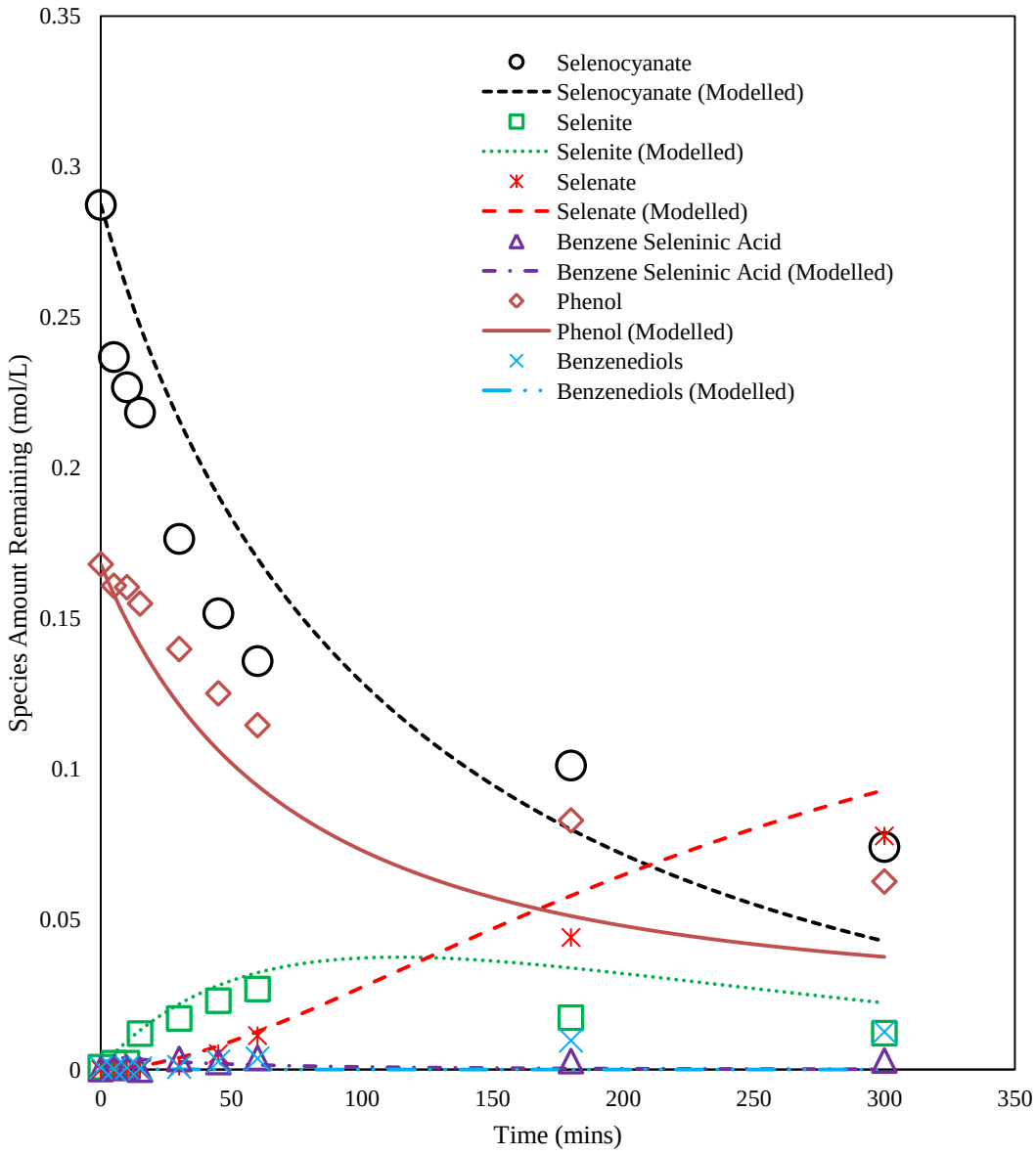

Figure A. 20: Experimental and kinetic modelling results for UV light competitive photocatalytic removal of selenocyanate and phenol at pH 4 (30 ppm selenocyanate, 15 ppm phenol, 150 ppm EDTA added at 5 hours).

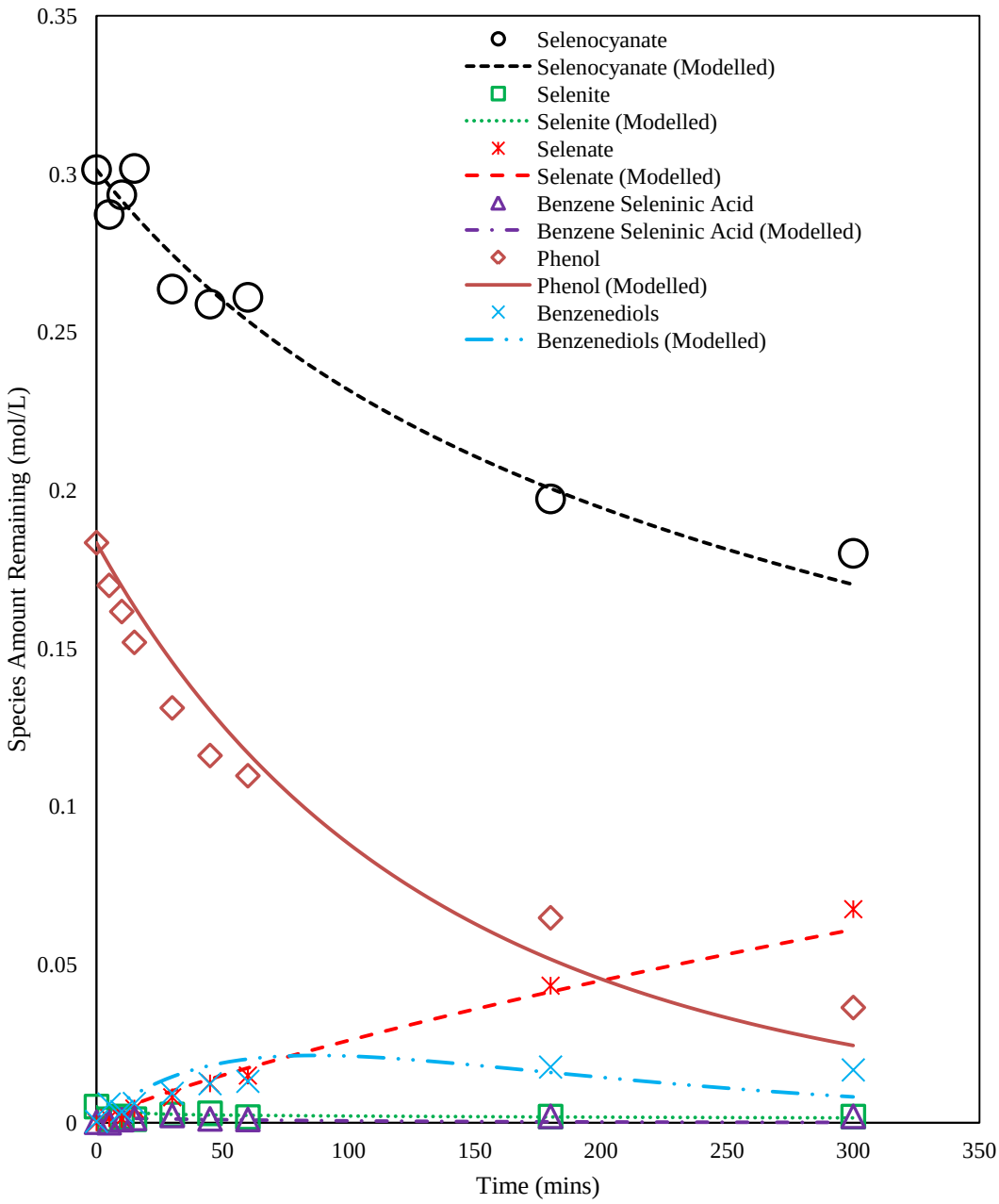

Figure A. 21: Experimental and kinetic modelling results for UV light competitive photocatalytic removal of selenocyanate and phenol at pH 8 (30 ppm selenocyanate, 15 ppm phenol, 150 ppm EDTA added at 5 hours).

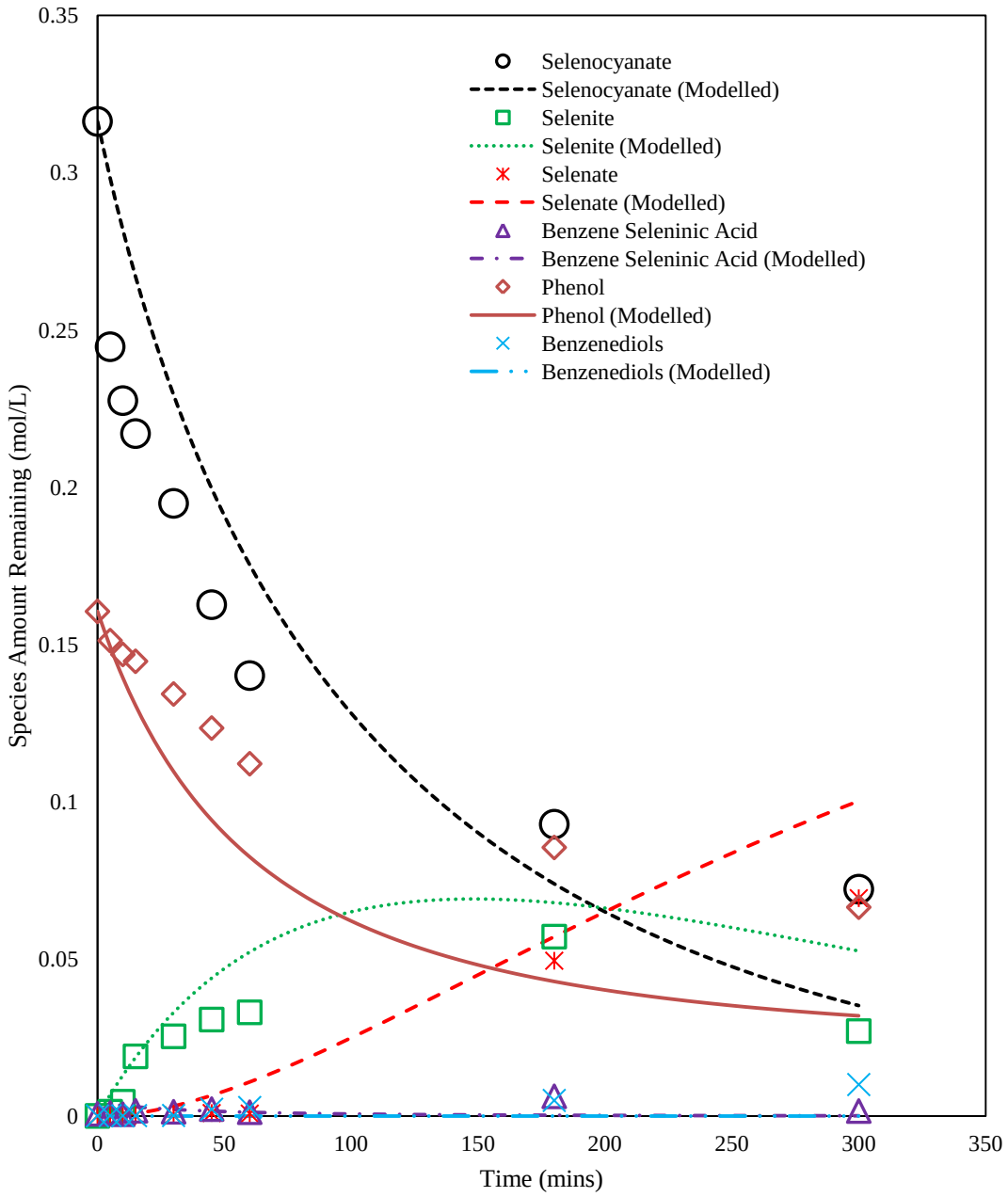

Figure A. 22: Experimental and kinetic modelling results for UV light competitive photocatalytic removal of selenocyanate and phenol at pH 4 (30 ppm selenocyanate, 15 ppm phenol, 450 ppm EDTA added at 5 hours).

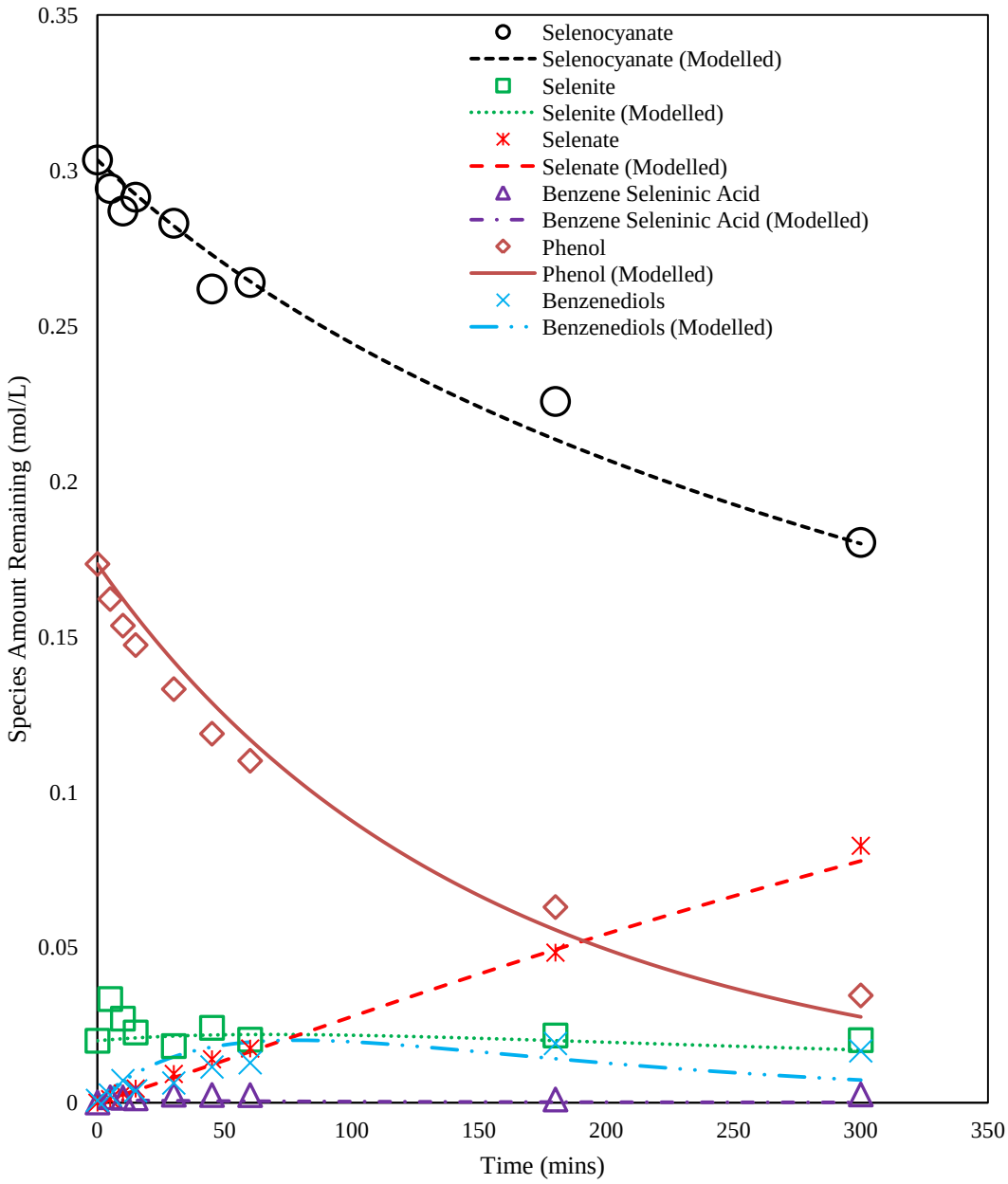

Figure A. 23: Experimental and kinetic modelling results for UV light competitive photocatalytic removal of selenocyanate and phenol at pH 8 (30 ppm selenocyanate, 15 ppm phenol, 450 ppm EDTA added at 5 hours).

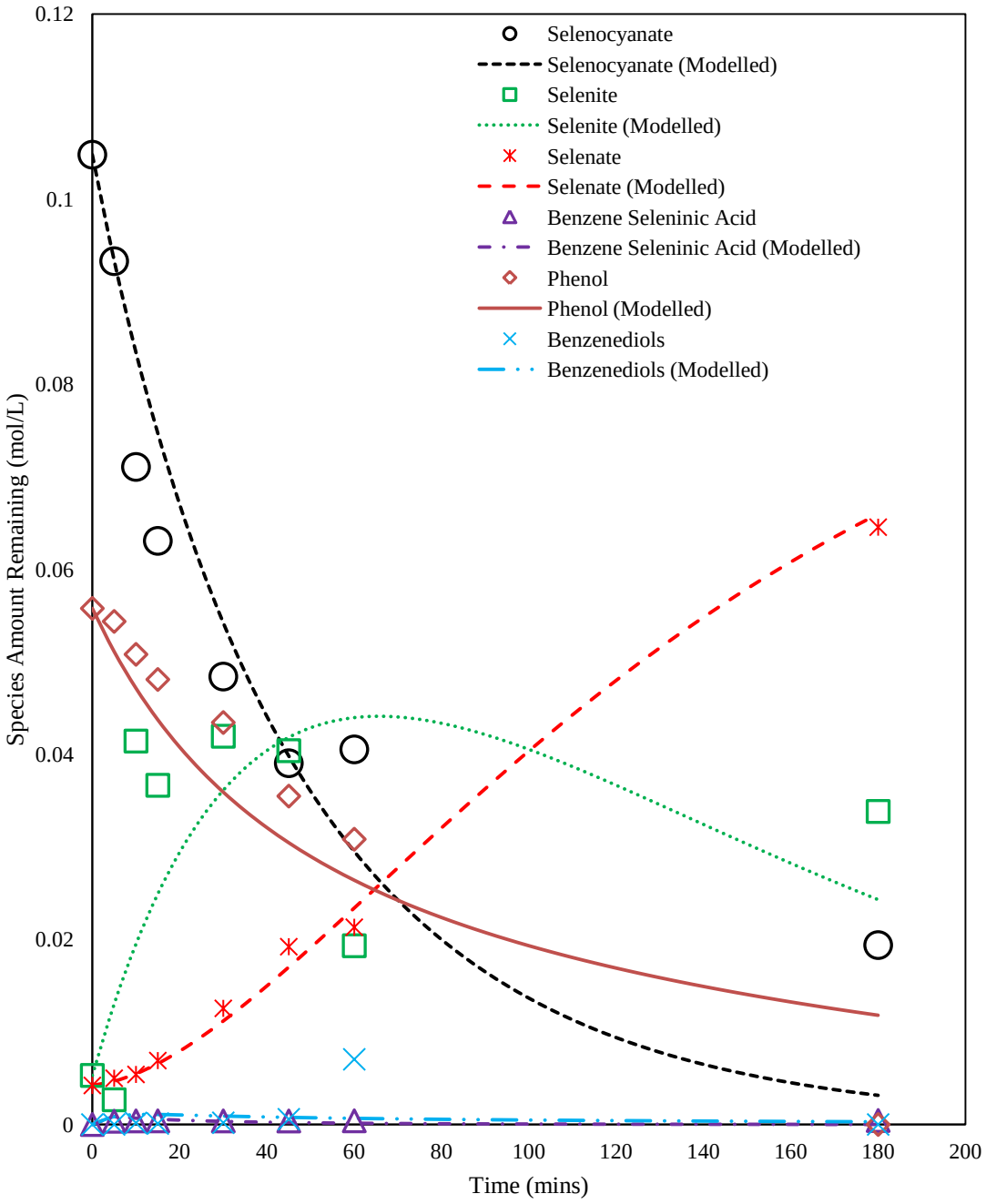

Figure A. 24: Experimental and kinetic modelling results for UV light competitive photocatalytic removal of selenocyanate and phenol at pH 4 (10 ppm selenocyanate, 5 ppm phenol, no EDTA).

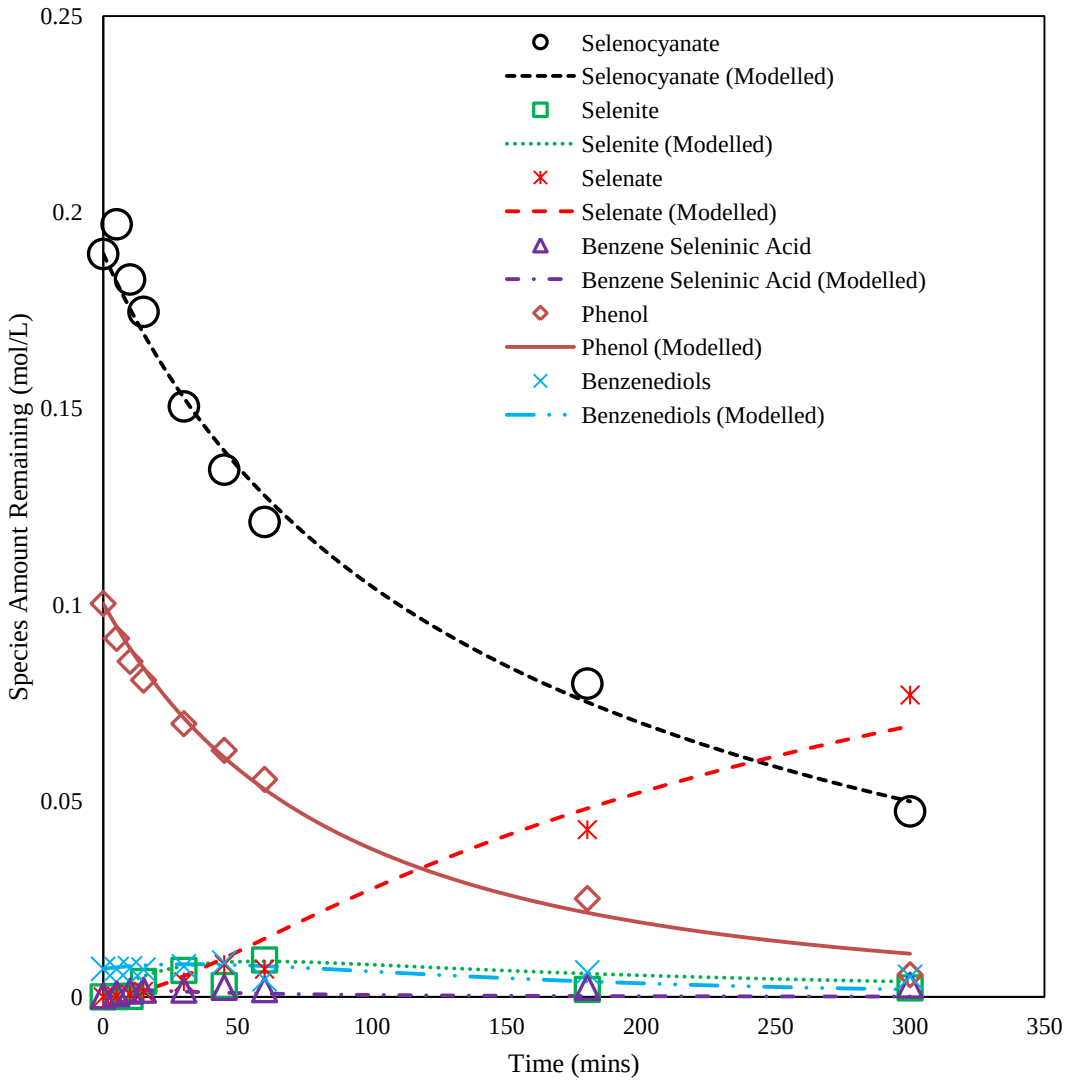

Figure A. 25: Experimental and kinetic modelling results for UV light competitive photocatalytic removal of selenocyanate and phenol at pH 6 (20 ppm selenocyanate, 10 ppm phenol, 150 ppm EDTA added at 5 hours).

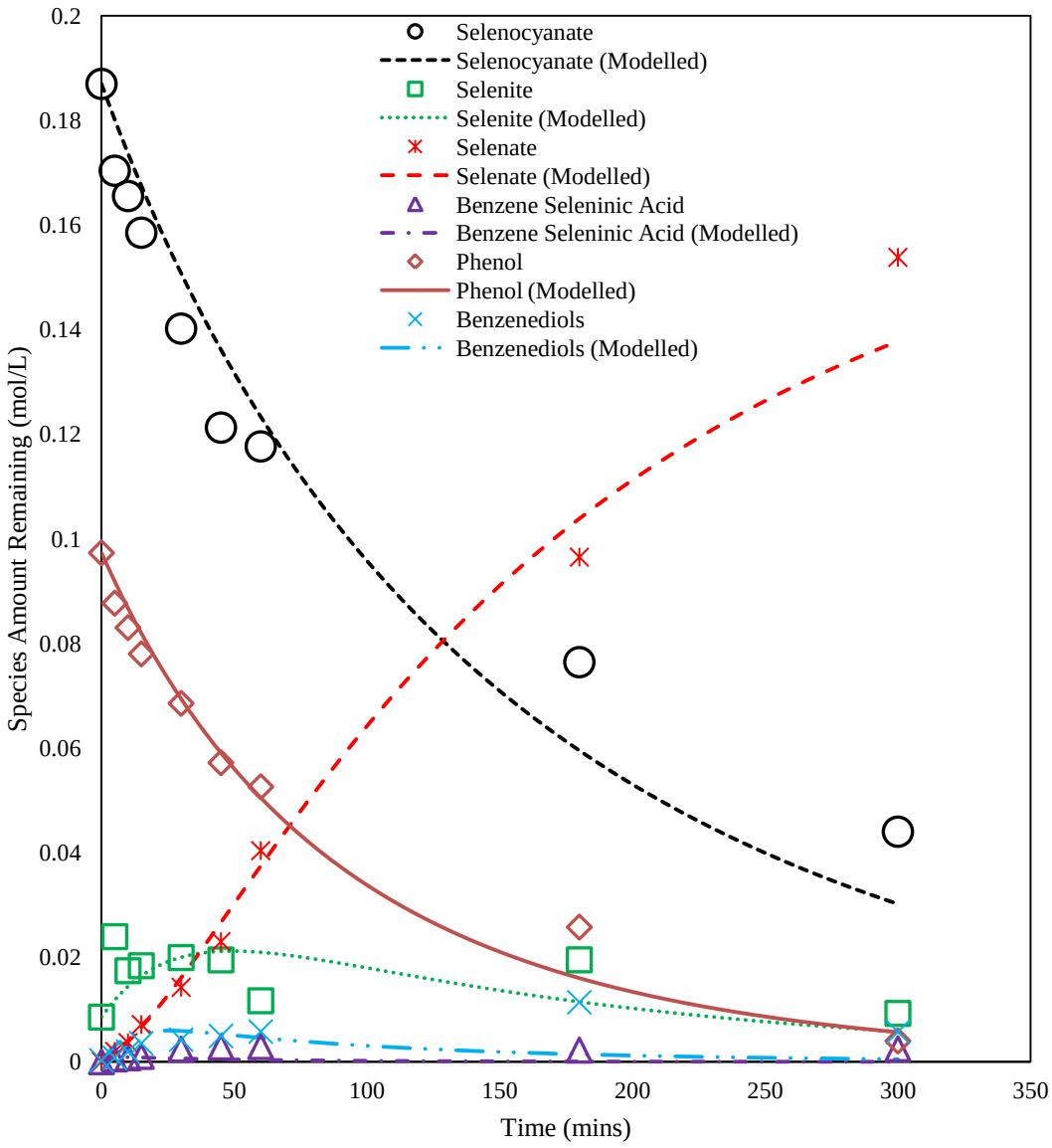

Figure A. 26: Experimental and kinetic modelling results for UV light competitive photocatalytic removal of selenocyanate and phenol at pH 6 (20 ppm selenocyanate, 10 ppm phenol, 450 ppm EDTA added at 5 hours).

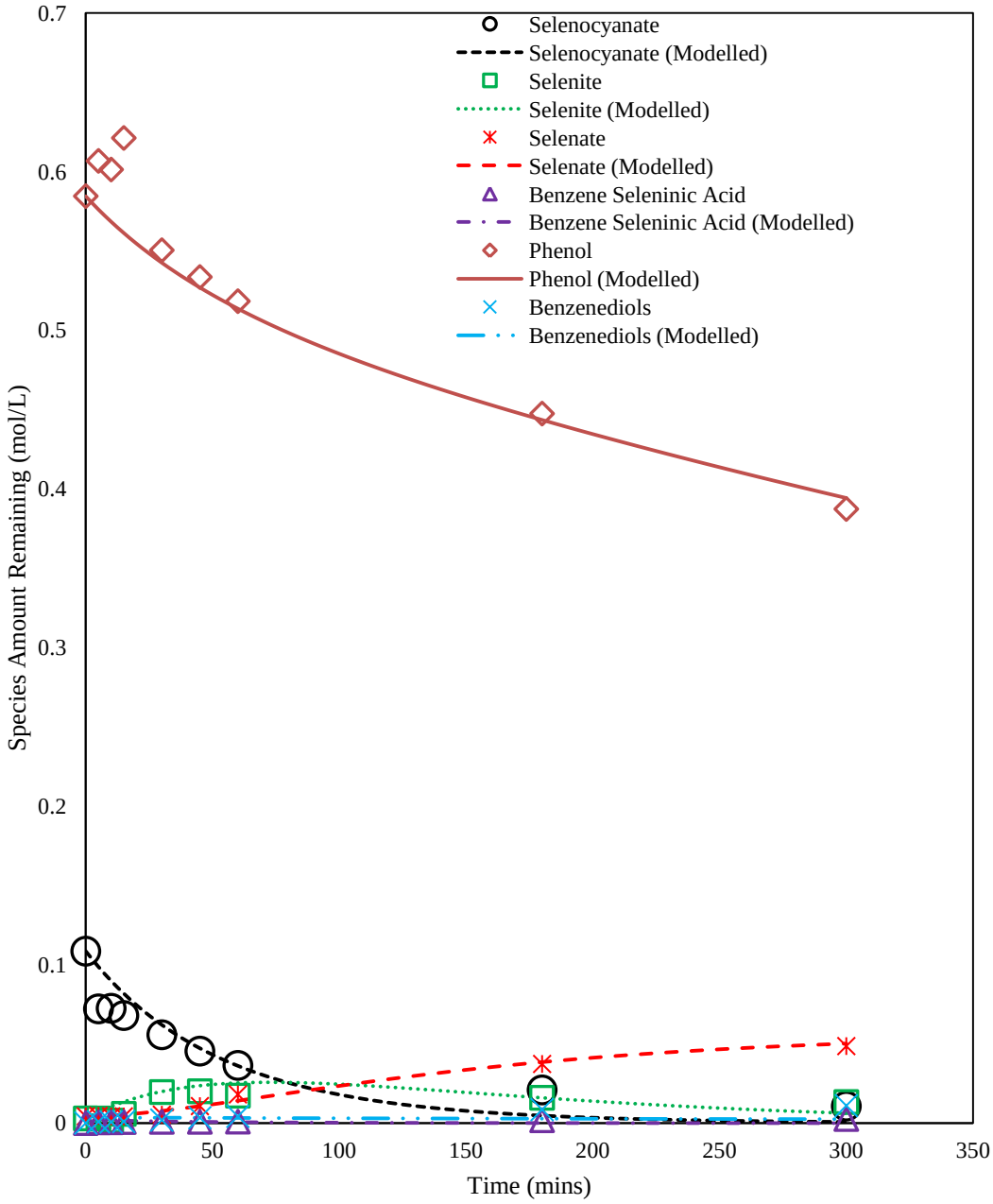

Figure A. 27: Experimental and kinetic modelling results for UV light competitive photocatalytic removal of selenocyanate and phenol at pH 4 (10 ppm selenocyanate, 50 ppm phenol, no EDTA).

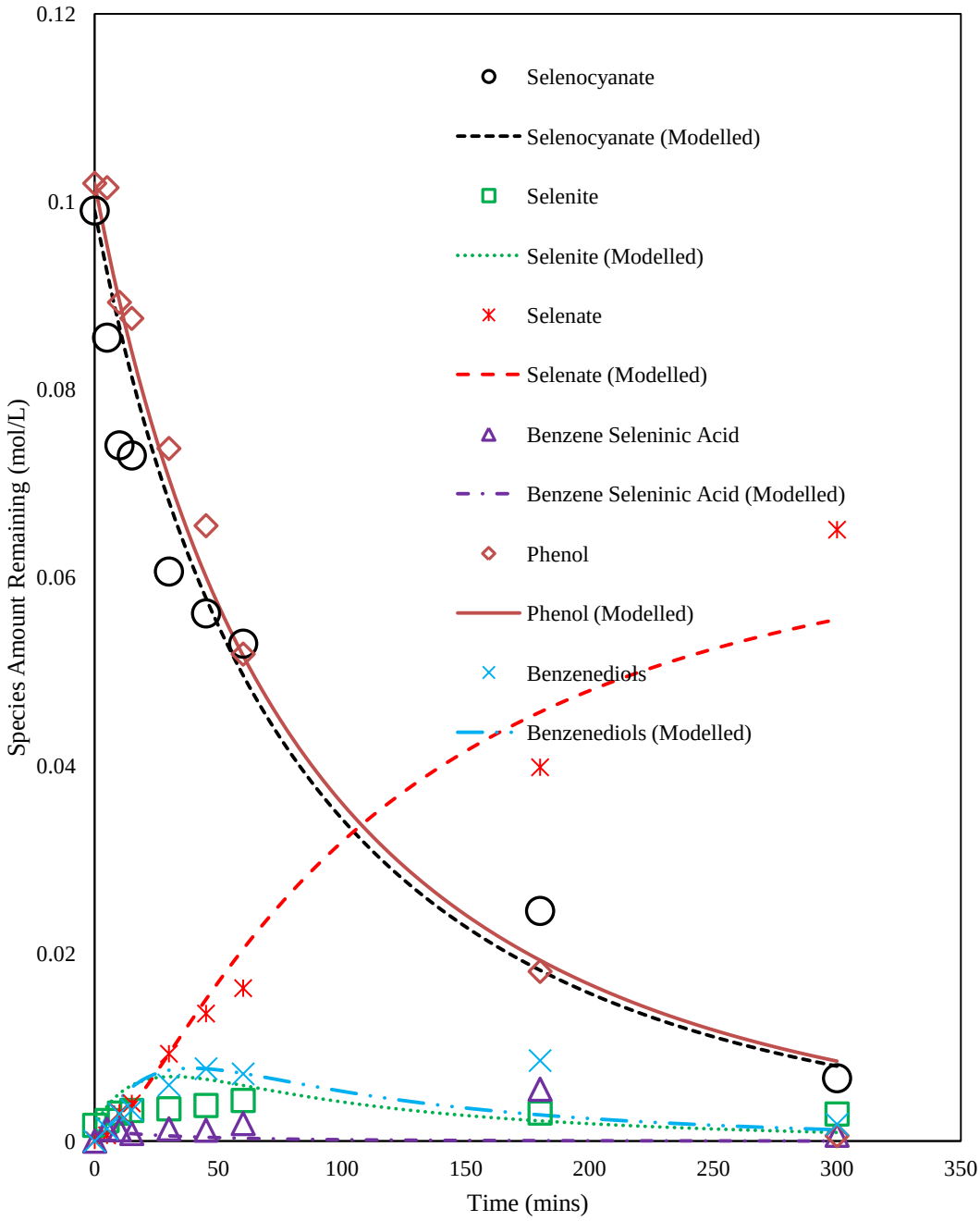

Figure A. 28: Experimental and kinetic modelling results for UV light competitive photocatalytic removal of selenocyanate and phenol at pH 6 (10 ppm selenocyanate, 10 ppm phenol, 300 ppm EDTA added at 5 hours).

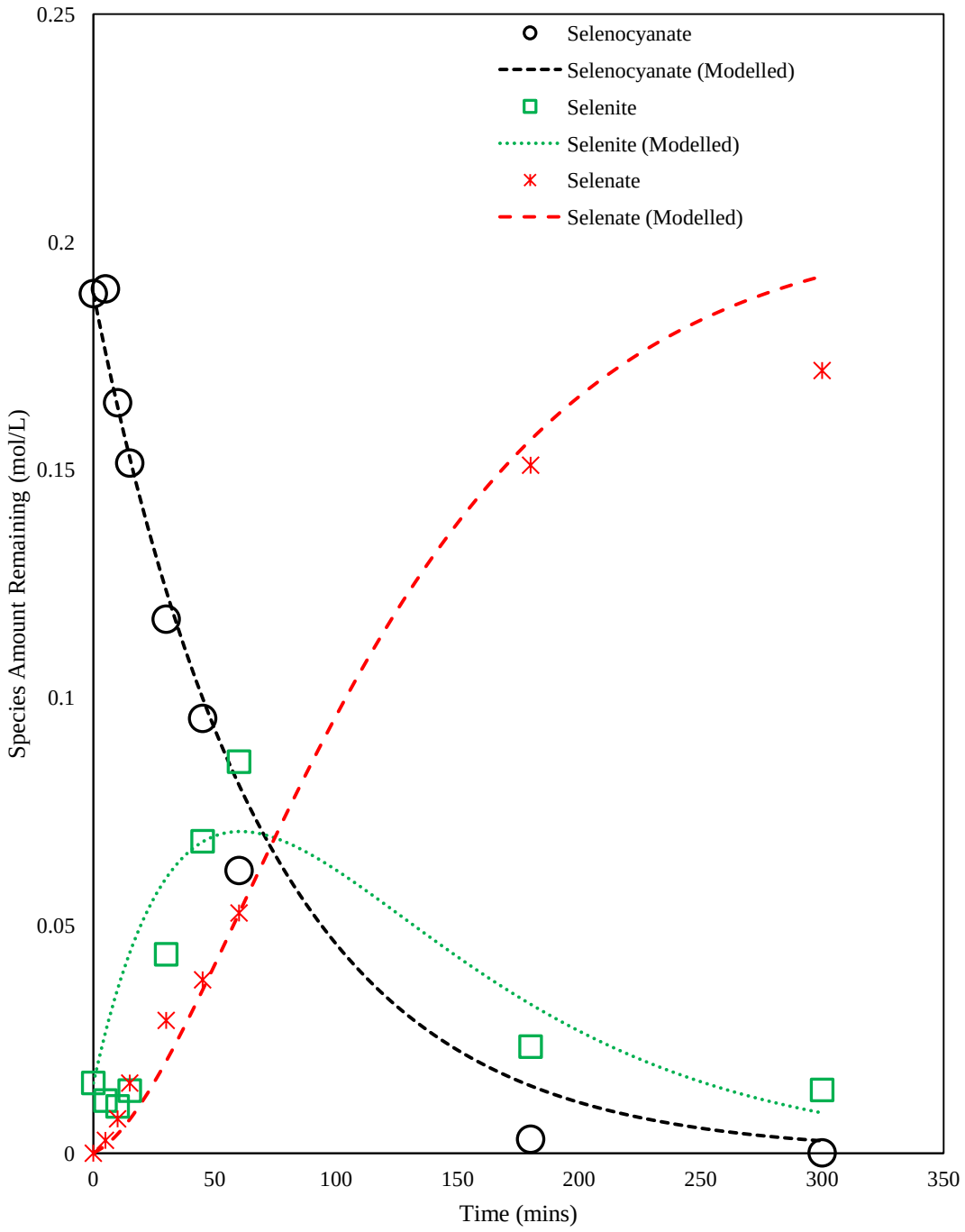

Figure A. 29: Experimental and kinetic modelling results for UV light competitive photocatalytic removal of selenocyanate and phenol at pH 6 (20 ppm selenocyanate, 0 ppm phenol, 300 ppm EDTA added at 5 hours).

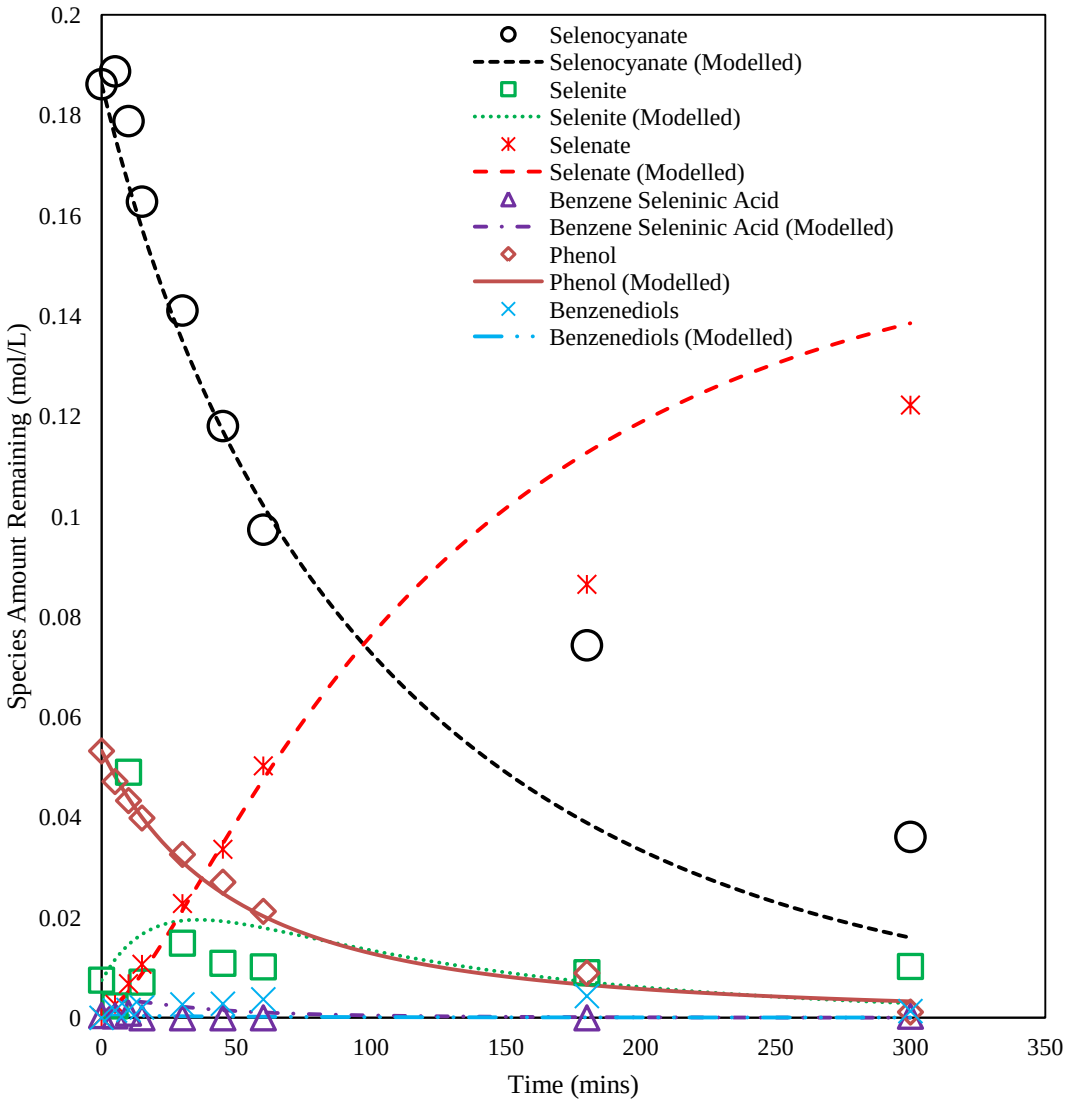

Figure A. 30: Experimental and kinetic modelling results for UV light competitive photocatalytic removal of selenocyanate and phenol at pH 6 (20 ppm selenocyanate, 5 ppm phenol, 300 ppm EDTA added at 5 hours).

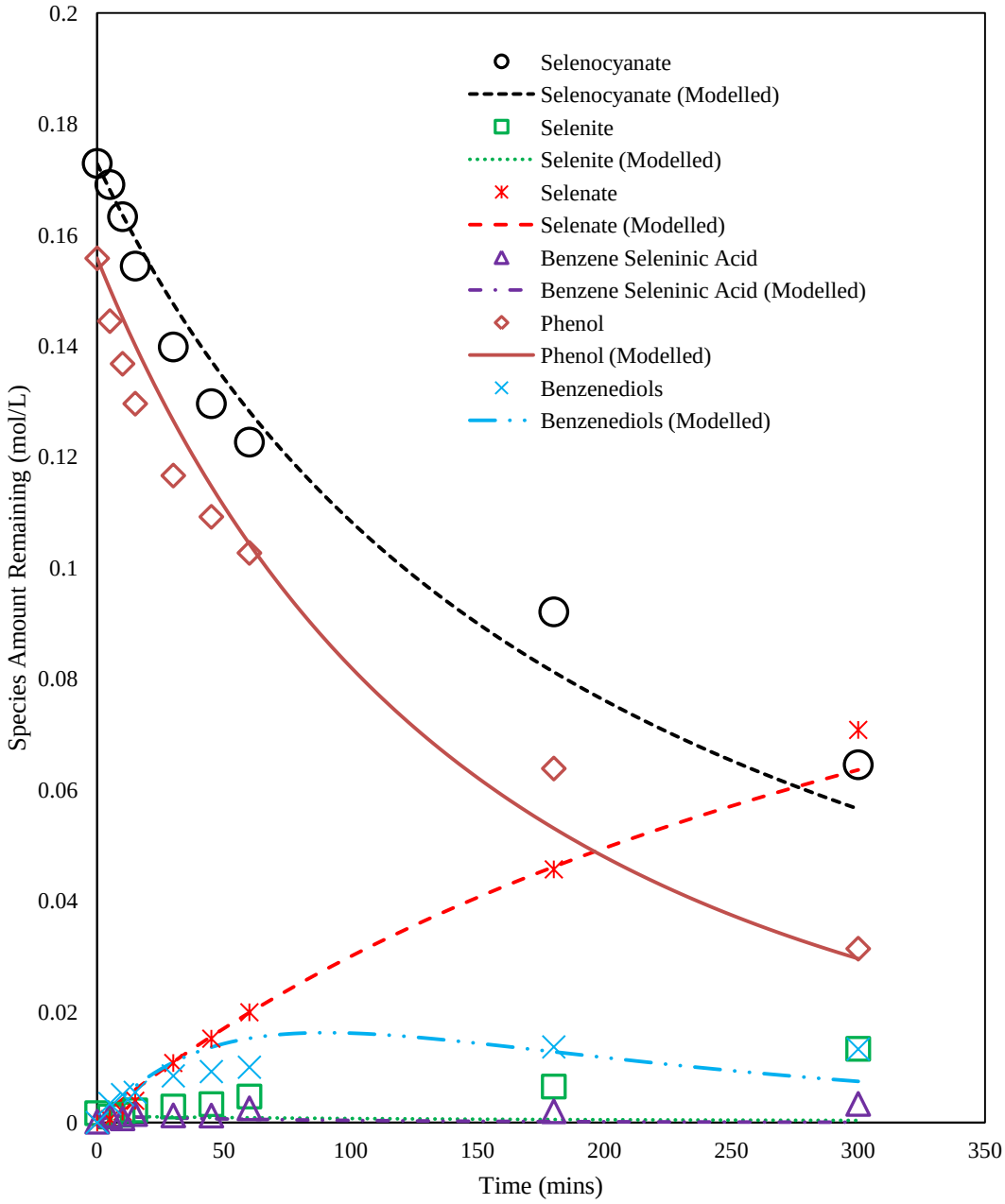

Figure A. 31: Experimental and kinetic modelling results for UV light competitive photocatalytic removal of selenocyanate and phenol at pH 6 (20 ppm selenocyanate, 15 ppm phenol, 300 ppm EDTA added at 5 hours).

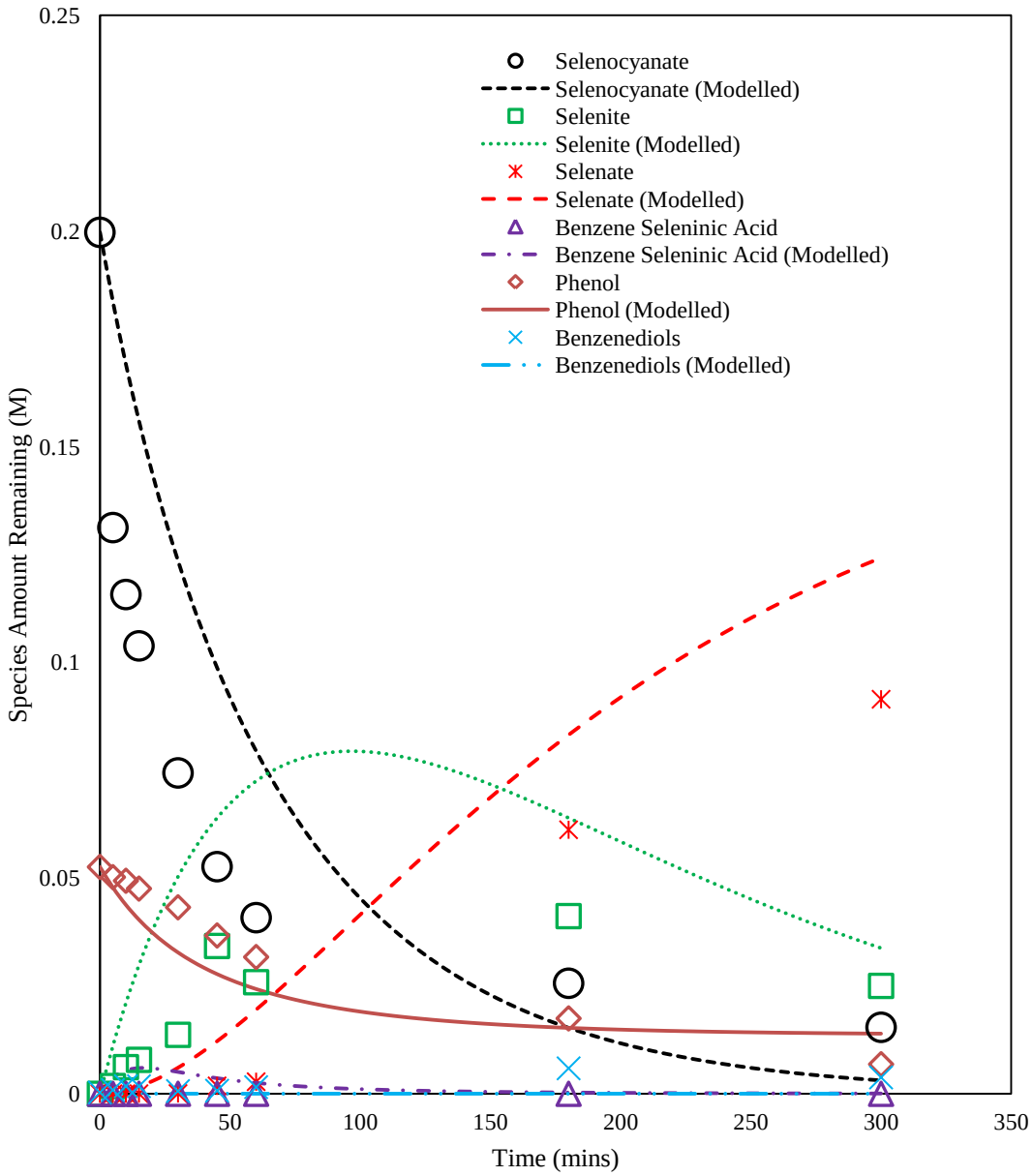

Figure A. 32: Experimental and kinetic modelling results for UV light competitive photocatalytic removal of selenocyanate and phenol at pH 4 (20 ppm selenocyanate, 5 ppm phenol, 450 ppm EDTA added at 5 hours).

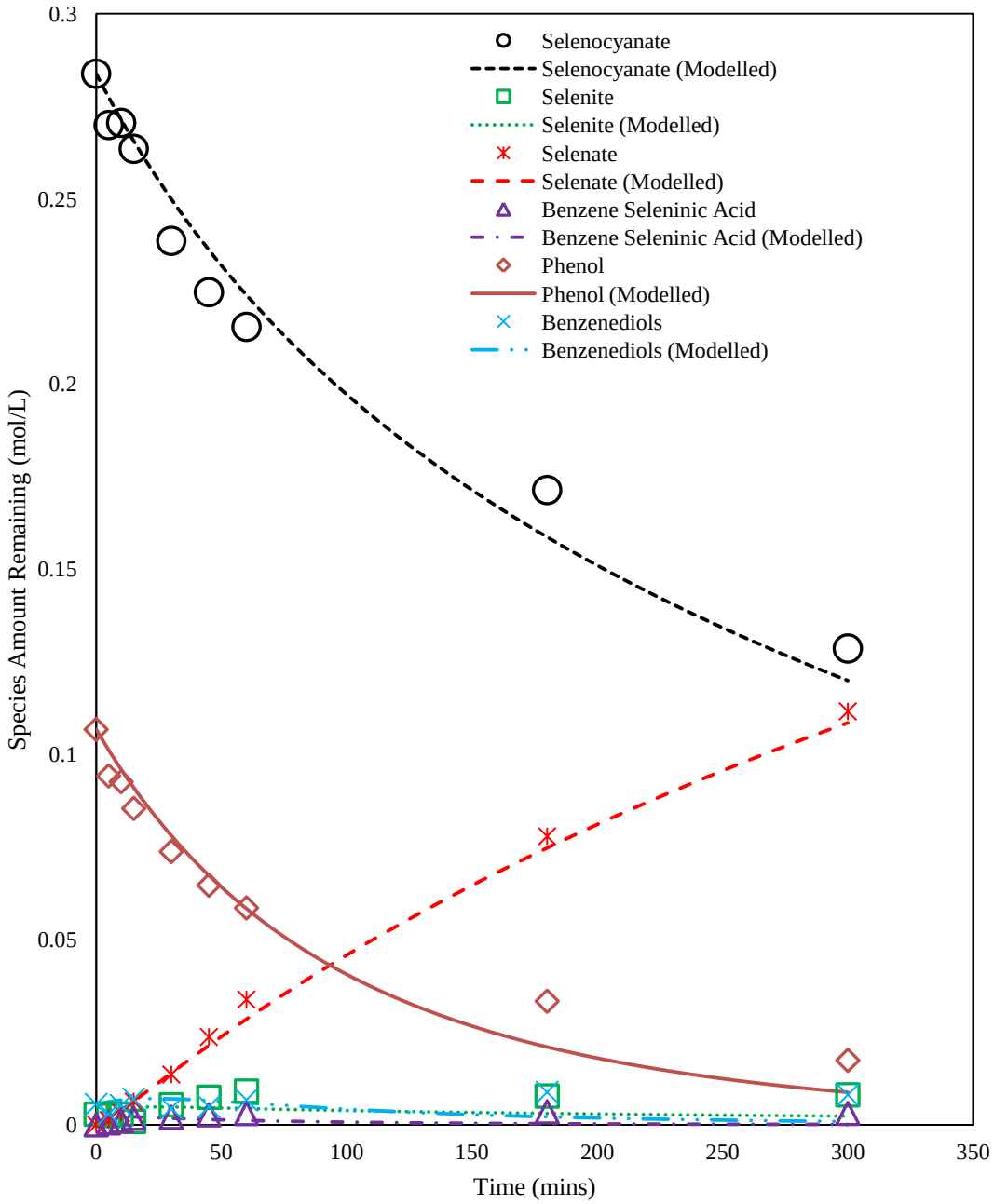

Figure A. 33: Experimental and kinetic modelling results for UV light competitive photocatalytic removal of selenocyanate and phenol at pH 6 (30 ppm selenocyanate, 10 ppm phenol, 300 ppm EDTA added at 5 hours).

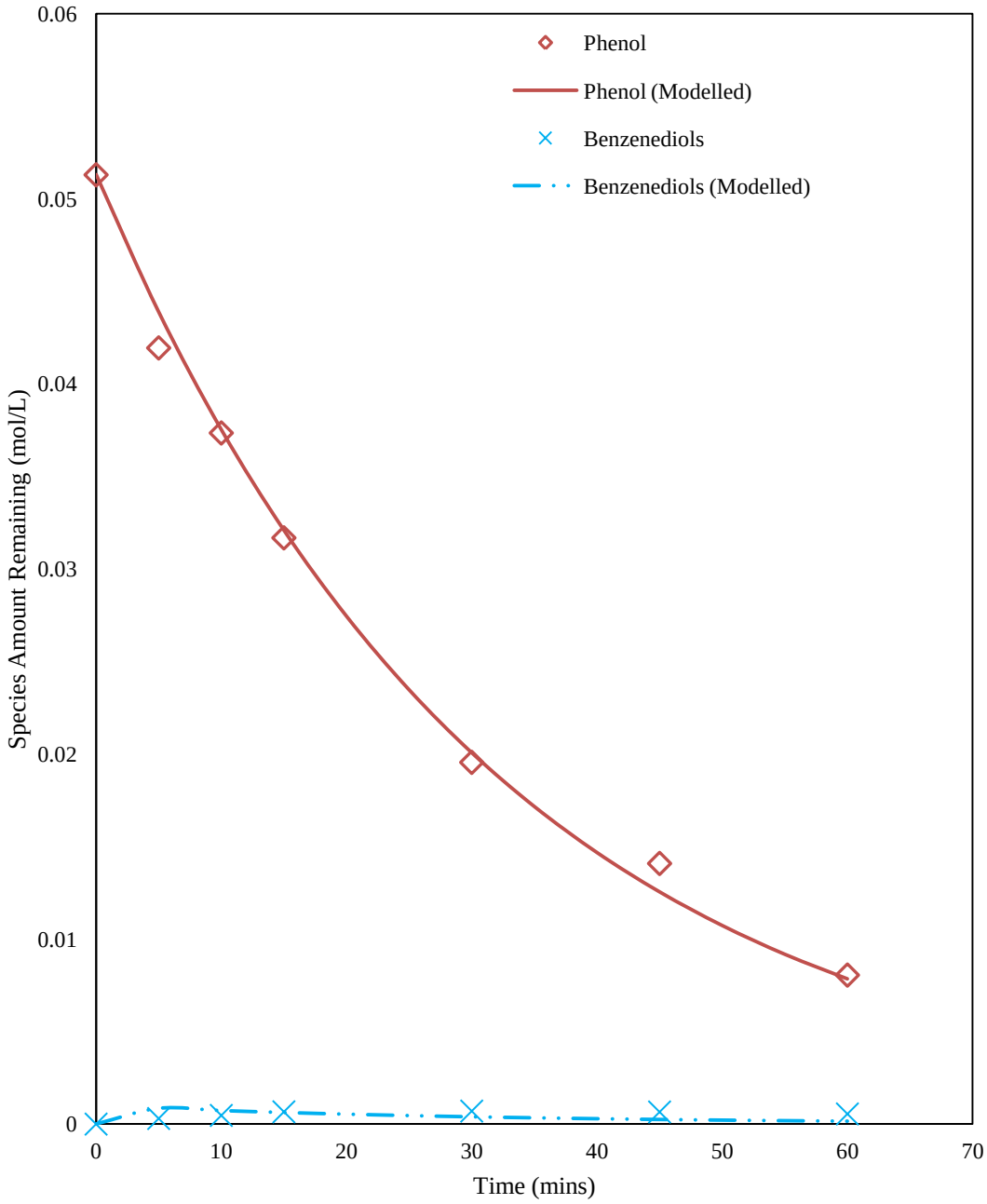

Figure A. 34: Experimental and kinetic modelling results for UV light competitive photocatalytic removal of 5 ppm phenol at pH 4.

References

1. Aman, N., et al., *Simultaneous photoreductive removal of copper (II) and selenium (IV) under visible light over spherical binary oxide photocatalyst.* Journal of hazardous materials, 2011. **186**(1): p. 360-366.
2. Bleiman, N. and Y.G. Mishael, *Selenium removal from drinking water by adsorption to chitosan–clay composites and oxides: batch and columns tests.* Journal of Hazardous Materials, 2010. **183**(1): p. 590-595.
3. Geoffroy, N. and G. Demopoulos, *The elimination of selenium (IV) from aqueous solution by precipitation with sodium sulfide.* Journal of hazardous materials, 2011. **185**(1): p. 148-154.
4. Hu, X., F. Wang, and M.L. Hanson, *Selenium concentration, speciation and behavior in surface waters of the Canadian prairies.* Science of the total environment, 2009. **407**(22): p. 5869-5876.
5. Manceau, A. and D.L. Gallup, *Removal of Selenocyanate in Water by Precipitation: Characterization of Copper− Selenium Precipitate by X-ray Diffraction, Infrared, and X-ray Absorption Spectroscopy.* Environmental science & technology, 1997. **31**(4): p. 968-976.
6. Sharmasarkar, S. and G.F. Vance, *Selenite–selenate sorption in surface coal mine environment.* Advances in environmental research, 2002. **7**(1): p. 87-95.
7. Torres, J., et al., *Selenium chemical speciation in natural waters: Protonation and complexation behavior of selenite and selenate in the presence of environmentally relevant cations.* Chemical Geology, 2011. **288**(1): p. 32-38.
8. Zhang, N., L.-S. Lin, and D. Gang, *Adsorptive selenite removal from water using iron-coated GAC adsorbents.* water research, 2008. **42**(14): p. 3809-3816.
9. Zhang, Y., et al., *Effect of zero-valent iron and a redox mediator on removal of selenium in agricultural drainage water.* Science of the total environment, 2008. **407**(1): p. 89-96.
10. de Almeida, C.M.S., et al., *Studies on the origin and transformation of selenium and its chemical species along the process of petroleum refining.* Spectrochimica Acta Part B: Atomic Spectroscopy, 2009. **64**(6): p. 491-499.
11. De Souza, M.P., et al., *Selenium assimilation and volatilization from selenocyanate-treated Indian mustard and muskgrass.* Plant physiology, 2002. **128**(2): p. 625-633.
12. Edwards, M., Kulas, J. E., Weakley, J. O., and Kuit, W. J., *Aquatic selenium at Cominco's Red Dog Mine: Sources, speciation, distribution, and control*, in *6th Tailings and mine waste*, A.A. Balkema, Editor. 1999: Fort Collins; CO. p. 535-542.
13. Miekeley, N., et al., *Inorganic speciation analysis of selenium by ion chromatography-inductively coupled plasma-mass spectrometry and its*

application to effluents from a petroleum refinery. Spectrochimica Acta Part B: Atomic Spectroscopy, 2005. **60**(5): p. 633-641.
14. Tonietto, G.B., et al., *Simultaneous speciation of arsenic (As (III), MMA, DMA, and As (V)) and selenium (Se (IV), Se (VI), and SeCN−) in petroleum refinery aqueous streams.* Analytical and bioanalytical chemistry, 2010. **397**(5): p. 1755-1761.
15. Wallschläger, D. and N.S. Bloom, *Determination of selenite, selenate and selenocyanate in waters by ion chromatography-hydride generation-atomic fluorescence spectrometry (IC-HG-AFS).* Journal of Analytical Atomic Spectrometry, 2001. **16**(11): p. 1322-1328.
16. Meng, X., S. Bang, and G.P. Korfiatis, *Removal of selenocyanate from water using elemental iron.* Water Research, 2002. **36**(15): p. 3867-3873.
17. Rader, W.S., et al., *Photocatalytic detoxification of cyanide and metal cyano-species from precious-metal mill effluents.* Environmental Pollution, 1995. **90**(3): p. 331-334.
18. Abdelwahab, O., N. Amin, and E.Z. El-Ashtoukhy, *Electrochemical removal of phenol from oil refinery wastewater*. Journal of hazardous materials, 2009. **163**(2): p. 711-716.
19. El-Naas, M.H., S. Al-Zuhair, and M.A. Alhaija, *Removal of phenol from petroleum refinery wastewater through adsorption on date-pit activated carbon.* Chemical Engineering Journal, 2010. **162**(3): p. 997-1005.
20. Ibrahim, M., et al., *Enzyme-catalyzed removal of phenol from refinery wastewater: feasibility studies.* Water environment research, 2001. **73**(2): p. 165-172.
21. Kapoor, A., et al., *Application of immobilized mixed bacterial culture for the degradation of phenol present in oil refinery effluent.* Journal of Environmental Science & Health Part A, 1998. **33**(6): p. 1009-1021.
22. Steevensz, A., et al., *Comparison of soybean peroxidase with laccase in the removal of phenol from synthetic and refinery wastewater samples.* Journal of chemical technology and biotechnology, 2009. **84**(5): p. 761-769.
23. Overman, S.D., *Process for removing selenium from refinery process water and waste water streams*. 1999, Google Patents.
24. Hoffmann, M.R., et al., *Environmental applications of semiconductor photocatalysis.* Chemical reviews, 1995. **95**(1): p. 69-96.
25. Serpone, N., et al., *Exploiting the interparticle electron transfer process in the photocatalysed oxidation of phenol, 2-chlorophenol and pentachlorophenol: chemical evidence for electron and hole transfer between coupled semiconductors.* Journal of Photochemistry and Photobiology A: Chemistry, 1995. **85**(3): p. 247-255.
26. Turchi, C.S. and D.F. Ollis, *Photocatalytic degradation of organic water contaminants: mechanisms involving hydroxyl radical attack.* Journal of catalysis, 1990. **122**(1): p. 178-192.

27. Vohra, M. and K. Tanaka, *Enhanced photocatalytic activity of nafion-coated TiO2.* Environmental science & technology, 2001. **35**(2): p. 411-415.
28. Labaran, B. and M. Vohra, *Photocatalytic removal of selenite and selenate species: effect of EDTA and other process variables.* Environmental technology, 2014. **35**(9): p. 1091-1100.
29. Nguyen, V.N.H., D. Beydoun, and R. Amal, *Photocatalytic reduction of selenite and selenate using TiO 2 photocatalyst.* Journal of Photochemistry and Photobiology A: Chemistry, 2005. **171**(2): p. 113-120.
30. Shi, K., et al., *Se (IV) sorption on TiO 2: Sorption kinetics and surface complexation modeling.* Colloids and Surfaces A: Physicochemical and Engineering Aspects, 2009. **349**(1): p. 90-95.
31. Tan, T., D. Beydoun, and R. Amal, *Effects of organic hole scavengers on the photocatalytic reduction of selenium anions.* Journal of Photochemistry and Photobiology A: Chemistry, 2003. **159**(3): p. 273-280.
32. Tan, T.T., D. Beydoun, and R. Amal, *Photocatalytic reduction of Se (VI) in aqueous solutions in UV/TiO 2 system: importance of optimum ratio of reactants on TiO 2 surface.* Journal of Molecular Catalysis A: Chemical, 2003. **202**(1): p. 73-85.
33. Tan, T.T., D. Beydoun, and R. Amal, *Photocatalytic reduction of Se (VI) in aqueous solutions in UV/TiO2 system: kinetic modeling and reaction mechanism.* The Journal of Physical Chemistry B, 2003. **107**(18): p. 4296-4303.
34. Tan, T.T.Y., et al., *Effects of nano-Ag particles loading on TiO 2 photocatalytic reduction of selenate ions.* Chemical Engineering Journal, 2003. **95**(1): p. 179-186.
35. Zhang, L., et al., *Sorption behavior of nano-TiO 2 for the removal of selenium ions from aqueous solution.* Journal of hazardous materials, 2009. **170**(2): p. 1197-1203.
36. Huang, M., et al., *Removal of silver in photographic processing waste by TiO2-based photocatalysis.* Environmental science & technology, 1996. **30**(10): p. 3084-3088.
37. Vohra, M.S., *SELENOCYANATE (SeCN-) CONTAMINATED WASTEWATER TREATMENT USING TiO2 PHOTOCATALYSIS: SeCN-COMPLEX DESTRUCTION, INTERMEDIATES FORMATION, AND REMOVAL OF SELENIUM SPECIES.* FRESENIUS ENVIRONMENTAL BULLETIN, 2015. **24**(3 B): p. 1108-1118.
38. Cheremisinoff, N.P. and P.N. Cheremisinoff, *Carbon adsorption for pollution control.* 1993.
39. Foo, K. and B. Hameed, *Insights into the modeling of adsorption isotherm systems.* Chemical Engineering Journal, 2010. **156**(1): p. 2-10.
40. Ho, Y.-S., *Review of second-order models for adsorption systems.* Journal of hazardous materials, 2006. **136**(3): p. 681-689.
41. Qiu, H., et al., *Critical review in adsorption kinetic models.* Journal of Zhejiang University-Science A, 2009. **10**(5): p. 716-724.

42. Schmuhl, R., et al., *Controlling the transport of cations through permselective mesoporous alumina layers by manipulation of electric field and ionic strength.* Journal of colloid and interface science, 2004. **273**(1): p. 331-338.
43. Su, C. and D.L. Suarez, *Selenate and selenite sorption on iron oxides an infrared and electrophoretic study.* Soil Science Society of America Journal, 2000. **64**(1): p. 101-111.
44. Saha, U., et al., *Kinetics of selenite adsorption on hydroxyaluminum-and hydroxyaluminosilicate-montmorillonite complexes.* Soil Science Society of America Journal, 2004. **68**(4): p. 1197-1209.
45. Yamani, J.S., A.W. Lounsbury, and J.B. Zimmerman, *Adsorption of selenite and selenate by nanocrystalline aluminum oxide, neat and impregnated in chitosan beads.* Water research, 2014. **50**: p. 373-381.
46. Li, S. and N. Deng, *Separation and preconcentration of Se (IV)/Se (VI) species by selective adsorption onto nanometer-sized titanium dioxide and determination by graphite furnace atomic absorption spectrometry.* Analytical and bioanalytical chemistry, 2002. **374**(7): p. 1341-1345.
47. Nguyen, V.N.H., R. Amal, and D. Beydoun, *Photocatalytic reduction of selenium ions using different TiO 2 photocatalysts.* Chemical engineering science, 2005. **60**(21): p. 5759-5769.
48. Sanuki, S., et al., *Photocatalytic reduction of selenate and selenite solutions using TiO2 powders.* Metallurgical and Materials Transactions B, 1999. **30**(1): p. 15-20.
49. Sanuki, S., et al., *Photocatalytic reduction of Se ions using suspended anatase powders.* Materials Transactions, JIM, 2000. **41**(7): p. 799-805.
50. Liu, G., et al., *Photooxidation pathway of sulforhodamine-B. Dependence on the adsorption mode on TiO2 exposed to visible light radiation.* Environmental science & technology, 2000. **34**(18): p. 3982-3990.
51. Pelet, S., J.-E. Moser, and M. Grätzel, *Cooperative effect of adsorbed cations and iodide on the interception of back electron transfer in the dye sensitization of nanocrystalline TiO2.* The Journal of Physical Chemistry B, 2000. **104**(8): p. 1791-1795.
52. Xu, Y. and C.H. Langford, *UV-or visible-light-induced degradation of X3B on TiO2 nanoparticles: the influence of adsorption.* Langmuir, 2001. **17**(3): p. 897-902.
53. Zhao, J., et al., *Photoassisted degradation of dye pollutants. 3. Degradation of the cationic dye rhodamine B in aqueous anionic surfactant/TiO2 dispersions under visible light irradiation: evidence for the need of substrate adsorption on TiO2 particles.* Environmental science & technology, 1998. **32**(16): p. 2394-2400.
54. Goh, K.-H. and T.-T. Lim, *Geochemistry of inorganic arsenic and selenium in a tropical soil: effect of reaction time, pH, and competitive anions on arsenic and selenium adsorption.* Chemosphere, 2004. **55**(6): p. 849-859.
55. Hingston, F., A. Posner, and J. Quirk, *Competitive adsorption of negatively charged ligands on oxide surfaces.* Discussions of the Faraday Society, 1971. **52**: p. 334-342.

56. Wu, C.-H., S.-L. Lo, and C.-F. Lin, *Competitive adsorption of molybdate, chromate, sulfate, selenate, and selenite on γ-Al 2 O 3.* Colloids and Surfaces A: Physicochemical and Engineering Aspects, 2000. **166**(1): p. 251-259.
57. Balistrieri, L.S. and T. Chao, *Adsorption of selenium by amorphous iron oxyhydroxide and manganese dioxide.* Geochimica et Cosmochimica Acta, 1990. **54**(3): p. 739-751.
58. Balistrieri, L.S. and T. Chao, *Selenium adsorption by goethite.* Soil Science Society of America Journal, 1987. **51**(5): p. 1145-1151.
59. Kabra, K., R. Chaudhary, and R.L. Sawhney, *Treatment of hazardous organic and inorganic compounds through aqueous-phase photocatalysis: a review.* Industrial & engineering chemistry research, 2004. **43**(24): p. 7683-7696.
60. Legrini, O., E. Oliveros, and A.M. Braun, *Photochemical processes for water treatment.* Chemical Reviews, 1993. **93**(2): p. 671-698.
61. Abdullah, M., G.K. Low, and R.W. Matthews, *Effects of common inorganic anions on rates of photocatalytic oxidation of organic carbon over illuminated titanium dioxide.* Journal of Physical Chemistry;(USA), 1990. **94**(17).
62. Kormann, C., D. Bahnemann, and M. Hoffmann, *Photolysis of chloroform and other organic molecules in aqueous TiO2 suspensions.* Environ. Sci. Technol, 1991. **25**(3): p. 494-500.
63. Matthews, R.W., *Photo-oxidation of organic material in aqueous suspensions of titanium dioxide.* Water Research, 1986. **20**(5): p. 569-578.
64. Matthews, R.W., *Kinetics of photocatalytic oxidation of organic solutes over titanium dioxide.* Journal of Catalysis, 1988. **111**(2): p. 264-272.
65. Matthews, R.W., *Purification of water with near—UV illuminated suspensions of titanium dioxide.* Water research, 1990. **24**(5): p. 653-660.
66. Ollis, D.F. and H. Al-Ekabi, *Photocatalytic purification and treatment of water and air: proceedings of the 1st International Conference on TiO2 Photocatalytic Purification and Treatment of Water and Air, London, Ontario, Canada, 8-13 November, 1992*. 1993: Elsevier.
67. Tinucci, L., et al. *Treatment of industrial wastewaters by photocatalytic oxidation on TiO2*. in *Proceedings of the 1st International Conference on TiO2 Photocatalytic Purification and Treatment of Water and Air*. 1993. Ontario, Canada.
68. Low, G.-C., S.R. McEvoy, and R.W. Matthews, *Formation of nitrate and ammonium ions in titanium dioxide mediated photocatalytic degradation of organic compounds containing nitrogen atoms.* Environmental science & technology, 1991. **25**(3): p. 460-467.
69. Wei, T.Y. and C.C. Wan, *Heterogeneous photocatalytic oxidation of phenol with titanium dioxide powders.* Industrial & Engineering Chemistry Research, 1991. **30**(6): p. 1293-1300.
70. Stumm, W., *Aquatic Surface Chemistry: Chemical Processes at the Particle-Water Interface*. 1987: Wiley.

71. Stumm, W., *Chemistry of the solid-water interface: processes at the mineral-water and particle-water interface in natural systems*. 1992: John Wiley & Son Inc.
72. Stone, A.T., et al., *Adsorption of organic compounds possessing ligand donor groups at the oxide-water interface.* ENVIRONMENTAL SCIENCE AND TECHNOLOGY-WASHINGTON DC-, 1993. **27**: p. 895-895.
73. Maruyama, T. and T. Nishimoto, *Hydrogen evolution over a powdered semiconductor photocatalyst.* Industrial & engineering chemistry research, 1991. **30**(7): p. 1634-1638.
74. Navio, J., et al., *A laser flash photolysis study of the reduction of methyl viologen by conduction band electrons of TiO2 and Fe ″ Ti oxide photocatalysts.* Journal of Photochemistry and Photobiology A: Chemistry, 1991. **55**(3): p. 319-322.
75. Heller, A., et al., *Controlled suppression and enhancement of the photoactivity of titanium dioxide (rutile) pigment.* J. Phys. Chem.;(United States), 1987. **91**(23).
76. Minero, C., et al., *Photocatalytic transformation of organic compounds in the presence of inorganic ions. 2. competitive reactions of phenol and alcohols on a titanium dioxide− fluoride system.* Langmuir, 2000. **16**(23): p. 8964-8972.
77. Kim, S. and W. Choi, *Kinetics and mechanisms of photocatalytic degradation of (CH3) n NH4-n+(0≤ n≤ 4) in TiO2 suspension: The role of OH radicals.* Environmental science & technology, 2002. **36**(9): p. 2019-2025.
78. Saquib, M. and M. Muneer, *TiO 2-mediated photocatalytic degradation of a triphenylmethane dye (gentian violet), in aqueous suspensions.* Dyes and pigments, 2003. **56**(1): p. 37-49.
79. Bekbölet, M. and G. Özkösemen, *A preliminary investigation on the photocatalytic degradation of a model humic acid.* Water Science and Technology, 1996. **33**(6): p. 189-194.
80. Wiszniowski, J., et al., *Photocatalytic decomposition of humic acids on TiO2: Part I: Discussion of adsorption and mechanism.* Journal of Photochemistry and Photobiology A: Chemistry, 2002. **152**(1–3): p. 267-273.
81. Ba-Abbad, M.M., et al., *Synthesis and catalytic activity of TiO2 nanoparticles for photochemical oxidation of concentrated chlorophenols under direct solar radiation.* Int. J. Electrochem. Sci, 2012. **7**: p. 4871-4888.
82. Dixit, A., A. Mungray, and M. Chakraborty, *Photochemical oxidation of phenol and chlorophenol by UV/H2O2/TiO2 process: a kinetic study.* International Journal of Chemical Engineering and Applications, 2010. **1**(3): p. 247.
83. Méndez-Arriaga, F., S. Esplugas, and J. Giménez, *Photocatalytic degradation of non-steroidal anti-inflammatory drugs with TiO 2 and simulated solar irradiation.* Water research, 2008. **42**(3): p. 585-594.
84. Liu, S., et al., *TiO2 photocatalysis of natural organic matter in surface water: impact on trihalomethane and haloacetic acid formation potential.* Environmental science & technology, 2008. **42**(16): p. 6218-6223.
85. Pham, H.N., et al., *Quantitative analysis of variations in initial Bacillus pumilus spore densities in aqueous TiO2 suspension and design of a photocatalytic*

reactor. Journal of Environmental Science & Health Part A, 1997. **32**(1): p. 153-163.
86. Bekbölet, M., *Destructive removal of humic acids in aqueous media by photocatalytic oxidation with illuminated titanium dioxide.* Journal of Environmental Science & Health Part A, 1996. **31**(4): p. 845-858.
87. Zang, Y. and R. Farnood, *Effect of hydrogen peroxide on the photocatalytic degradation of methyl tert-butyl ether.* Topics in Catalysis, 2006. **37**(2-4): p. 91-96.
88. Chang-ming, D., et al., *Degradation of acid Orange 7 solution by air-liquid gliding arc discharge in combination with TiO2 catalyst.* Journal of Advanced Oxidation Technologies, 2011. **14**(1): p. 17-22.
89. Tang, W.Z. and H. An, *UV/TiO2 photocatalytic oxidation of commercial dyes in aqueous solutions.* Chemosphere, 1995. **31**(9): p. 4157-4170.
90. Peterson, M., J. Turner, and A. Nozik, *Mechanistic studies of the photocatalytic behavior of TiO2. Particles in a photoelectrochemical slurry cell and the relevance to photodetoxification reactions.* Journal of physical chemistry, 1991. **95**(1): p. 221-225.
91. Schmuhl, R., H. Krieg, and K. Keizer, *Adsorption of Cu (II) and Cr (VI) ions by chitosan: Kinetics and equilibrium studies.* Water Sa, 2001. **27**(1): p. 1-8.
92. Al-Degs, Y.S., et al., *Effect of solution pH, ionic strength, and temperature on adsorption behavior of reactive dyes on activated carbon.* Dyes and pigments, 2008. **77**(1): p. 16-23.
93. Abdus-Salam, N. and F. Adekola, *The influence of pH and adsorbent concentration on adsorption of lead and zinc on a natural goethite.* African Journal of Science and Technology, 2005. **6**(2).
94. Weber Jr, W.J., *ADSORPTION PROCESSES*, in *XXIVth International Congress of Pure and Applied Chemistry*. 1974, Butterworth-Heinemann. p. 375-392.
95. Toth, J., *Adsorption*. 2002: Taylor & Francis.
96. Goldberg, S., *Surface complexation modeling.* Reference Module in Earth Systems and Environmental Sciences, 2013.
97. Hayes, K.F., et al., *Surface complexation models: an evaluation of model parameter estimation using FITEQL and oxide mineral titration data.* Journal of colloid and interface science, 1991. **142**(2): p. 448-469.
98. Selim, H.M. and M.C. Amacher, *Reactivity and transport of heavy metals in soils*. 1996: CRC Press.
99. Goldberg, S., S. Hyun, and L.S. Lee, *Chemical modeling of arsenic (III, V) and selenium (IV, VI) adsorption by soils surrounding ash disposal facilities.* Vadose Zone Journal, 2008. **7**(4): p. 1231-1238.
100. Brezonik, P. and W. Arnold, *Water chemistry: an introduction to the chemistry of natural and engineered aquatic systems*. 2011: OUP USA.
101. Delgado, A.V., *Interfacial Electrokinetics and Electrophoresis*. 2001: Taylor & Francis.

102. Delgado, A.V., et al., *Measurement and interpretation of electrokinetic phenomena.* Journal of Colloid and Interface Science, 2007. **309**(2): p. 194-224.
103. Vithanage, M., et al., *Mechanistic modeling of arsenic retention on natural red earth in simulated environmental systems.* Journal of Colloid and Interface Science, 2006. **294**(2): p. 265-272.
104. Komárek, M., et al., *Competitive adsorption of Cd (II), Cr (VI), and Pb (II) onto nanomaghemite: a spectroscopic and modeling approach.* Environmental science & technology, 2015. **49**(21): p. 12851-12859.
105. Tertre, E., et al., *Europium retention onto clay minerals from 25 to 150 °C: Experimental measurements, spectroscopic features and sorption modelling.* Geochimica et Cosmochimica Acta, 2006. **70**(18): p. 4563-4578.
106. Lim, J.K. and S.-W. Joo, *Comparative adsorption of phenyl selenolate and selenocyanate on Au nanoparticle surfaces.* Applied surface science, 2007. **253**(11): p. 4830-4835.
107. Ye, Z., et al., *Possible use of constructed wetland to remove selenocyanate, arsenic, and boron from electric utility wastewater.* Chemosphere, 2003. **52**(9): p. 1571-1579.
108. Davis, A. and C. Huang, *Removal of phenols from water by a photocatalytic oxidation process.* Water Science and Technology, 1989. **21**(6-7): p. 455-464.
109. Davis, A.P. and C. Huang, *The removal of substituted phenols by a photocatalytic oxidation process with cadmium sulfide.* Water Research, 1990. **24**(5): p. 543-550.
110. Wei, T.-Y., Y.-Y. Wang, and C.-C. Wan, *Photocatalytic oxidation of phenol in the presence of hydrogen peroxide and titanium dioxide powders.* Journal of Photochemistry and Photobiology A: Chemistry, 1990. **55**(1): p. 115-126.
111. Zhijie, X.Y.C.W.Z., *PHOTODEGRADATION OF PHENOL AND CHLORINATED PHENOLS USING A TiO_2-COATED PHOTOREACTOR [J]*. Environmental Chemistry, 1990. **6**: p. 003.
112. Peral, J., J. Casado, and X. Doménech, *Competitive processes in photocatalysis. Phenol-sulphide and phenol-cyanide competitive photooxidation over ZnO.* Electrochimica acta, 1989. **34**(9): p. 1335-1338.
113. Lin, C. and K.-S. Lin, *Photocatalytic oxidation of toxic organohalides with TiO 2/UV: the effects of humic substances and organic mixtures.* Chemosphere, 2007. **66**(10): p. 1872-1877.
114. Kashif, N. and F. Ouyang, *Parameters effect on heterogeneous photocatalysed degradation of phenol in aqueous dispersion of TiO2.* Journal of Environmental Sciences, 2009. **21**(4): p. 527-533.
115. Selvam, K., et al., *The influence of inorganic oxidants and metal ions on semiconductor sensitized photodegradation of 4-fluorophenol.* Chemical Engineering Journal, 2007. **128**(1): p. 51-57.
116. Tunesi, S. and M. Anderson, *Influence of chemisorption on the photodecomposition of salicylic acid and related compounds using suspended*

titania ceramic membranes. The Journal of Physical Chemistry, 1991. **95**(8): p. 3399-3405.
117. Robert, D., et al., *Chemisorption of phenols and acids on TiO 2 surface.* Applied Surface Science, 2000. **167**(1): p. 51-58.
118. Bekkouche, S., et al., *Study of adsorption of phenol on titanium oxide (TiO2).* Desalination, 2004. **166**: p. 355-362.
119. Bekkouche, S., et al., *Competitive adsorption of phenol and heavy metal ions onto titanium dioxide (Dugussa P25).* Desalination and Water Treatment, 2012. **37**(1-3): p. 364-372.
120. GoLDBERG, S., *Chemical modeling of anion competition on goethite using the constant capacitance model.* Soil Science Society of America Journal, 1985. **49**(4): p. 851-856.
121. Hayes, K., et al., *In Situ X-ray Absorption Study of Surface Complexes: Selenium Oxyanions on agr-FeOOH.* Science (New York, NY), 1987. **238**(4828): p. 783.
122. Goldberg, S. and R. Glaubig, *Anion sorption on a calcareous, montmorillonitic soil-selenium.* Soil Science Society of America Journal, 1988. **52**(4): p. 954-958.
123. Hayes, K.F., C. Papelis, and J.O. Leckie, *Modeling ionic strength effects on anion adsorption at hydrous oxide/solution interfaces.* Journal of Colloid and Interface Science, 1988. **125**(2): p. 717-726.
124. Ghosh, M.M., C.D. Cox, and J.R. Yuan- Pan, *Adsorption of selenium on hydrous alumina.* Environmental progress, 1994. **13**(2): p. 79-88.
125. Duc, M., et al., *Sorption of selenium anionic species on apatites and iron oxides from aqueous solutions.* Journal of Environmental Radioactivity, 2003. **70**(1): p. 61-72.
126. Gabos, M.B., S. Goldberg, and L.R.F. Alleoni, *Modeling selenium (IV and VI) adsorption envelopes in selected tropical soils using the constant capacitance model.* Environmental toxicology and chemistry, 2014. **33**(10): p. 2197-2207.
127. Jordan, N., et al., *Sorption of selenium (IV) onto magnetite in the presence of silicic acid.* Journal of colloid and interface science, 2009. **329**(1): p. 17-23.
128. Jordan, N., et al., *Competition between selenium (IV) and silicic acid on the hematite surface.* Chemosphere, 2009. **75**(1): p. 129-134.
129. Nsir, K., et al., *Transport of selenium oxyanions through TiO 2 porous media: Column experiments and multi-scale modeling.* Journal of contaminant hydrology, 2014. **160**: p. 30-41.
130. Goldberg, S., *Macroscopic Experimental and Modeling Evaluation of Selenite and Selenate Adsorption Mechanisms on Gibbsite.* Soil Science Society of America Journal, 2014. **78**(2): p. 473-479.
131. Vohra, M.S. and A.P. Davis, *Adsorption of Pb (II), EDTA, and Pb (II)-EDTA onto TiO2.* Journal of colloid and interface science, 1998. **198**(1): p. 18-26.
132. Brady, P.V., *The physics and chemistry of mineral surfaces*. 1996: CRC Press.
133. Papelis, C., et al., *X-ray-absorption spectroscopic studies of cadmium and selenite adsorption on aluminum-oxides.* Langmuir, 1995. **11**(6): p. 2041-2048.

134. Boyle-Wight, E.J., L.E. Katz, and K.F. Hayes, *Macroscopic studies of the effects of selenate and selenite on cobalt sorption to γ-Al2O3.* Environmental science & technology, 2002. **36**(6): p. 1212-1218.
135. Huang, J., et al., *Surface complexation modeling of adsorption of Cd (II) on graphene oxides.* Journal of Molecular Liquids, 2015. **209**: p. 753-758.
136. Papelis, C., P.V. Roberts, and J.O. Leckie, *Modeling the rate of cadmium and selenite adsorption on micro-and mesoporous transition aluminas.* Environmental science & technology, 1995. **29**(4): p. 1099-1108.
137. Gurkan, Y.Y., E. Kasapbasi, and Z. Cinar, *Enhanced solar photocatalytic activity of TiO 2 by selenium (IV) ion-doping: characterization and DFT modeling of the surface.* Chemical engineering journal, 2013. **214**: p. 34-44.
138. Sartz Jr, W.E., K.J. Wynne, and D.M. Hercules, *X-ray photoelectron spectroscopic investigation of Group VIA elements.* Analytical Chemistry, 1971. **43**(13): p. 1884-1887.
139. Smith, K.S., *Metal sorption on mineral surfaces: an overview with examples relating to mineral deposits.* The Environmental Geochemistry of Mineral Deposits. Part B: Case Studies and Research Topics, 1999. **6**: p. 161-182.
140. Hamada, S., *ACID DECOMPOSITION EQUILIBRIUM OF SELENOCYANATE ION.* Nippon Kagaku Zasshi, 1961. **82**(10): p. 1327-&.
141. Drioli, E. and L. Giorno, *Comprehensive Membrane Science and Engineering*. 2010: Elsevier Science.
142. Vohra, M., S. Selimuzzaman, and M. Al-Suwaiyan, *Aqueous phase thiosulfate removal using photo catalysis.* International Journal of Environmental Research, 2010. **5**(1): p. 247-254.
143. Christy, A.A. and P.K. Egeberg, *Oxidation of thiocyanate by hydrogen peroxide — a reaction kinetic study by capillary electrophoresis.* Talanta, 2000. **51**(6): p. 1049-1058.
144. Zhu, X., et al., *Effects of pH and catalyst concentration on photocatalytic oxidation of aqueous ammonia and nitrite in titanium dioxide suspensions.* Environmental science & technology, 2005. **39**(10): p. 3784-3791.
145. Vohra, M., S. Selimuzzaman, and M. Al- Suwaiyan, *NH4+- NH3 removal from simulated wastewater using UV- TiO2 photocatalysis: effect of co- pollutants and pH.* Environmental technology, 2010. **31**(6): p. 641-654.
146. Combs, M.T., M. Ashraf-Khorassani, and L.T. Taylor, *pH effects on the direct supercritical fluid extraction of phenols from aqueous matrices.* The Journal of Supercritical Fluids, 1996. **9**(2): p. 122-127.
147. Das, J. and K. Parida, *Catalytic Ketonization of Acetic Acid on Zn/Al Layered Double Hydroxides.* Reaction Kinetics and Catalysis Letters, 2000. **69**(2): p. 223-229.
148. Ernst, W. and K. Weber, *Chlorinated phenols in selected estuarine bottom fauna.* Chemosphere, 1978. **7**(11): p. 867-872.

149. Etter, M.C., J.C. MacDonald, and J. Bernstein, *Graph-set analysis of hydrogen-bond patterns in organic crystals.* Acta Crystallographica Section B, 1990. **46**(2): p. 256-262.
150. Sinisterra, J.V., et al., *The nature of active sites in Ba(OH)2 catalyst.* Reaction Kinetics and Catalysis Letters, 1984. **25**(3): p. 277-282.
151. Torres, I.J., C.L. Litterst, and A.M. Guarino, *Transport of Model Compounds across the Peritoneal Membrane in the Rat.* Pharmacology, 1978. **17**(6): p. 330-340.
152. O'Shea, K.E. and C. Cardona, *The reactivity of phenol in irradiated aqueous suspensions of TiO2. Mechanistic changes as a function of solution pH.* Journal of Photochemistry and Photobiology A: Chemistry, 1995. **91**(1): p. 67-72.
153. Shardt, Y.A.W., *Statistics for Chemical and Process Engineers: A Modern Approach*. 2015: Springer International Publishing.
154. Hibbert, D.B., *Quality Assurance in the Analytical Chemistry Laboratory*. 2007: Oxford University Press, USA.
155. Narayanan, S. and R.N. IYENGAR, *IUTAM Symposium on Nonlinearity and Stochastic Structural Dynamics: Proceedings of the IUTAM Symposium held in Madras, Chennai, India 4–8 January 1999*. 2001: Springer Netherlands.
156. Breyfogle, F.W., *Statistical Methods for Testing, Development, and Manufacturing*. 1992: John Wiley & Sons.
157. Bartz-Beielstein, T., et al., *Experimental Methods for the Analysis of Optimization Algorithms*. 2010: Springer Berlin Heidelberg.
158. Vuchkov, I.N. and N.L. Boyadjieva, *Quality Improvement with Design of Experiments: A Response Surface Approach*. 2013: Springer Netherlands.
159. Box, G.E.P. and D.R. Cox, *An Analysis of Transformations.* Journal of the Royal Statistical Society. Series B (Methodological), 1964. **26**(2): p. 211-252.
160. Cook, R.D. and S. Weisberg, *Residuals and Influence in Regression*. 1982: Chapman & Hall.
161. Piñeiro, G., et al., *How to evaluate models: Observed vs. predicted or predicted vs. observed?* Ecological Modelling, 2008. **216**(3–4): p. 316-322.
162. Gaya, U.I., *Kinetic Concepts of Heterogeneous Photocatalysis*, in *Heterogeneous Photocatalysis Using Inorganic Semiconductor Solids*. 2014, Springer Netherlands: Dordrecht. p. 43-71.

Vitae

Name	Bashir Alhaji Labaran
Nationality	Nigerian
Date of Birth	15th September 1982
Email	iklima4bash@yahoo.com
Address	No. 2 Gawo Street, Sabongari, Jega, Nigeria
Academic Background	B.Eng. Civil Engineering, Bayero University Kano (2008)
	M. Sc. Civil Engineering, King Fahd University of Petroleum and Minerals (2013)
	PhD. Civil Engineering, King Fahd University of Petroleum and Minerals (2017)